



University of
Strathclyde
Glasgow

New Methods for the Production of Oral Dosage Forms

by

Alice Jane Turner

A thesis in fulfilment of the requirements for the degree of Doctor of
Philosophy

Strathclyde Institute of Pharmacy and Biomedical Sciences,

The University of Strathclyde,

Glasgow, United Kingdom

2018

Declaration of Authenticity and Author's Rights

This is the result of the author's original research. It has been composed by the author and has not been previously submitted for examination which has led to the award of a degree.

The copyright of this thesis belongs to the author under the terms of the United Kingdom Copyright Acts as qualified by University of Strathclyde Regulation 3.50. Due acknowledgement must always be made of the use of any material contained in, or derived from, this thesis.

Signed:

Date:

Alice J. Turner

Acknowledgments

I would like to thank my supervisor Gavin Halbert for his patience, guidance and support throughout the project, and for telling me to “keep calm and experiment on!”. I would like to thank my second supervisor Alastair Florence for his guidance and support. I would also like to thank all the members of CMAC’s secondary processing team, John Robertson, Elke Prasad, Ali Anwar, Elanor Brammer, Ecaterina Bordos, Tariq Islam, Carlota Mendez-Torrecillas and Sarahjane Wood, for all their guidance and support throughout my work. I would further like to thank Ali Anwar, Deborah Bowering, Matthew Bunker, Lauren Connor, Frederik Doerr, Kelly Etherson, Anne Goudie, Shashwat Gupta, Laura Harvey, Maruf Hussain, Gerry Johnston, Ibrahim Khadra, Alan Martin, Thomas McGlone, Eleonora Paladino, Savitha Panikar, Elke Prasad, Sonia Razavi, Lennart Ramakers, Murray Robertson, Jennifer Seaton, Fiona Sillars, Vaclav Svoboda, Kevin Treacher, Antony Vassileiou, Bruce Wareham, Monika Warzecha and Sarahjane Wood for all their technical support. I would also like to thank Bilal Ahmed, Magdalene Chong, Michael Chrubasik, Lauren Connor, Andrew Dunn, Clarissa Forbes, Arabella McLaughlin, Carlota Mendez-Torrecillas, Georgia Sanxaridou, Vaclav Svoboda, Antony Vassileiou, Bruce Wareham and Sarahjane Wood for keeping me smiling. I would also like to thank everyone else in CMAC for their continuing teaching and support over the course of the past 4 years.

I would like to thank my industry mentors, particularly Liz Meehan, Elizabeth Swain and Helen Wheatcroft, and everyone else at AstraZeneca for allowing me to have such a wonderful placement there. I would like to thank C-SOPS for welcoming me into their labs for a month and for all their support throughout that month.

I would like to acknowledge that this work was carried out in the CMAC National Facility supported by UKRPIF (UK Research Partnership Investment Fund) award from the Higher Education Funding Council for England (HEFCE) (Grant ref HH13054). I would also like to thank the International Institute for Advanced

Pharmaceutical Manufacturing (I2APM) (Grant ref EP/M02166/1) and the EPSRC Doctoral Training Centre in Continuous Manufacturing and Crystallisation for funding this work.

Last but certainly not least, I would also like to thank my friends and family for their constant support and encouragement over the last 4 years, I could not have completed this project without them. I would especially like to thank my mother, the woman who believed in me when I didn't believe in myself, fed my thirst for knowledge, drove me to be the best version of myself and made me the woman I am today.

Published Conference Papers

Turner A.J., Florence A.J. & Halbert G.W., Aerosol Jet Printing Oral Dosage Forms to Increase Dissolution of Class II Drugs, CMAC Open Day 2018, The Technology and Innovation Centre, Glasgow, 25-26th October 2018

Turner A.J., Florence A.J. & Halbert G.W., New Methods for the Production of Oral Dosage Forms, CMAC Summer School 2018, Peebles Hydro, Peebles, 14th June 2018

Turner A.J., Florence A.J. & Halbert G.W., Inkjet Printing of Oral Dosage Forms to Solubilize BCS Class II Drugs, SCI Formulation Forum Launch Event 2018, SCI, London, 17-18th January 2018

Turner A.J., Florence A.J. & Halbert G.W., Inkjet Printing Scalable Oral Dosage Forms Capable of Increasing Solubility of BCS Class II Drugs, AAPS Annual Meeting and Exposition 2017, San Diego Convention Centre, San Diego, CA, USA, 15th November 2017

Turner A.J., Florence A.J. & Halbert G.W., New Methods for the Production of Oral Dosage Forms, C-SOPS Fall 2017 Industry Meeting, Busch Campus, Rutgers University, Piscataway, NJ, USA, 16-17th October 2017

Turner A.J., Florence A.J. & Halbert G.W., New Methods for the Production of Oral Dosage Forms, CMAC Open Day 2017, The Technology and Innovation Centre, Glasgow, 23-24th March 2017

Turner A.J., Florence A.J. & Halbert G.W., Inkjet Printing Oral Dosage Forms, International Institute of Advanced Pharmaceutical Manufacturing (I2APM) Symposium 2016, The Technology and Innovation Centre, Glasgow, 30th November-1st December 2016

Turner A.J., Florence A.J. & Halbert G.W., Inkjet Printing Oral Dosage Forms, APS PharmSci 2016, The Technology and Innovation Centre, Glasgow, 5-7th September 2016

Turner A.J., Florence A.J. & Halbert G.W., New Methods for the Production of Oral Dosage Forms, CMAC Summer School 2016, Dunblane Hydro, Dunblane, 16th June 2016

Turner A.J., Florence A.J. & Halbert G.W., New Methods for the Production of Oral Dosage Forms, CMAC Open Day 2015, The Technology and Innovation Centre, Glasgow, 23-24th September 2015

Turner A.J., Florence A.J. & Halbert G.W., New Methods for the Production of Oral Dosage Forms, CMAC Summer School 2015, Crieff Hydro, Crieff, 25 June 2015

Papers in Preparation

Turner A.J., Florence A.J. & Halbert G.W., 2019, Investigation of Aerosol Jet Printing for the Preparation of Solid Dosage Forms, (publication TBA)

Patents in Preparation

Turner A.J., Florence A.J. & Halbert G.W., 2019, Aerosol Jet Printed Pulsatile Systems, (publication TBA)

Abstract

Oral drug delivery remains the preferred method of API administration, but Biopharmaceutical Classification System Class II drugs are not ideally suited to this due to their inherent poor solubility. The current study aims to utilise the innovative formulation technique of aerosol jet printing to increase the dissolution capability of poorly soluble drugs.

Aerosol jet printing Class II drugs with an appropriate stabilising polymer reduces crystallinity, increasing drug solubility. Furthermore, in the presence of sufficient polymer content, fully amorphous products can be produced resulting in enhanced dissolution capabilities. The intrinsic dissolution rate of fenofibrate was found to increase by 10-fold on printing with PVP K30. A lesser increase was typically seen on printing the materials as separate layers, but a slight loss of crystallinity does suggest that there are some interactions happening at the interface. Printing with PVP K30 was also found to increase the intrinsic dissolution rate of ibuprofen, with 3-fold increase on formation of amorphous material.

Aerosol jet printing also allows a high degree of precision, enabling control of drug location to the micrometre, production of scalable dosage forms and control of drug distribution within solid dispersions. This high degree of precision has also enabled design of more complex dosage forms with a view to generating a pulsatile release profile in an entirely novel manner. Scale up of printing was attempted to allow demonstration of high precision printing of a full-size tablet. Unfortunately, dissolution testing of the full-size tablet failed but it is hoped this technology could be developed further in the future.

Overall this thesis demonstrates the ability of the aerosol jet technology to be applied to pharmaceutical manufacturing in a precise manner to increase dissolution of poorly soluble compounds. Future work could include development of the technique for use in production of more complex customisable dosage forms.

Table of Contents

Declaration of Authenticity and Author's Rights	i
Acknowledgments	ii
Published Conference Papers.....	iv
Papers in Preparation	v
Patents in Preparation	vi
Abstract.....	vii
Abbreviations	xi
List of Figures.....	xiii
List of Tables	xxii
Chapter 1: Introduction	1
1.1 Background.....	1
1.1.1 Dosage Forms	1
1.1.2 Oral Solid Dosage Forms.....	1
1.2 Class II drugs	6
1.3 Methods of Improving Solubility of Class II Drugs	7
1.3.1 Conventional Methods to Improve the Solubility of Class II Drugs	8
1.3.5 Continuous Manufacture of Oral Drug Delivery Systems to Improve the Solubility of Class II Drugs: Basic Concepts of and Reasons for Continuous Manufacture	21
1.3.6 Methods for Continuous Manufacture of Oral Drug Delivery Systems for Class II Drugs.....	24
1.4 The Current Study	32
1.4.4 Basic Concepts.....	32
1.4.5 Theory	34
1.4.6 The Model Drugs.....	35
1.4.7 Excipient Selection	37
1.5 Research Questions	38
1.6 Aims and Objectives.....	38

Chapter 2: The Effect of Ink Formulation and Aerosol Jet Printing on Physical Form	39
2.1 Introduction	39
2.2 Materials and Methods	39
2.2.1 Materials	39
2.2.2 Methods.....	40
2.3 Results & Discussion	47
2.3.1 Ink Rheology.....	47
2.3.2 Powder X-Ray Diffraction.....	53
2.3.3 Differential Scanning Calorimetry	71
2.3.4 Raman Spectroscopy.....	82
2.3.5 Scanning Electron Microscopy	86
2.3.6 Size Exclusion Chromatography	98
2.4 Conclusions	100
Chapter 3: Aerosol Jet Printer Capabilities	101
3.1 Introduction	101
3.2 Materials and Methods	101
3.2.1 Materials	101
3.2.2 Methods.....	101
3.3 Results & Discussion	107
3.3.1 Dosage Form Construction	107
3.3.2 Drug Distribution.....	117
3.4 Conclusions	131
Chapter 4: The Effect of Aerosol Jet Printing on Dissolution	132
4.1 Introduction	132
4.2 Materials and Methods	132
4.2.1 Materials	132
4.2.2 Methods.....	132
4.3 Results & Discussion	140
4.3.1 Drug Content.....	140
4.3.2 Dissolution	144
4.3.3 Contact Angle	169
4.4 Conclusions	187

Chapter 5: Aerosol Inkjet Printing Pulsatile Release Systems Utilising Fenofibrate.....	188
5.1 Introduction	188
5.2 Materials and Methods	190
5.2.1 Materials.....	190
5.2.2 Methods.....	190
5.3 Results & Discussion	192
5.4 Conclusions	195
Chapter 6: Aerosol Inkjet Printing Pulsatile Release Systems Utilising Ibuprofen	196
6.1 Introduction	196
6.2 Materials and Methods	196
6.2.1 Materials.....	196
6.2.2 Methods.....	196
6.3 Results & Discussion	205
6.3.1 SDI Samples.....	205
6.3.2 Full-Size Tablet	228
6.4 Conclusions	239
Chapter 7: Conclusions, Challenges and Future Work.....	240
7.1 Conclusions	240
7.2 Challenges	243
7.2.1 Limitations of the Instrument.....	243
7.2.2 Challenges due to the Nature of the Manufacturing Technique.....	246
7.2.3 Challenges Arising from the Drugs Utilised	248
7.3 Future Work	251
7.3.1 Alterations to the method.....	251
7.3.2 Applications	252
References	255
Appendices	295

Abbreviations

ABS – absolute

ACN -acetonitrile

API – Active Pharmaceutical Ingredient

BP – British Pharmacopoeia

ccm - Cubic Centimetres per minute

CAD – computer aided drawing

CMAC – The EPSRC Centre for Innovative Manufacturing in Continuous Manufacturing and Crystallisation (until December 2016)/ The EPSRC Continuous Manufacturing and Advanced Crystallisation (CMAC) Future Manufacturing Research Hub (as of 2017)

cP – Centipoise (1 = 0.001 Pa.s)

d – SDI path length

DSC – Differential Scanning Calorimetry

FaSSIF – Fasted state simulated intestinal fluid

FeSSIF – Fed state simulated intestinal fluid

FNF - Fenofibrate

GIT – Gastrointestinal Tract

HPLC – High Performance Liquid Chromatography

HPMC – Hydroxypropyl Methylcellulose

IBU – Ibuprofen

IDR – Intrinsic dissolution rate

MEC – Molar extinction coefficient

MDCK - Madin-Darby Canine Kidney cells for permeability testing

Mn – Number Average Molecular Weight

Mn/Mw – Molecular weight distribution

Mw – Weight Average Molecular Weight

Mz – Z-Average Molecular Weight

PAT – Process Analytical Technology

PEG – Polyethylene glycol

psi – Pounds per Square Inch (1 = 0.0689476 bar)

PVP 10,000 - Polyvinylpyrrolidone average molecular weight 10,000

PVP K30 – Polyvinylpyrrolidone average molecular weight 40,000

PVP K90 - Polyvinylpyrrolidone average molecular weight 360,000

PXRD – Powder X-ray Diffraction

Rpm – rate per minute

SDI – Surface Dissolution Imager

SEC – Size Exclusion Chromatography

SEM – Scanning Electron Microscopy

SIF – Simulated intestinal fluid without enzymes

TOF-SIMS – Time of Flight Secondary Ion Mass Spectroscopy

USP I/II/IV – United States Pharmacopoeia I/II/IV dissolution method

UHPLC-MS – Ultra High Performance Liquid Chromatography coupled with Mass Spectrometry

XRD – X-ray diffraction

List of Figures

Figure 1: Structure of an ideal solid dispersion with the drug.....	11
Figure 2: Basic structure of a polymer-drug conjugate	15
Figure 3: Micro and nanoparticle structures	16
Figure 4: Basic structure of micelles	18
Figure 5: Solvent Activated Systems	19
Figure 6: Chemically Controlled Systems	20
Figure 7: The Continuous Pharmaceutical Pipeline	23
Figure 8: Twin-screw extrusion	25
Figure 9: Optomec AJ200 3D Inkjet Printer	32
Figure 10: Changes to the conventional tablet manufacturing process.....	33
Figure 11: Schematic of theoretical dosage forms	34
Figure 12: Structure of fenofibrate.....	35
Figure 13: Structure of Ibuprofen.....	37
Figure 14: The pneumatic atomisation process.....	41
Figure 15: Comparison of the effect of increasing polymer content on the viscosity water and ethanol- based solutions.....	48
Figure 16: Comparison of shear rate sweeps	49
Figure 17: The effect of PVP K30 content on viscosity of formulation inks prepared in ethanol taken at 1000 1/s	51
Figure 18: Comparison of example shear rate sweeps of formulation inks	52
Figure 19: Comparison of printing on Kapton film vs. printing on standard printer paper: XRD on the Bruker D8 Advance II	54
Figure 20: Limitation of the Bruker D8 Advance	55
Figure 21: Comparison of printing on Kapton film vs. printing on rice paper with the rice paper signal subtracted.....	56
Figure 22: Subtraction of the rice paper signal: XRD on the Bruker D8 Discover	57
Figure 23: X-ray diffraction of fenofibrate powder and physical mixtures of fenofibrate:PVP 2:1, 1:1, 2:3, 1:2, 1:3 and 1:4.....	59

Figure 24: X-ray diffraction of printed fenofibrate and printed mixtures fenofibrate:PVP 2:1, 1:1, 2:3, 1:2, 1:3 and 1:4.....	61
Figure 25: X-ray diffraction of printed fenofibrate and layered printed samples.....	67
Figure 26: X-ray diffraction of ibuprofen powder, ibuprofen printed and printed mixtures of ibuprofen:PVP 1:1, 1:2, 1:3 and 1:4.....	70
Figure 27: Differential scanning calorimetry of fenofibrate powder and physical mixtures of fenofibrate:PVP 2:1, 1:1, 2:3, 1:2, 1:3 and 1:4.....	73
Figure 28: Differential scanning calorimetry of printed fenofibrate and mixtures of fenofibrate:PVP 2:1, 1:1, 2:3, 1:2, 1:3 and 1:4.....	75
Figure 29: Differential scanning calorimetry of printed fenofibrate and layered printed samples.....	77
Figure 30: Differential scanning calorimetry of ibuprofen powder and physical mixtures of ibuprofen:PVP 1:1, 1:2, 1:3 and 1:4.....	79
Figure 31: Differential scanning calorimetry of printed ibuprofen and mixtures of ibuprofen:PVP 1:1, 1:2, 1:3 and 1:4.....	81
Figure 32: Raman spectra of fenofibrate and PVP K30 based printed samples.....	84
Figure 33: Raman spectra of fenofibrate alone in raw powder form and as part of an inkjet printed 1:3 fenofibrate:PVP solid dispersion.....	85
Figure 34: SEM of 2mm samples of PVP K90 4 layers at x35 magnification.....	87
Figure 35: SEM of 2mm samples of PVP K30 1 layer x35 magnification	88
Figure 36: SEM of PVP K30 with different starting ink concentrations taken at x1.5K magnification.....	89
Figure 37: SEM of printed fenofibrate and PVP mixtures taken at x1.5K magnification.....	92
Figure 38: SEM of fenofibrate:PVP layered samples.....	94
Figure 39: SEM of tori style printed samples.....	95
Figure 40: SEM of printed ibuprofen, and ibuprofen:PVP 1:1, 1:2, 1:3 and 1:4 taken at x1.5K magnification.....	97
Figure 41: Size exclusion chromatograph of raw and printed PVP.....	98

Figure 42: The effect of speed on mass of drug printed.....	108
Figure 43: The effect of nozzle size on mass of drug printed.....	110
Figure 44: The effect of deposition size on mass of drug printed.....	112
Figure 45: The effect of layer number on mass of drug printed.....	114
Figure 46: Thickness of depositions based on polymer content as detected by laser triangulation.....	116
Figure 47: 3D Raman images of dosage forms consisting of 2:1 and 1:1 fenofibrate:PVP.....	119
Figure 48: 3D Raman images of dosage forms consisting of 2:3 and 1:2 fenofibrate:PVP.....	120
Figure 49: 3D Raman images of dosage forms consisting of 1:3 and 1:4 fenofibrate:PVP.....	121
Figure 50: Raman spectra comparing the spectral regions of rice paper, PVP and fenofibrate.....	122
Figure 51: A 3D Raman mapping images of fenofibrate and PVP K30 aerosol jet printed as separate layers and tori-based regions.....	125
Figure 52: A TOF-SIMS image and its starting deposition design depicting a 6mm diameter deposition consisting of 2 distinct areas of fenofibrate and 2 distinct areas of PVP K30 of 5 printed lines each.....	128
Figure 53: TOF-SIMS images taken of the 2 areas highlighted in Figure 52 with measurements for fenofibrate and PVP K30.....	128
Figure 54: A TOF-SIMS image and its starting deposition design depicting a 6mm diameter deposition consisting of 4 distinct areas of fenofibrate and 5 distinct areas of PVP K30 of 2 printed lines each.....	129
Figure 55: TOF-SIMS images taken of the area highlighted in Figure 34 with measurements for fenofibrate and PVP K30.....	129
Figure 56: A TOF-SIMS image and its starting deposition design depicting a 6mm diameter deposition consisting of 9 distinct areas of fenofibrate and 9 distinct areas of PVP K30 of 1 printed line each.....	130
Figure 57: TOF-SIMS images taken of the 2 areas highlighted in Figure 36 with measurements for fenofibrate and PVP K30.....	130
Figure 58: Designs of Dosage Forms.....	136

Figure 59: SDI process.....	136
Figure 60: Percentage Drug Release from fenofibrate and PVP compacts	146
Figure 61: Percentage Drug Release from printed samples of fenofibrate and PVP.....	148
Figure 62: Intrinsic Dissolution Rate obtained from compacts of fenofibrate and PVP.....	151
Figure 63: Intrinsic Dissolution Rate obtained from printed samples of fenofibrate and PVP.....	152
Figure 64: Comparison of intrinsic dissolution rate of powder and printed	153
Figure 65: Images taken from the Sirius SDI Data Analysis software of fenofibrate and PVP compacts and printed samples.....	154
Figure 66: Percentage drug release of printed fenofibrate compared to layered with PVP.....	156
Figure 67: Intrinsic dissolution rate of printed fenofibrate compared to layered with PVP.....	157
Figure 68: Comparison of percentage drug release of 1:1 layered samples	158
Figure 69: Comparison of intrinsic dissolution rate of 1:1 layered samples,	159
Figure 70: Images taken from the Sirius SDI Data Analysis software of fenofibrate and PVP layered samples.....	160
Figure 71: Percentage drug release of 5 layered printed premixed fenofibrate and PVP.....	161
Figure 72: Intrinsic dissolution rate of 5 layered printed premixed fenofibrate and PVP.....	162
Figure 73: Comparison of the percentage drug release of fenofibrate and ibuprofen raw powder compacts.....	163
Figure 74: Percentage drug release of 5 layered printed ibuprofen compared to printed premixed ibuprofen and PVP.....	165
Figure 75: Comparison of the intrinsic dissolution rate of fenofibrate and ibuprofen raw powder compacts.....	166
Figure 76: Intrinsic dissolution rate of 5 layered printed ibuprofen compared to printed premixed ibuprofen and PVP.....	168

Figure 77: Images taken from the Sirius SDI Data Analysis software of ibuprofen and PVP samples.....	169
Figure 78: The effect of polymer ink concentration on the contact angle of PVP spin coated samples measured at point zero.....	171
Figure 79: Comparison of initial contact angle images of spin coated PVP samples.....	172
Figure 80: The effect of polymer concentration on the contact angle of fenofibrate and PVP spin coated samples measured at point zero.....	174
Figure 81: Comparison of initial contact angle images of fenofibrate and PVP spin coated samples.....	176
Figure 82: Average contact angle values of printed fenofibrate and PVP taken at point zero.....	179
Figure 83: Comparison of printed samples to spin coated samples based on contact angle values taken at point zero.....	181
Figure 84: Comparison of initial contact angle images of printed fenofibrate and PVP samples.....	183
Figure 85: Average contact angle of ibuprofen and PVP printed samples measured at point zero.....	186
Figure 86: Drug Release from fenofibrate containing sandwich-style systems.....	193
Figure 87: Intrinsic dissolution rate from fenofibrate containing sandwich-style systems.....	194
Figure 88: Drug release from sandwich-style prototype pulsatile dosage forms.....	206
Figure 89: Intrinsic Dissolution Rate from sandwich-style prototype pulsatile dosage forms.....	207
Figure 90: Drug release from tori based dome-style prototype pulsatile dosage forms.....	209
Figure 91: Intrinsic dissolution rate from tori based dome-style prototype pulsatile dosage forms.....	210
Figure 92: Drug release from encapsulated prototype pulsatile dosage forms.....	211

Figure 93: Intrinsic dissolution rate from encapsulated prototype pulsatile dosage forms consisting of 2 5 layer 1:4 ibuprofen:PVP layers to 1 5 layer PVP buffer layer and 2 10 layer 1:4 ibuprofen:PVP layers to 1 10 layer PVP buffer layers.....	212
Figure 94: Intrinsic dissolution rate from encapsulated prototype pulsatile dosage forms consisting of 2 5 layer 1:4 ibuprofen:PVP layers to 1 5 layer PVP buffer layer.....	213
Figure 95: Intrinsic dissolution rate from encapsulated prototype pulsatile dosage forms consisting of 2 10 layer 1:4 ibuprofen:PVP layers to 1 10 layer PVP buffer layers.....	214
Figure 96: Drug release from encapsulated prototype pulsatile dosage forms consisting of 2 5 layer 1:4 ibuprofen:PVP layers to 1 5 1.1mm layer PVP buffer layer, 1.4mm buffer layer and 1.7mm buffer layer	215
Figure 97: Intrinsic dissolution rate from encapsulated prototype pulsatile dosage forms consisting of 2 5 layer 1:4 ibuprofen:PVP layers to 1 5 1.1mm layer PVP buffer layer, 1.4mm buffer layer and 1.7mm buffer layer.....	216
Figure 98: Drug release from encapsulated prototype pulsatile dosage forms consisting of 2 5 layer 1:4 ibuprofen:PVP layers to 1 5 1.1mm layer PVP buffer layer.....	217
Figure 99: Intrinsic dissolution rate from encapsulated prototype pulsatile dosage forms consisting of 2 5 layer 1:4 ibuprofen:PVP layers to 1 5 1.1mm layer PVP buffer layer.....	218
Figure 100: Drug release from encapsulated prototype pulsatile dosage forms consisting of 2 5 layer 1:4 ibuprofen:PVP layers to 1 5 1.7mm layer PVP buffer layer.....	219
Figure 101: Intrinsic dissolution rate from encapsulated prototype pulsatile dosage forms consisting of 2 5 layer 1:4 ibuprofen:PVP layers to 1 5 1.7mm layer PVP buffer layer.....	220
Figure 102: Drug release from encapsulated prototype pulsatile dosage forms consisting of 2 10 layer 1:4 ibuprofen:PVP layers to 1 10 1.4mm layer PVP buffer layer, 2 5 layer 1:4 ibuprofen:PVP layers to 1 5 1.4mm layer PVP buffer layer, 1 5 layer 1:4 ibuprofen:PVP outer layer and 1 10 layer 1:4	

ibuprofen:PVP core to 1 5 1.4mm layer PVP buffer layer and 1 10 layer 1:4 ibuprofen:PVP outer layer and 1 20 layer 1:4 ibuprofen:PVP core to 1 10 1.4mm layer PVP buffer layer.....	221
Figure 103: Intrinsic Dissolution Rate from encapsulated prototype pulsatile dosage forms consisting of 2 10 layer 1:4 ibuprofen:PVP layers to 1 10 1.4mm layer PVP buffer layer, 2 5 layer 1:4 ibuprofen:PVP layers to 1 5 1.4mm layer PVP buffer layer, 1 5 layer 1:4 ibuprofen:PVP outer layer and 1 10 layer 1:4 ibuprofen:PVP core to 1 5 1.4mm layer PVP buffer layer and 1 10 layer 1:4 ibuprofen:PVP outer layer and 1 20 layer 1:4 ibuprofen:PVP core to 1 10 1.4mm layer PVP buffer layer.....	222
Figure 104: Drug release from encapsulated prototype pulsatile dosage forms consisting of 1 5 layer 1:4 ibuprofen:PVP outer layer and 1 10 layer 1:4 ibuprofen:PVP core to 1 5 1.4mm layer PVP buffer layer.....	223
Figure 105: Intrinsic dissolution rate from encapsulated prototype pulsatile dosage forms consisting of 1 5 layer 1:4 ibuprofen:PVP outer layer and 1 10 layer 1:4 ibuprofen:PVP core to 1 5 1.4mm layer PVP buffer layer	224
Figure 106: Drug release from encapsulated prototype pulsatile dosage forms consisting of 1 10 layer 1:4 ibuprofen:PVP outer layer and 1 20 layer 1:4 ibuprofen:PVP core to 1 10 1.4mm layer PVP buffer layer	225
Figure 107: Intrinsic dissolution rate from encapsulated prototype pulsatile dosage forms consisting of 1 10 layer 1:4 ibuprofen:PVP outer layer and 1 20 layer 1:4 ibuprofen:PVP core to 1 10 1.4mm layer PVP buffer layer.....	226
Figure 108: Drug release from encapsulated prototype pulsatile dosage forms consisting of 3 5 layer 1:4 ibuprofen:PVP layers to 2 5 1.4mm layer PVP buffer layers and 3 10 layer 1:4 ibuprofen:PVP layers to 2 10 1.4mm layer PVP buffer layers.....	227
Figure 109: Intrinsic dissolution rate from encapsulated prototype pulsatile dosage forms consisting of 3 5 layer 1:4 ibuprofen:PVP layers to 2 5 1.4mm layer PVP buffer layers and 3 10 layer 1:4 ibuprofen:PVP layers to 2 10 1.4mm layer PVP buffer layers.....	228
Figure 110: Nano CT image of the full size ibuprofen and PVP K30 tablet at different angels.....	229

Figure 111: Nano CT image of the full size tablet sliced horizontally from above with the full tablet being sliced a third of the way down to show the start of the PVP buffer, then another third to show the drug containing core and right down to the substrate.....	230
Figure 112: Nano CT image of the full size tablet sliced horizontally from above as 2D cutaway images of the tablet uncut, a third removed and 2 thirds removed.....	231
Figure 113: Nano CT image of the full size tablet sliced horizontally from below.....	233
Figure 114: Nano CT image of the full size tablet sliced vertically gradually revealing the tablet core from two angles.....	235
Figure 115: Drug release from a full size pulsatile ibuprofen and PVP prototype.....	238
Figure 116: Theoretical design of a dual atomiser and print head system.	244
A1.1: SEM of PVP K30 (A), fenofibrate (B), 2:1 (C) and 1:1 (D) fenofibrate:PVP K30 taken at x20K magnification.....	295
A1.2: SEM of 2:3 (A), 1:2 (B), 1:3 (C) and 1:4 (D) fenofibrate:PVP K30 taken at x20K magnification.....	296
A2.2: Average calibration curve for UHPLC of fenofibrate over a range of 5-100µg/ml.....	299
A3.1: Average calibration curve for UHPLC of ibuprofen over a range of 5-100µg/ml.....	300
A3.2: Calibration curve generated using the Sirius Analytical SDI for fenofibrate over a range of 1-10µg/ml.....	301
A3.3: Calibration curve generated using the Sirius Analytical SDI for ibuprofen over a range of 1-10µg/ml in SIF.....	302
A4.1: Contact angle of glass coverslips over a 30 second period.....	303
A4.2: Contact angle of PVP spin coated samples over a 30 second period.	304
A4.3: Contact angle of fenofibrate and PVP spin coated samples over a 30 second period.....	305
A4.4: Contact angle of fenofibrate and PVP printed samples over a 30 second period.....	306

A5: Calibration curve for ibuprofen in SIF generated using the USP IV flow cell system coupled with the UV spectrometer.....	307
--	-----

List of Tables

Table 1: Classification of a number of drugs via the Biopharmaceutical classification System.....	5
Table 2: Formulations generated on inkjet printing.....	43
Table 3: Crystalline content of fenofibrate containing physical mixtures measured by powder X-ray diffraction.....	58
Table 4: Crystalline content of printed premixed fenofibrate containing samples measured by powder X-ray diffraction.....	62
Table 5: Percentage crystallinity obtained from a stability study on fenofibrate-based printed samples over a 6 month period.....	64
Table 6: Crystalline content of printed fenofibrate containing layered samples measured by powder X-ray diffraction.....	66
Table 7: Crystalline content of printed ibuprofen containing samples measured by powder X-ray diffraction.....	69
Table 8: DSC peak and peak enthalpy Fenofibrate powder alone and as physical mixtures with PVP K30.....	72
Table 9: DSC peak and peak enthalpy Fenofibrate printed alone and with PVP K30.....	74
Table 10: DSC peak and peak enthalpy Fenofibrate printed alone and layered with PVP K30.....	76
Table 11: DSC peak and peak enthalpy ibuprofen powder alone and physical mixtures with PVP K30.....	78
Table 12: DSC peak and peak enthalpy ibuprofen printed alone and with PVP K30.....	80
Table 13: Size exclusion chromatography results.....	99
Table 14: UHPLC method selection parameters and effects.....	102
Table 15: Percentage content detected by the H2Optix mPAT Python script from premixed samples.....	123
Table 16: Percentage content detected by the H2Optix mPAT Python script.....	126

Table 17: Method development for UHPLC of ibuprofen.....	133
Table 18: Formulations to increase dissolution of Class II Drugs.....	134
Table 19: Samples prepared for contact angle.....	139
Table 20: Drug content of printed fenofibrate alone and premixed with PVP as 25 layer x 0.9 mm ² circle depositions, generated using a 300µm nozzle at 3 mm/s, measured at 280 nm by UHPLC.....	142
Table 21: Drug content of printed fenofibrate alone and premixed with PVP as 5 layer x 0.9 mm ² circle depositions, generated using a 300µm nozzle at 3 mm/s, measured at 280 nm by UHPLC.....	143
Table 22: Drug content of printed ibuprofen alone and premixed with PVP as 5 layer x 0.9 mm ² circle depositions, generated using a 300µm nozzle at 3 mm/s, measured at 214 nm by UHPLC.....	144
Table 23: The effect of concentration of polymer used to prepare spin coated samples on the contact angle measured at point zero.....	173
Table 24: Average contact angle for each type of printed sample taken at point zero from lowest to highest polymer content.....	178
Table 25: Average contact angle values obtained for printed ibuprofen and ibuprofen:PVP printed mixtures.....	185
Table 26: Fenofibrate formulations to achieve pulsatile release.....	190
Table 27: Ibuprofen formulations to achieve pulsatile release.....	197
Table 28: Full Size Tablet Design.....	203
Table 29: Drug content of full size tablet components.....	237
A2.1: Examples of percentage success and failure of printing using the aerosol jet, based on the number of samples discarded.....	297

Chapter 1: Introduction

1.1 Background

1.1.1 Dosage Forms

In the broadest sense, dosage forms can be considered the means by which an active pharmaceutical ingredient is administered. These systems aim to ensure the drug reaches its site of action at the required dose, within the appropriate therapeutic index and produces a therapeutic response (Panakanti and Narang 2015). Drug delivery systems can take a number of forms such as parenteral, topical, ocular, transdermal and oral. The latter is of particular interest to the current study

1.1.2 Oral Solid Dosage Forms

1.1.2.1 Basics of Oral Drug Delivery

Currently oral drug delivery is the preferred method of administration of medication for many conditions as it allows patients to self-administer and when administered correctly allows highly accurate dosing. From an economic point of view this is more beneficial than any other dosage form as it does not necessarily require any additional personnel to be present, as is often the case with some parenteral routes such as intravenous, subcutaneous, intramuscular or intraperitoneal administration. In terms of patient compliance, it is also much less invasive than other administration methods which does make it more favourable to some. This is particularly significant for paediatric patients, to whom the pain associated with parenteral administration can prove greater than most adult patients, and for elderly patients for whom finding a vein may prove more difficult resulting in higher risk of pain. It is said that approximately 90% of all drugs in existence can be used in an oral form and over 50% of dosage forms sold are oral drug formulations (Pavurala & Achenie 2013). There are a range of oral drug delivery systems available such as tablets, liquid formulations, hard and soft capsules, and particle systems. For oral drug delivery to be effective, it is necessary that the active pharmaceutical ingredient (API) reaches its site of action, and

that its formulation succeeds in generating the required pharmacokinetic profile and therefore gives rise to the anticipated pharmacodynamic effect (Mrsny, 2012). This means the drug, which may be aided by its manner of delivery, must interact effectively with the body on both a tissue and cellular level to achieve the required effect. Additionally, in order to achieve this the solid oral dosage form must facilitate dissolution in the gastrointestinal fluid to allow the drug to be in a state which is amenable to absorption.

Generally oral solid dosage forms consist of a mixture of API and excipients such as diluents, binders, disintegrants, glidants and lubricants. This blend should ideally result in an optimum flowability and distribution of all components to ensure successful compression, disintegration, wettability and dissolution. Conventionally a tablet consists of a powder blend. The powder blend defines these properties by governing hardness, porosity and friability. Production is highly controlled and monitored to ensure the quality of the dosage forms generated from these powders. Tablet manufacture conventionally takes the form of direct compression or granulation followed by compression. The former method is often favoured for large scale manufacturing as it remains the cheapest method of tablet manufacturing, however it is not suitable for all powder blends. The latter method is generally employed when the powders utilised produce poor flowability and/or fail to maintain a good distribution of components. The latter issue often results from differing particle sizes and densities resulting in some powders segregating within the blend. Granulation enables generation of particles featuring a mixture of the components achieving a more uniform particle size. Granulation can take multiple forms, most notably wet and dry granulation. Wet granulation involves the addition of liquid, generally water but ethanol or propanol may also be used, and the binding of particles by this means, before sieving. Wet granulation is sometimes unsuitable however as certain APIs are prone to aqueous hydrolysis or polymorphic changes through this process. Dry granulation by slugging or roller compaction is often employed as an alternative. Slugging and roller compaction can both be considered means of compaction, with the former resulting in a powder compact and the latter resulting in a sheet of agglomerated material, both of which can then be milled to give granules. However there is still a

risk of polymorph transformation associated with this as the powder is still exposed to mechanical stress, but the risk hydrolysis is removed (Andrews 2007, Leane et al. 2015). However not all drugs are perfectly suited to oral drug delivery and a number of issues can arise.

1.1.2.2 The Importance of the Biopharmaceutical Classification System

Drugs delivered orally can be categorised within the Biopharmaceutical Classification System by solubility and permeability. This is a method of characterising drugs which was originally suggested by Amidon et al. over twenty years ago to understand the relationship between dissolution, absorption and bioavailability of an orally administered drug (Amidon et al. 1995). It aims to classify drugs in terms of the rate limiting steps of dissolution in the body, including the initial drug release, preservation of the solubilised state of the drug while it is in the alimentary canal and finally the stage during which the drug is absorbed from the gastrointestinal tract (GIT) through the surrounding tissues into the blood (Vikaas and Arun 2012).

Solubility within the Biopharmaceutical Classification System is defined by the highest dose strength of a drug. As a broad rule, solubility can be considered as the mass of a material which dissolves in a particular volume of solvent at a particular temperature. An agent is categorised as having high solubility when the highest dose can dissolve in up to 250ml of a water-based solution. This volume is based on the recommended water intake with an oral dose. Studies should be carried out across a pH range of 1-7.5 at 37°C (body temperature) to allow examination of the drug's fate at all regions of the gastrointestinal tract, moving from the approximately neutral region of the mouth to the acidic region of the stomach to the increasingly less acidic region of the intestine. Solubility can be tested using a shake-flask or titration method. More recently it has been suggested the guidelines should be modified to testing solubility within a 500ml aqueous solution as this is more indicative of the fluid volume in a fasted gastrointestinal tract (Kawabata et al. 2011, Puranik et al. 2011).

Permeability within the Biopharmaceutical Classification System is defined by the rate of mass transfer of drug through the tissues lining the gastrointestinal tract into the blood and the amount of drug absorbed *in vivo*. Agents are said to have a high absorption capacity when 90% of the substance is absorbed based on pharmacokinetic analysis of blood samples (Puranik et al. 2011). *In vitro* studies can also be carried out on Caco-2 or MDCK cells or simulated tissues for prognosis of agent permeability from the gastrointestinal tract into the systemic circulation (Kawabata et al. 2011).

The Biopharmaceutical Classification System allows drug bioavailability prediction. When new drug moieties are introduced, solubility testing and *in vitro* transport studies are initially used to estimate the oral absorption of a drug *in vivo* (Buckley et al. 2013). Drugs must exhibit a good *in vivo/in vitro* correlation. This is defined as the formation of an effective association between a biological property or response induced by a drug in a living organism, and a physicochemical property, such as dissolution rate and extent, of the same drug outwith a living organism (Emami 2006). In order to accurately simulate *in vivo* conditions *in vitro*, the make-up, volume and hydrodynamics of the GIT fluid must be accurately mimicked. In the fasted state this can take the form of pH 1-3 simulated gastric fluid, pH 6.8 simulated intestinal fluid without enzymes and pH 5.4-6.5 FaSSIF within the USP method dissolution apparatus (Bou-Chacra et al. 2017). The fed state can be mimicked by carrying out dissolution testing in milk or pH 5-6.5 FeSSIF (Dressman and Reppas 2000, Bou-Chacra et al. 2017). However, *in vitro* testing cannot simulate all the parameters exhibited *in vivo*. For example, first pass metabolism via the hepatic portal vein leading to degradation of the drug cannot yet be simulated effectively (Tiwari et al. 2011). As a result, *in vivo* dissolution testing must be carried out in animal models with pharmacokinetic analysis of blood samples to interpret the drug concentrations present (Buckley et al. 2013). This process of testing can be highly useful as if carried out early it allows drugs with problems too severe or too costly to fix to be removed from study before too many resources are wasted (Puranik et al. 2011). The drugs are placed in one of four categories based on their solubility and permeability.

1.1.2.3 Oral Drug Classes of the Biopharmaceutical Classification System

Class I drugs are categorized as those with good solubility and permeability (Lindenberg et al. 2004). Class II drugs have poor solubility but good permeability (Kawabata et al. 2011). Class III drugs have good solubility but poor permeability. Class IV drugs fall in to the category of those with both poor permeability and poor solubility (Lindenberg et al. 2004, Puranik et al. 2011). Examples of each of the four categories can be observed in Table 1. Drugs with low solubility struggle or fail to dissolve in the gastrointestinal fluid and thus are poorly absorbed, as the undissolved drug is not in a suitable state for absorption to occur properly. Drugs with low permeability cannot be properly absorbed into the systemic circulation as, often due to low lipophilicity, they cannot transverse the gastrointestinal wall. This can result in poor bioavailability and reduced therapeutic effect possibility signified by breakthrough symptoms (Blagden et al. 2007). At present 40% of all drugs on the market fall into the category of either Class II or IV drugs (Roberts and Zhang 2013). Class II agents are a major area of interest in oral drug development in the current study as alone their activity is suppressed by their incapacity to dissolve in the gastrointestinal fluid but, unlike Class IV agents, their permeability allows them to be absorbed effectively if they are effectively solubilised by formulation (Sant et al. 2004).

Table 1: Classification of a number of drugs via the Biopharmaceutical classification System (Lindenberg et al. 2004, Golovenko and Borisyuk 2008, Puranik et al. 2011, Lennernäs 2014)

	Highly Soluble		Poorly Soluble	
Highly Permeable	Class I		Class II	
	Drug	Use/ Pharmacology	Drug	Use/ Pharmacology
	Chloroquine	Antimalarial agent	Carbamazepine	Antiepileptic agent
	Digoxin		Griseofulvin	

	Paracetamol	Cardiac glycoside	Hydrocortisone	Antifungal agent
	Salbutamol	Analgesic agent	Nifedipine	Cortisol Replacement Therapy
		β -blocker, bronchodilator		Calcium channel blocker
Poorly Permeable	Class III		Class IV	
	Drug	Use/ Pharmacology	Drug	Use/ Pharmacology
	Abacavir	Antiretroviral agent	Hydrochlorothiazide	Thiazide diuretic
	Atenolol	β -blocker	Ritonavir	Antiretroviral agent
	Metformin	Hypoglycaemic agent	Talinolol	β -blocker
	Ranitidine	H ₂ -antagonist	Paclitaxel	Anticancer agent

1.2 Class II drugs

Class II drugs have been estimated to make up 17% of the official WHO list of essential medicines (Lindenberg et al. 2004). These active pharmaceutical ingredients include well used substances such as griseofulvin, digoxin, phenytoin, carbamazepine, trimethoprim, dapsone, ibuprofen, nifedipine, nitrofurantoin, sulfamethoxazole and hydrocortisone (Leuner and Dressman 2000, Lindenberg et al. 2004). Unfortunately, the problem is also on the rise as it is estimated in recent years 70% of APIs in

development have exhibited poor aqueous dissolution (Ku and Dulin 2012). This is believed by some to be partly due to the growing number of complex synthetic compounds being manufactured, however as many synthetic compounds have been produced without this problem the source of the issue is debatable (Kawakami 2012).

Class II drugs have a rate limiting dissolution step which means absorption does not occur as fully or sometimes as rapidly as Class I drugs (Vikaas and Arun 2012). Class II drugs can result in a range of issues in drug delivery due to their failure to dissolve properly. If the drug cannot dissolve efficiently or fully, the mass entering the systemic circulation is reduced and the rate at which it is absorbed can fluctuate leading to poor bioavailability (Blagden et al. 2007). However, once their dissolution has been improved, Class II drugs do generally have an *in vitro/in vivo* correlation which is comparable to Class I drugs, which as a whole generally have the best correlations and overall performance of all the drug types (Vikaas and Arun 2012). This suggests that solubility and absorption exhibited *in vitro* is more likely to be comparable to that observed *in vivo*. Thus there is a great deal of interest in increasing the bioavailability of these drugs as if the solubility is increased without compromising the pharmacodynamics of the agent, they can exhibit a level of permeability comparable to that of Class I drugs (Puranik et al. 2011, Buckley et al. 2013).

1.3 Methods of Improving Solubility of Class II Drugs

Even a small increase in solubility of an API can make an impact on increasing bioavailability by increasing the overall dissolution rate. A number of physiochemical factors influence the dissolution rate such as the agitation applied, the surface area, the diffusion coefficient, the saturation solubility, the mass of agent to be dissolved and the volume of liquid available for dissolution (Kawabata et al. 2011). The overall solubility of a drug can be increased via changes to the crystal structure, molecular modification and formulation. As the current study focuses on the work of CMAC, batch methods will be detailed briefly but latterly the methods given will be primarily continuous.

1.3.1 Conventional Methods to Improve the Solubility of Class II Drugs

1.3.1.1 Solid State Modification

1.3.1.1.1 Salt Formation

Salt formation can be used to increase dissolution as the ionised form of the drug is often more soluble. Salts can be formed by the movement of protons from an acid to a base and a stable ionic bond can be established if the variation between the pKa values of an acid and a base is over 3. The salt counter ions alter the pH at the surface of the salt particle, leading to a greater solubility than the original molecule (Kawabata et al. 2011). For example, celecoxib, an acidic agent with poor aqueous solubility, exhibited an increased dissolution rate and oral bioavailability when formulated as a sodium salt, in comparison to the unionised molecule (Guzman et al. 2007). In another example, Skořepová et al. demonstrated the ability of salt formation to increase the solubility of agomelatine. On formation of salts with hydrogen sulphate, mesylate and besylate, 3.2-fold, 51.43-fold and 200-fold increases in intrinsic dissolution rate respectively were observed relative to the drug alone (Skořepová et al. 2017).

1.3.1.1.2 Polymorphism

Polymorphism can also be utilised to increase dissolution. Polymorphism is defined as the ability of a substance to exist in a number of forms (Fabbiani and Pulham 2006). This generally refers to substances with identical chemical composition but dissimilar lattice structures and/or molecular shapes. This ability is found very prominently in the field of pharmaceuticals. Each polymorphic form of a substance exhibits different physiochemical properties, including melting point, density, solubility and stability. As a general rule, the metastable polymorphic form has a kinetically higher solubility than the polymorphic form with greater thermodynamic stability. However, polymorphism is limited as the metastable form often reverts back into the more thermodynamically stable form (Kawabata et al. 2011). An example of increasing the dissolution of a poorly soluble drug in this manner is oxytetracycline as the metastable form of the drug exhibited 95% dissolution compared to only 55% dissolution

exhibited by the thermodynamically more stable form in a previous study (Savjani et al. 2012). Another more prominent example is the polymorphism of paracetamol as the metastable form II of this drug was established to have a greater dissolution capacity and to be more compactable than the thermodynamically more stable form I. This is as a result of form II's more layered structure (Thomas et al. 2011).

1.3.1.1.3 Amorphous Material Formation: Solid dispersions

Polymorphism can also exist as the transition of crystalline drugs into the amorphous state. Amorphous forms of drugs also possess higher solubility than their crystalline forms. The solubility can increase on generating the amorphous form by 1.1 to 1000 times. Solid dispersion techniques can be used to generate a stable amorphous form of the drug within a formulation by encapsulating the drug particles within a polymer matrix to stabilise this disordered state. The formation of amorphous material is highly desirable to increase solubility as breaking down the lattice energy of the crystalline form results in a higher entropy, enthalpy and free energy, and thus a higher dissolution capability (Baghel et al. 2016). This typically occurs when the drug loading is considered to be lower than the equilibrium solubility of the drug in the stabilising material, creating a thermodynamically stable homogenous solution (Huang and Dai 2014).

Solid dispersions can be considered to be a collection of formulation methods which are made up of two or more materials, which normally include a water soluble matrix and a poorly soluble drug (Figure 1). Solid dispersions can be formulated by spray drying, melt extrusion, lyophilisation and by utilising supercritical fluids with polymeric transporters and/or surfactant (Kawabata et al. 2011). An example of amorphous material formation was shown in a study investigating a poorly soluble VR1 antagonist in solid dispersions of hydroxypropyl methylcellulose acetate succinate (Kennedy et al. 2008). Largely these systems utilise polymers such as polyvinylpyrrolidone (PVP) and polyethylene glycols (PEG), however surfactants such as Tween-80, docusate sodium and sodium lauryl sulphate or other excipients

such as cyclodextrin may also be included (Moribe et al. 2012, Savjani et al. 2012). These have the advantage of smaller particle size, better wettability and higher porosity which all provide a greater surface area for dissolution to occur (Vasconcelos et al. 2007) There are a number of methods for generating solid dispersions including hot-melt methods, solvent evaporation, nanosuspension, media milling, high pressure homogenization, supercritical fluid process, inclusion complex formulation based techniques, kneading, micellar solubilisation, hydrotrophy, crystal engineering and cryogenic techniques (Savjani et al. 2012).

Examples of improving dissolution in this manner include a previous study involving spray drying of probucol and PVP K30 increased the dissolution relative to the drug alone by more than 6-fold (Thybo et al. 2008). Another study demonstrated the effect of thin film freezing of fenofibrate with HPMC E5 resulting in an increase from 40% release on physical mixing to 100% release on formation of amorphous FNF-HPMC E5. Additionally, film freezing with HPMCAS resulted in an increase from 60% release on physical mixing to 100% release on formation of amorphous FNF-HPMCAS (Zhang et al. 2012). A further study demonstrated solvent evaporation of ethanol, carbamazepine, Neusilin UFL2 and Kollidon VA64 resulting in an increase from 30% drug release from the drug alone to up to 70% release from the solid dispersions (Vojinović et al. 2018). Additionally, a previous study demonstrated co-milling of ibuprofen and microcrystalline cellulose resulting in an increase from about 60-70% release to about 100% release after 20 minutes of milling (Varghese and Ghoroi 2017). Hot-melt techniques will be discussed later in this chapter.

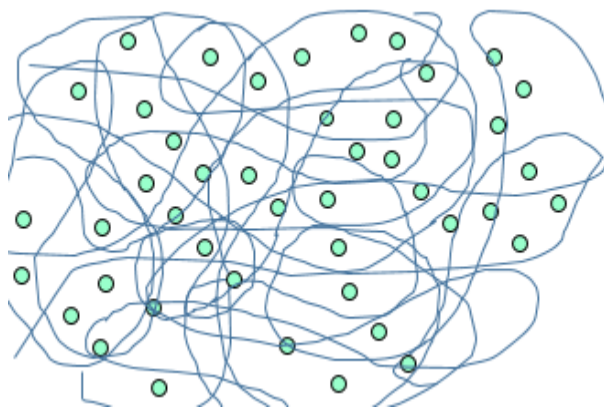


Figure 1: Structure of an ideal solid dispersion with the drug (green) evenly distributed throughout the polymer (blue chains) (Huang and Dai, 2014).

1.3.1.1.4 Co-crystallisation

Co-crystal formation is another method of increasing dissolution capability. Co-crystals can be defined as substances consisting of two or more different constituents within the same crystal lattice tied to each other by non-covalent interactions (Blagden et al. 2007, Kawabata et al. 2011). In the case of drug-based co-crystals they tend to consist of the drug plus another molecule, for example an inert excipient (Kawabata et al. 2011). Co-crystallisation is particularly useful as it can improve the physicochemical properties of a drug without altering its chemical characteristics or pharmacological activity (Yadav and Yadav 2009, Aakeröy et al. 2011). Previous evidence of using co-crystals to improve solubility was exemplified using glutamic acid to improve dissolution of a poorly soluble API by 8-fold (McNamara et al. 2006), and using saccharin to improve dissolution of indomethacin with the time to reach 100% dissolution rate decreasing by 9-fold on co-crystallisation (Jung et al. 2010). More recently, Pan et al. employed oxalic acid to improve dissolution of azelnidipine by a third (Pan et al. 2017).

1.3.1.2 Prodrug Formation

Prodrugs have also been used to great effect in previous research into improving solubility. A prodrug is defined as a virtually or entirely pharmacologically inactive

precursor which releases the active drug on hydrolysis, oxidation, reduction or enzymatic degradation (Testa 2004). One major way of achieving greater solubility is to create prodrugs with higher polarity than the drug alone. Water and water-soluble drugs can be considered to be polar due to their ability to form dipoles and the latter can dissolve in the former due to their shared character. The solubility of class II drugs is low due to the fact they possess a higher number of non-polar groups, as is often exhibited by organic molecules as the electronegativity of the carbons and hydrogens is very alike. This causes the overall character of the molecule to be non-polar and thus more hydrophobic than hydrophilic. They are therefore less likely to dissolve in water due to the fact the polar and non-polar groups cannot interact. Thus, the addition of polar groups to the structure can be used to increase the overall polarity of the molecule and therefore its solubility (Rasenack and Müller 2005). An example of this is the agent sulindac which can be solubilised to sulfoxide and then converted back to sulindac to achieve effective anti-inflammatory activity (Stella and Nti-Addae 2007).

Prodrugs can also take the form of carrier-linked prodrugs, where the drug is released from a carrier molecule, bioprecursors, which behave similarly to carrier-linked prodrugs but lack a promoiety, and macromolecular prodrugs, which consist of a macromolecule like PEG bound to the drug. Amino acid derivatives of dapsone, such as glycyl, alanyl, leucyl and lysyl dapsone, were effectively used to as prodrugs with a higher solubility than the drug alone, however the most useful precursor was found to be lysyl dapsone with a solubility value of over 460-fold higher than the drug alone in pH7.4 phosphate buffer (Testa 2004). Phosphate esters can be used as prodrugs to improve the solubility of poorly soluble agents via their dianionic phosphate group and can be transformed into the active drug via enzymatically cleavage of the phosphate group by alkaline phosphatases. This has been used to great effect on the drugs fosamprenavir, prednisolone and fludarabine (Rautio et al. 2008).

1.3.1.3 Cyclodextrin Complexes

The complexation of a drug with cyclodextrins can also increase the overall solubility of the formulation. Cyclodextrins are cyclic oligomers of glucose which in their pure and derivative forms can alter the physicochemical characteristics of the drug thus increasing dissolution capacity. Unlike some excipients cyclodextrins also have no interactions with the GIT tissue and thus allow the drug to be effectively taken up into the systemic circulation but are not taken up with it, reducing the change of toxicity development (Balint 2001)

1.3.1.4 Drug Delivery Methods

1.3.1.4.1 Lipid Systems

Lipid drug delivery systems, although generally used to increase permeability, can also be used for oral administration of poorly soluble drugs. Phospholipids have amphiphilic properties which lead to them forming micelles or lipid bilayers with the hydrophobic regions surrounded by the hydrophilic regions of the molecule. The hydrophobic regions can be used to encase poorly soluble drugs, while the system evokes an overall solubility higher than the drug itself. Lipid drug delivery systems can affect the uptake of the drug by altering processes and issues such as the release of the drug by controlling its dissolution rate, increasing bioavailability, inducing the lymphatic transport of drugs and reducing toxicity. Phospholipids can also safeguard drugs from breaking down before reaching their target. Phospholipids applied to oral drug delivery include soybean phosphatidylcholine, egg phosphatidylcholine, synthetic lecithin/ phosphatidylcholine and hydrogenated phosphatidylcholine. Phospholipids can form emulsions, in which one liquid is present in another liquid but not miscible and thus forms droplets. They can consist of either an oil in water or water in oil model. A previous study exemplified the use of phospholipids by studying the effect of using phospholipid 1,2-dimyristoyl-sn-glycero-3-phosphatidylcholine with PEG to solubilise piroxicam (Prabhu et al. 2005).

Lipids can also be applied as part of micro and nanoemulsions. They generally are created by high-pressure homogenization resulting in droplets of the non-miscible substance or between 50 and 500 nm. Poorly soluble drugs which can be delivered within nanoemulsions or microemulsions include griseofulvin and cyclosporin A. The latter can also form self-emulsifying drug delivery systems (SEDDS). SEDDS consist of blends of oil and surfactants, which emulsify in the presence of moderate agitation in the form of the muscle contractions of the gastrointestinal tract. Solid lipid nanoparticles are also an option for drug delivery using phospholipids. They consist of melt-emulsified lipids which are solid at 25°C. Poorly soluble drugs which can be carried by these include nifedipine, celecoxib and camptothecin (Fricker et al. 2010, Song et al. 2014). It is also possible to generate self nano-emulsifying drug delivery systems (SNEDDS), which are made up of lipids, surfactants and co-solvents. For example, SNEDDS were created using amiodarone and talinolol with Tween 20, Span 80, Cremophor RH40 and lecithin and showed enhanced solubility for both drugs, while reducing the effects of metabolism (Elgart et al. 2013). Likewise, it is also possible to produce self micro-emulsifying drug delivery systems (SMEDDS) as exemplified by a formulation of cyclosporine A in a soft gelatine capsule created by Novartis and a hard gelatine capsule generated by Abbott Laboratories (Prachi et al. 2012).

1.3.1.4.2 Polymer Systems

Poorly soluble drugs can also be solubilised for use orally through arrangement of polymers and agents within formulations with a range of conformations including reservoir, microparticulate, nanoparticulate, micellular and polymer-drug conjugate forms.

1.3.4.2.1 *Polymer Drug Conjugates*

Polymer-drug conjugates can be used to deliver poorly soluble drugs efficiently. In general, the conjugated form is a prodrug which can be converted to the active form of the drug when subjected to acid/base hydrolysis or enzyme cleavage (Kim et al. 2009). The drug can be attached to the polymeric backbone with or without a linker (Figure 2). The polymeric mainchain is vital in determining the pharmacokinetics and pharmacodynamics of the drug and therefore is involved in solubilising the poorly soluble drug utilising its own hydrophilic properties (Markovsky et al. 2012). An example of this is the formation of conjugates of atorvastatin, ketoconazole or Itraconazole with chitosan via hydrogen bonding (Al-Hilal et al. 2013)

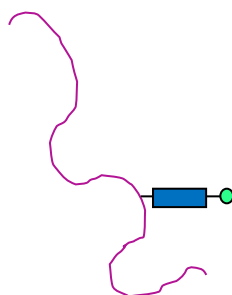


Figure 2: Basic structure of a polymer-drug conjugate made up of a polymer backbone (purple), a linker group (blue) and a drug molecule (green).

1.3.4.2.2 *Polymeric Nano and Microparticles*

Polymeric nanoparticles and microparticles (Figure 3) can also be utilised to greatly improve solubility of drugs. This ability can be particularly associated with the larger surface area generated by their smaller particle size (Lee et al. 2010, Kumar et al. 2011). The drug can either be distributed throughout the polymer during manufacture of the particles themselves by mixing or used to coat the outside of the particle using a concentrated solution of API latterly (Agnihotri et al. 2004). Nanoparticles are largely described as systems between 200-300 nm in size, and this can be changed to affect the overall drug release rate and thus the time period for drug delivery (Cho et al. 2008). Nanoparticles can be categorised as nanocapsules and nanospheres. The former are conformationally similar to vesicles and are made up of a polymer membrane which surrounds a central cavity where the drug is held. In the latter the

drug is dispersed throughout a polymer matrix. As such the release pattern from these two system types can be quite different (Soppimath et al. 2001). In the case of poorly soluble drugs, the nanoparticle must have an overall hydrophilic character which can be used to impart solubility on the drug and enable the drug to be carried effectively. This can be accomplished using a water-soluble coating, with a polymer such as polyethylene glycol or dextran, or by utilising block copolymers with a mixture of poorly soluble and highly soluble characteristics, with the latter imparting the overall effect. There are a number of examples of nanoparticle dosage forms such as polyglycolic acid (PGA) nanoparticles with camptothecin, and Celecoxib nanoparticles with ethyl cellulose, sodium caseinate and bile salts (Cho et al. 2008, Morgen et al. 2012).

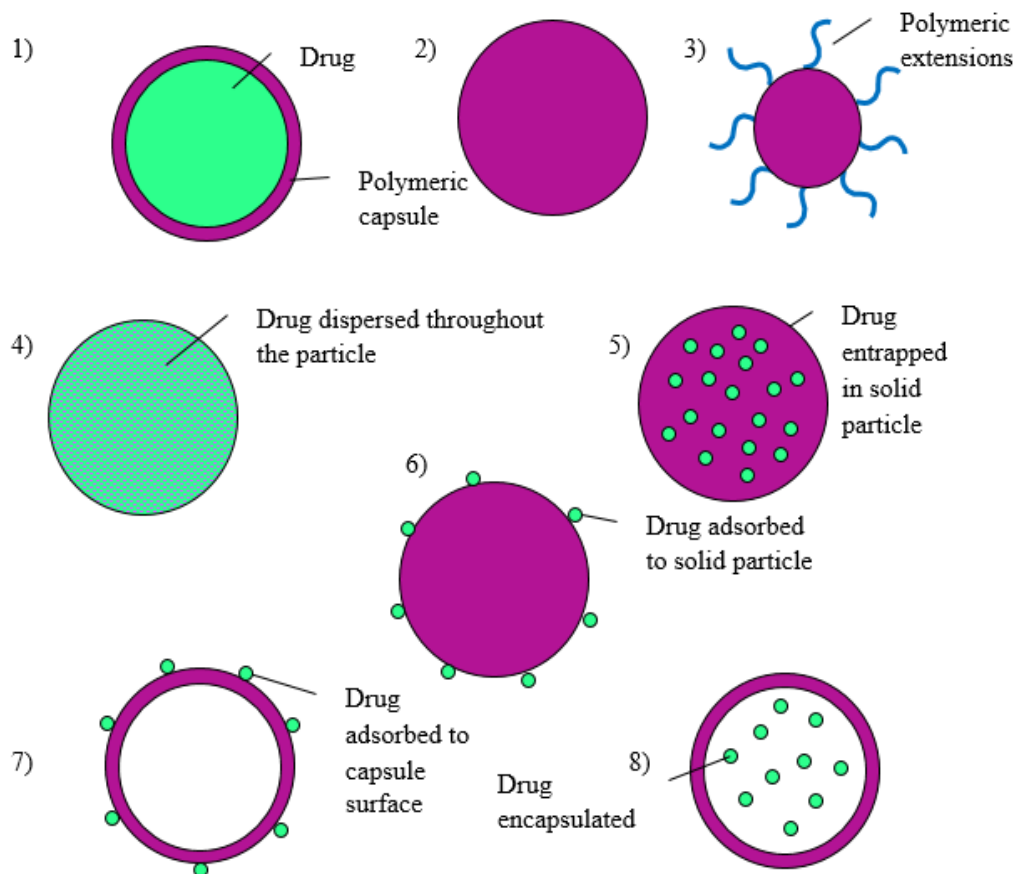


Figure 3: Micro and nanoparticle structures: 1) capsule, 2) solid particle, 3) solid particle with polymeric extensions, 4) solid particle with the drug dispersed, 5) solid particle entrapping a drug, 6) solid particle with the drug adsorbed to the surface, 7) capsule with the drug adsorbed to the surface and 8) capsule with a drug containing core

Microparticles generally are slightly larger than nanoparticles with a particle size typically ranging between 0.1 and 200 μm (Satheesh Madhav and Kala 2011). Microcapsules have a conformation which is comparable to nanocapsules. However, unlike nanoparticles they can exhibit either one central hollow (monocored microcapsules) or multiple hollows within their structure (polycored microcapsules). The polymeric layer also has the capacity for drug loading, giving rise to matrix type polymeric microcapsules. Microspheres are very conformationally similar to nanospheres in that the drug is dispersed throughout a polymer matrix. Like the nanoparticles, microcapsules and microspheres can exhibit different release patterns due to their different structures and the way the drug is held within the system (Kumar et al. 2011). Microparticles have effectively been applied to the delivery of poorly soluble drugs such as paclitaxel, aclacinomycin, Carvedilol and camptothecin (Takale et al. 2012, Zhang et al. 2013).

1.3.4.2.3 *Polymeric Micelles*

Polymeric micelles are another system suitable for delivery of poorly soluble drugs. A typical micelle consists of an external hydrophilic layer, encapsulating a drug and excipient containing hydrophobic core, which is particularly useful for carrying class II drugs (Figure 4) (Kim et al. 2009, 2011). Micelles are generally made up of many amphiphilic molecules grouped together to form aggregates at what is known as the critical micelle concentration. They have a nearly entirely spherical configuration in which the hydrophobic regions of the amphiphilic molecules are found to form a central cavity, which is capable of increasing the aqueous solubility of hydrophobic drugs (Torchilin 2011). Polymers with good aqueous solubility, such as polyethylene glycol, are utilised within the external membrane of the micelle, while more lipophilic polymers, including those made up of propylene oxide, aspartic acid and spermine monomers, are used within the hydrophobic core of the micelle (Torchilin 2004). A number of polymers have been used to generate self-assembled micelles. Most of these are linear block copolymers and have main chains made up of hydrophilic polymers such as polyethylene glycol, poly(N-vinyl-2-pyrrolidone) and poly(vinyl

alcohol), with hydrophobic regions made up of polymers such as polyester and poly(amino acid)s (Guo et al. 2012). An example of micellation of poorly soluble drugs was given in a previous study where the solubility of chemotherapeutic agent paclitaxel was increased by combining the drug with poly(2-(4-(vinylbenzyloxy)-N,N diethylnicotinamide) and polyethylene glycol block copolymers in micelles (Huh et al. 2005).

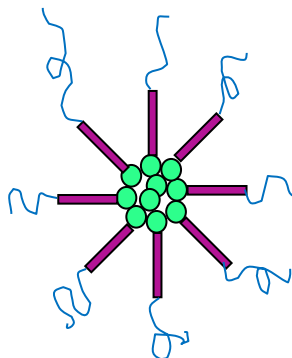


Figure 4: Basic structure of micelles: The drug (green) is entrapped by hydrophobic blocks (purple), which is in turn entrapped by hydrophilic blocks (blue).

1.3.4.2.4 Reservoir-based systems

Reservoir based systems are a commonly utilised polymeric dosage form. Within this type of system, the drug is entrapped by a polymer film which acts as a barrier layer (Yang and Pierstorff 2012). Although generally used within injectables or implants, there is recent research for the use of this system orally. Alza Corporation developed an osmotic reservoir system suitable for oral use called OROS®, consisting of a soft gelatine capsule, surrounded by a barrier layer, an osmotic push layer and finally a rigid semi-permeable membrane with a 0.5-1.4mm laser-drilled hole. After the capsule has been swallowed by the patient, the gastrointestinal fluid permeates through the membrane into a central reservoir containing the drug and this forces this agent out of the laser-drilled hole as the osmotically active polymer push layer swells (Stevenson et al. 2012).

1.3.4.2.5 Solvent-activated systems

Solvent-activated systems can be categorised into osmotically controlled systems and swelling controlled systems (Figure 5). Osmotically controlled systems are characterised by the fact release is induced by the movement of the gastrointestinal fluid from an area of low drug concentration outside the drug carrier to a high drug concentration inside the carrier. The pressure of the fluid accumulation within the system forces the drug out of a hole in the tablet or capsule surface (Khandare and Haag, 2010). Recently a carvedilol nanosuspension was packaged into an osmotic pump capsule to increase its solubility and was observed to be a favourable new method of delivery of hydrophobic drugs (Liu et al. 2014). Swelling-controlled systems are characterised by the fact the polymer draws in gastrointestinal fluid from the surrounding environment, causing the whole system to become turgid. The swollen layer becomes more permeable which allows the drug to be gradually released into the surrounding fluid (Lao et al. 2008).

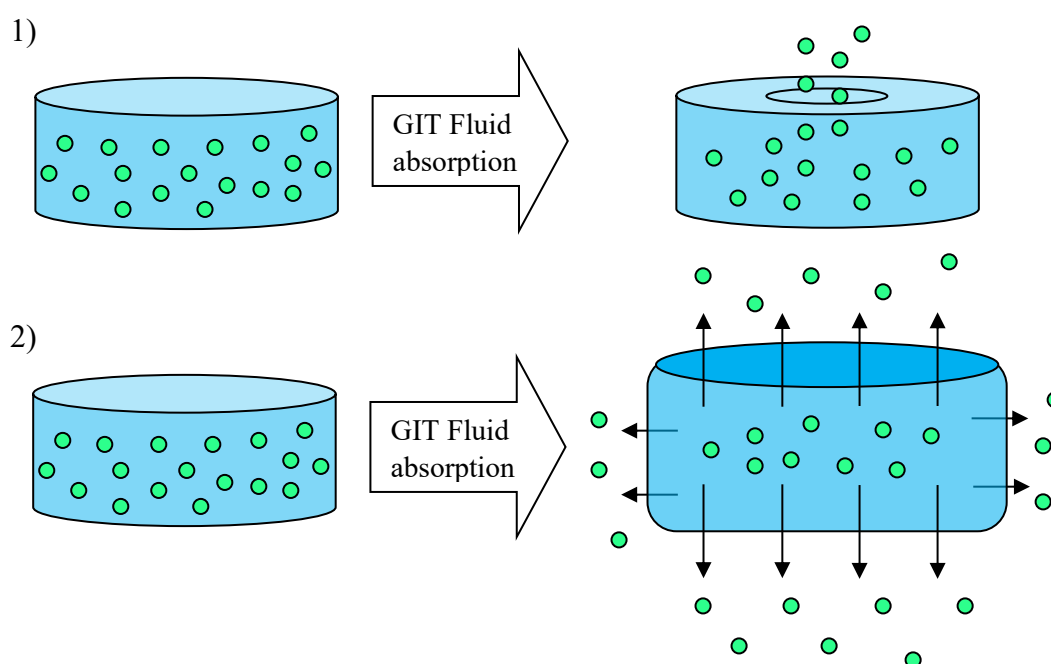


Figure 5: Solvent Activated Systems: 1) Osmotically-controlled and 2) Swelling-controlled models (Adapted from Khandare and Haag, 2010; Lao et al., 2008).

1.3.4.2.6 Chemically Controlled systems

Chemically controlled systems can be divided into “pendant-chain” and biodegradable systems (Figure 6). In “pendant-chain” systems the agent is chemically connected to the polymer mainchain and the API is released by chemical hydrolysis or enzyme degradation of the system. In biodegradable systems, the agent is evenly dispersed throughout the polymer mass and as this mass degrades via erosion the drug is released at a constant rate in a controlled manner. This particular type of system is highly efficient as it degrades in the gastrointestinal fluid, does not need to be eradicated from the body due to a risk of toxicity and has been observed to be effective in delivering poorly soluble drugs (Ranade and Hollinger, 2004).

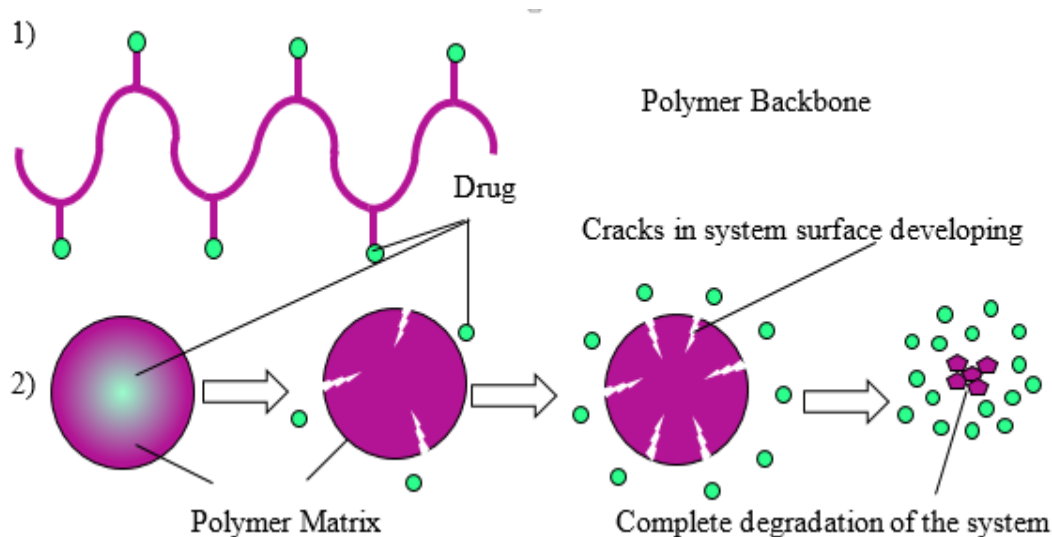


Figure 6: Chemically Controlled Systems: 1) Pendant chain systems and 2) Biodegradable systems (Ranade and Hollinger, 2004).

Although many of the techniques discussed in the current section are batch processes, formulations with enhanced dissolution capabilities can also be generated in a continuous manner with a view to increasing efficiency of production.

1.3.5 Continuous Manufacture of Oral Drug Delivery Systems to Improve the Solubility of Class II Drugs: Basic Concepts of and Reasons for Continuous Manufacture

It is believed by many scientists that continuous manufacture is the future of pharmaceutical production as it is believed to have great potential for reducing the expense of these processes as well as enhancing the quality and yield of the pharmaceuticals produced (Schaber et al. 2011).

Batch processing has long been used in the field of pharmaceuticals. It has the advantage of allowing small scale production and ease of variation in the presence of problems. However, there are a number of issues which exist with standard batch processing in pharmaceutical manufacture. Batch processing can potentially take much longer than continuous methods to produce usable dosage forms as the materials have to be transported. Additionally, intermediate and end product analysis can take a long time. All of this leads to sizeable and costly inventories, as well as loss of product should the end product testing identify any issues necessitating disposal of the batch. Continuous processes on the other hand enables a more rapid reaction to any issues, allowing inventories which are less sizeable, leading to reduced need for personnel and lower overall costs (Mascia et al. 2013). Batch manufacturing also is not as suitable for scale up as continuous manufacturing processes as many batch methods utilise agitated containers such as stir tank vessels. These are difficult to scale up because there is less guarantee of consistency throughout the batch as the velocity within a single vessel can vary considerably resulting in different heat, momentum and mass transfer levels, and thus inconsistent temperature and distribution of substances throughout the batch. This leads to a poorer quality end product. It is also challenging to generate a consistent product over several batches, leading to poorer quality overall than can be achieved with a continuous set up. By-products generated can also result in adverse events *in vivo* if undetected and extracted from the formulation. However the conditions and consistency of continuous manufacture are much easier to control, and thus a better quality product can be produced (Plumb 2005).

Previously manufacture has relied on batch processes as regulations demanded that all procedures were carried out in an identical manner for the period of the particular formulation's use. It was also previously favoured because quality control can be carried out on each batch or manufacturing stage before beginning another one. However, it is now growing more challenging for industry to achieve the required profit margin as a result of greater research and development expenditure and opposition in the market from companies producing generics. For large scale manufacture, continuous manufacture proves more profitable as overall manufacturing expenses are less, enhanced by less wastage of valuable substances, any reusable excess is recycled, and lower labour costs as less cleaning, quality control checks and movement of materials is required for continuous manufacture than standard batch procedures (Schaber et al. 2011, Giridhar et al. 2014).

Continuous processes are not an entirely new concept in the scientific world, as continuous flow stirred reactors have been in existence for a number of years with large scale chemical production of simple synthetic organic compounds such as ethylene dichloride and methanol being carried out previously. However, it is still a relatively small field compared with manufacture as a whole (Calabrese and Pissavini 2011). However, companies are becoming interested in continuous manufacture with a view to increasing efficacy, safety, reliability and sustainability of manufacturing procedures (Cervera-Padrell et al. 2012), and over the last fifteen years it has slowly began to replace some standard batch processes for pharmaceutical product manufacture (Giridhar et al. 2014). The introduction of process analytical technology (PAT) was a major step forward in the use of continuous manufacture in the pharmaceutical industry as it allowed processes such as crystallisation, blending, drying, distillation and granulation to be monitored, allowing contamination detection, feedback control, end point establishment and quality assurance (Giridhar et al. 2014).

Continuous manufacturing can occur throughout the pharmaceutical pipeline, but the stages of production are generally divided into primary and secondary manufacture (Figure 7). The former is a collection of processes by which the drug is produced either by chemical synthesis or extraction from biological sources, and then undergoes a number of stages of physical treatments including drying, purification and micronisation. The drug is then transferred to secondary manufacture in which the drug is made into its end product dosage form by combining it with various excipient molecules, such as glidants, disintegrants, diluents, binders and lubricants, within a formulation to improve delivery to the active site *in vivo*. The formulation might be subjected to further treatments during this process including drying, micronisation, size amplification and filtration. The drug mixture is then packaged as its final administration form suitable for human consumption (Plumb 2005). The current study is focused on the latter stage of manufacturing which may be carried out by a number of continuous manufacturing processes.

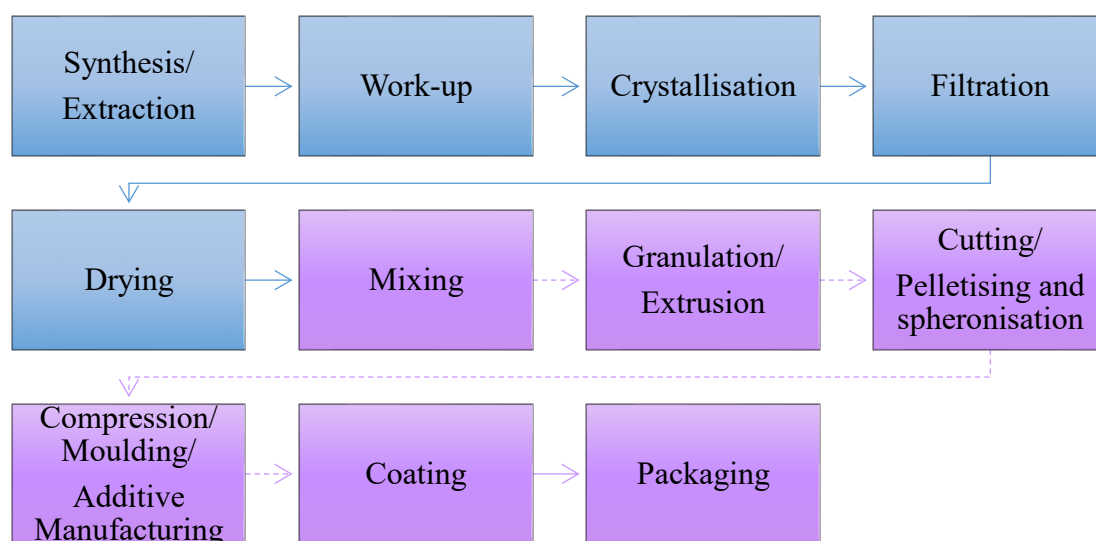


Figure 7: The Continuous Pharmaceutical Pipeline with primary steps shown in blue and secondary steps shown in purple. Dashed lines denote optional steps to indicate the possibility of the use of direct compression, or tablet production without compression or coating (for example by 3D-printing).

1.3.6 Methods for Continuous Manufacture of Oral Drug Delivery Systems for Class II Drugs

There are a number of possible methods to increase the solubility of class II drugs via innovative manufacturing processes.

1.3.6.2 Hot Melt Extrusion

Hot melt extrusion (Figure 8) is a possible method of secondary manufacture which may be utilised to increase the solubility of class II drugs. It was originally introduced by the plastics industry, although it was not used in the pharmaceutical industry until polymers such as PVP and PEG came into use. Hot melt extrusion utilises thermoplastic polymers to produce a range of different drug delivery systems, such as granules, pellets and tablets, while circumventing issues of drug instability, flammable solvents and lengthy drying processes, thus decreasing the overall time taken to manufacture a dosage form. On a simple level it generates a product with a consistent density and conformation by compressing, mixing and transforming a powder blend. An extruder can contain a single or twin screw system within a barrel, with the latter having co-rotating screws (Figure 8). The barrel has three sections known as the feed region, the compression region and the metering region, which all apply their own level of pressure on the mixture as it is heated, due to the fact they have varying depths which decreases in order of region to increase the pressure. The feed region allows moderate blending, the compression region allows greater blending and compression to melt and bring together the components of the blend, and the meter region controls the viscosity of the blend using high pressure to make it constant throughout the product. Hot melt extrusion offers a number of benefits over other methods to produce oral formulations. It is more stable than typical wet granulation techniques as it does not require any additional fluid to be added to the blend. The product extracted from the extruder can often be cut into tablets or pellets without further processing reducing the risk of degrading the drug with over handling (Andrews 2007). It was demonstrated in a previous study that melt extrusion can effectively be used to continuously produce a formulation to increase the solubility of indomethacin using the polymer polyvinylpyrrolidone (PVP) (Forster, Hempenstall, Tucker, et al. 2001).

In another study the class II drug 3-methoxy-1,5-bis(4-methoxyphenyl)-1H-1,2,4-triazole was melt extruded within a polymer mixture of hydroxypropyl methylcellulose ether with PVP to increase its solubility due to hydrogen bonding between the agent and the carboxylic acid groups of the PVP (Shah et al. 2013). Another technique which may be utilised to increase solubility is injection moulding.

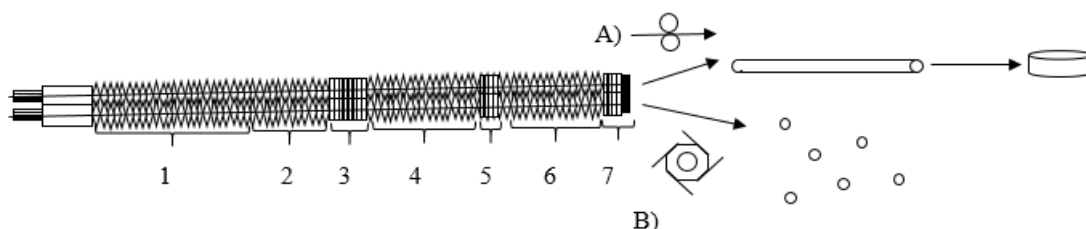


Figure 8: Twin-screw extrusion: Regions 1 to 7 above illustrate the feeding region (1), the transition zone (2), the mixing region (3), a transport region (4), a second mixing region (5), another transport region (6) and finally a die feeding region (7). In route (A) the product is squeezed through a die to form a rod or cable-like structure which can be cut to form tablets. In route (B) the product is spheronised to form pellets. (Leuner and Dressman 2000, Keleb et al. 2004).

1.3.6.3 Injection Moulding

Injection moulding is not an entirely new process as it has been used for many years within the plastics industry, but its use for formulation of drug delivery systems is a relatively recent notion. Within the field of formulation, it generally involves the application of high pressures and temperatures to polymers to cause them to melt. These molten polymers can then be injected into cold metal moulds and set hard in the required conformation. In continuous manufacture the resultant product can then be forced out of the mould in an automated fashion before the mould realigns with the injection portion of the device ready for the next sample. Various polymers, such as PVP and PEG, have been previously shown to form effective products using this method of production (Zema et al. 2012).

This method of dosage form production has a number of advantages. For example, it can be completely solvent free and thus should produce drug delivery systems safe for patient consumption. The high pressures and temperatures exerted on the dosage form decrease the chance of microbial growth, improving the quality of the overall product, reducing product rejection and reducing the risk of harm to the patient. It also promotes interactions between the drug and the excipients which help improve solubility (Quinten, Gonnissen, et al. 2009, Zema et al. 2012).

There is also evidence for integration of injection moulding into the continuous manufacturing pipeline. Extrusion followed by injection moulding to achieve a more uniform matrix dosage form has been demonstrated previously in a number of studies. For example, Quinten et al. effectively produced solid dispersion tablets in this manner using HPMC and sustained release tablets in this manner using Eudragit® (Quinten, Beer, et al. 2009, Quinten, Gonnissen, et al. 2009, Quinten et al. 2012). Bouman et al. also demonstrated this continuous process to produce caplets using zein protein by directly linking the outflow pipe of the extruder to the inflow point of the injection moulder (Bouman et al. 2015).

1.3.6.4 Additive Manufacturing

Additive manufacturing can be thought of as building a 3-dimensional construct from the bottom up and, unlike conventional manufacturing processes, has the flexibility to create almost any object which can be designed on a computer (Gao et al. 2015). It aims to achieve highly accurate customised production, and reduce wastage of materials by depositing material in a highly precise manner (Huang et al. 2013). One important application of this is personalised medicine.

1.3.6.4.1 Personalised Medicine

Personalised medicine can be thought of as different dosing frequency, drug release or overall dose required by different patients based on their individual physiology. The

aim of this is to increase the likelihood of the drug reaching its site of action and produce a response in a safe and effective manner (Alomari et al. 2015). Patient response to the same drug can vary hugely with some patients responding in the intended manner, some responding to a lesser degree, some exhibiting greater adverse effects and some failing to respond. This may come down to a number of factors such as physiology, genetics, gender, race and body mass (Hampton 2005, Xie and Frueh 2005, Hartman and Helft 2007, Lauschke and Ingelman-Sundberg 2016, Legato et al. 2016, Pickard 2017). Patient groups which are particularly suited to personalised medicine include paediatrics and the elderly (Alomari et al. 2015). Paediatric dosing can be challenging as individuals grow and change at varying rates. As such currently dosing is based on patient weight in kilograms and is perhaps not as flexible as required. Elderly patients may exhibit reduced metabolic activity and reduced patient compliance. As such personalised medicine is vital to ensure medications are taken in the necessary manner. Personalised medicine may be particularly important for drugs with narrow therapeutic indices as the margin for error with dosing is significantly less than drugs with wide therapeutic indices. Personalised medicine can be applied to poorly soluble drugs through a number of additive manufacturing techniques.

1.3.6.4.2 Fused-filament Fabrication

Fused-filament fabrication is a well utilised additive manufacturing technique which may be employed to increase the dissolution capability of poorly soluble drugs (Goyanes, Robles Martinez, et al. 2015). It builds on the standard extrusion process by re-melting the extruded cord and feeding it through a print head to allow assembly of the required dosage form design. This technique is still in its infancy but Goyanes et al., effectively showed its ability to solubilise fluorescein and also to form a range of conformations (Goyanes et al. 2014, Goyanes, Robles Martinez, et al. 2015).

1.3.6.4.3 Inkjet Printing

Inkjet printing is a highly innovative formulation technique which may be used to solubilise poorly soluble drugs (Scoutaris et al. 2011, Rajjada et al. 2013). Inkjet printing is generally employed for home and office use but in recent years it has been developed for use in dosage form production to allow rapid manufacturing. Inkjet printing may be considered to be a broad term for a number of methods for the digitally-controlled formation and placement of small liquid drops onto a surface (Daly et al. 2015). A liquid binder may be applied to a drug and excipient powder substrate in a liquid droplet form in a similar way to how ink is applied to paper. This droplet then allows the powder particles to adhere. Equally so the drug and excipient may be made into a suspension or another liquid formulation to use as “ink” (Yun, Kim, Lee, Cho, et al. 2009a, Daly et al. 2015). Polymers and other excipients can be inkjet printed to create dosage forms by either solid free form fabrication or layered manufacturing. This consists of manufacturing structures from the bottom up in a mould-less fashion by layering slices of material (Yun, Kim, Lee, Cho, et al. 2009a). This can be performed as layers of drug alone and excipient alone or layers of pre-prepared formulation (Wickström et al. 2015). It has also been previously demonstrated that inkjet printing can be used to generate polymer-based films. This can be achieved by printing on to acetate, from which they may be peeled off, or starch, which is integrated into the delivery system (Wang, 2013).

Inkjet printing allows a level of precision which many conventional formulation techniques cannot achieve. It may enable design of structures which can take the form of anything created using computer aided drawing software. As the droplets produced can be as tiny as nano or even pico-litres, very complex dosage forms may be created in this manner (Scoutaris et al. 2011). Precise control of the deposition pattern, size and distribution can enable highly effective control of the drug content and quality of a dosage form (Ursan et al. 2013, Vakili et al. 2015). By extension this may allow better control over drug release and overall performance. This type of technique may even allow us to predetermine the exact position of a drug within a final dosage form (Vakili et al. 2015). The choice of instrument can have a major effect on the degree

of precision achieved as the nozzle tip size, tubing diameter, pressure exerted on the system and maximum viscosity allowed by the particular system can all influence the amount of deposition achieved. Ink formulations are required to have a viscosity and surface tension which enables the ink to pass through the deposition head in a continuous fashion, flowing and adhering to the substrate in a reproducible, controlled manner (Genina et al. 2012, Ursan et al. 2013). The precise nature of this type of technique may allow highly accurate, scalable dosing with reduced wastage of material resulting in lower costs (Singh et al. 2010, Vakili et al. 2015). It can also be considered to be a contactless process and thus may result in less damage to the final product and perhaps a lower risk of contamination (Werner et al. 2013).

The final dose in the dosage form produced can be defined by the drug concentration in the ink, the computer aided design utilised and, the number of droplets and layers deposited on the substrate (Vakili et al. 2015). The latter of these factors is particularly significant. To generate a comparable dosage form to existing methods, using inkjet printing, layering is required as deposition cannot achieve as high a dose as compression can in one step (Genina et al. 2013). Layering inkjet depositions can also allow 3D printing via additive manufacturing. Inkjet printing has been suggested to hold advantages over moulding such as reduced wastage and, greater precision and intricacy (Lu, Zheng, et al. 2014). As such the drug content of a dosage form should be able to be controlled more easily, simply by changing patterns or the number of layers deposited (Wickström et al. 2015). As a result, inkjet printing holds a lot of potential for use in personalised medicine as the dose and rate of release should be able to be easily tailored to the individual requirements of the patient. In theory, due to the on-demand nature of these systems, prescriptions could be prepared from “ink” formulations in pharmacies in the future (Cheow et al. 2015).

From a solid state perspective, it has been suggested previously that inkjet printing may result in formation of amorphous material. Wickström et al. suggested that the amorphous form of indomethacin could be generated by inkjet printing, even in the absence of polymer, leading to greater overall solubility (Wickström et al. 2015).

Likewise greater solubility was generated by forming an amorphous form of felodipine in another study by Scoutaris et al. (Scoutaris et al. 2011). However, both studies concede a need for greater solid state investigation.

Inkjet printing can take the form of either continuous inkjet printing or drop on demand printing. The former consists of application of a continuous stream of fluid from a nozzle on to a surface. The surface tension causes the stream to form drops. Any excess is caught in a gutter and recirculated. The latter method of inkjet printing consists of injection of fluid on to the surface in a drop-wise fashion when required, as such the capacity of this technique is considerably less than that of the continuous method (Daly et al. 2015). Much of previous work investigating dosage form production in this manner has used standard inkjet printers but the current study utilises the innovative technique of aerosol jet printing.

1.3.2.3.3. Aerosol Jet Printing

Aerosol jet technology functions by passing pressurised nitrogen through ink to cause atomisation, forming small droplets which are then propelled through a virtual impactor, extracting any excess nitrogen to condense the stream before transversing the instrument tubing and then condensing further to form a usable stream at the print head. Aerosol jet printing can be thought of as a miniaturised version of spray drying as the use of volatile solvent in combination with atomisation results in formation of microdroplets followed by rapid drying of particles (King and Renn 2008, King 2014, Hyun et al. 2015).

Aerosol jet printing is a technique which has never been applied in pharmaceutical manufacturing previously. Much of the initial work with this particular type of printer has involved conductive silver ink in printed electronics (Shankar et al. 2011, Mahajan et al. 2013, Seifert, Baum, et al. 2015, Agarwala et al. 2017, 2018, Abt et al. 2018, Clifford et al. 2018, Elmogi et al. 2018). Previous use has also included production of ceramic aqueous suspensions for micropatterning (Holthaus et al. 2011).

Additionally, it has been used for metal inks for use in 3D chip interconnects (Seifert, Baum, et al. 2015, Lan et al. 2017), sensors on non-planar surfaces, antennae, solar cells and solder-free electronics (King and Renn 2008, Pavec et al. 2018), anode interlayers (Sukeshini A. et al. 2013), batteries, fuel cells, and supercapacitors (Deiner and Reitz 2017), metal grids for organic solar cells and light emitting diodes (Eckstein et al. 2014) and electrolyte-gated transistors (Hong, Kim, Kim, et al. 2014, Hong, Kim, Mahajan, et al. 2014). Furthermore, it has been used for printing polymer lines for organic light emitting diodes (Tait et al. 2015), polyimide (PI)/carbon nanotube (CNT) (Wang et al. 2016), graphene channels (Kim and Frisbie 2014, Pandhi et al. 2018), interconnects for photovoltaic modules (Fields et al. 2017), tin films (Fortier et al. 2017), carbon nanotube pH sensors (Goh et al. 2018) and polymer solar cells (Yang et al. 2011). This previous work has demonstrated a number of advantages of the technology.

This method holds significant benefits over standard inkjet printing techniques as it is contactless and thus eliminates the sweeping and tugging actions normal printers exhibit. It is hoped this will reduce the chance of accidental removal of the previous surface on the application of a new surface (Buanz et al. 2011). Unlike conventional inkjet printing it also dries more quickly allowing a fresh layer to be added more efficiently (Werner et al. 2013). It may also allow significantly narrower deposition lines to be achieved compared with conventional inkjet printing as the more focused nozzle stream allows greater control (Werner et al. 2013, Seifert, Sowade, et al. 2015). Additionally, aerosol jet printing has previously shown greater freedom with regards to ink particle materials, loading and size, as well as the ink viscosity and surface tension. It has also been shown to be more applicable to thin layer production as the overall droplet size generated is often smaller. As such it may be possible to achieve a higher level of precision in this manner (Seifert, Sowade, et al. 2015).

1.4 The Current Study

1.4.4 Basic Concepts

Although a number of formulation methods already exist to increase the solubility of poorly soluble drugs and improve their bioavailability, there is a need for formulations which reduce the risk of damage to the drug and have greater flexibility and precision to allow tailoring to the needs of the patient. Thus, the current study attempts to increase solubility and improve control over the dosage form design and drug distribution using the innovative technique of aerosol jet printing (Figure 9) (King 2014).



Figure 9: Optomec AJ200 3D Inkjet Printer

As can be observed in Figure 10, the conventional manufacturing process will be significantly altered with a view to removing steps, such as compression and wet granulation, which have a risk of causing damage to the drug via over handling or exposure. This is highly important as drugs can be very vulnerable to degradation, for example due to water exposure, or polymorphism, due to over handling. Granulation, drying and compression will be replaced by inkjet printing as shown in Figure 10.

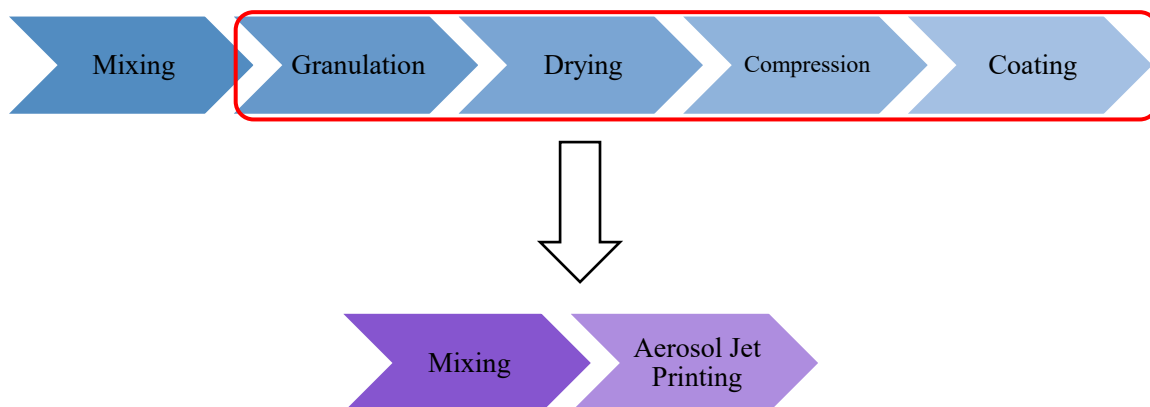


Figure 10: Changes to the conventional tablet manufacturing process

The precision allowed by aerosol jet printing in the current study has the potential to allow personalised medicine. The dose and release could be altered by changing the deposition pattern drawn on CAD software, the nozzle size used, the ink formulation content and/or the number of layers deposited. From a macro issue point of view this could hold potential in reducing wasted medicines and increasing patient compliance, as dosing could be specifically tailored to the patient reducing side effects, and thus reducing costs to the health service. Likewise, dosage forms produced could hold potential for controlled release as control over deposition could ensure the drug is evenly dispersed throughout the matrix for a sustained release effect or even could allow a delayed or pulsatile release effect with regions of the dosage form consisting of only excipient to form a buffer to release (Figure 11). As the dosage forms produced would be scalable, they could increase the compliance of paediatric and elderly patients, as these may prove easier to swallow than some conventional formulations.

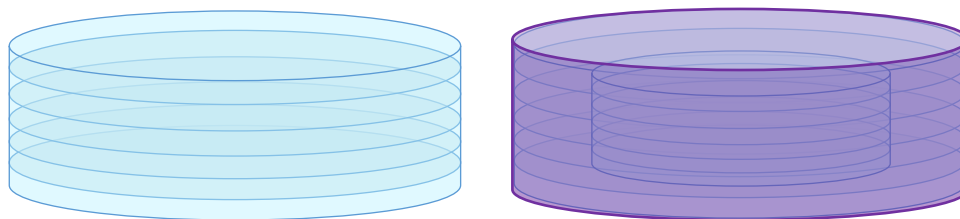


Figure 11: Schematic of theoretical dosage forms built by inkjet printing with layers or regions of drug and excipient for immediate or sustained release (left), or pulsatile or delayed release (right).

1.4.5 Theory

The fluid flow associated with inkjet printing is often governed by what are known as Reynold's number (Re) and Weber number (We). The former is defined as a dimensionless parameter which is based on the ratio of the inertial forces of the moving solution to the viscosity of the solution which reduces the flow (Newbury and Bates 2017). This can be defined by the equation: $Re = \rho \vartheta d / \eta$, where ρ is fluid density, ϑ is drop velocity, d is orifice diameter and η is viscosity (Eckstein 2016). Weber is defined by as the ratio between surface energy and kinetic energy, given by the equation $We = \vartheta^2 \rho d / \sigma$, where ρ is fluid density, ϑ is drop velocity, d is orifice diameter and σ is the surface tension of the fluid (Eckstein 2016, Barui et al. 2017). By taking the square root of Webber and dividing it by Reynolds it is possible to determine what's known as the inverse of Ohnesorge number (Z). Ohnesorge number can be defined as a variable which determines the relative importance of viscosity and surface forces. By taking the inverse it is possible to obtain a value which indicates if an ink is printable. If the ink has a Z -value of less than 1 it is considered too viscous but if the value is over 10 it is liable to produce droplets that are too small to control (Eckstein 2016, Barui et al. 2017).

In the case of aerosol jet printing, the Reynolds equation is more complicated to define than in a standard inkjet printer and thus may be inapplicable to the current study. This is because the ink is atomised and thus is a function of the pressure exerted by

nitrogen application in combination with the viscosity. The flow rate through the aerosol jet printer in standard cubic centimetres per minute (Q) must be taken into account. Additionally, there is a constant mass flow rate coupled with a variable volumetric nitrogen flow, which changes with temperature and pressure giving what is known as the jet mass flux. This can be defined by the equation: $\rho U = 4\rho_s Q / (\pi D^2)$, which is a constant for a given flow rate (Q) and nozzle diameter (D), where p is actual gas density and ps is gas density under standard conditions at 0°C and 105 Pa. So for aerosol jet, Reynolds can be considered to be $Re = \rho U D / \eta$, where η is considered to be a measure of gas viscosity rather than ink viscosity (Feng 2018). The only issue is there is no prior evidence of Reynolds with regards to ink viscosity and thus determination of printability in this manner may not be possible in the current study.

1.4.6 The Model Drugs

The model drug initially utilised in the current study is the class II drug fenofibrate (Figure 12). Fenofibrate is a hypolipidemic agent utilised to reduce low density lipoprotein cholesterol, the total cholesterol concentration and triglycerides in patients with a risk of cardiovascular disease (Tran et al. 2014). It is a neutral substance, with a Log P value of 5.24, and exhibits an expected solubility value of less than 500 µg/L, which makes it highly favourable for the current study (Hu et al. 2011).

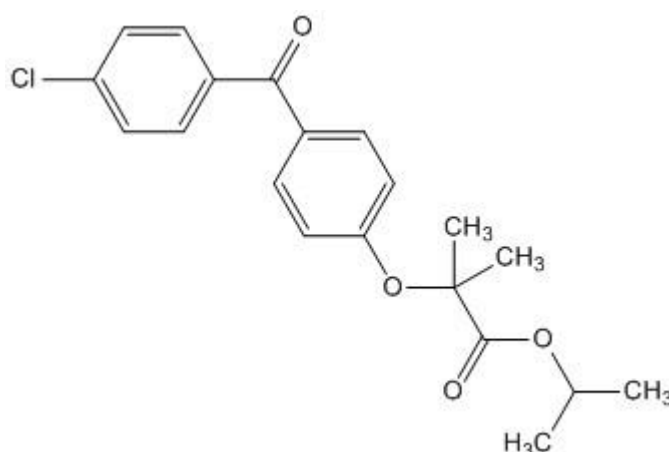


Figure 12: Structure of fenofibrate

This drug is particularly interesting from a personalised medicine perspective as the patients who take this drug can vary considerably as they may suffer from type II diabetes or metabolic syndrome, be renal impaired, overweight, young or elderly (Steiner 2008). The British National Formulary lists fenofibrate daily doses of 200-267 mg capsules or 160 mg tablets for non-renally impaired adults. However, this drops to 134 mg or even 67 mg per tablet in the presence of renal impairment due to reduced glomerular filtration rates (British National Joint Formulary Committee, 2018). Likewise, paediatric doses are considerably lower with capsules based on 67mg/20kg/day being given as standard (British National Paediatric Formulary Committee, 2018). The use of continuous manufacture with this drug in the current study is highly advantageous as in recent years there has been increasing demand within the pharma industry for cheaper more effective formulations of this drug as generic formulations emerge on the market (Chachad et al. 2014).

The drug latterly used in the current study is ibuprofen (Figure 13). Ibuprofen was selected as, although it too is a BCS class II drug, it has the advantage of being slightly acidic in nature and thus dissolves more efficiently in less acidic buffers (Al Masum et al. 2015). Ibuprofen is one of the most common anti-inflammatory drugs in existence currently and thus it is primarily used for mild to moderate analgesic purposes but it may also be used to treat rheumatoid arthritis, osteoarthritis and psoriatic arthritis, and other musculoskeletal conditions (Deng et al. 2016). Ibuprofen is another ideal candidate for personalised medicine as for paediatric use doses can range between 50mg 3 times daily to 400mg 3-4 times daily, and for adult use the dose can increase as high as 600mg 4 times a day for severe pain (British National Joint Formulary Committee, 2018).

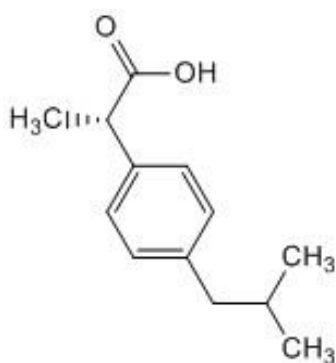


Figure 13: Structure of Ibuprofen

1.4.7 Excipient Selection

The excipient selection for fenofibrate was highly significant in the current study as they had to be able to withstand printing, help form a stable dosage form and effectively solubilise the drug. One study showed PVP K30 to have the greatest effect in solubilising fenofibrate when compared to HPMC, Carbopol and ethyl cellulose (Choi, Lee, et al. 2013). Nanoparticles were shown to increase drug release on dissolution testing from only 20% to 80% (Choi, Lee, et al. 2013). As such PVP was selected. Ethanol was selected as an ink medium as it is biocompatible, fenofibrate dissolves well in it and it has been shown before to generate effective formulations with fenofibrate (Vialpando et al. 2012, Hossen et al. 2014). Interestingly fenofibrate has not previously been paired with PVP in a printed formulation but felodipine, another class II drug has been. PVP was combined with a 95% ethanol solution to generate a formulation in this case (Scoutaris et al. 2011). As such it will be interesting to see if an effective dosage form can be produced by printing PVP and fenofibrate in ethanol. There is also previous evidence for the use of ibuprofen in ethanol (Li, Oh, et al. 2008, Shen 2011, Melzig et al. 2018). There is also previous evidence for the use of ibuprofen with PVP to create amorphous particles but only in complexes with PEG or using ibuprofen sodium rather than ibuprofen itself (Labuschagne et al. 2011, Rossmann et al. 2014). However, there is one study by Kazarian and Martirosyan where PVP was impregnated with ibuprofen using supercritical CO₂, showing a loss of crystalline material (Kazarian and Martirosyan 2002). However, there is little

evidence for the use of ethanol and PVP together with ibuprofen, so the current work is quite novel in that regard.

1.5 Research Questions

1.5.4 How effective is aerosol inkjet printing as a method for producing an oral dosage form?

1.5.4.2 Could this method of manufacture potentially replace or at least supplement standard methods of tablet manufacture?

1.5.4.3 Could this system be used to increase control over drug and excipient location within a dosage form?

1.5.4.4 As a result of this, could this system be used for personalised medicine and/or controlled release?

1.5.5 Can a class II drug be effectively solubilised by this new method?

1.5.5.2 How does dissolution compare to conventional powder-based systems?

1.5.5.3 Does the crystalline form play a part or are the excipients causing the most significant effect?

1.6 Aims and Objectives

Overall, the current study aims to generate an innovative oral dosage form capable of solubilising class II drugs. This dosage form design will replace conventional steps in the tablet production process in the hope of reducing damage to the drug. It is hoped by using aerosol jet printing a more flexible dosage form will be generated.

Chapter 2: The Effect of Ink Formulation and Aerosol Jet Printing on Physical Form

2.1 Introduction

The current chapter details the effects of aerosol jet printing on the solid state of fenofibrate and ibuprofen alone and in the presence of PVP K30. Inks were developed in a range of concentrations with a view to understanding the printability of the compounds and the implications of changing the ratio of drug to polymer on the overall formulation. Samples were produced by printing mixtures of drug and polymer in different ratios and printing the drug and polymer alone in layers, with a view to testing the effect of configuration on solid state. Utilising physical mixtures as a control, samples were initially tested by x-ray diffraction (XRD), Raman microscopy, scanning electron microscopy (SEM) and differential scanning calorimetry (DSC). As fenofibrate was the initial model drug, the work on this compound is more extensive. Samples using this compound were also analysed in their ink form by rheology to test the effect of polymer content on viscosity, and thus droplet size and particle size. Additionally, the effect of printing on the polymer was tested both by SEM and by size exclusion chromatography.

2.2 Materials and Methods

2.2.1 Materials

Fenofibrate, PVP 10,000, PVP K30, PVP K90, HPMC and phosphoric acid were obtained from Sigma-Aldrich (Dorset, U.K.). Sodium hydroxide and potassium dihydrogen phosphate were obtained from Merck Millipore (Burlington, MA, USA). Ibuprofen was obtained from Alfa Aesar (Haverhill, Massachusetts, USA). Ethanol (ABS), acetonitrile and propanol-2 were obtained from VWR International (Lutterworth, U.K.) and Honeywell International (Bucharest, Romania).

2.2.2 Methods

2.2.2.1 Dosage Form Manufacture by Inkjet Printing

2.2.2.1.1 Basic Concepts and Formulation Manufacture

Ink was prepared by mixing ethanol with either the API or PVP alone, or a combination of the two, to achieve a viscosity of less than 1000 cP as required by the instrument. Fenofibrate-based inks were prepared with a drug concentration of 30 mg/ml as standard and the concentration of polymer present was altered as follows: 0 mg/ml, 15 mg/ml, 30 mg/ml, 45 mg/ml, 60 mg/ml, 90 mg/ml and 120 mg/ml. Ibuprofen-based inks were prepared with a drug concentration of 30 mg/ml as standard and the concentration of polymer present was altered as follows: 0 mg/ml, 30 mg/ml, 60 mg/ml, 90 mg/ml and 120 mg/ml.

Aerosol jet printing was carried out using an Optomec AJ200 3D Inkjet Printer (Optomec Ltd., Albuquerque, U.S.A). The chosen ink solution was added to the pneumatic atomiser and atomised to an aerosol capable of transversing the tubing and the deposition head. Pneumatic atomisation was achieved by applying nitrogen to the printer at 90 psi, lowering this to 45 psi within the printer and using this pressurised nitrogen to vaporise the ink (Figure 14). The Optomec program KEWA Process Control 2.5.6 was used to control the pressure entering the atomiser, tubing and deposition head by setting the sheath flow rate to 60 cm³/min, the exhaust flow rate to 550 cm³/min and the atomiser flow rate to 600 cm³/min.

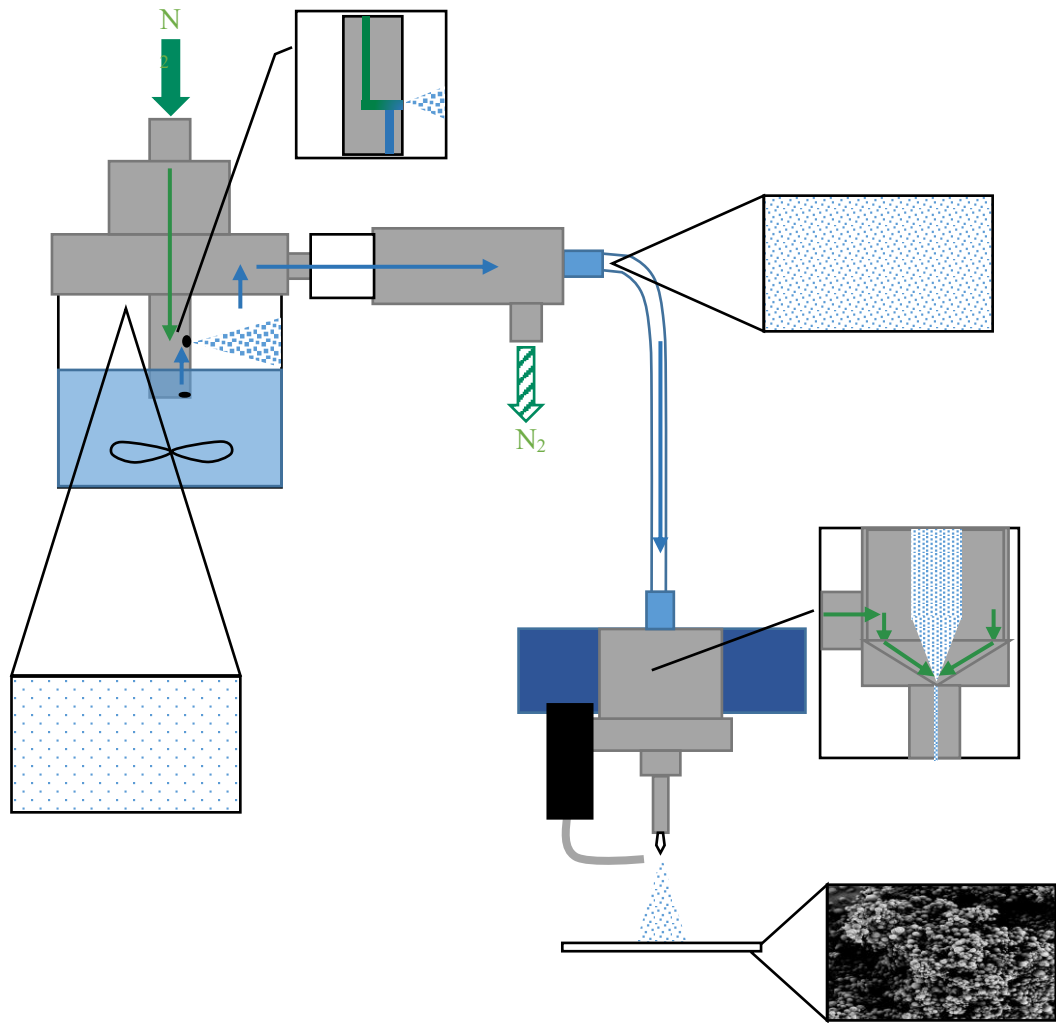


Figure 14: The pneumatic atomisation process – Pressurised nitrogen (green) is forced through formulation ink (blue), drawing it up into the jet stem and propelling it out into the atomisation chamber, enabling droplet mist formation. This is drawn up into the virtual impactor and excess nitrogen is extracted by the exhaust, forming a more condensed mist. This mist transverses the tubing, reaching the print head where a sheath flow condenses and directs the mist forming a precise jet stream which then dries forming particles on the substrate surface.

2.2.2.1.2 *Printing Formulations*

Ink was deposited on to different substrates depending on the needs of the study. Glass slides were used for microscopy and Raman spectroscopy studies, rice paper was used for powder x-ray diffraction (PXRD) and the ink was printed directly into metal pans for differential scanning calorimetry (DSC) and onto metal plates for scanning electron microscopy (SEM). Care was taken to ensure substrates were completely free of dust or contamination.

The ink deposition was programmed by creating a shape on AutoCAD 2015 with precise measurements and then running the file using KEWA Motion 2.5.0. To build up layers, generating a 3D structure, the file was rerun multiple times until the desired height was reached. Dosage forms were produced with layers of drug alone and polymer alone, as well as with pre-mixed formulations to allow analysis of the instrument's role in solubility vs. drug and excipient interactions (Table 2). Samples were then analysed and compared using the analytical techniques described in the following section.

Table 2: Formulations generated on inkjet printing

Formulation	Concept	Components and Ink	Variations
I	Drug alone	30mg/ml Fenofibrate or ibuprofen in ethanol	
II	Fenofibrate layer and polymer layer	30mg/ml Fenofibrate and PVP K30 in ethanol	Fenofibrate printed first (FNFPVP) vs. polymer printed first (PVPFNF)
III	Fenofibrate sandwiched between polymer layers	30mg/ml Fenofibrate and PVP K30 in ethanol	Layers of fenofibrate:PVP in ratios of 1:1, 1:2, 1:3, 1:4 w/w
IV	Fenofibrate or ibuprofen and polymer premixed	30mg/ml Fenofibrate or ibuprofen premixed with different concentrations of Polymer in ethanol (see right)	Fenofibrate:PVP 1:1, 1:2, 1:3, 1:4, 2:1, 2:3 w/w Ibuprofen:PVP 1:1, 1:2, 1:3, 1:4 w/w

2.2.2.2 Rheology of Ink Formulations

Initially, 2 different sets of samples were prepared to test the effect of ethanol use on viscosity using PVP alone. Following this, an additional set of samples using fenofibrate was prepared to test the impact of adding the drug into the mix and mimic the printing inks. For the PVP in water and PVP in ethanol solutions, 150mg, 300mg, 450mg, 600mg, 900mg and 1.2g of drug were dissolved in each of the solvents to result in 15mg/ml, 30mg/ml, 45mg/ml, 60mg/ml, 90-mg/ml and 120mg/ml solutions respectively. Samples were prepared by leaving the polymer to dissolve in less than 10ml and then topping up and inverting. For the fenofibrate and PVP ethanol solutions, 300mg fenofibrate was used as a standard base with 0mg, 150mg, 300mg, 450mg, 600mg, 900mg, 1.2g dissolved in 10ml ethanol. The fenofibrate containing

samples proved more difficult to dissolve due to fenofibrate's inherent poor solubility and thus once the PVP had fully dissolved a stirring bar was added to dissolve any remaining API particles.

Samples were run using a Thermoscientific Haake Mars Liquid Rheometer with a double cone DC60/1°TiL and a TMP60DC lower plate using Haake Rheowin Job Manager. Samples were measured over a range of 0-1000 shear taking incremental measurements at 25°C. Data was analysed using Haake Rheowin Data Manager. The results were plotted and statistical analysis was carried out using Origin Pro 2017.

2.2.2.3 Powder X-ray Diffraction

Initial Powder x-ray diffraction (PXRD) studies were carried out using a Bruker AXS D8 Advance II (Plate Priscilla) x-ray diffractometer (Bruker Corporation, Massachusetts, USA). Samples were tested over a range of 5-35 degrees 2θ at 0.01s. The only samples run on this were very early tests on fenofibrate and PVP printed. Initial runs comparing Kapton and standard printer paper were run on this ruling out printer paper as a valid substrate. However, experimental work was not continued on this instrument as it was found the detection level was not high enough for printed samples.

PXRD was latterly carried out using a Bruker D8 Discover x-ray diffractometer (Bruker Corporation, Massachusetts, USA). Following on from initial studies on the D8 Advance II, fenofibrate samples were printed onto Kapton film and rice paper initially. For the latter, the signal generated by the rice paper was subtracted using the analysis software Diffrac. EVA. V4.1. As the Kapton film was seen to hold little advantage over rice paper after subtraction, all other samples (Table 2) were only tested on rice paper. Samples were tested over a range of 5-35 degrees 2θ at 0.01s. Additionally, a stability study was carried out on samples over a period of 6 months, taking readings at 1, 2, 3, 4, 5, 8, 15, 22, 29, 60 and 180 days. Samples were analysed using Diffrac. EVA.V4.1 and Origin Pro 2017. Crystallinity was measured using the

software algorithm for percentage crystallinity which divides the peak area by the overall area of the diffraction pattern.

2.2.2.4 Differential Scanning Calorimetry

Differential Scanning Calorimetry (DSC) was carried out using a Netzsch STA449 F1 Jupiter (NETZSCH-Gerätebau GmbH, Wolverhampton, West Midlands, UK). Powder samples were prepared in the standard manner, weighing the pans before and after loading. Dosage form samples were prepared by printing directly into the pans for a period of 20 minutes to produce samples of 1-5mg. Analysis was carried out over a range of room temperature to 150°C, at 10 degrees a minute, cooling with liquid nitrogen between samples. Samples were analysed using the Netzsch program Proteus Analyser and Origin Pro 2017.

2.2.2.5 Raman Spectroscopy

Raman spectroscopy was carried out using a Horiba Xplora Raman Microscope using LabSpec 6 (Horiba Ltd., Stanmore, U.K.) to conclude where changes to the chemical structure of the drug occur on formation of solid dispersions. Studies were carried out using a 532 nm laser at x10 objective. The optimal parameters used to capture data on Labspec 6 were 6 minute acquisition, 2 minutes retention and 2 minutes delay with a 50 µm slit, 300 µm hole and 1200 filter. The results were plotted and statistical analysis was carried out using Origin Pro 2017.

2.2.2.6 Scanning Electron Microscopy

SEM was carried out using a Hitachi SU660 Field Emission SEM (FE-SEM) (Hitachi Ltd., Chiyoda, Tokyo, Japan) and a U9320B Field Emission Scanning Electron Microscope (Keysight, USA) using back scattering mode. Ink was deposited directly on to SEM stubs, using a circular deposition pattern, before the samples were subjected to a 20nm gold coat and then measured at x1,500 and x10,000 magnifications.

2.2.2.7 Size Exclusion Chromatography

Samples were prepared by printing PVP K30 in the manner detailed in section 2.1.2 as 1 cm diameter circles on glass slides, layering and weighing until 30mg was achieved. The PVP printed samples were dissolved in a solution of 50:50 methanol:0.1M lithium nitrate in water overnight. A raw powder control was produced by dissolving 30mg in the solvent. The following day the solutions were diluted to 10ml and inverted 12 times to give 3mg/ml solutions.

Size exclusion chromatography was carried out using a Malvern ObniseC Resolve coupled with a Malvern ObniseC Reveal using a 2xTSKgel GMPWXL 300x7.8mm column and a mobile phase of 50:50 methanol:0.1M lithium nitrate in water at 1ml/min for 40 minutes. A standard of polyethylene oxide (1.5mg/ml) was run through the instrument to calibrate. 3 x 100 µl injections were run of the raw and printed solutions and the results compared using OmniSEC.

2.3 Results & Discussion

2.3.1 Ink Rheology

2.3.1.1 Analysis of the Use of Volatile Solvents

PVP was run in both ethanol and water and compared. Figure 15 shows viscosity increases with polymer content in both solutions but this effect is augmented in ethanol, which may be due to evaporation. This is supported by an ANOVA with significant differences exhibited by the 60mg/ml, 90mg/ml and 120mg/ml PVP K30 samples at 1000 1/s. Figure 16 supports this showing very similar patterns of results but ever so slightly higher for ethanol. This effect seems to become more pronounced with concentration.

On comparison to the literature, a previous paper showed higher viscosity of PVP in water than ethanol which contradicts the current study (Vialpando et al. 2012). However, another paper supports the current study as the viscosity of ethanol is 1.2 mPa.s, compared to water at 0.88 mPa.s (Chuangchote, Surawut Sagawa and Yoshikawa 2009). Additionally, previous papers have shown the effect of increasing polymer concentrations in solution on the viscosity. For example Krull demonstrates an increase in viscosity with HPMC concentration in water (Krull et al. 2017). Additionally there are studies with PVP showing the relationship between viscosity and concentration such as one by Pawar et al. and Swei and Talbot in water, and by Mehrdad et al. in 1-hexyl- 3-methylimidazolium bromide (Swei and Talbot 2002, Mehrdad et al. 2013, Pawar et al. 2014).

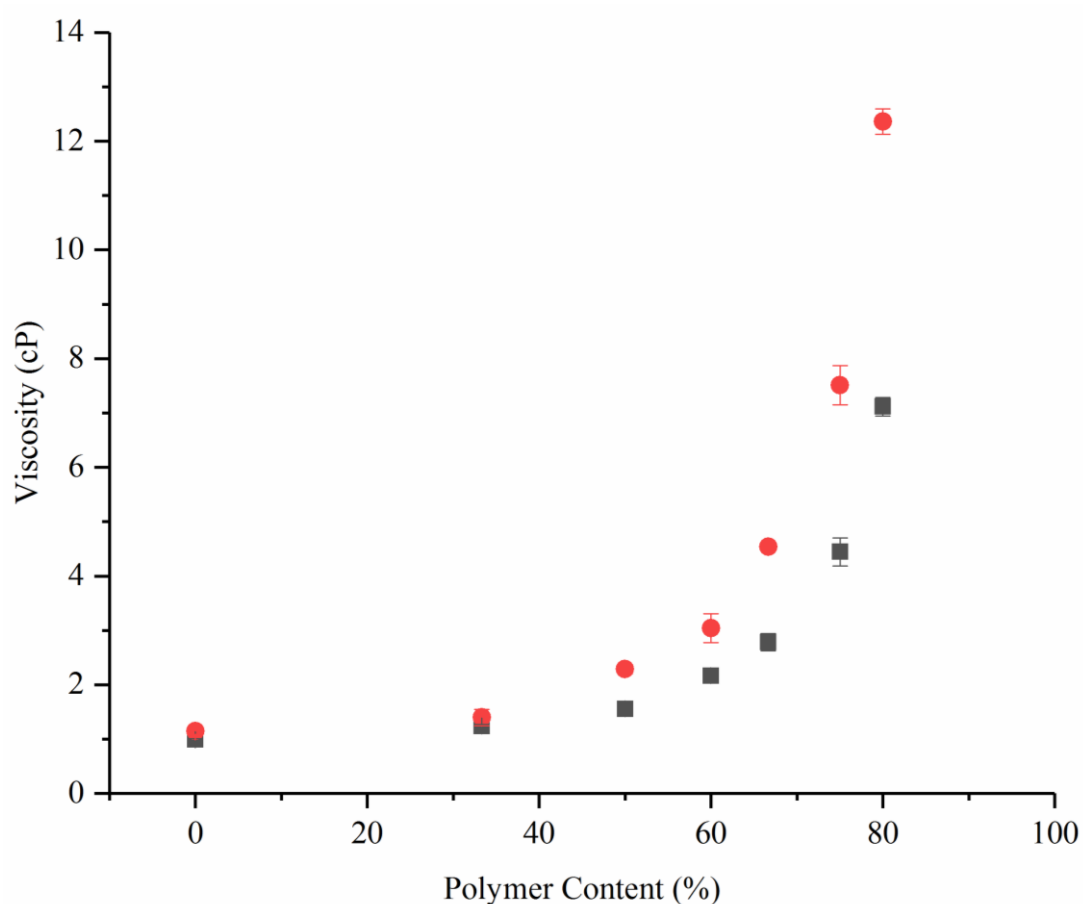


Figure 15: Comparison of the effect of increasing polymer content on the viscosity water (black) and ethanol (red) based solutions taken at 1000 1/s where $n=3 \pm$ standard error. The 95% confidence intervals in water are 0.92 cP and 1.06 cP, 1.10 cP and 1.38 cP, 1.22cP and 1.90 cP, 1.74 cP and 2.60 cP, 2.09 cP and 3.47 cP, 3.34 cP and 5.55 cP, and 6.59 cP and 7.79 cP for 0, 15, 30, 45, 60, 90, 120mg/ml PVP K30. The 95% confidence intervals in ethanol are 0.89 cP and 1.41 cP, 0.75 cP and 2.05 cP, 1.93 cP and 2.65 cP, 1.90 cP and 4.18 cP, 4.17 cP and 4.91 cP, 5.97 cP and 9.06 cP, and 11.36 cP and 13.36 cP for 0, 15, 30, 45, 60, 90 and 120mg/ml PVP K30. $P=0.99999$ for 0mg/ml, $P=0.99999$ for 15mg/ml, $P=0.23615$ for 30mg/ml, $P=0.07983$ for 45mg/ml, $P=1.59535 \times 10^{-5}$ for 60mg/ml, $P=1.40369 \times 10^{-6}$ for 90mg/ml and $P=0$ for 120mg/ml for comparisons of ethanol and water solutions of PVP K30 at 1000 1/s respectively.

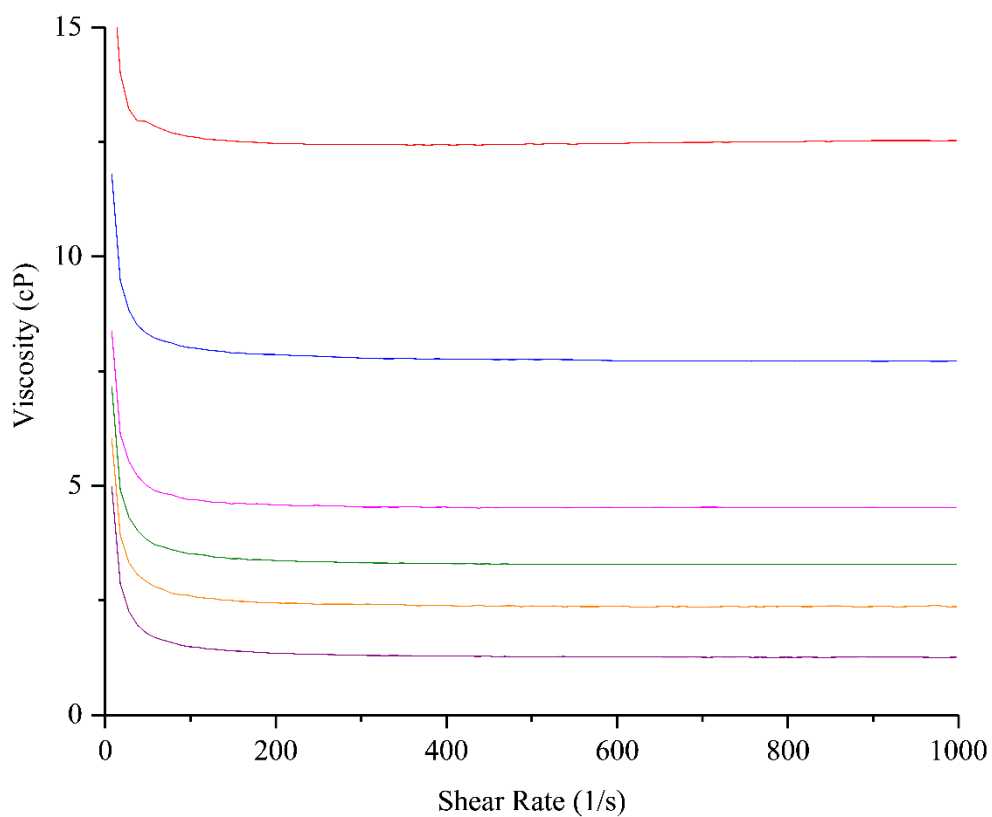
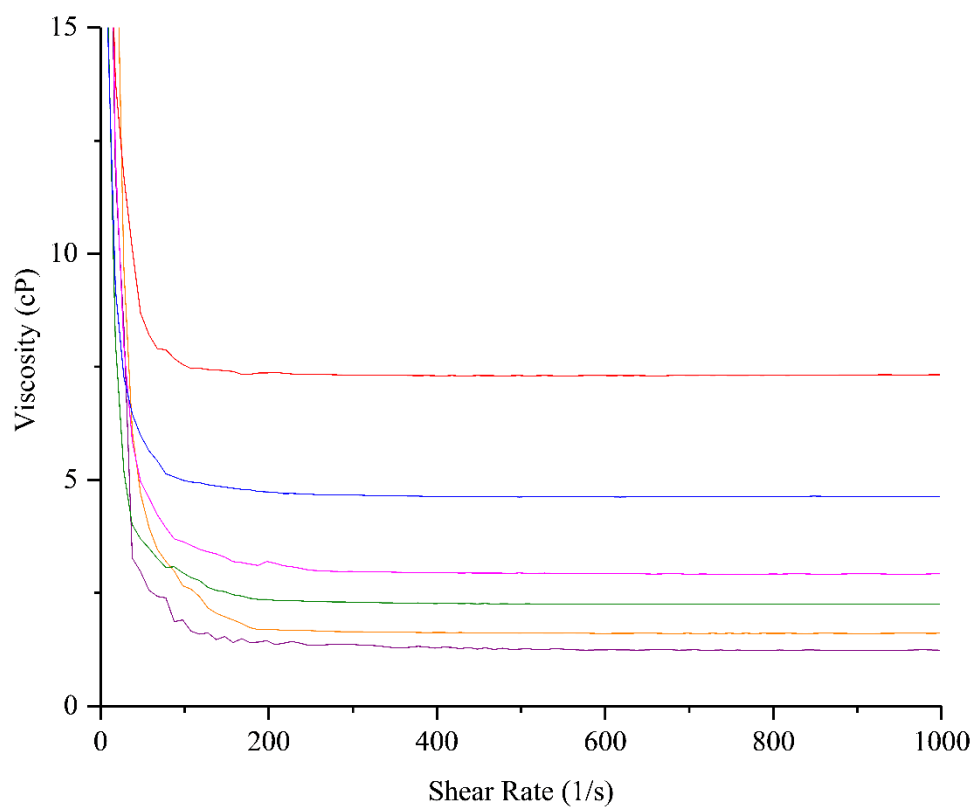


Figure 16: Comparison of shear rate sweeps of 15mg/ml (purple), 30mg/ml (orange), 45mg/ml (green), 60mg/ml (magenta), 90mg/ml (blue) and 120mg/ml (red) PVP in water (top) and ethanol (bottom).

2.3.1.2 Analysis of Viscosity of Ink Formulations

The ink formulations show an increase in viscosity with polymer concentration as demonstrated both by a comparison of the viscosity taken at the shear rate value of 1000 1/s (Figure 17) and by comparison of example shear rate sweeps (Figure 18). The relationship is linear with the exception of the latter two concentrations which start to raise the curve in a more exponential fashion (Figure 17), resulting in the r-squared value of 0.96871. Statistical analysis in Origin Pro 2017 gave a P-value of 5.94805×10^{-5} demonstrating the relationship between polymer concentration and viscosity is significant. Considering Figure 17, an ANOVA was performed using Origin Pro 2017 on the samples demonstrating no significant difference between the lower viscosity samples up to 45mg/ml PVP K30. However, the P-values are decreasing suggesting the difference is increasing. On increasing the polymer concentration there is a statistically significant increase in viscosity from 60 to 120mg/ml. Unfortunately, due to timings and availability of appropriate equipment this set of experiments was carried out on placement at AstraZeneca, prior to introduction of ibuprofen but based on the relationship between the ink viscosity and PVP it is believed that the ibuprofen ink may behave in a similar manner.

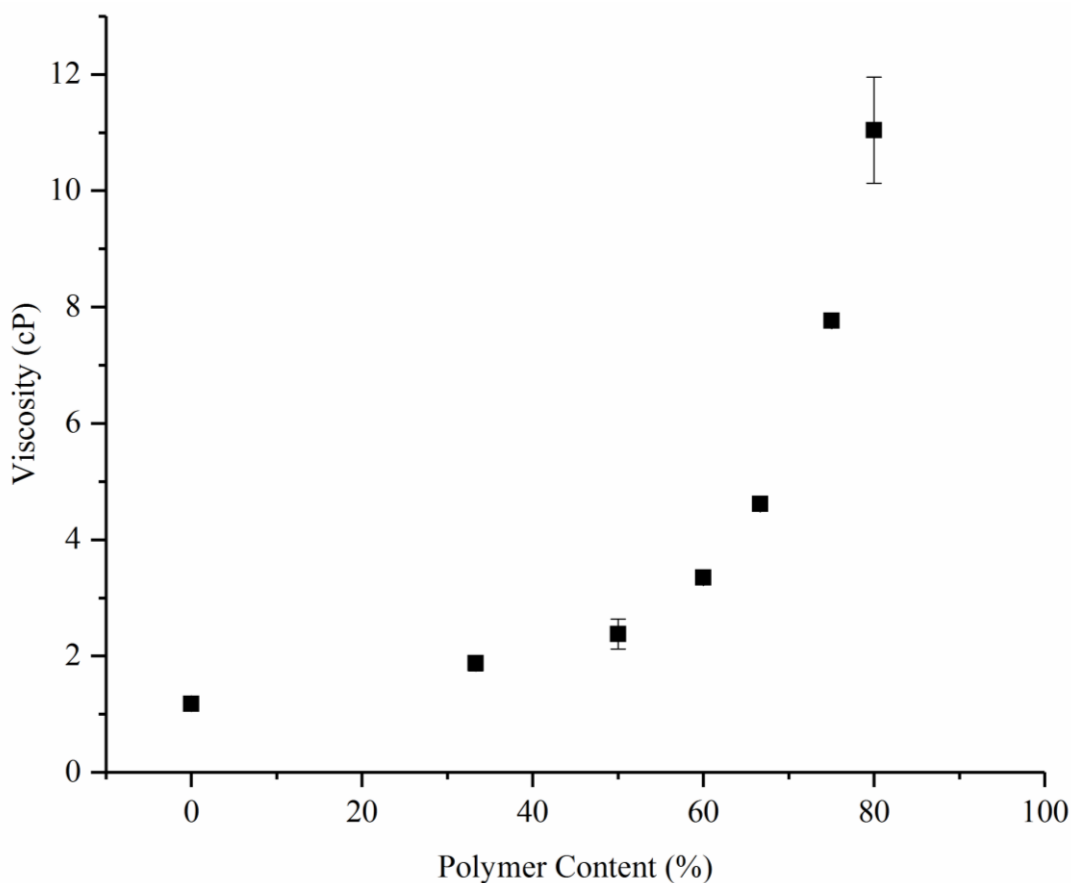


Figure 17: The effect of PVP K30 content on viscosity of formulation inks prepared in ethanol taken at 1000 1/s, where the polymer is 0mg/ml, 15mg/ml, 30mg/ml, 45mg/ml, 60mg/ml, 90mg/ml and 120mg/ml with a drug concentration of 30mg/ml throughout where $n=3 \pm$ standard error with 95% confidence intervals of 1.03 cP and 1.34 cP, 1.30 cP and 2.46 cP, 1.27 cP and 3.49 cP, 2.87 cP and 3.83 cP, 4.24 cP and 4.99 cP, 7.23 cP and 8.30 cP, and 7.12 cP and 14.96 cP for 0, 15, 30, 45, 60, 90 and 120mg/ml PVP K30. $P=0.8075$ for 0 to 15mg/ml, $P=0.94814$ for 15mg/ml to 30mg/ml, $P=0.51494$ for 30mg/ml to 45mg/ml and $P=0.24477$ for 45mg/ml to 60mg/ml, $P=6.76051 \times 10^{-4}$ for 60mg/ml to 90mg/ml and $P=4.75277 \times 10^{-4}$ for 90mg/ml to 120mg/ml PVP K30 in ethanol.

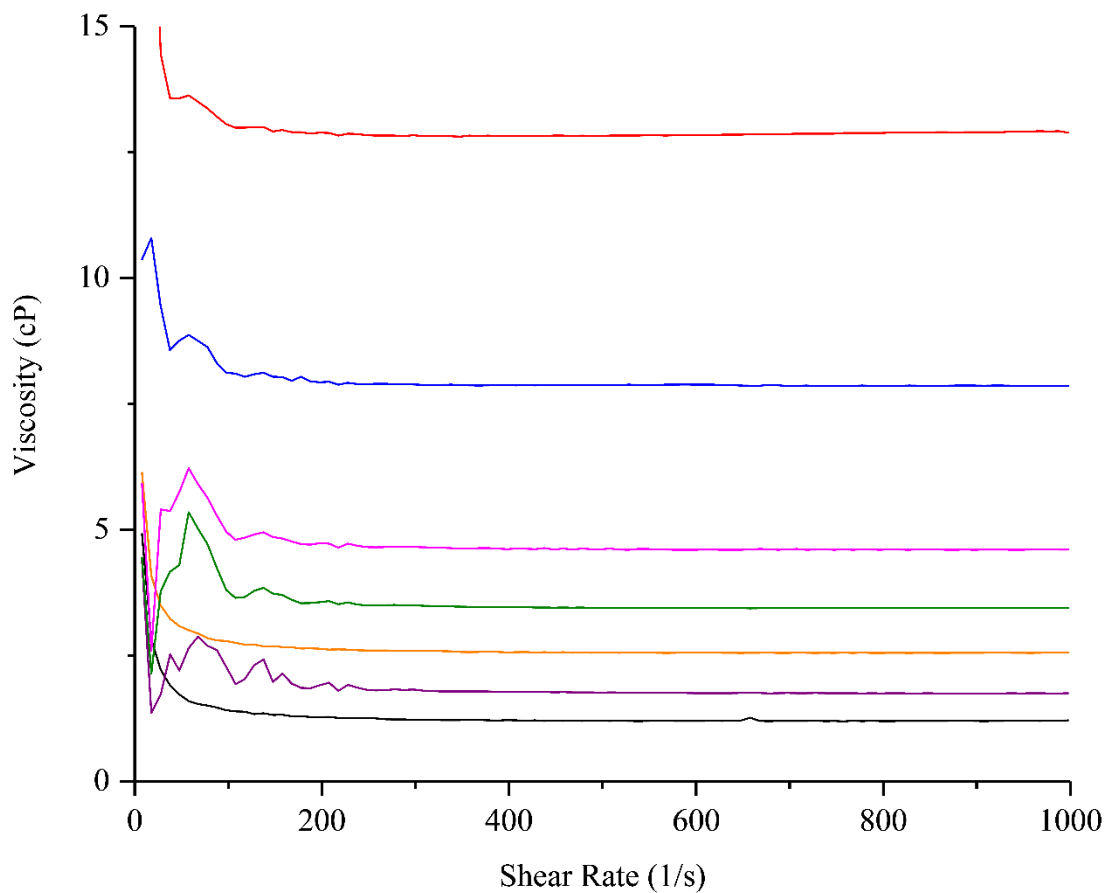


Figure 18: Comparison of example shear rate sweeps formulation inks - FNF 30mg/ml (black) and premixed FNF:PVP 2:1 (30mg/ml:15mg/ml) (purple), 1:1 (30mg/ml:30mg/ml) (orange), 2:3 (30mg/ml:45mg/ml) (green), 1:2 (30mg/ml:60mg/ml) (magenta), 1:3 (30mg/ml:90mg/ml) (blue) and 1:4 (30mg/ml:120mg/ml) (red)

On comparison to the literature, PVP and fenofibrate viscosity has been analysed previously but only in a 50:50 ethanol and dichloromethane. A 20% solution resulted in a viscosity measurement of 20 mPa.s, however no other concentrations were analysed in this study (Ng et al. 2013). As such the current study is fairly novel.

2.3.2 Powder X-Ray Diffraction

2.3.2.1 Substrate Selection

Samples were printed on Kapton film, standard printer paper and rice paper to establish if these substrates had any effect on crystallinity observed in the x-ray diffraction pattern. Initial samples were run on a Bruker D8 Advance II and it was established this instrument was not particularly suitable for use with printed samples. However, the effect of printing on standard printer paper was established using this instrument as can be observed in Figure 19. Additional peaks were observed in the diffraction pattern on comparison to the raw sample. On consulting the literature, it was established these are likely to be representative of cellulose in the printer paper (Foner and Adan 1983). Kapton film was also compared in this study but this, in combination with printing various samples on this surface, (Figure 20) suggested that this particular instrument was not suitable for analysing printed samples.

Therefore, all the other samples in this study were analysed using a Bruker D8 Discover. Analysis of the effect of printing on Kapton film was repeated and compared to printing on rice paper, which was selected due to its biocompatibility (Figure 21). As the rice paper gave a signal this was subtracted using Diffrac EVA V.4.1 (Figure 22). Printing on Kapton film was found to give a rougher baseline overall, whereas printing on rice paper was found to give more defined crystalline peaks despite the subtraction. As a result, rice paper was carried forward for use throughout the study with the exception of DSC, TOF-SIMS and SEM.

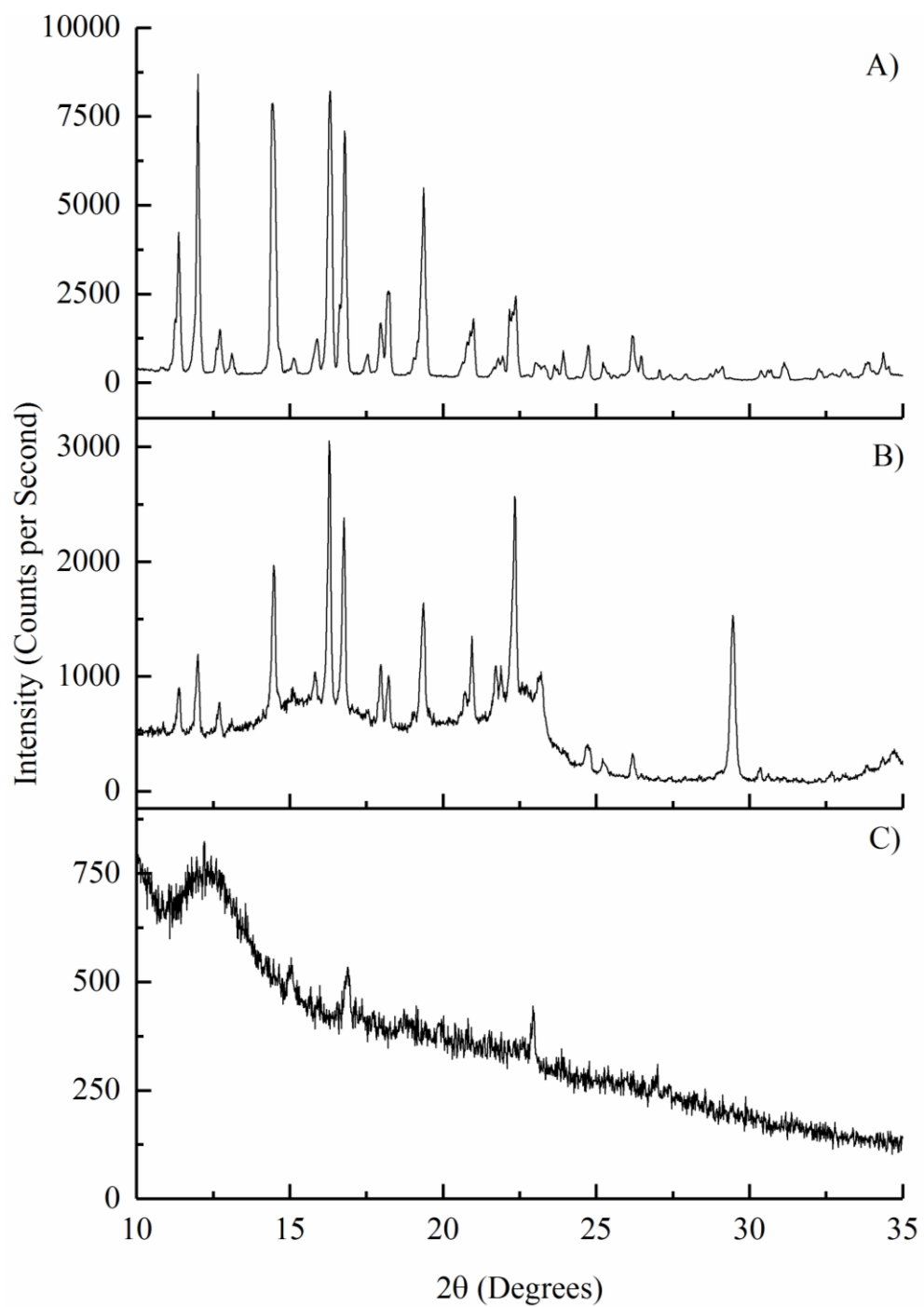


Figure 19: Comparison of printing on Kapton film vs. printing on standard printer paper - XRD on the Bruker D8 Advance II of (A) raw powder fenofibrate, (B) fenofibrate printed on printer paper and (C) fenofibrate printed on Kapton film.

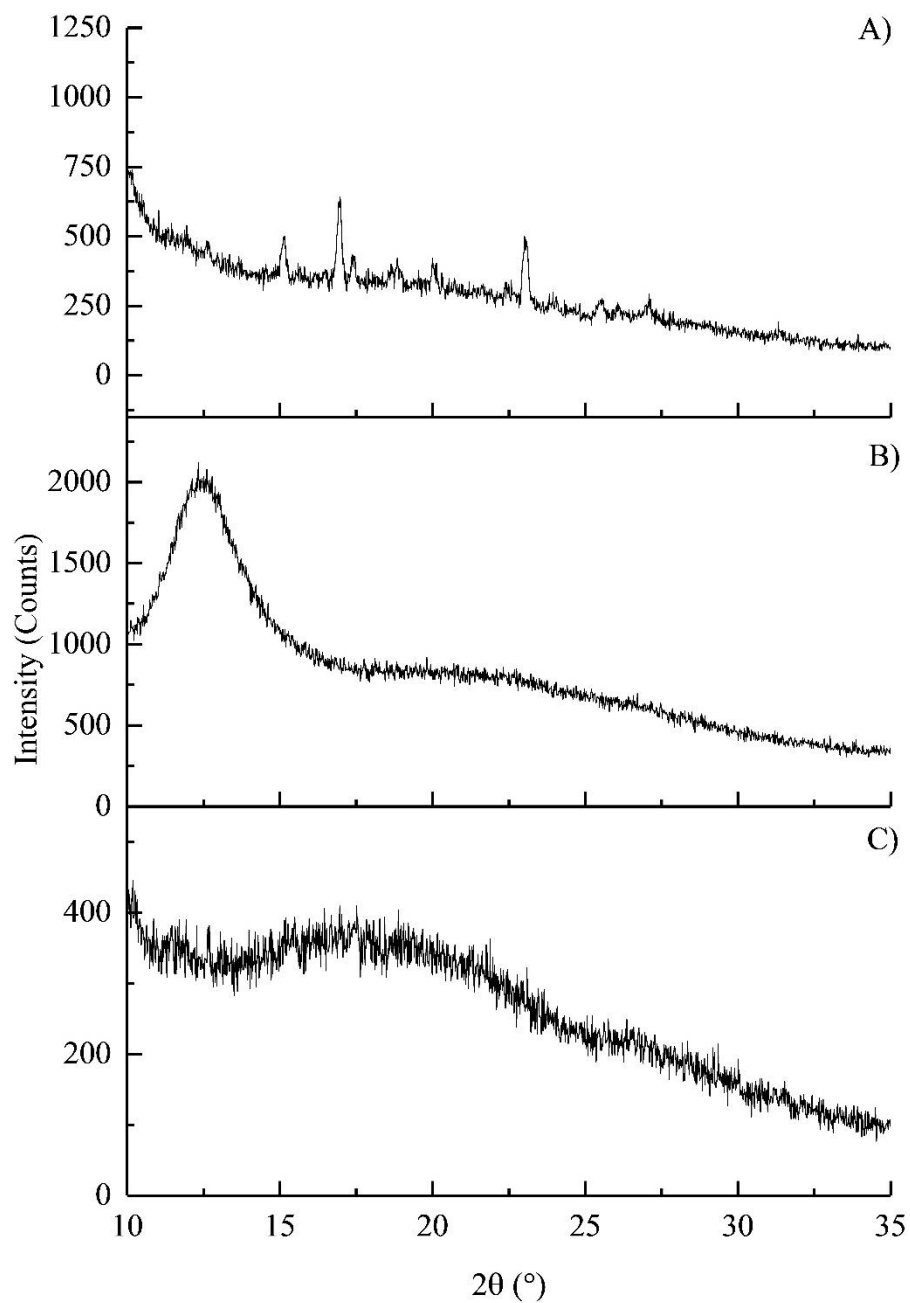


Figure 20: Limitation of the Bruker D8 Advance - (A) PVP and FNF single layers, (B) sandwiched fenofibrate between PVP (1:1) and (C) 1:1 premixed fenofibrate:PVP

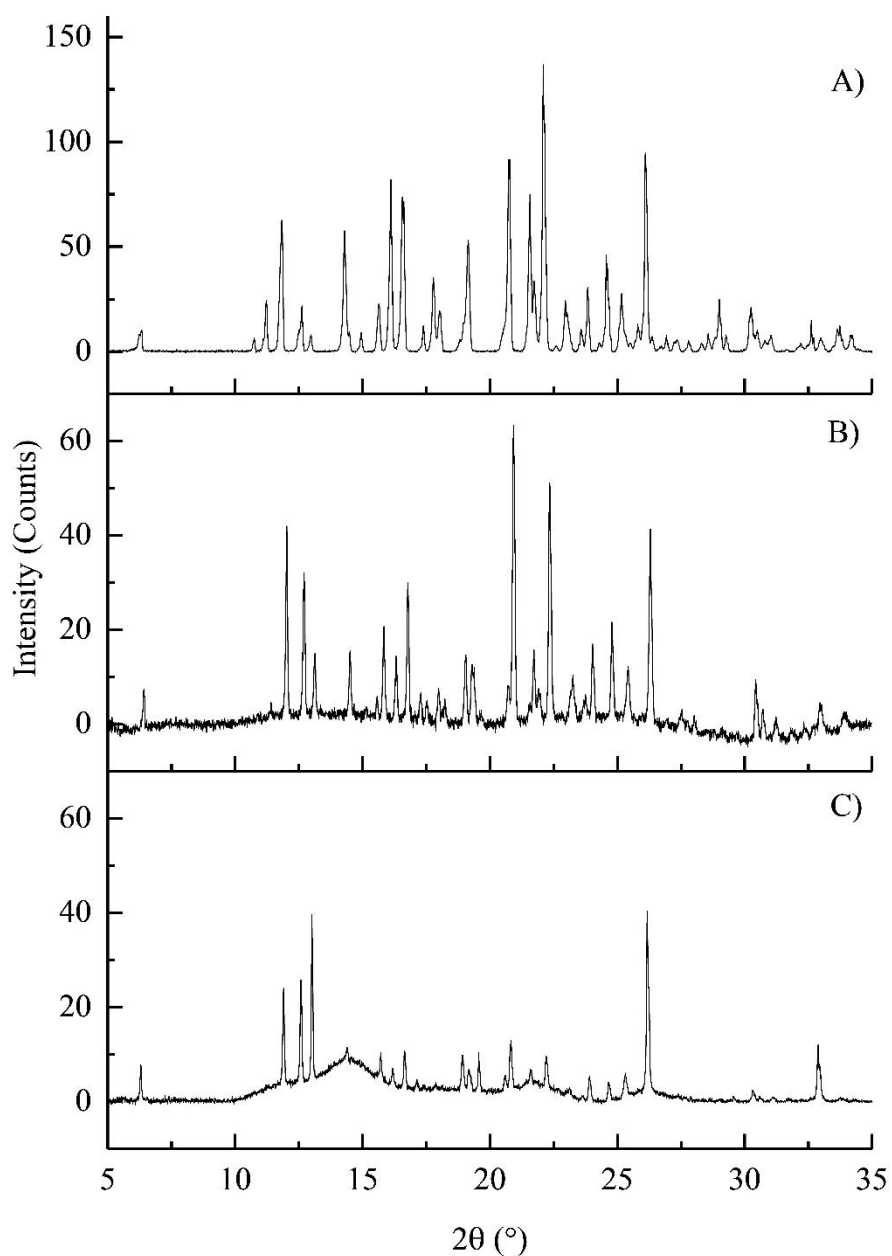


Figure 21: Comparison of printing on Kapton film vs. printing on rice paper with the rice paper signal subtracted - XRD on the Bruker D8 Discover of (A) raw powder fenofibrate, (B) fenofibrate printed on rice paper with the subtraction and (C) fenofibrate printed on Kapton film.

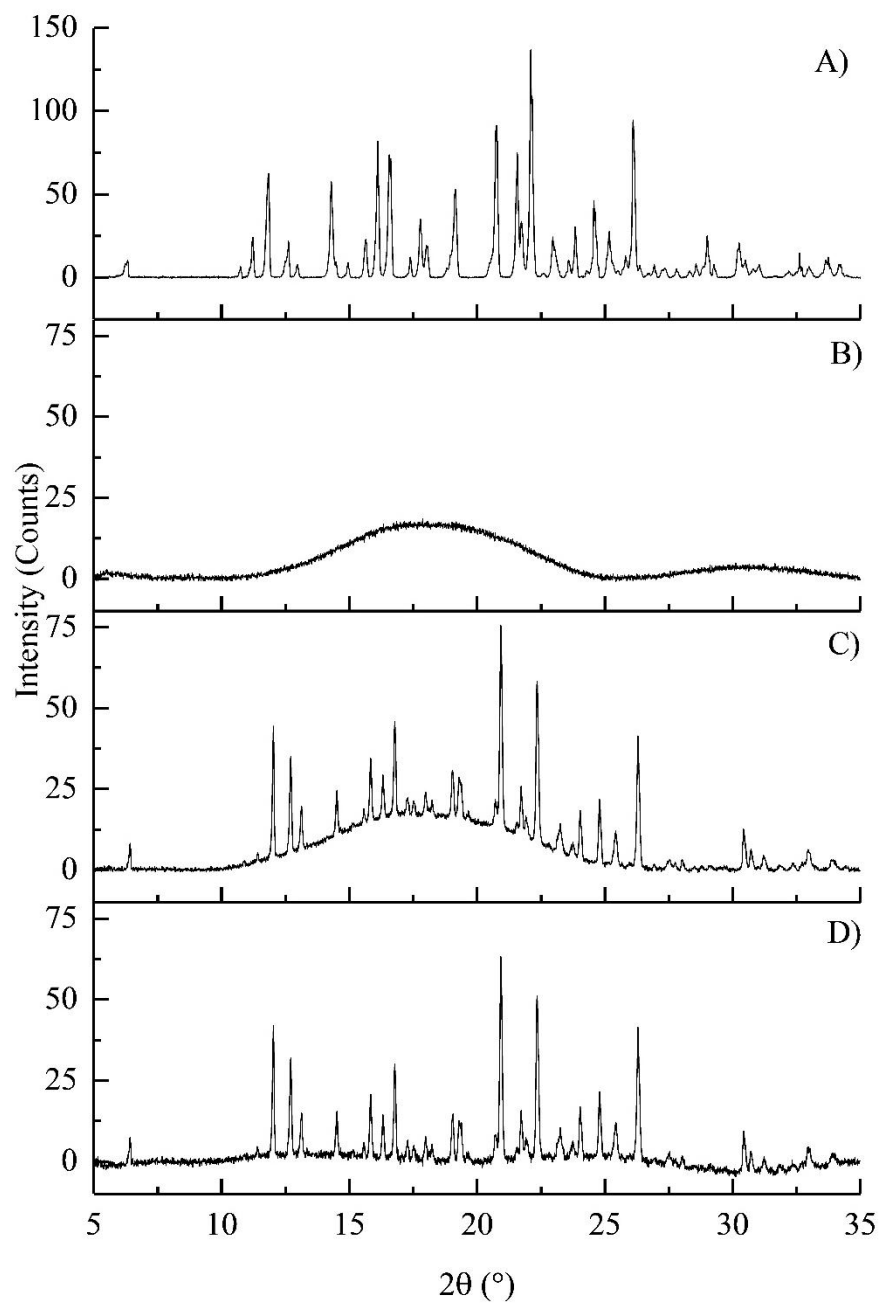


Figure 22: Subtraction of the rice paper signal - XRD on the Bruker D8 Discover of (A) fenofibrate raw powder, (B) rice paper, (C) printed fenofibrate on rice paper without subtraction and (D) printed fenofibrate on rice paper with the subtraction

2.3.2.2 Fenofibrate

2.3.2.2.1 Powder

XRD shows significant effects on the physical form of the drug on printing alone and with polymer. Figure 23 and Table 3 compare the raw drug powder alone to physical mixtures with polymer. The crystalline peaks are observed to reduce with polymer content but do not fully disappear. This is supported by a 44.4% crystallinity value for 1:4 fenofibrate:PVP suggesting the crystallinity is retained within the physical mixture. It should be noted that the calculation by Diffrac. EVA V.4.1 may be limited slightly by noise as the PVP control shows 0.6% crystallinity.

Table 3: Crystalline content of fenofibrate containing physical mixtures measured by powder X-ray diffraction

FNF:PVP ratio	Crystalline content (% , n=1)
1:0	94.2
2:1	86.6
1:1	77.9
2:3	67.1
1:2	55.8
1:3	47.4
1:4	44.4
0:1 (control)	0.6%

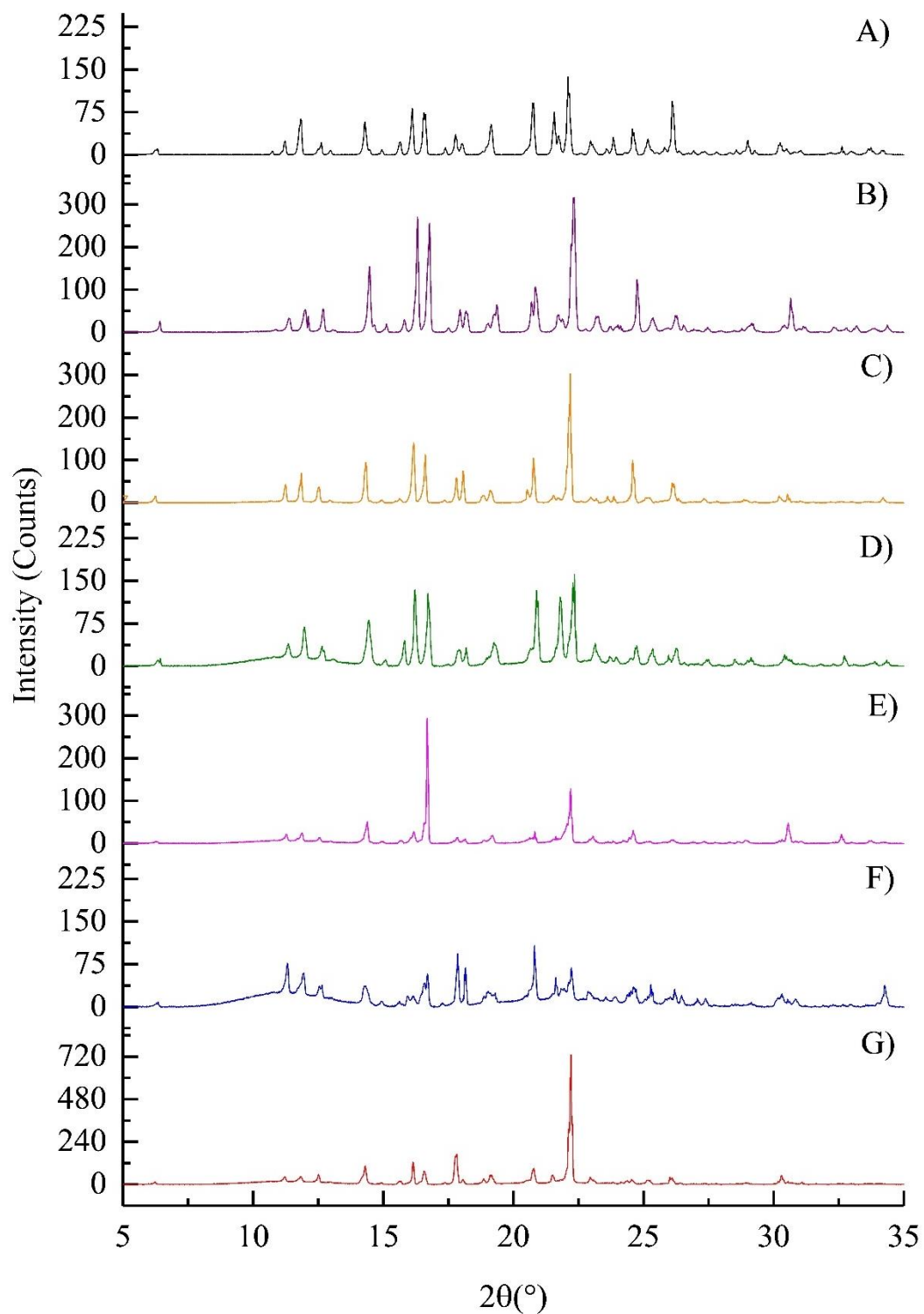


Figure 23: X-ray diffraction of (A) fenofibrate powder and (B-G) physical mixtures of fenofibrate:PVP 2:1, 1:1, 2:3, 1:2, 1:3 and 1:4.

2.3.2.2.2 *Premix*

Figure 24 and Table 4 compare printed drug alone to printed drug and polymer mixtures. In this case, the addition of polymer reduces the crystallinity of the overall formulation gradually until a fully amorphous product is achieved on printing formulations with a 75% polymer content or higher.

Table 4 demonstrates the gradual loss of crystallinity. Fenofibrate printed shows less crystallinity overall compared to the raw sample which is believed to be due to the lower mass present rather than reduced crystallinity. The gradual loss of peaks observed in Figure 24 is reflected in a decrease in percentage crystallinity. Ultimately, the difference between the printed drug alone and the printed drug-polymer mixtures becomes statistically significant on addition of 75% polymer or more, as the amorphous material reduces the crystalline signal. Again, it should be noted that printing polymer alone, as well as the 1:3 and 1:4 samples, shows a slight percentage crystallinity which is believed to be noisiness in the diffraction pattern. The comparison between these samples and the control allows us to conclude that they are amorphous due to this being consistent.

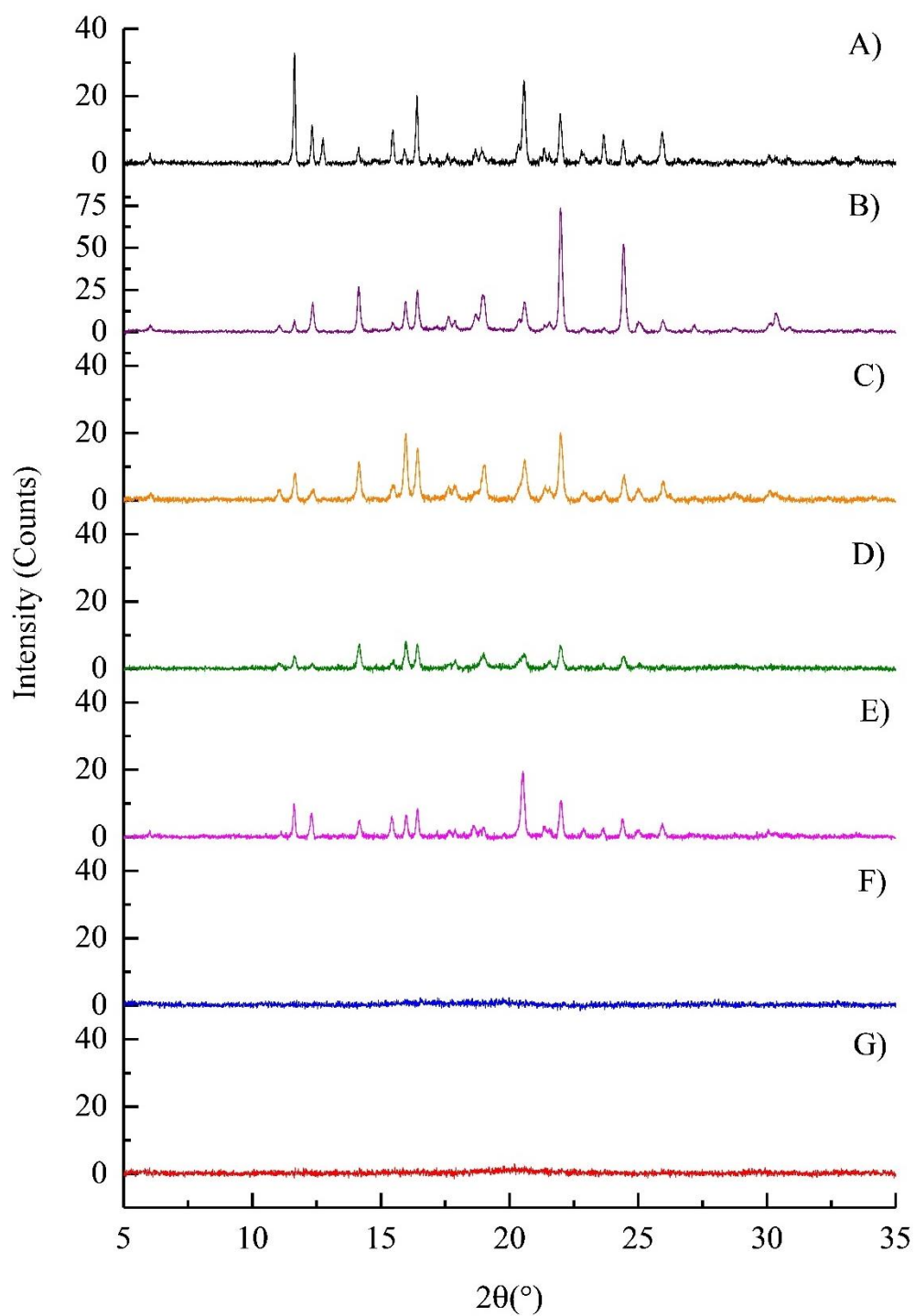


Figure 24: X-ray diffraction of printed (A) fenofibrate and (B-G) printed mixtures fenofibrate:PVP 2:1, 1:1, 2:3, 1:2, 1:3 and 1:4. $P=0.12674$ for FNF to 2:1, $P=0.99999$ for 2:1 to 1:1, $P=0.98249$ for 1:1 to 2:3, $P=1$ for 2:3 to 1:2, $P=0.03558$ for 1:2 to 1:3 and $P=1$ for 1:3 to 1:4.

Table 4: Crystalline content of printed premixed fenofibrate containing samples measured by powder X-ray diffraction

FNF:PVP ratio	Crystalline content (% , n=3)	SE	ANOVA Crystalline Content Relative to printed drug alone P-value
1:0	19.1	5.23864	
2:1	15	5.67186	0.99959
1:1	13.83	1.91862	0.99465
2:3	8.1	1.65025	0.45267
1:2	8.03	2.71437	0.44333
1:3	1.07	0.1453	0.01779
1:4	1.73	0.38442	0.02571
0:1 (control)	1.23	0.31798	0.01952

Comparisons can be made to spray drying in the literature as aerosol jet can be thought of as a miniaturised version of this. Spray drying has been observed to result in amorphous material formation in a number of papers and there are two previous papers using fenofibrate in particular. Vogt et al. investigated nanosizing coupled with spray drying of fenofibrate, resulting in complete loss of crystallinity measured by XRD (Vogt et al. 2008). Varshosaz and Ghassami demonstrated amorphous material formation by XRD and SEM on spray drying fenofibrate with Eudragit E100, Solutol HS15 and HPMC (Varshosaz and Ghassami 2015). Additionally, Yousaf et al. demonstrates the effect of spray drying with insufficient PVP K30. This fails to result in fully amorphous products as the samples generated contained only 1:1.8 fenofibrate:PVP which exhibited peaks very similar to 1:2 fenofibrate:PVP in Figure 24 (Yousaf et al. 2015). Comparisons can also be made to solvent evaporation as the

initial particle formation is the result of the ethanol evaporation. In a study by Choi et al., fenofibrate and PVP nanoparticles were prepared in ethanol in a 1:1 ratio. This resulted in fully amorphous particles with a loss of the crystalline peaks (Choi, Lee, et al. 2013).

Samples were analysed over 6 months as can be seen in Table 5. Fenofibrate remains relatively constant throughout the 6 months only increasing in detected crystallinity at the 2 month point. 2:1 fenofibrate:PVP also seems to maintain a similar level of crystallinity and is very similar to the drug alone in the initial readings but it then doubles between 2 and 6 months. The greatest changes can be observed in the 1:1, 2:3 and 1:2 fenofibrate:PVP with the greatest evidence of crystal growth being again observed between 2 and 6 months. 1:1 shows a gradual increase in crystalline content, while 2:3 and 1:2 only seem to increase substantially over the last 4 months. 1:3 fenofibrate:PVP shows a small amount of crystal growth but only between months 2 and 6 and substantially less than the lower polymer content samples. 1:4 fenofibrate:PVP is the most stable overall with no additional crystal growth being observed over the 6 month period.

Table 5: Percentage crystallinity obtained from a stability study on fenofibrate-based printed samples over a 6 month period

Days (n)	Percentage Crystallinity Detected (%)							
	FNF Powder	FNF Printed	2:1 FNF:PVP	1:1 FNF:PVP	2:3 FNF:PVP	1:2 FNF:PVP	1:3 FNF:PVP	1:4 FNF:PVP
1	94.3	29.5	28	6.9	5.1	2.1	2.1	2.7
2	95.3	29.1	20.1	6.5	2.1	2.7	1.6	2.6
3	95.6	27.7	19.4	13.3	2	6	2.1	3.1
4	95.7	19.1	17.9	17	3.8	6	1.4	1
5	94.8	19.5	19.4	11.7	4.3	7	1.4	1.7
8	95	20	18	8.7	5.9	5.7	1.4	2
15	94.8	27.6	26.9	15	8.2	13.2	1.9	3.4
22	93.4	20	21.2	12.4	3.7	5	1.2	1.7
29	94	28.9	26.4	13.7	5.8	4.4	1.8	2
60	94.2	35	22.3	13.6	5.3	3.2	1	1.5
180	94	31	56.8	27	21.4	15.6	2.6	2.5
Percentage Increase (%)	N/A	5.08	102.86	291.31	319.61	642.86	23.81	N/A

2.3.2.2.3 Layered

Layered samples with fenofibrate between 2 layers of PVP and as 2 separate layers were compared with drug alone (Figure 25 and Table 6). The diffraction patterns of 1:1 fenofibrate:PVP K30 with fenofibrate printed first, 1:1 fenofibrate:PVP K30 with PVP printed first and 1:1 fenofibrate:PVP K30 with fenofibrate sandwiched between

2 layers of PVP are fairly similar. Table 6 interestingly demonstrates a slight reduction in crystallinity between fenofibrate and the single layer 1:1 samples but 1:1 in the sandwich style shows lower crystallinity overall. This is potentially due to the overall higher PVP content and the configuration. As the PVP content is increased with the outer sandwiching layers increasing the ratio to 1:2 the crystallinity increases slightly. Then on increasing the polymer content to 1:3 fenofibrate:PVP, the crystallinity falls slightly before increasing slightly on increasing the polymer content to 1:4 fenofibrate:PVP. Although the crystallinity is not reduced as dramatically as premixing, the percentage crystallinity is still less than that of the physical mixtures suggesting there is some kind of interaction occurring. However, on performing an ANOVA none of the samples are considered statistically different from the drug alone.

On comparison to the literature, there is little previous evidence for the effect of layering. However, there is a paper comparing the crystallinity using IR-ATR on spin coating PVP and fenofibrate films separately. On comparison of 1:1 premixed to layered, premixing and putting down PVP seemed to result in more crystallinity than layering PVP on top of a fenofibrate layer, which is a little different than detected in the current study which may be attributed to the slightly different techniques. However, all of the samples retain their crystallinity to a degree which is consistent with the current study (Ng et al. 2013).

Table 6: Crystalline content of printed fenofibrate containing layered samples measured by powder X-ray diffraction

FNF:PVP ratio	Crystalline content (% , n=3)	SE	ANOVA relative to printed drug P-value
1:0	19.1	5.23864	
1:1 (PVP-FNF)	16.17	2.18658	0.99999
1:1 (FNF-PVP)	17.10	2.96142	1
1:1 (PVP-FNF-PVP)	10.23	5.57654	0.76051
1:2	14.10	3.15013	0.99676
1:3	11.93	3.3982	0.93198
1:4	12.93	0.76884	0.9783

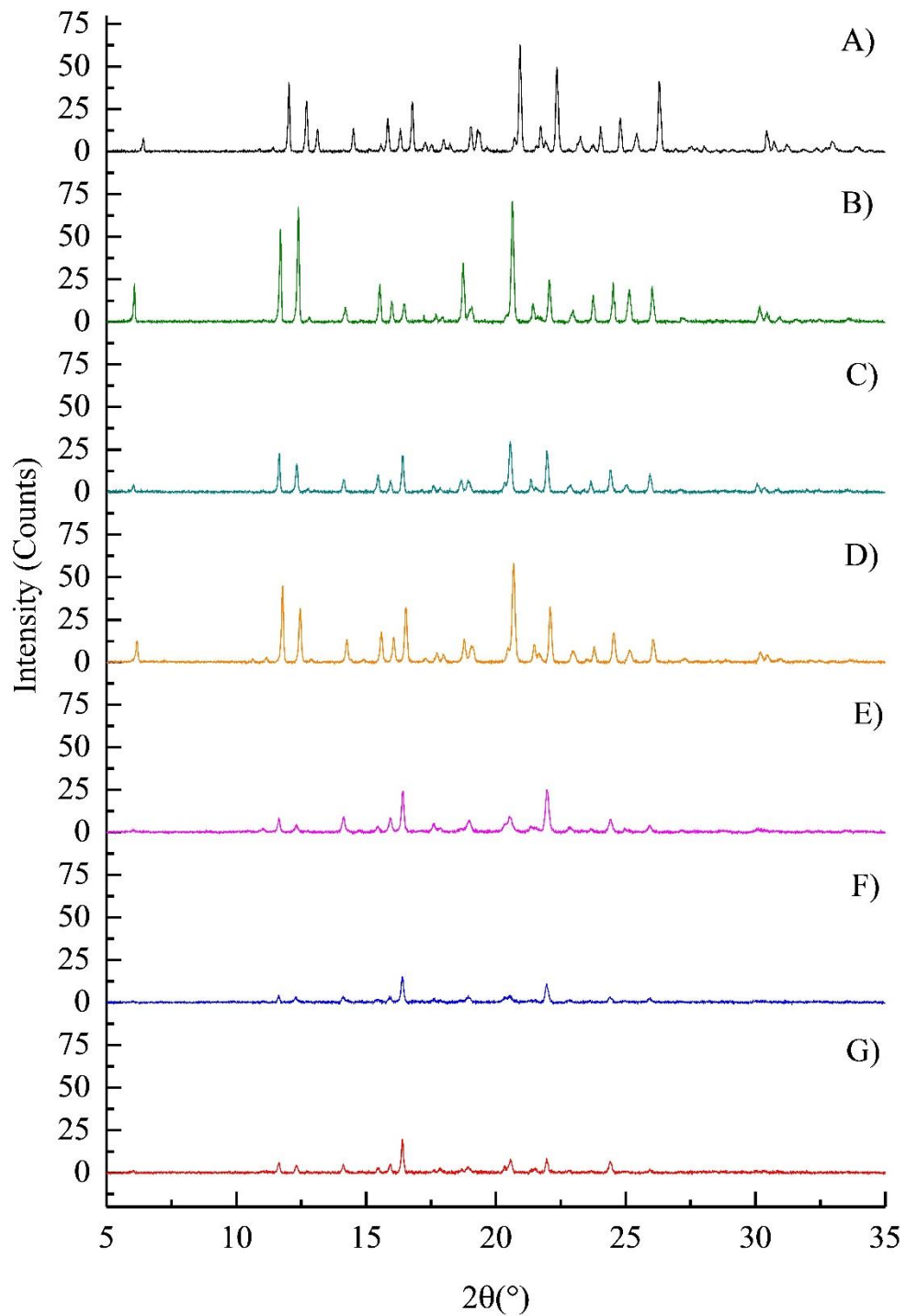


Figure 25: X-ray diffraction of printed fenofibrate and layered printed samples as follows: (A) fenofibrate, fenofibrate:PVP (B) 1:1 FNF printed first (FNFPVP), (C) 1:1 PVP printed first (PVPFNF) and (D-G) sandwiched 1:1, 1:2, 1:3 and 1:4. $P=0.14649$ FNF for FNFPVP, $P=0.4875$ for FNF to PVPFNF, $P=6.32509 \times 10^{-4}$ for FNF to 1:1 sandwiched, $P=0.99999$ for FNF to 1:2 sandwiched, $P=1$ for FNF to 1:3 sandwiched, $P=1$ for FNF to 1:4 sandwiched,

2.3.2.3 Ibuprofen

As can be observed in Figure 26, X-ray diffraction of printed ibuprofen alone exhibits a similar pattern to the powdered API. However, on printing with polymer present the crystallinity is diminished entirely and a fully amorphous product is achieved with even 50% polymer present in the ink. This is considerably less than was required for fenofibrate suggesting ibuprofen is more amenable to this change. Table 7 demonstrates a reduction in crystallinity relative to the raw sample on printing the drug alone, which is again believed to be a result of the reduced mass present. On addition of polymer the crystallinity is significantly reduced. Again, the crystallinity value is not zero but, as the PVP measurement in Table 6 demonstrated, there is a chance the inherent noisiness of the diffraction pattern may be resulting in the software measuring crystallinity. As such, on comparison to PVP, it can be concluded that the samples are amorphous.

On comparison to the literature, the XRD of aerosol jet printed ibuprofen reflects similar results using spray drying. Shen et al. demonstrated fully amorphous product formation from ibuprofen and SBA-15 with a 50:50 ratio in ethanol and a complete loss of crystalline peaks in two papers (Shen et al. 2010, 2011). Additionally, a very similar effect was achieved using ibuprofen and gelatine in ethanol in a paper by Li et al. again featuring a complete loss of the crystalline peak on co-spray drying (Li, Oh, et al. 2008).

Table 7: Crystalline content of printed ibuprofen containing samples measured by powder X-ray diffraction

IBU:PVP ratio	Crystalline content (% , n=1)
1:0 powder	96.2
1:0	66.9
1:1	2.2
1:2	1.3
1:3	1
1:4	1.6

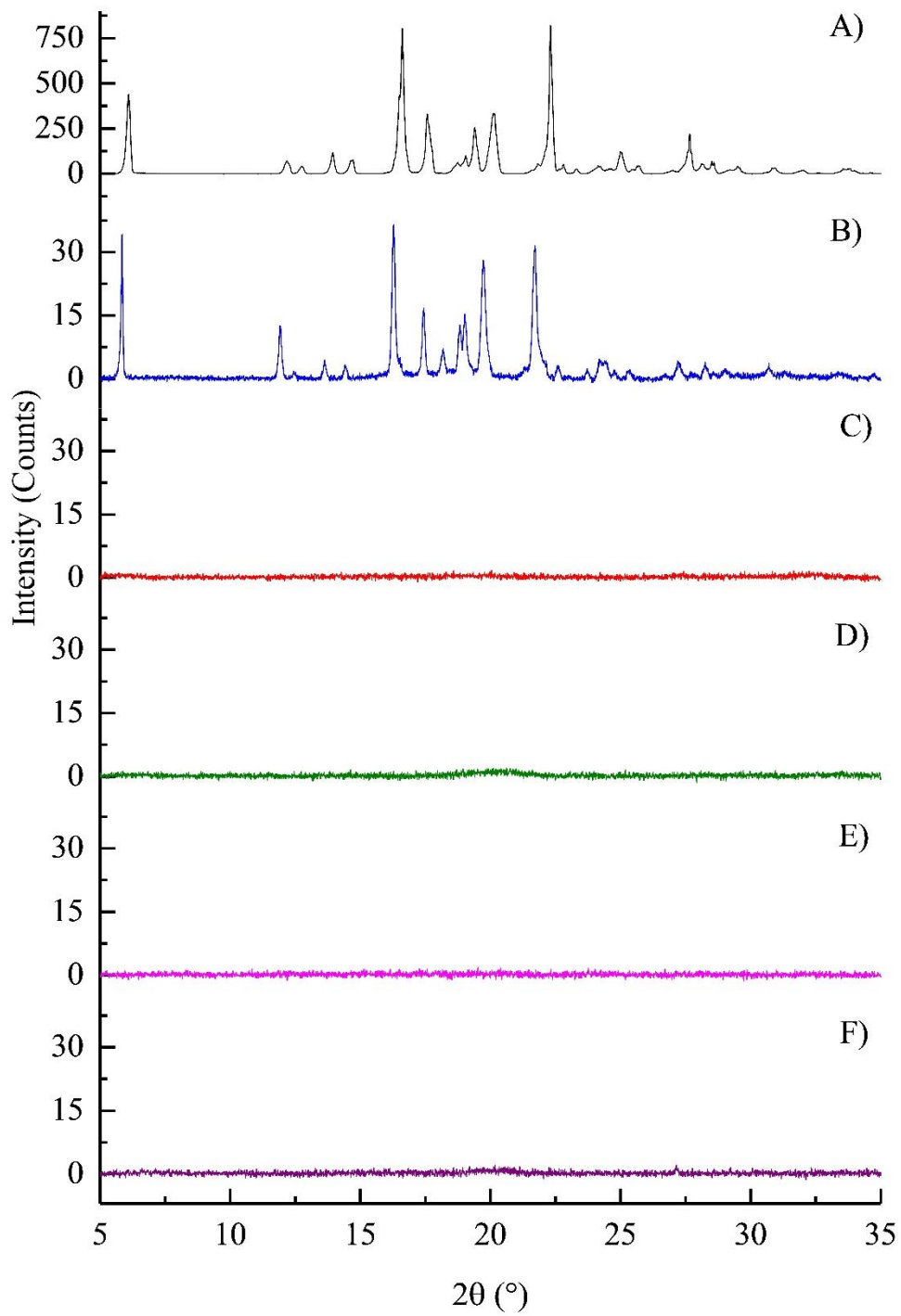


Figure 26: X-ray diffraction of (A) ibuprofen powder, (B) ibuprofen printed and (C-F) printed mixtures of ibuprofen:PVP 1:1, 1:2, 1:3 and 1:4.

2.3.3 Differential Scanning Calorimetry

2.3.3.1 Fenofibrate

The differential scanning calorimetry (DSC) results support the XRD results (Figures 23 and 24). Although the crystallinity decreases slightly with polymer content in the physical mixtures (Figure 27 and Table 8), a much more defined loss of crystallinity is observed in the comparable printed samples (Figure 28 and Table 9). Printing the drug alone seems to result in less crystallinity relative to the powdered sample, shown by the significantly reduced peak. Premixing the drug and polymer in a 2:1 or 1:1 ratio seems to reduce the peak further suggesting a reduction in crystalline character. There is a slight shift in the trough for these samples which suggests an interaction may be occurring between the PVP and fenofibrate even if the crystalline state is maintained. This effect has been seen previously with fenofibrate and has been associated with increased solubility (Grimling et al. 2012, 2013). The crystalline trough gradually decreases in size until it is undetectable at 1:2 fenofibrate:PVP content. This suggests the PVP is having a stabilising effect on the amorphous state of fenofibrate. The decrease in peak enthalpy from 1:1 to 2:3 is considerably less than the previous samples which may be due to 2:3 continuing to exhibit larger more agglomerated crystals as well as amorphous particles.

Interestingly, all of the powder samples and the printed drug alone exhibit Form I of fenofibrate with exothermal peaks of approximately 80°C, whereas printed 2:1 and 2:3 fenofibrate:PVP exhibit evidence of Form II with exothermal peaks of approximately 74°C. Form II has previously been associated with formation and recrystallisation of amorphous fenofibrate (Tipduangta et al. 2015). This suggests that printing does convert fenofibrate to the amorphous form in these samples but they lack sufficient PVP to stabilise the drug in this form.

There is very little previous literature on DSC of fenofibrate and PVP, however Choi et al. demonstrates a loss of the crystalline trough using nanoparticles produced by solvent evaporation with a 1:1 ratio of fenofibrate:PVP (Choi, Lee, et al. 2013).

Table 8: DSC peak and peak enthalpy Fenofibrate powder alone and as physical mixtures with PVP K30

Drug:Polymer Ratio	Peak (°C)	Peak Enthalpy (J/g)
1:0	82.9	-807.333
2:1	81.3	-78.61
1:1	80.6	-66.15
2:3	80.8	-36.79
1:2	80.7	-68.98
1:3	79.9	-20.55
1:4	80.3	-18.17

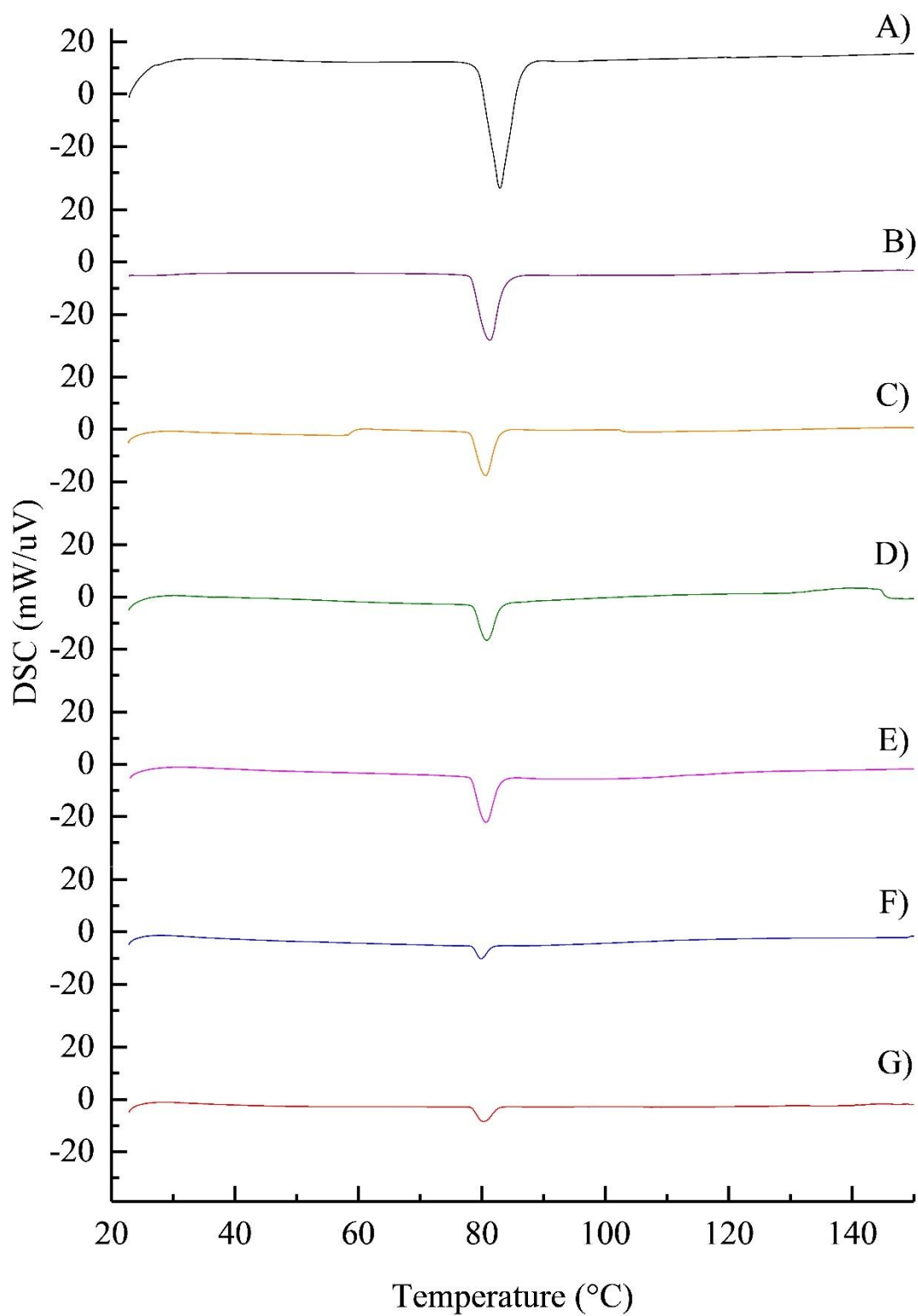


Figure 27: Differential scanning calorimetry of (A) fenofibrate powder and (B-G) physical mixtures of fenofibrate:PVP 2:1, 1:1, 2:3, 1:2, 1:3 and 1:4.

Table 9: DSC peak and peak enthalpy Fenofibrate printed alone and with PVP K30

Drug:Polymer Ratio	Peak (°C)	Peak Enthalpy (J/g)
1:0	79.4	-92.11
2:1	74.8	-67.31
1:1	78.9	-23.97
2:3	74.1	-20.40
1:2	N/A	N/A
1:3	N/A	N/A
1:4	N/A	N/A

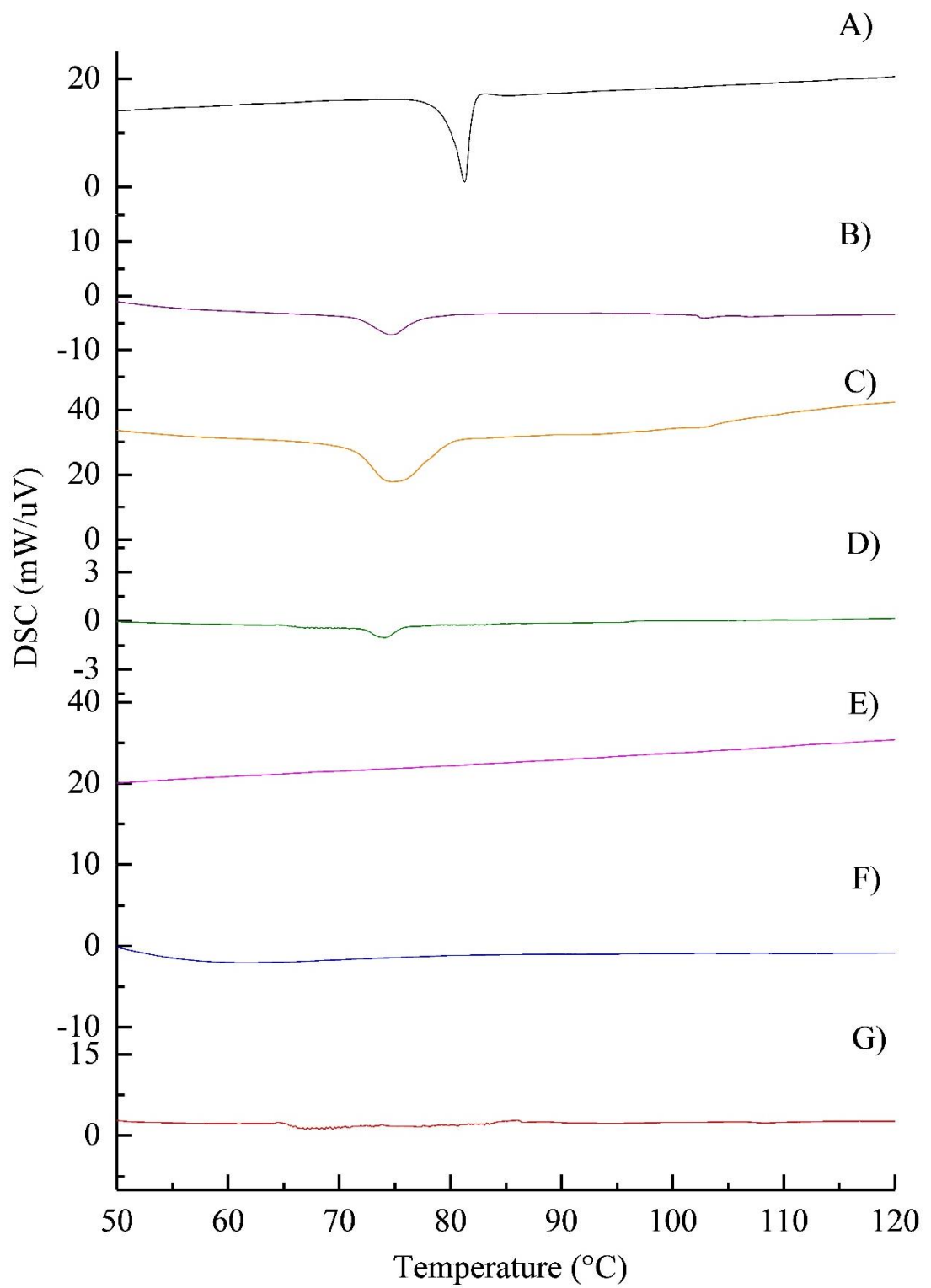


Figure 28: Differential scanning calorimetry of printed (A) fenofibrate and (B-G) mixtures of fenofibrate:PVP 2:1, 1:1, 2:3, 1:2, 1:3 and 1:4.

As can be observed in Figure 29 and Table 10, much like the XRD results (Figure 25), the layered 1:1 samples behave fairly similarly with the trough being considerably reduced relative to the drug alone. However, the single layer style samples (A and B) exhibit a slight secondary hump which is thought to be due to movement in the pan rather than a secondary event. The trough then reduces with polymer content in the sandwiched style samples. Similar to the XRD results (Figure 25), some crystallinity is retained, as shown by the reduced but not completely lost trough, as the inks are not exposed to the supersaturated atomisation state together. On comparison to the literature, there is very little previous evidence as, since as previously stated in the XRD section of this thesis, the only study existing investigating layering PVP and fenofibrate seems to be Ng et al., which unfortunately does not include a DSC measurement (Ng et al. 2013). As such this is a novel study and set of results.

Table 10: DSC peak and peak enthalpy Fenofibrate printed alone and layered with PVP K30

Drug:Polymer Ratio	Peak (°C)	Peak Enthalpy (J/g)
1:0	79.4	-92.11
1:1 (PVPFNF)	78.7	-26.91
1:1 (FNFPVP)	79.5	-37.32
1:1 (sandwiched FNF)	79.4	-26.11
1:2	79.2	-25.91
1:3	78.9	-32.56
1:4	79	-34.99

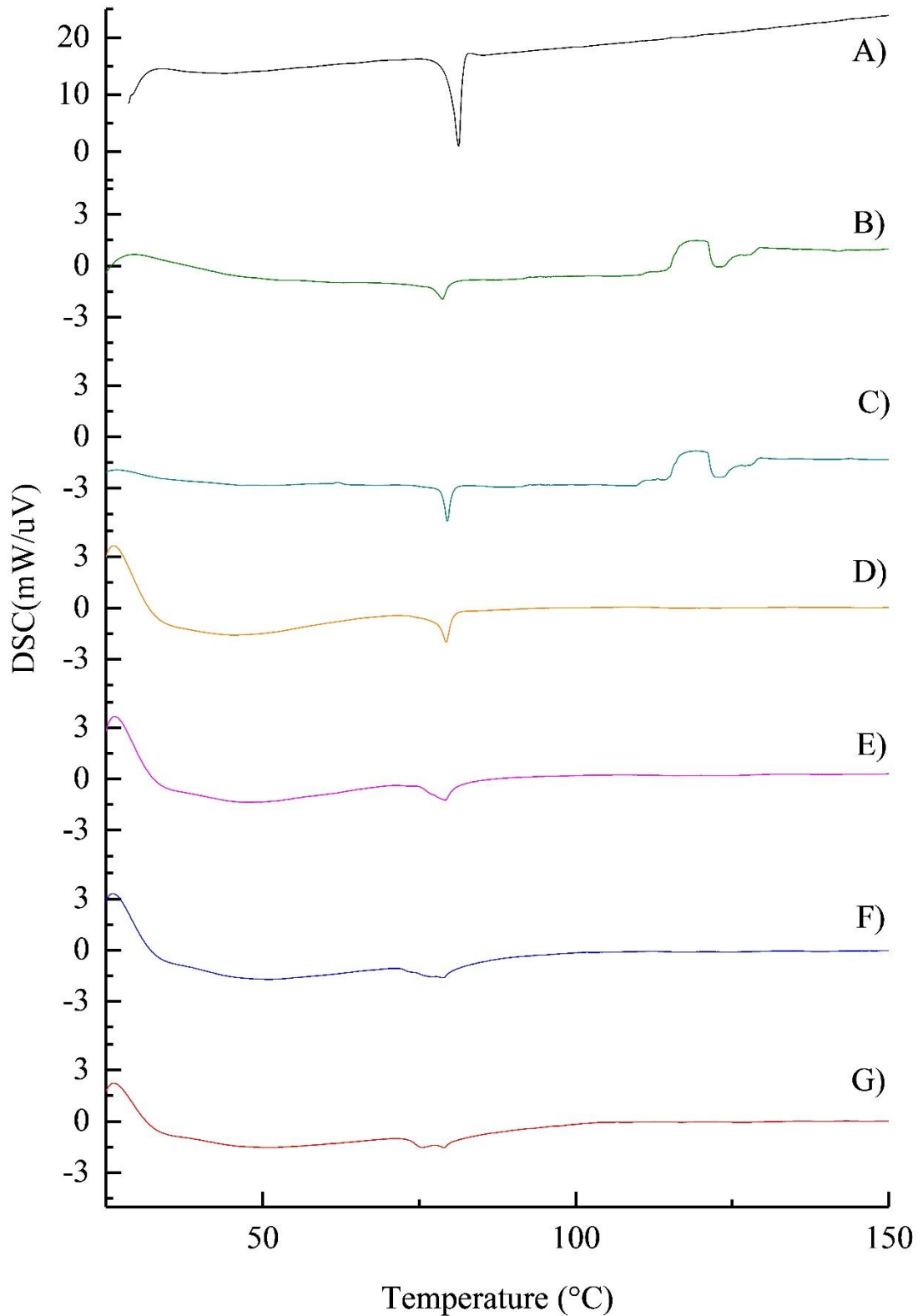


Figure 29: Differential scanning calorimetry of printed fenofibrate and layered printed samples as follows: (A) fenofibrate alone and fenofibrate:PVP (B) 1:1 PVP printed first, (C) 1:1 FNF printed first and (D-G) sandwiched 1:1, 1:2, 1:3 and 1:4.

2.3.3.2 Ibuprofen

Initially powdered ibuprofen was compared to physical mixtures of the API with PVP (Figure 30 and Table 11). The crystalline trough is observed to decrease in size with increasing polymer content but even at ibuprofen:PVP 1:4 the trough is not fully lost, suggesting the crystallinity is retained as a solid dispersion is not formed.

Table 11: DSC peak and peak enthalpy ibuprofen powder alone and physical mixtures with PVP K30

Drug:Polymer Ratio	Peak (°C)	Peak Enthalpy (J/g)
1:0	77.3	-171.76
1:1	74.6	-113.22
1:2	74.3	-46.37
1:3	74.6	-45.77
1:4	74.3	-7.45

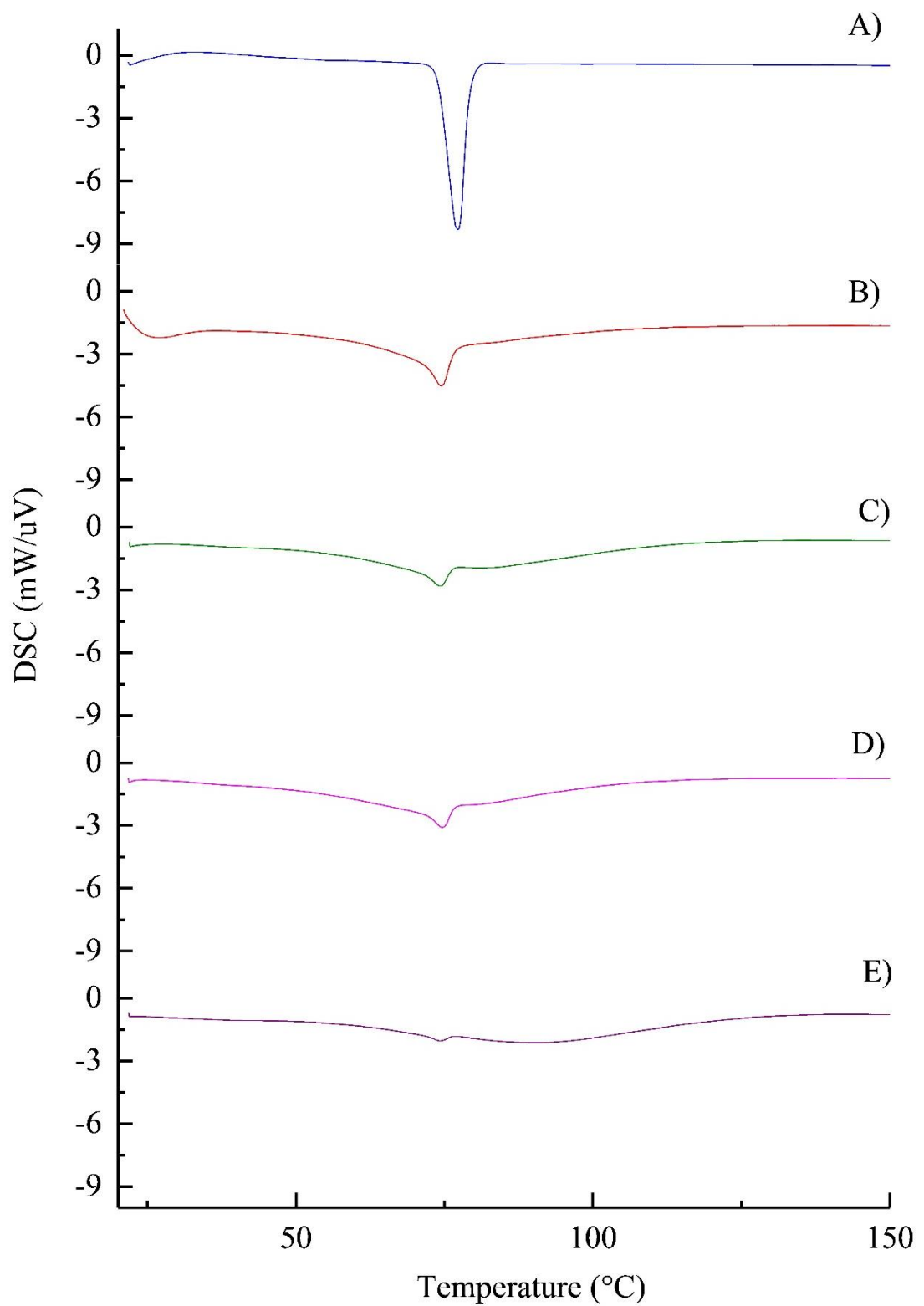


Figure 30: Differential scanning calorimetry of (A) ibuprofen powder and (B-E) physical mixtures of ibuprofen:PVP 1:1, 1:2, 1:3 and 1:4.

Similar to the XRD results (Figure 26), on printing ibuprofen alone the drug is observed to be fully crystalline (Figure 31 and Table 12). As the polymer is introduced the crystalline trough disappears and a fully amorphous product is produced and any variation in the line is caused by trace solvent evaporation.

Table 12: DSC peak and peak enthalpy ibuprofen printed alone and with PVP K30

Drug:Polymer Ratio	Peak (°C)	Peak Enthalpy (mJ)
1:0	75.5	-117.44
1:1	N/A	N/A
1:2	N/A	N/A
1:3	N/A	N/A
1:4	N/A	N/A

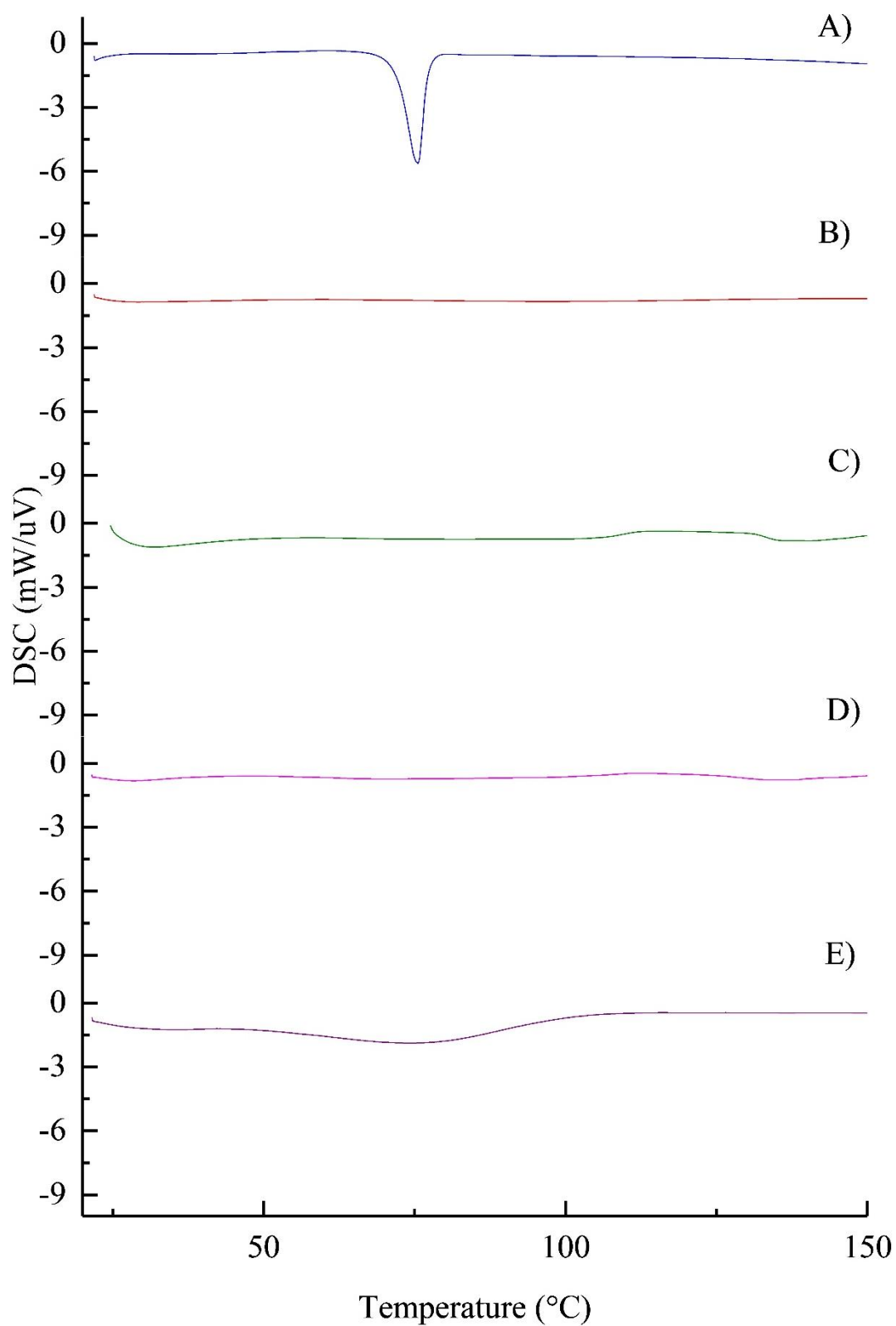


Figure 31: Differential scanning calorimetry of printed (A) ibuprofen and (B-E) mixtures of ibuprofen:PVP 1:1, 1:2, 1:3 and 1:4.

On comparison to the literature, papers on spray drying of ibuprofen and a co-former result in very similar DSC results. Like the XRD results, Li et al. produced a complete loss of the crystalline trough using gelatine and Shen et al. achieved a similar effect using SBA-15 (Li, Oh, et al. 2008, Shen et al. 2010, 2011). Melzig et al. achieved a similar effect using polysorbate 80 but only in the aqueous nanosuspension phase as the final product was not analysed in this manner (Melzig et al. 2018).

2.3.4 Raman Spectroscopy

Raman spectroscopy (Figures 32 and 33) demonstrates the major signals responsible for the loss of fenofibrate crystallinity observed in the XRD and DSC samples. Initially comparing the drug alone to the polymer and the drug-polymer printed mixtures (Figure 32) it can be observed that the distinct fenofibrate peaks decrease in size relative to the PVP peaks as the polymer content increases, reflecting the increasing polymer concentration, similar to the crystalline peaks observed in the XRD and DSC samples. Looking more closely (Figure 33), changes in the terahertz, 1130-1160 cm^{-1} , 1500-1650 cm^{-1} and 3050-3100 cm^{-1} regions can be observed. This suggests changes are occurring in the crystal lattice vibrations, the carbonyl stretching region, the C16-O3 stretching region, and the CH stretching region respectively. In particular the 1150 cm^{-1} peak is associated with methyl group bending within the C16-O3 stretch at C12 and C17, and the 1656 cm^{-1} peak is associated with C1=O4 stretch. In Figure 32 it can be observed that the latter fenofibrate terahertz peak and the definition in the 3050-3100 cm^{-1} region is lost as the peak broadens after addition of 60% PVP. The latter effect may be due to bond rotations in the aliphatic region of the molecule (Heinz et al. 2009). The 1500-1650 cm^{-1} region smooths, broadens and decreases in size on addition of 75% PVP. Additionally, the 1650 cm^{-1} peak shifts to 1656 cm^{-1} and the 1147 cm^{-1} peak shifts to 1150 cm^{-1} . These regions have been shown to change on formation of amorphous material previously with the 1130-1160 cm^{-1} , 1500-1650 cm^{-1} and the 3050-3100 cm^{-1} regions smoothing as the bonds stretch (Heinz et al. 2009).

Previously the change from crystalline to amorphous fenofibrate has been established to be due to a mixture of hydrogen bonding and non-hydrogen bonding interactions. The former is associated with the carbonyl bonds represented by the 1650cm^{-1} region (Sailaja et al. 2016). Van der Waals forces may also govern the interaction between the carbonyl group and the acidic CH group (Tipduangta and Pharm 2016).

Inkjet printing has demonstrated the formation of amorphous material in Raman studies previously. For example piezoelectric printing has been used previously to generate amorphous products detectable by Raman spectroscopy from w/w 0.50% Irgacure 2959 photoinitiator, 30%, 2.00 % ropinirole HCl and polyethylene glycol diacrylate (Clark et al. 2017).

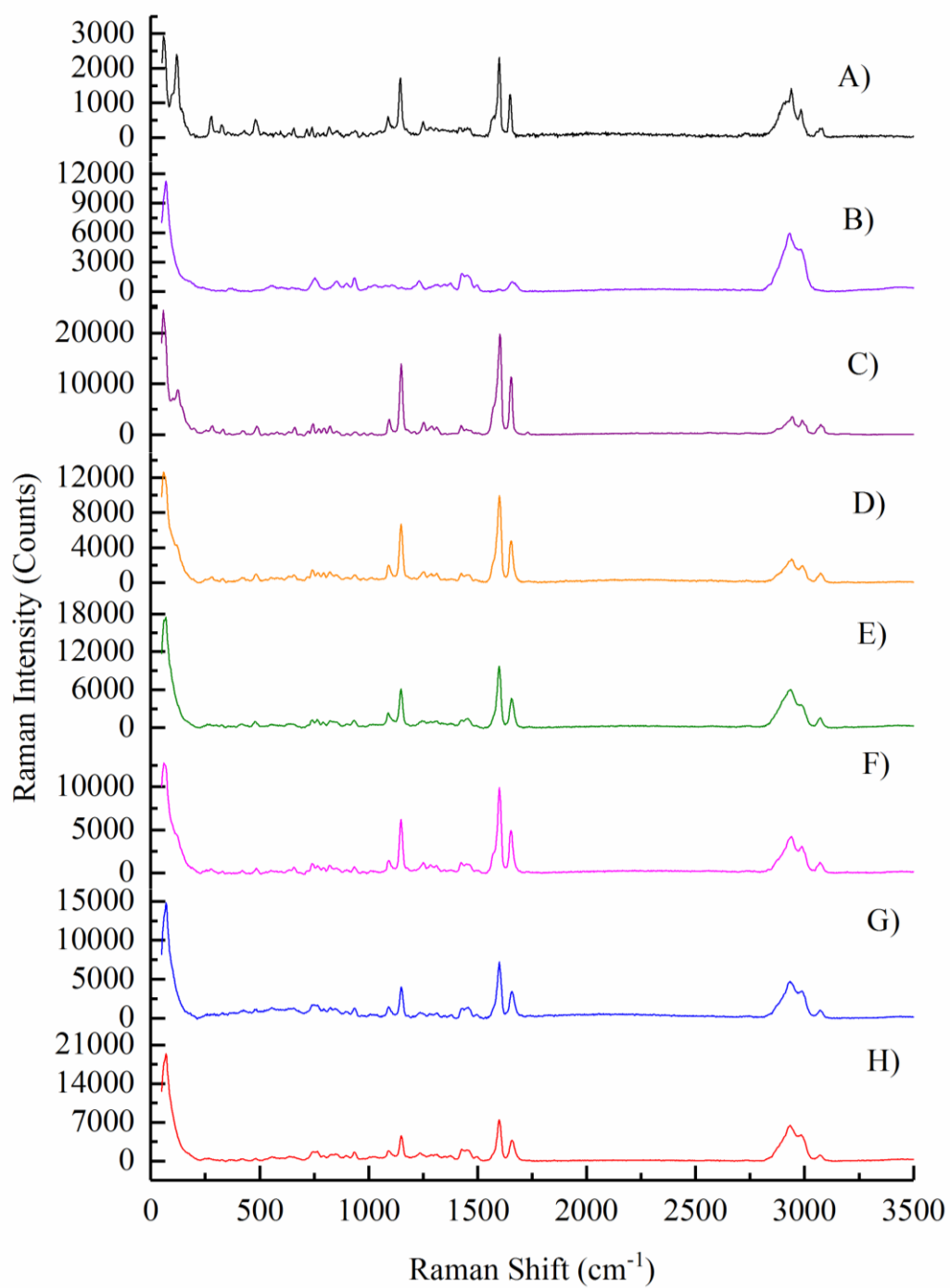


Figure 32: Raman spectra of fenofibrate and PVP K30 based printed samples: (A) fenofibrate, (B) PVP K30, (C-H) 2:1, 1:1, 2:3, 1:2, 1:3 and 1:4 fenofibrate:PVP K30.

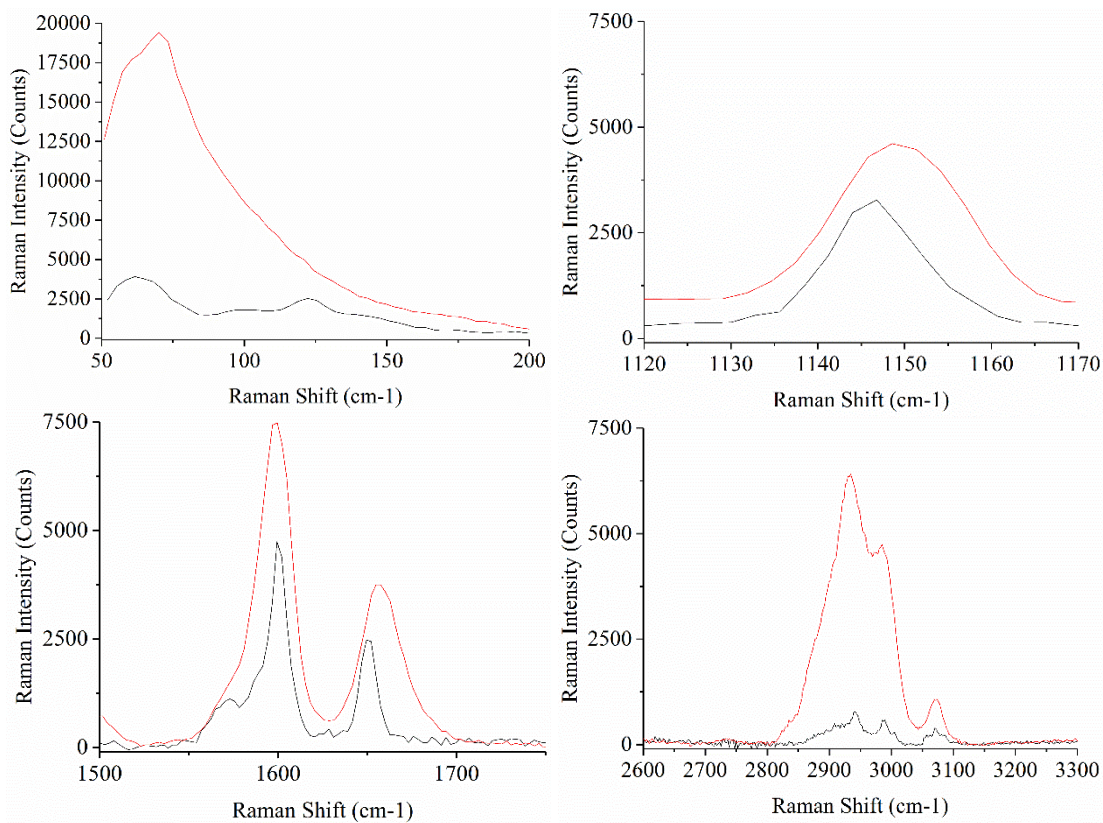


Figure 33: Raman spectra of fenofibrate alone in raw powder form (black) and as part of an inkjet printed 1:3 fenofibrate:PVP solid dispersion (red) showing the terahertz (top left), 1130-1160 cm^{-1} (top right), 1550-1700 cm^{-1} (bottom left) and 2700-3200 cm^{-1} regions (bottom right).

2.3.5 Scanning Electron Microscopy

2.3.5.1 Polymers

PVP 1000, K30 and K90 were printed as 1, 2, 3 and 4 layer samples initially to compare the effect of printing different molecular weights on the structures formed. In Figure 34, it can be observed that printing PVP 1000 results in a very scant distribution of particles until 4 layers are printed. This is believed to be due to its low viscosity resulting in small particles of less than 5 μ m. Additionally, it can be observed that PVP K90 also resulted in a very scant distribution of particles, suggesting the viscosity of this ink has been too high for the printer resulting in less deposition overall. In Figure 35, the effect of printing PVP K30 can be observed. Consistent spherical particles, which were smaller overall than that of K90, were achieved, reflected in the fact that the printer very seldom blocked with this ink. It can be observed how layering PVP K30 alters the structure of the deposition. Starting from a very porous single layer, the spherical particles become more and more tightly packed with each additional layer. As this ink proved the most reliable, this form of the polymer was taken forward. In Figure 36, the effect of changing the concentration of the starting ink was analysed. As can be observed the structure changes from very scant, spread out small particles which are less than 5 μ m in size on application of 15mg/ml PVP in ethanol, gradually increasing in size until nearly 10 μ m particles were produced on application of 120mg/ml PVP in ethanol was applied. On comparison with the rheology work (Figures 15 and 16), it is thought the overall density and particle size increases with viscosity.

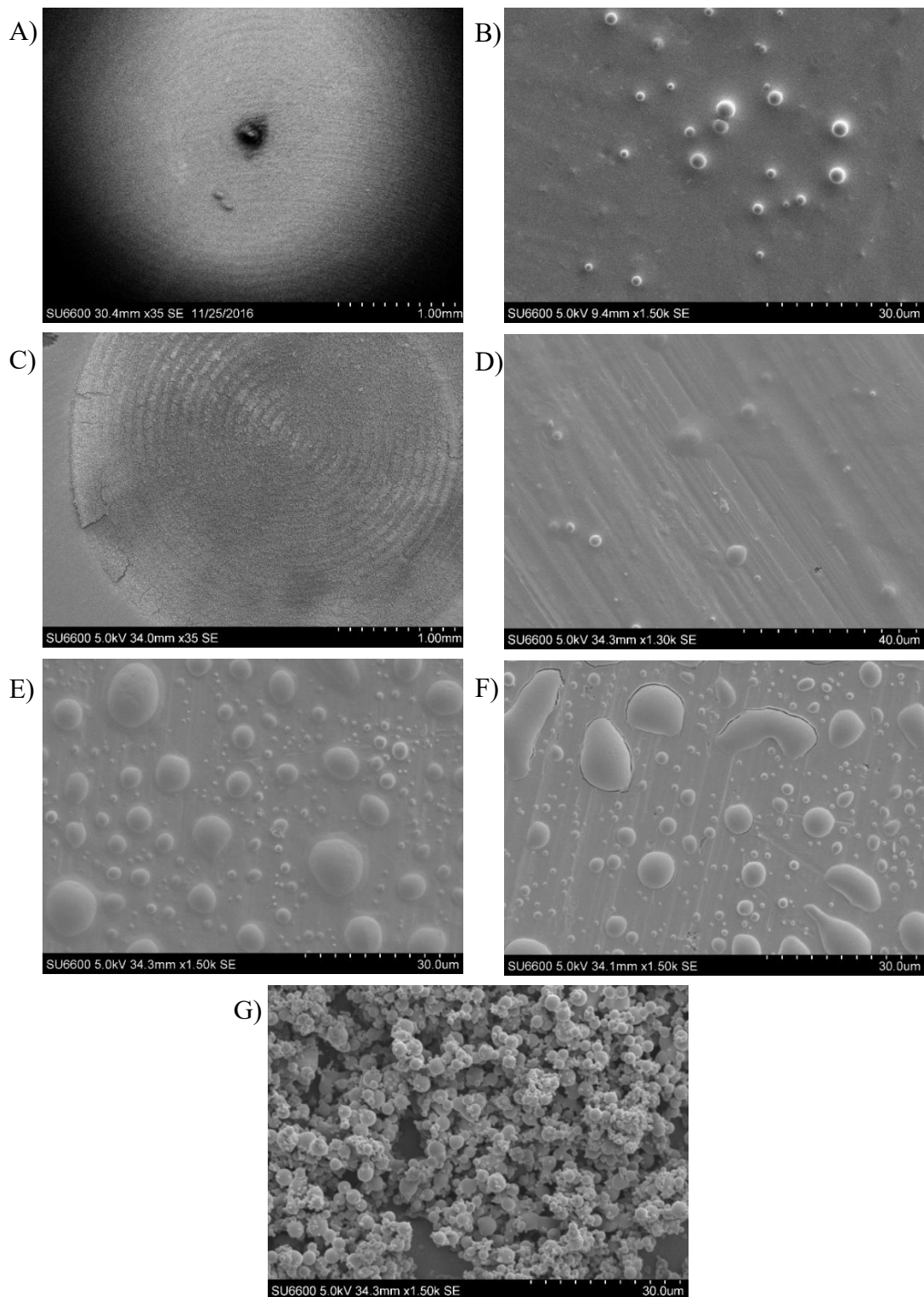


Figure 34: SEM of 2mm samples of PVP K90 4 layers at (A) x35 magnification and (B) x1.5K magnification and 2mm samples of PVP 10,000 (C) 4 layers at x35 magnification, (D) 1 layer at x1.3K magnification, (E) 2 layers at x1.5K magnification, (F) 3 layers at x1.5K magnification and (G) 4 layers at x1.5K magnification.

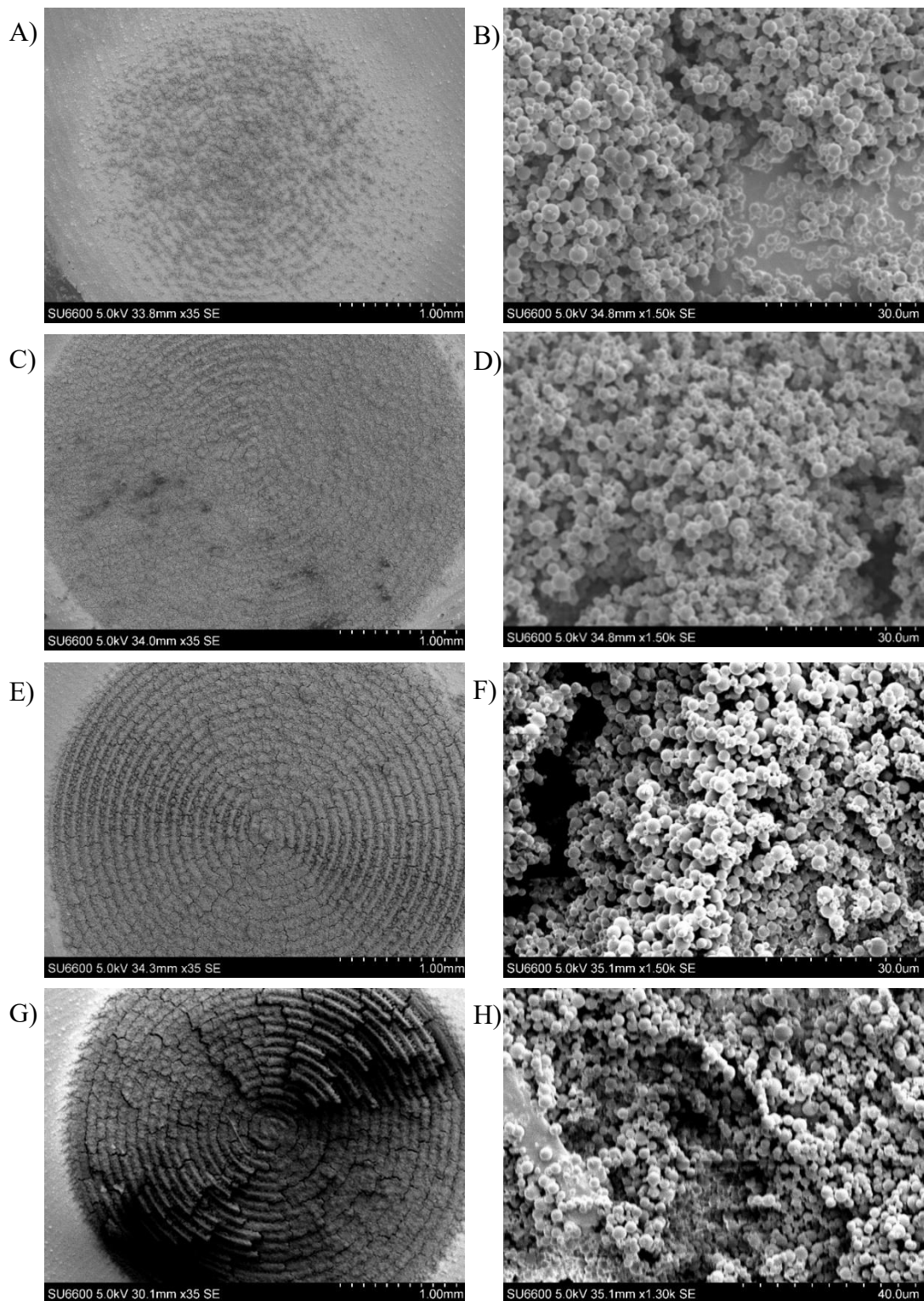


Figure 35: SEM of 2mm samples of PVP K30 (A) 1 layer x35 magnification, (B) 1 layer x1.5K magnification, (C) 2 layers x35 magnification, (D) 2 layers x1.5K magnification, (E) 3 layers x35 magnification, (F) 3 layers x1.5K magnification, (G) 4 layers x35 magnification and (H) 4 layers x1.5K magnification

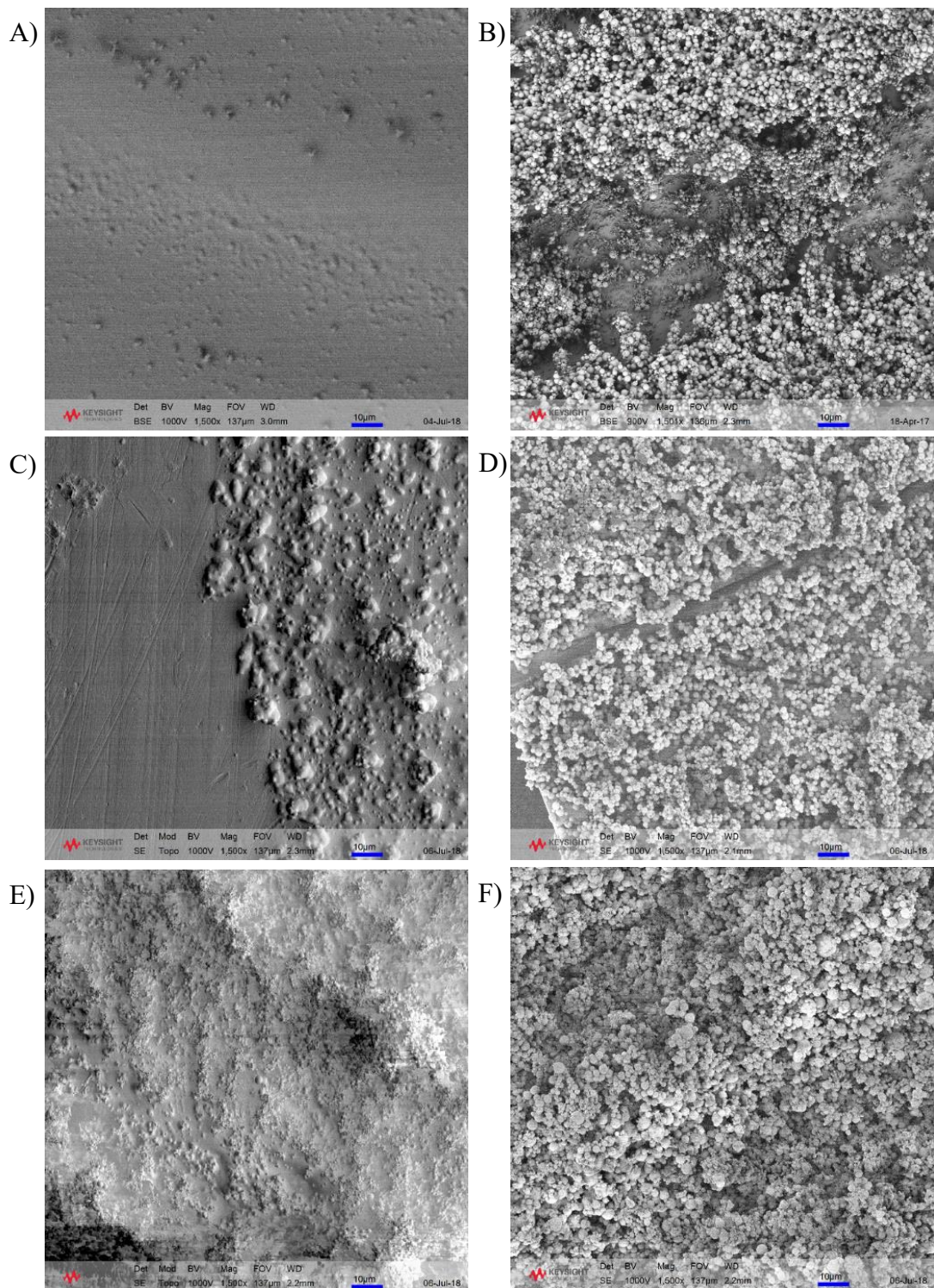


Figure 36: SEM of PVP K30 with different starting ink concentrations taken at x1.5K magnification – (A)15mg/ml, (B) 30mg/ml, (C) 45mg/ml, (D) 60mg/ml, (E) 90mg/ml and (F) 120mg/ml

2.3.5.2 Fenofibrate

2.3.5.2.1 Fenofibrate vs. Premixes

Observing the formulations at x1.5K magnification (Figure 37), it can be observed the formulations with lower concentrations of PVP as stated previously continue to exhibit a degree of crystallinity, with the addition of 33% polymer resulting in a change from driftwood-like crystalline particles to more plate-like and elongated crystals. On addition of 50% polymer the drug starts to form cuboidal crystalline particles of more than 10µm and squamous crystalline particles of approximately 5µm with a light covering of polymer. On addition of 60% polymer the drug starts to agglomerate more with large crystalline particles and some more amorphous looking particles. The individual amorphous particles are typically 5µm or less but on agglomeration with each other they form masses of more than 10µm. The crystalline particles are cuboidal and as large as 20 or 30µm in length. However, on increasing the concentration of the formulation to 67% polymer the formulation starts to look more amorphous with a slight crystallinity present. The amorphous particles are largely less than 5µm. Ultimately on addition of 75% and 80% polymer the formulation is fully amorphous as characterised by spherical particles throughout. On addition of 75% polymer, the particle size is typically about 5µm or less but on addition of 80% polymer the particles are mostly about 5µm or larger. Higher magnification images can be observed Appendix 1.

Higher viscosity has been shown previously to result in larger droplets. Furthermore, it has been demonstrated previously in spray drying that particle size distribution is a function of the droplet size. Sander demonstrated parallel curves for droplet size and particle size with the curve moving to the left as the solvent dries (Sander 2014). This appears to be the case here, with 1:3 fenofibrate:PVP exhibiting larger particles than 1:1 and 1:2 fenofibrate:PVP, and 1:4 fenofibrate:PVP exhibiting larger agglomerates. The agglomeration of the latter may explain why less material is deposited overall for 1:4 fenofibrate:PVP, as it may be reasonable to assume that the agglomerated particles will not flow as easily through the nozzle cavity as smaller individual particles.

There are a number of papers showing this formation of amorphous spherical particles. Fenofibrate and PVP has demonstrated this effect previously on solvent evaporation with the generation of amorphous particles using a 1:1 ratio of drug: polymer in ethanol (Choi, Lee, et al. 2013). The formation of mixed crystalline and spherical amorphous particles has also been demonstrated previously with spray drying of a solution with too low a PVP concentration to result in full amorphous material formation in a paper by Yousaf et al (Yousaf et al. 2015). However, inkjet printing has not demonstrated formation of spherical amorphous particles with fenofibrate previously. For example inkjet printing has been used in combination with amorphous nanoparticle formation of ciprofloxacin with dextran sulphate suspended and mixed with polyethylene glycol resulting in spherical particles as demonstrated by SEM (Cheow et al. 2015). The closest inkjet printing paper to the current work is a study by Scoutaris et al. featuring piezoelectric inkjet printing of felodipine and PVP in an ethanol:DSMO 95:5 solution resulting in amorphous material as demonstrated by TOF-SIMS. However, unlike the current study it was found extended spray times resulted in the amorphous state being lost (Scoutaris et al. 2011). Interestingly, there is no prior literature with the degree of control over the particles formed with different concentrations as in the current study. As such the current study is relatively novel.

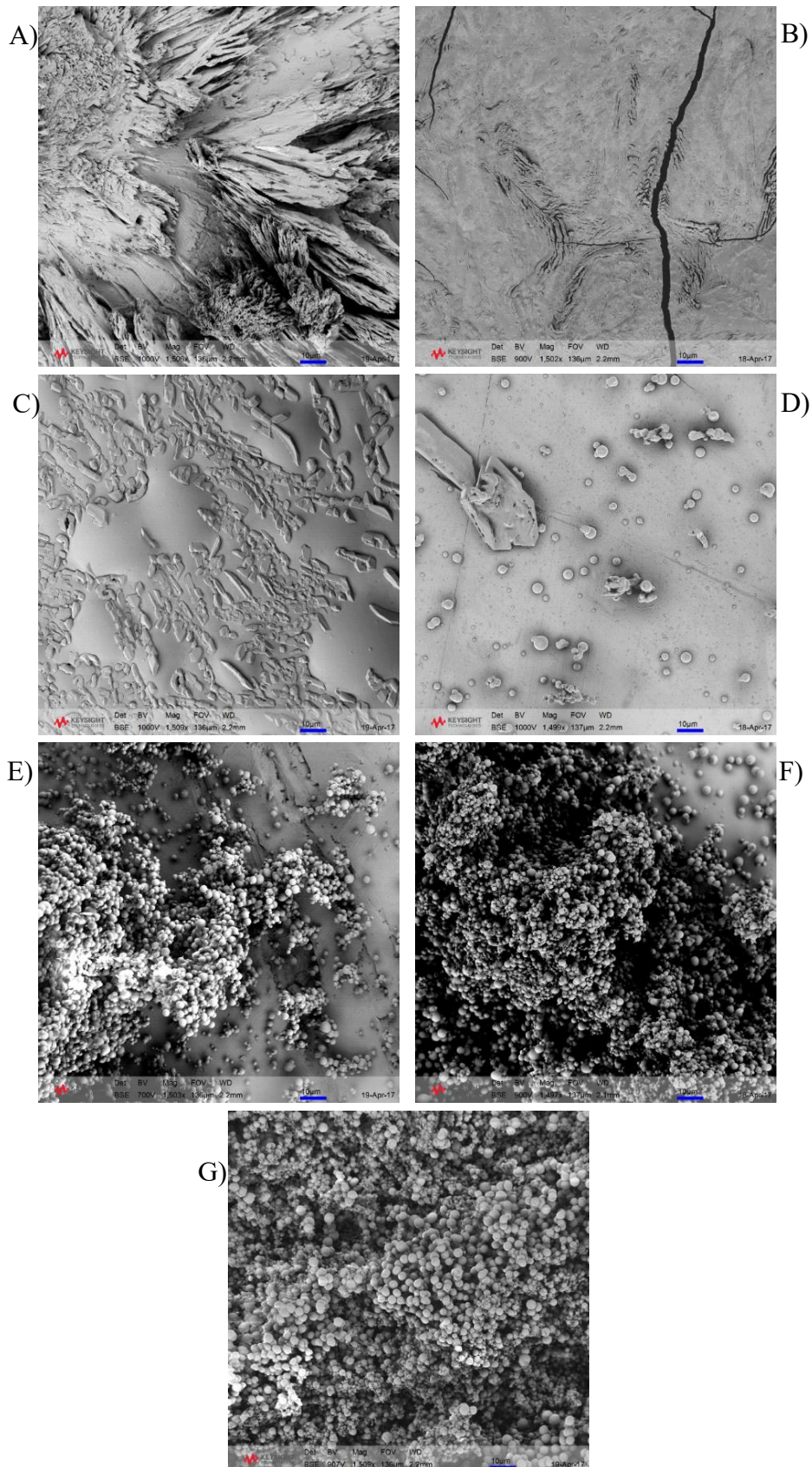


Figure 37: SEM of printed fenofibrate and PVP mixtures taken at x1.5K magnification – (A) FNF, (B) 2:1, (C) 1:1, (D) 2:3, (E) 1:2, (F) 1:3 and (G) 1:4 FNF:PVP.

2.3.5.2.2 *Layered*

On layering (Figure 38), the SEM images exhibit a mixture of crystalline and amorphous particles with the distinct areas of PVP and fenofibrate quite apparent. Additionally, there is evidence of agglomeration on the crystalline particle surface. There is evidence of interactions with the particles transitioning at the interface. This supports the reduced crystallinity observed in the XRD and DSC data (Figures 25 and 29).

On comparison to the literature, there is only one previous paper investigating the effect of layering films of PVP and fenofibrate. Although it is based around spin coating, there are similar particle morphologies observed with striated crystals. However, there is less evidence of amorphous material which may be attributed to the absence of the atomisation step (Ng et al. 2013).

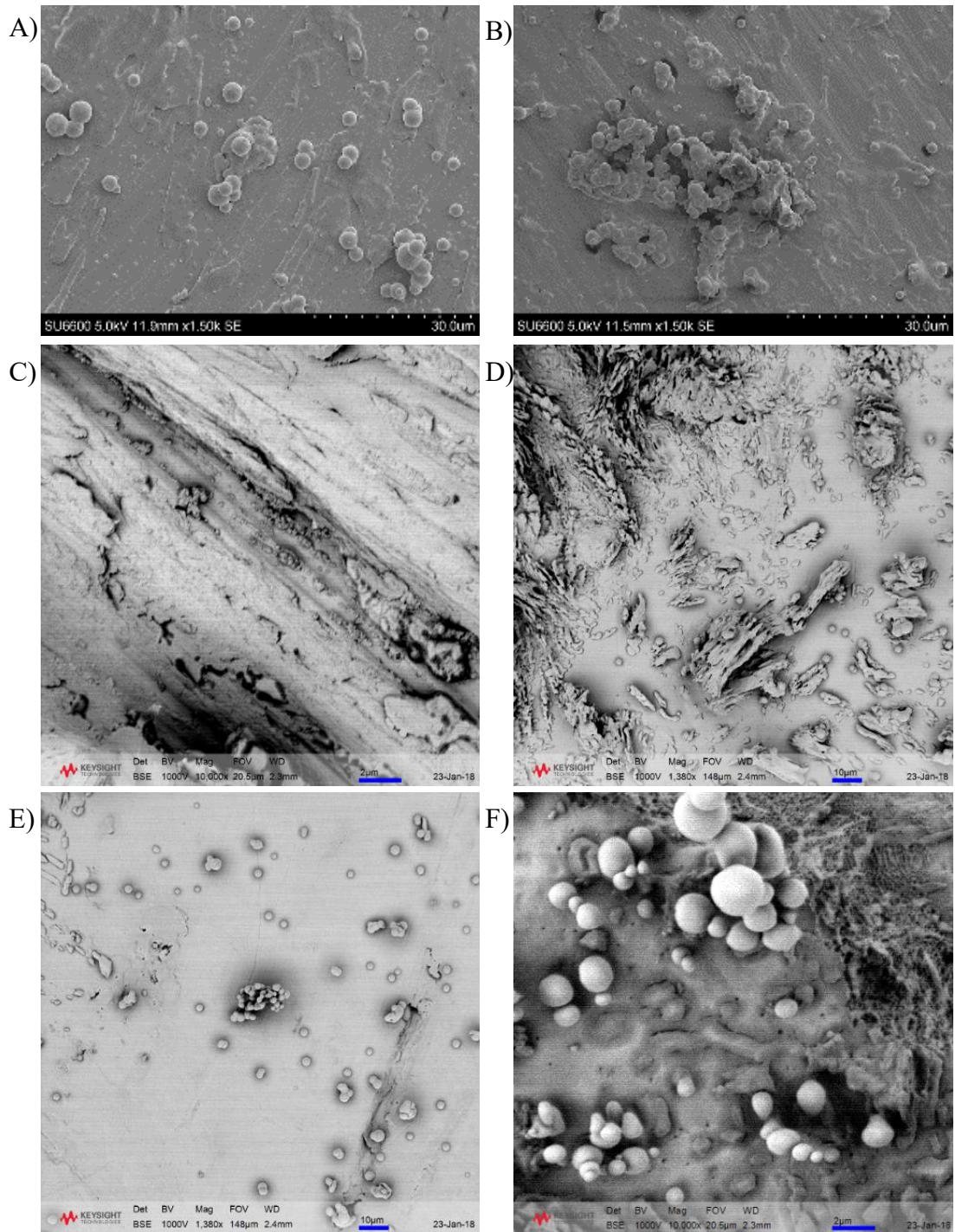


Figure 38: SEM of fenofibrate:PVP layered samples – (A) 1:1 PVP printed first, (B) 1:1 fenofibrate printed first, (C) 1:1 sandwiched, (D) 1:2 sandwiched, (E) 1:3 sandwiched and (F) 1:4 sandwiched taken at x1.5K.magnification.

2.3.5.2.3 Torus

On printing tori (Figure 39), interfaces between the drug and polymer can be observed, with the polymer coating the crystalline particles and forming adjacent amorphous particles. There is a fusing appearance to the particles at the interface with a mixture of agglomerates.

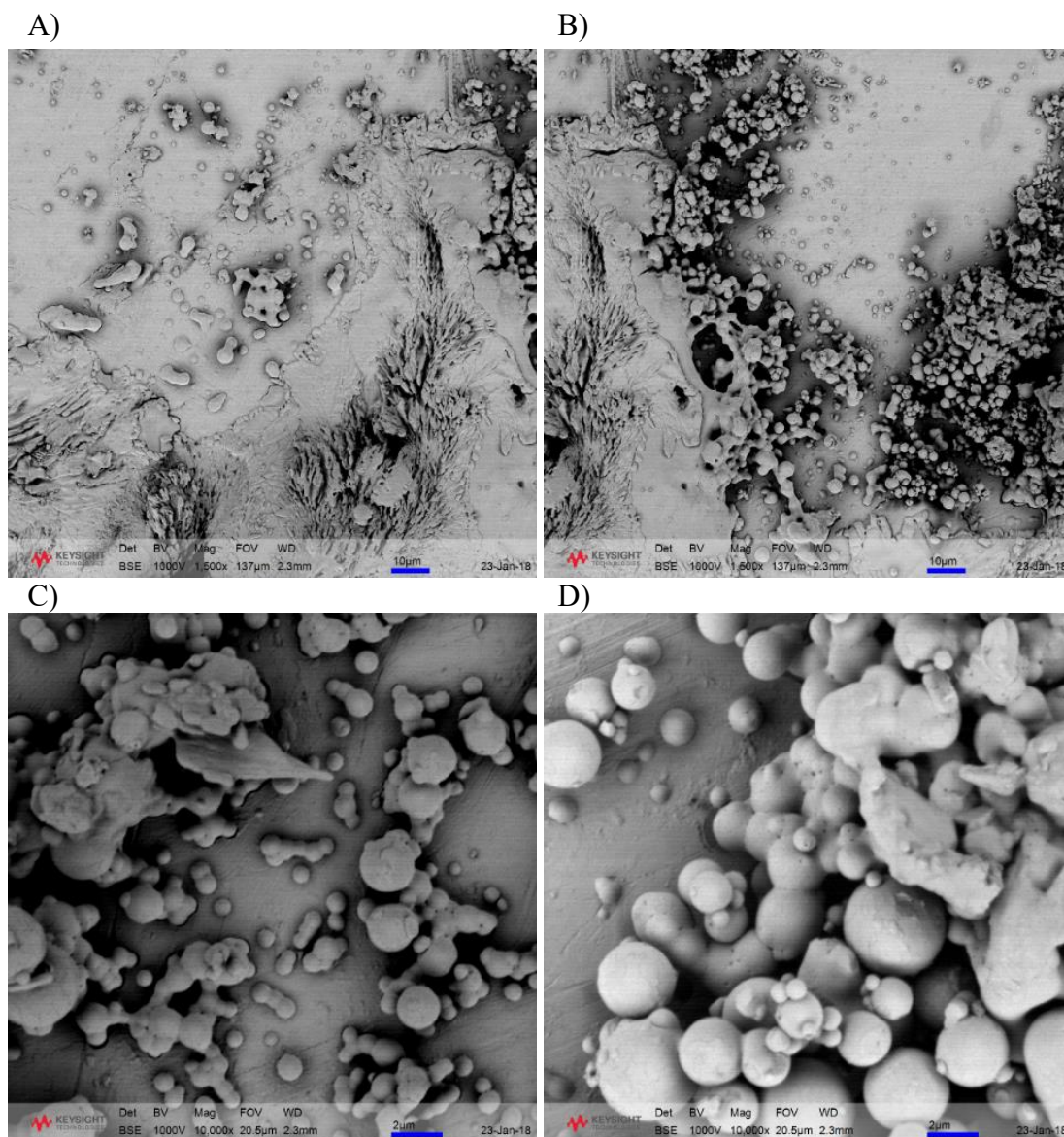


Figure 39: SEM of tori style printed samples with fenofibrate and PVP printed separately taken at (A and B) x1.5K and (C and D) x10K.

2.3.5.3 Ibuprofen

As can be observed in Figure 40, printing drug alone once again results in a fully crystalline product with mountain range like features being observed. On addition of polymer, supporting the XRD and DSC results (Figures 26 and 31), fully amorphous spherical particles are observed. 1:1 ibuprofen:PVP initially shows quite sparse, flat particles between 2 and 10 μ m, 1:2 ibuprofen:PVP shows more closely distributed particles about 5 μ m overall mixed with a few small agglomerates, 1:3 ibuprofen:PVP shows more closely distributed flat larger particles between 5 and 10 μ m and 1:4 ibuprofen:PVP ultimately shows densely packed spherical particles about 1 to 5 μ m and some agglomeration. The particles generated are smaller than that of fenofibrate:PVP 1:4 which may suggest the overall droplet size is smaller and thus explain why this type of ink was easier to print.

On comparison to the literature, the most similar data is that achieved by spray drying. Shen et al. demonstrated the effect of co-spray drying ibuprofen and mesoporous SBA-15 with ethanol. Interestingly, due to the more squamous nature of the co-former their amorphous particles were more squamous than spherical but the effect is still comparable (Shen et al. 2010, 2011). Interestingly on utilising a loose pore version of the SBA-15 the particles formed agglomerates similar to the particles achieved in the current study (Shen et al. 2011). Li et al. achieved very similar spherical particles to the current study by co-spray drying with gelatine and ethanol, as did Melzig et al. with polysorbate 80 and ethanol (Li, Oh, et al. 2008, Melzig et al. 2018).

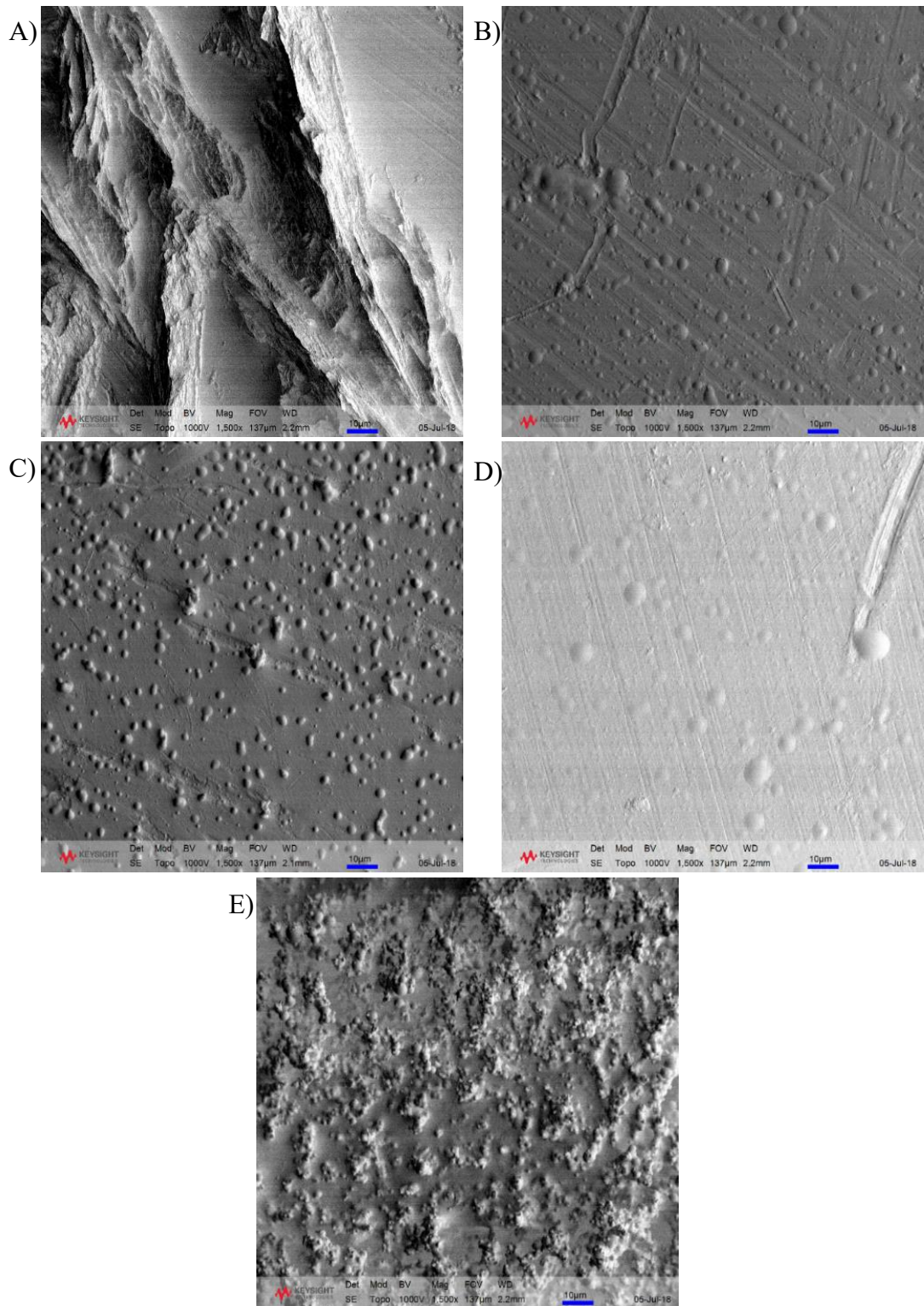


Figure 40: SEM of printed (A) ibuprofen, and ibuprofen:PVP (B) 1:1, (C) 1:2, (D) 1:3 and (E) 1:4 taken at x1.5K magnification.

2.3.6 Size Exclusion Chromatography

Figure 41 demonstrates the effect of printing on the molecular weight distribution of PVP K30. The chromatographs for both printed and raw PVP K30 are nearly identical in nature suggesting there is little effect on the polymer. On analysis of the data, it can be observed in Table 13 that the M_n , M_w , M_z and M_n/M_w are very similar confirming printing has little effect on the polymer. On performing a T-test without the Welch correction only the M_n and molecular weight distribution values are found to be statistically non-significant. On performing a Welch correction all but the M_z were found to be statistically non-significant. This implies processing does not affect the tensile or impact strength and the brittleness of the material.

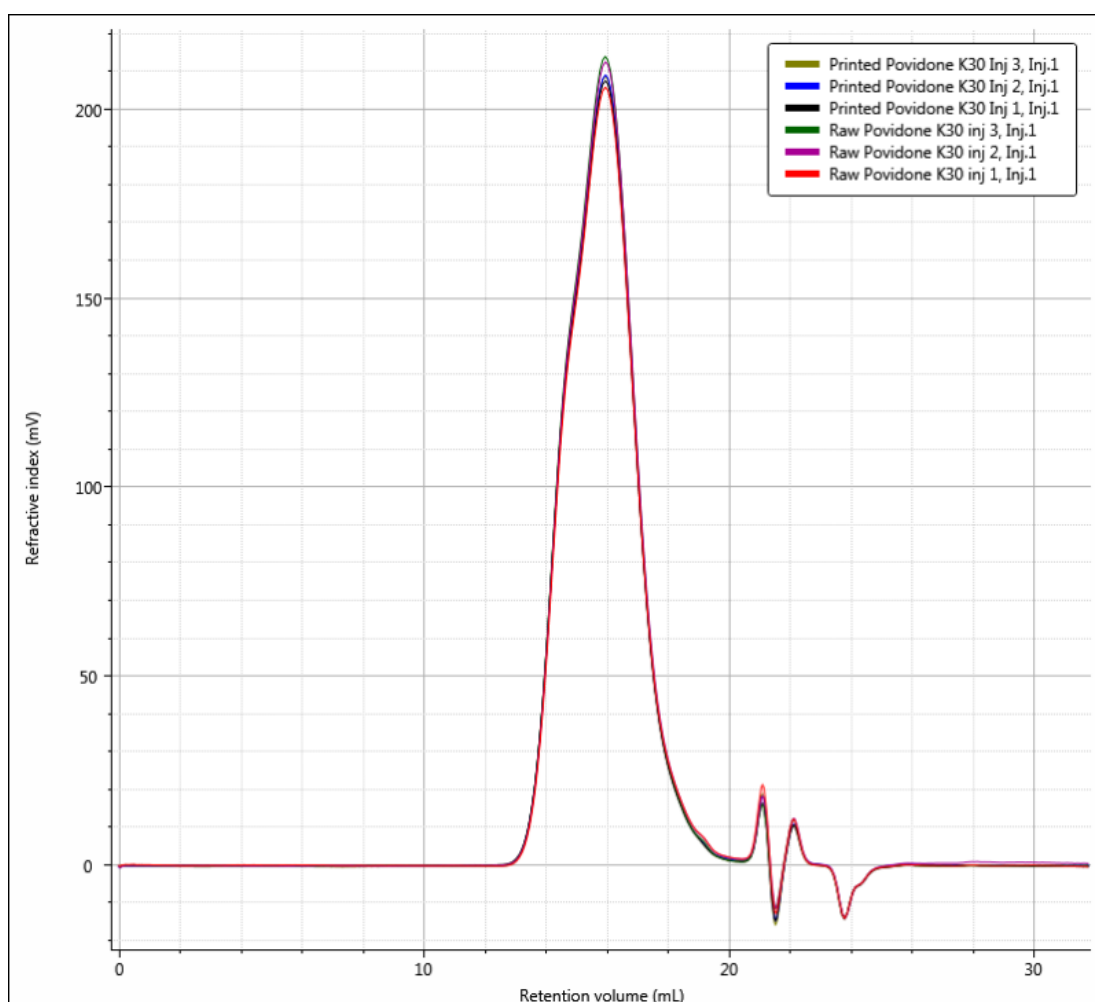


Figure 41: Size exclusion chromatograph of raw and printed PVP where $n=3$. The colours representing each sample are shown in the legend.

Table 13: Size exclusion chromatography results

Parameter	Raw Powder (n=3)	Standard Error	Printed Sample (n=3)	Standard Error	T-test	T-test (Welch Correction)
Mn (g/mol)	26,670	1,657.84	25,420	525.39	Non-significant	Non-significant
Mw (g/mol)	61,833	839.77	64,613	366.71	Significant	Non-significant
Mz (g/mol)	150,667	733.33	160,800	503.32	Significant	Significant
Mw/Mn	2.332	0.11	2.544	0.04	Non-significant	Non-significant

On comparison with the literature, it can be said that aerosol jet is potentially less damaging than other polymer processing techniques. Previous studies have demonstrated polymer degradation during processing. For example Wheeler et al. showed continuous inkjet printing of polymethyl methacrylate using a Dimatix DMP-2800 resulted in a reduction in molecular weight as a result of mechanochemical degradation (Wheeler et al. 2014, 2016). Additionally, Alexy et al. demonstrated degradation of polyvinyl alcohol on thermal exposure by extrusion, which is relevant as many solid dispersive techniques such as hot melt extrusion and injection moulding are subjected to similar conditions. In this case the molecular weight increased with each pass through the extruder (Alexy et al. 2004).

2.4 Conclusions

Ink solutions were found to increase in viscosity with polymer content. Printing either fenofibrate or ibuprofen alone seemed to result in a fully crystalline product. For fenofibrate, on addition of polymer the crystallinity was observed to reduce with a fully amorphous product generated when the drug was premixed with 75% PVP or more as demonstrated by Raman spectroscopy, DSC and XRD. Additionally, this was observed to have considerable effects on the morphology as demonstrated by SEM with the amorphous material exhibiting spherical particles. The particle size seemed to increase with viscosity which may be explained by the effect of viscosity on atomisation. On layering without premixing, the crystallinity is reduced but not to the same degree as premixing. Interestingly, for ibuprofen, on addition of as little as 50% polymer within a premixed ink, an amorphous product is formed as demonstrated by SEM, DSC and XRD. Interestingly, there is no prior literature with the degree of control over the particles formed with different concentrations as in the current study. This suggests the aerosol jet printer presents greater control over solid state than seen previously. Additionally, the effect of printing on the polymer was analysed and fortunately the act of printing seemed to have minimal effects on the physical state of the polymer and thus any other effects should be comparable to physical mixtures. This may also suggest that aerosol jet printing is less damaging than some other solid dispersive techniques. The capabilities of the printer will be explored in Chapter 3.

Chapter 3: Aerosol Jet Printer Capabilities

3.1 Introduction

The current chapter is concerned with the capabilities of the aerosol jet printer as this technique has never been used in pharmaceutical manufacturing previously. Utilising the inks developed in Chapter 2, a number of parameters can be tested. As the printer has the flexibility of a free moving stage and a range of nozzle sizes, in addition to its ability to be programmed, the current chapter investigates the ability of the printer to achieve scalable and precise deposition patterns. Scalability was investigated by changing the area of deposition designed on AutoCAD, the nozzle size utilised, the speed of deposition selected and the number of layers deposited. Precision was investigated using TOF-SIMS and Raman mapping.

3.2 Materials and Methods

3.2.1 Materials

As in Chapter 2

3.2.2 Methods

3.2.2.1 Dosage Form Construction

3.2.2.1.1 Scalability

Scalability was tested by programming different shapes and sizes precisely using AutoCAD 2015 and running them using KEWA Motion 2.5.0. The effect of speed was tested by varying the speed settings on KEWA Motion 2.5.0. Different nozzle sizes ranging between 150 and 300 μm were utilised to generate different sized lines from the same ink using the same AutoCAD file. Samples were tested for content using UHPLC to test for a linear relationship between nozzle size, and the size and/or speed of deposition and dose.

3.2.2.1.2 Ultra High Pressure Liquid Chromatography

3.2.2.1.2.1 Method Selection

Initially the British Pharmacopoeia method at 286nm (British Pharmacopoeia Commission, 2018) was used but due to issues with curve uniformity and degradation of the samples a method selection study was performed running samples as shown in Table 14 (calibration curve in Appendix 2). The detection wavelength was changed to 280nm to reflect the SDI studies (Chapter 4). Additionally, the average retention time was found to have a standard deviation of 0.25 minutes amounting to only 3.7% variation.

Table 14: UHPLC method selection parameters and effects

Method	Mobile Phase (ACN: Acidified Water)	Diluent	Temperature	Flow (ml/min)	Observations
1 (BP)	70:30	Mobile phase	25°C	1 ml/min	Noisy and sloping baseline with additional peaks, average retention time 1.983

2	70:30	Acetonitrile	25°C	1 ml/min	Some noise and sloping baseline, average retention time 2.082
3	70:30	Mobile phase	25°C	0.5 ml/min	Noisy baseline with additional peaks, average retention time 11.581
4	70:30	Acetonitrile	25°C	0.5 ml/min	Noisy baseline, average retention time 11.884
5	70:30	Mobile phase	30°C	1 ml/min	Noisy baseline with additional peaks, average retention time 1.191
6	70:30	Acetonitrile	30°C	1 ml/min	Noisy baseline, average retention time 1.467
7	80:20	Mobile phase	25°C	1 ml/min	Additional peaks,

					average retention time 6.672
8	80:20	Acetonitrile	25°C	1 ml/min	Flat baseline, similar to literature (Sahoo et al. 2014), average retention time 6.589
9	Gradient (30:70, 50:50, 70:30, 100:0 ACN:Water)	Mobile phase	25°C	1 ml/min	Very noisy baseline with extra peaks, average retention time 15.708
10	Gradient (30:70, 50:50, 70:30, 100:0 ACN:Water)	Acetonitrile	25°C	1 ml/min	Very noisy baseline with extra peaks, average retention time 15.8

3.2.2.1.2.2 Sample Analysis

Ultra High Performance Liquid Chromatography (UHPLC) was carried out using an Agilent 1290 UHPLC, 6530 Q-TOF (Agilent Technologies, Santa Clara, California, USA) at 280 nm with a mobile phase consisting of acetonitrile: acidified water 80:20 running at 1 ml per minute on a C-18(2) 100Å silica reversed phase column. Samples were prepared by printing on rice paper for ease of dissolution and dissolved in 5 or 10ml acetonitrile. Calibration curves covering a range of 5-1000 µg/ml were

produced for each UHPLC session using the area under the curve and concentrations of samples were calculated using the resultant equation of the line (see Appendix 2). UHPLC was used to measure the drug content of the fenofibrate alone and fenofibrate with PVP samples and test for uniformity between samples, as well as for the effects of deposition size, speed, layering and nozzle size. The chromatographs were collected using MassHunter Workstation Software Data Collection and Qualitative Analysis B.07.00. The results were plotted, and statistical analysis was carried out using Origin Pro 2017.

3.2.2.1.3 Laser triangulation for Depth Analysis

Printed samples were analysed by laser triangulation using an LK-H057 (Keyence Corporation of America, Illinois, USA). Samples of each formulation were prepared by printing 5mm circles consisting of 5 layers each on rice paper. Samples were analysed by initially taking a background measurement of the rice paper and then moving the sample so the centre was in line with the laser. Sample height was then collected on the LK-navigator software and compared. The results were plotted and statistical analysis was carried out using Origin Pro 2017.

3.2.2.2 Drug Distribution

3.2.2.2.1 Raman Mapping

Raman mapping was carried out using an H2Optx mPAT 3D Raman spectrometer (H2Optx, San Jose, California, USA). This system holds a significant advantage as it enabled samples to be taken in slices from the same dosage form and stacked to a 3D image and also covers a larger area. The mPAT was run at 754 nm, with a Class 3B laser (Innovative Photonics Solutions, New Jersey, USA) with a 160mA current, 90mW power and 10s exposure time. The instrument was driven using the H2Optx program MetaScan. Samples were measured over a 4mmx4mm area taking readings at 10µm intervals along the x and y-axes in a 6x6 grid. Normally the mPAT would shave the surface of tablets in an automated process but due to the fragile nature of inkjet printed samples compared to standard tablets, samples were sheared using a

diamond blade. Due to the lack of control of manual cutting the exact thickness of slices is unknown but the slices were approximately about half way and three quarters of the original tablet thickness. The 3 layers were measured per sample and the data was fed into the H2Optx program MetaAnalyser and using raw powder reference spectra a base map was generated. This base map was then fed into a company provided Python script to generate the required maps and a pixel value for each substance.

3.2.2.2.2 *TOF-SIMS*

25 layer, 6mm diameter samples were prepared on silicon wafers using the standard 3mm/s, 300 μ m nozzle printing method. Laying down the polymer first, 3 samples were prepared consisting of 4 quintuplicate rings, 18 single rings and 9 double rings respectively. Samples were run on an IONTOF TOF.SIMS V (ION-TOF GmbH, Münster, Germany), based at the Wolfson Foundation Pharmaceutical Surfaces Laboratory in the Technology and Innovation Centre, University of Strathclyde. The instrument is equipped with a Bismuth Liquid Metal Ion Gun (LMIG) and a gridless reflection time-of-flight mass analyser. To overcome charge build-up on the isolative samples, a low-energy electron beam (21 eV) flood gun was employed and the sample surface potential was optimised for each analysis. The surface analysis conditions were selected and adjusted to keep the primary ion dose density (PIDD) below the static limit of 1013 primary ions/cm² to minimise surface damages during the analysis. All the mass spectral information was recorded in the m/z range of 0–900.

Samples were analysed to collect reference spectra. These were acquired in the positive secondary ion polarities, in three replicates, from 100 μ m \times 100 μ m areas in various points of the sample. The total PIDD for each analysis was approximately 5 \times 1012 (primary ions/cm²). The spectra were used to visually select characteristic mass peaks for each compound.

A 30 kV Bi³⁺ primary ion beam was employed to generate macro images rotating the stage and the ion beam across the whole area of interest. The total area analysed was 6.51 mm × 6.51 mm and the mass spectral information was collected in the positive secondary ion polarity, applying a delayed extraction of 0.050 μs to improve mass resolution and decrease topographic artefacts potentially generated by the rough surface. The total PIDD delivered during the acquisition of each raster was approximately 9 × 10¹⁰ (primary ions/cm²).

A 30 kV Bi³⁺ primary ion beam was operated in an un-bunched mode to collect high lateral resolution secondary ion images of specific spots on the sample's surface. These were acquired over an area of 500 μm × 500 μm, with a pixel size of 0.488 μm, in the positive secondary ion polarity, selecting an extraction delay of 0.050 μs, with a final PIDD of approximately 5 × 10¹² (primary ions/cm²). The images were then processed using SurfaceLab 6.7 software (ION-TOF, Münster, Germany) to generate colour overlays of the selected peaks for FNF and PVP.

3.3 Results & Discussion

3.3.1 Dosage Form Construction

3.3.1.1 Speed of Deposition

On speed testing using the KEWA settings, an increase in mass with decreasing speed is observed, with a P-value of 0.0671 suggesting a significant relationship (Figure 42). However, this is not particularly linear in nature with an r-squared value of 0.79657, and the ANOVA does not show a significant difference between the samples resulting from the lack of linearity. The linear curve fitting therefore may be entirely due to the 1mm/s point rather than a reflection of the results as a whole. At lower speeds, the printer seems to block much more easily, resulting in large error bars, and at higher speeds, the print head is simply moving too fast to deposit much at all. Additionally, the standard error exhibited increases with decreasing speed. This is supported by the 95% confidence intervals given in Figure 42. Thus, this is inadvisable as a method of scaling.

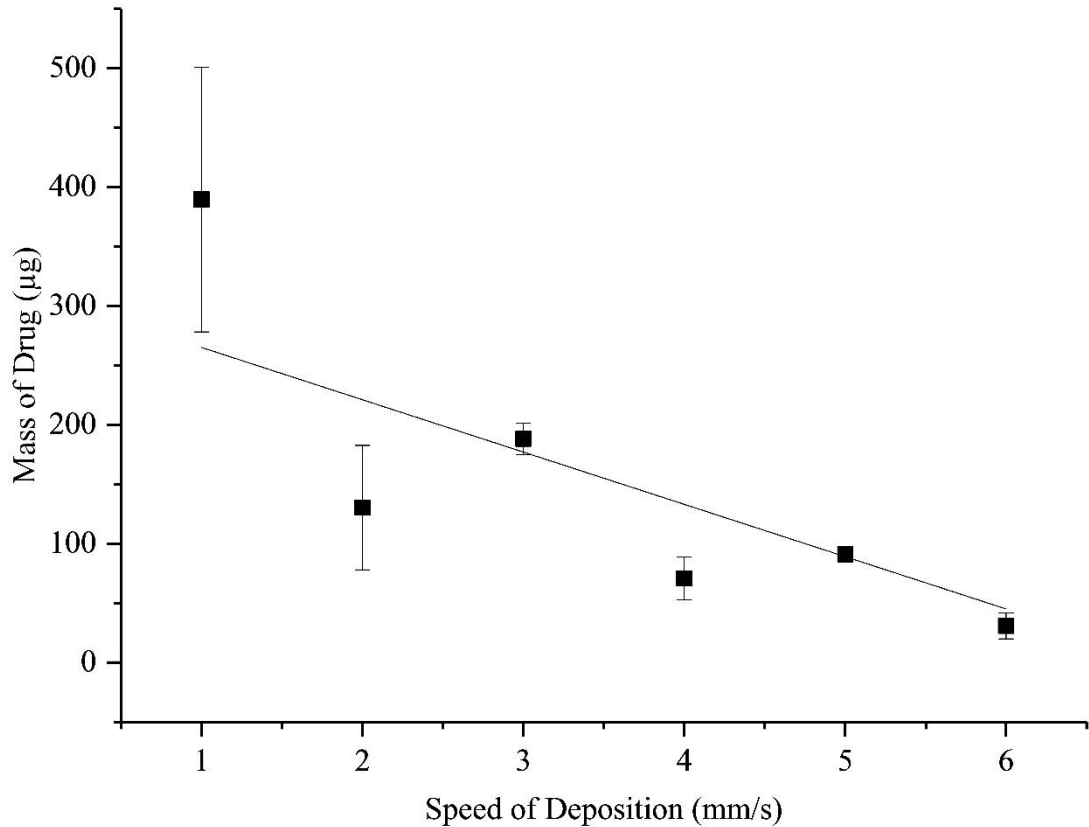


Figure 42: The effect of speed on mass of drug printed using a 1:1 fenofibrate:PVP K30 premixed ink with a 250 µm nozzle, where $r^2=0.77446$ and $n=6 \pm$ standard error with 95% confidence intervals of 103.23 µm and 675.75 µm, -4.10 µm and 264.77 µm, 153.77 µm and 222.57 µm, 23.97 µm and 117.65 µm, 84.14 µm and 97.74 µm, and 3.00 µm and 58.54 µm for 1, 2, 3, 4, 5 and 6 mm/s respectively. $P=0.0079$ for 1 to 2mm/s, $P=0.97396$ for 2 to 3mm/s, $P=0.57643$ for 3 to 4mm/s, $P=0.99992$ for 4 to 5mm/s and $P=0.9684$ for 5 to 6mm/s. P of the slope= 0.01671 .

There is no prior literature changing the dose using speed however, in other studies the effect of speed on thickness and line width is compared. In Mahajan et al., the effect of the stage speed on line width and thickness was tested by printing silver nanoparticles using an Optomec Aerosol Jet M³D Printer, which behaves similarly to the AJ200 but uses an ultrasonic atomiser rather than a pneumatic one. Using a 200 µm nozzle, printing at 1 and 2mm/s a similar effect of larger error bars is observed, as in the current study. The line width and thickness decrease in a similar manner to the

mass. This is relatable as it would follow that the area covered by the printer should increase with line width and the thickness is a function of the number of layers. From 1mm/s to 3mm/s the thickness and line width are observed to decrease with speed quite rapidly before levelling off slightly towards the faster speed settings. As with the current study the results are not perfectly linear and as such the authors have opted for a dot-to-dot curve rather than a linear fit (Mahajan et al. 2013).

Additionally, Goh et al. demonstrates a similar effect on printing carbon nanotubes using aerosol jet printing with ultrasonic atomisation. There is a drop in the line width after 4mm/s and considerably bigger error bars exhibited on printing at 6mm/s, followed by a levelling off affect. Again the dot-to-dot approach is utilised as the line is not linear (Goh et al. 2018).

In another paper by Wang et al., polyimide/carbon nanotube nanocomposite was printed using an Optomec AJP 300® Aerosol Jet Printer using both pneumatic and ultrasonic atomisation steps to generate the final ink from polyamide and carbon nanotube inks, combining them in a static mixer before printing. The speed was analysed by comparison to thickness similar to Mahajan et al. but only 3 points were utilised reducing the curve appearance (Wang et al. 2016).

In a study by Elmogi et al., silver nanoparticles were printed using the aerosol jet technology but the printer utilised is not specified. Stage speed is once again compared to thickness and line width and a similar curvature to the line is observed with 1mm/s and 2mm/s being considerably higher than 3mm/s before the line levels off. This is once again not fully linear and it appears to be based on a single set of data, or if not, the standard deviation and/or error are not displayed. The only difference between the line width and thickness curves are the 9mm/s and 10mm/s points, which drop for the line thickness. The shape of the curve is quite similar to Mahajan et al. (Elmogi et al. 2018)

3.3.1.2 Nozzle Size

Nozzle size shows a linear relationship with mass of drug deposited with a r-squared value of 0.91999 (Figure 43). On statistical analysis a P-value of 0.04084 was obtained suggesting there is a significant relationship between nozzle size and drug mass deposited. Changing the nozzle size from the minimum to the maximum allows a 3-fold increase in mass deposited. The error is slightly higher for the smaller nozzle sizes which reduces the overall linearity. A significant change was recorded on performing an ANOVA for 150 to 200 μm but the latter samples show insignificant differences.

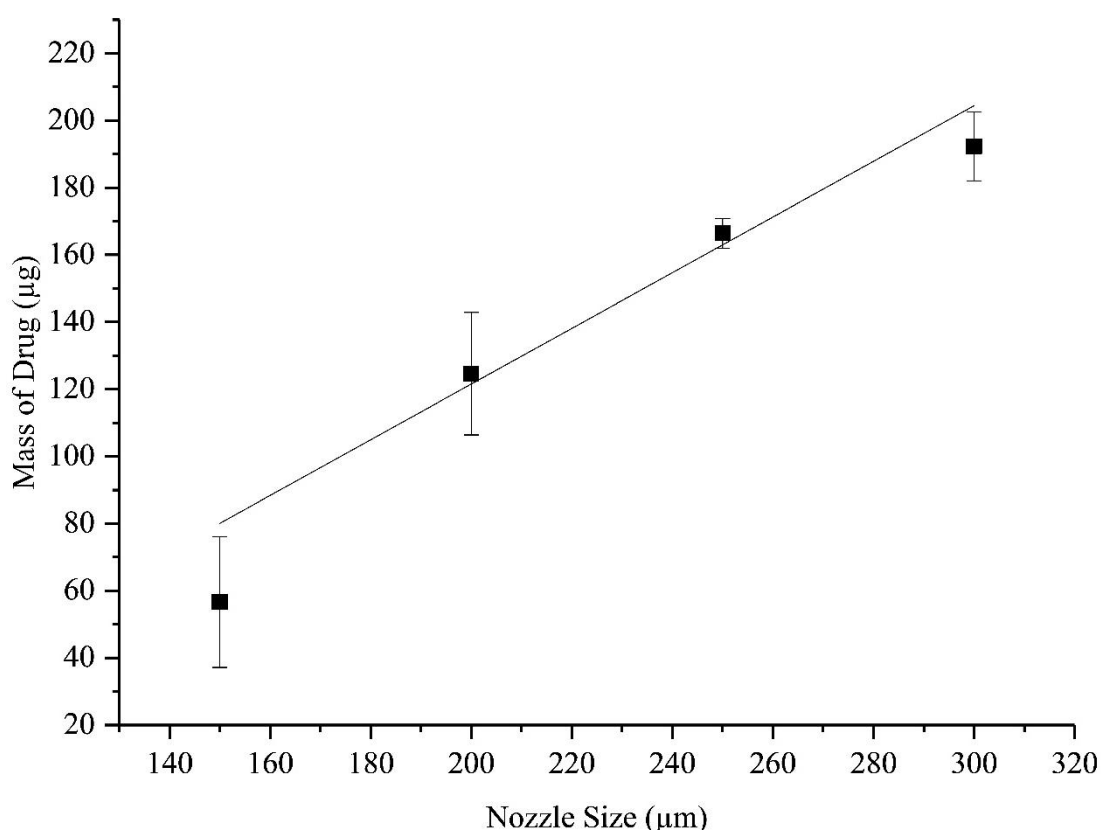


Figure 43: The effect of nozzle size on mass of drug printed using a 1:1 fenofibrate:PVP K30 premixed ink at 3 mm/s to print a 5mm diameter circle, where $r^2=0.91999$ and $n=6 \pm$ standard error with 95% confidence intervals of 6.53 μm and 106.74 μm , 77.79 μm and 171.46 μm , 154.78 μm and 177.96 μm , and 165.78 μm and 218.82 μm for 150 μm , 200 μm , 250 μm and 300 μm respectively. $P=0.00229$ for 150 to 200 μm , $P=0.06496$ for 200 to 250 μm and $P=0.35644$ for 250 to 300 μm . P of the slope=0.04084

Although, nozzle size has a relatively linear relationship with mass, it has the disadvantage of being dependent on the manufacturer's stated nozzle diameters and, as it is such a small scale, any slight variation is magnified. Thus, there is a chance of variation between nozzles of the same size and also a chance that nozzles are not exactly the size specified. Nozzles of 150 and 200 μm also suffer from bigger variations between samples as they are less forgiving of viscosity and thus droplet size than 250 and 300 μm as exhibited by bigger error bars than the latter two nozzle sizes.

Although there is little evidence of study of the relationship between nozzle size and mass previously, nozzle size has been studied as a means of changing droplet size previously in a DOD PIJ (EPSON C45) piezoelectric printer (Liou et al. 2010). Linearity is observed between the droplet size and nozzle size which may explain the linearity between nozzle size and mass observed in the current study. The effect of line width has also been previously tested using an aerosol jet printer using silver ink. Different pressures were applied using an Optomec Aerosol Jet M³D Printer with 100, 150 and 200 μm nozzles. Line width increases with nozzle diameter but again this does not reflect a drug mass directly (Mahajan et al. 2013). As such this is relatively novel.

3.3.1.3 Single Layer Deposition Size

Area was determined using AutoCAD 2017. Good linearity was observed between different deposition areas with an r-squared value of 0.99869 (Figure 44). This was also found to be also highly reproducible as the error bars are often too small to be observed. On statistical analysis a P-value of 6.57601×10^{-4} was obtained suggesting a significant relationship between size and mass of drug deposited. Increasing the area deposited up to a 40-fold increase in the mass deposited is achieved. On performing an ANOVA all the samples show a P-value of 0.00 suggesting changing the size has significant effects. This P-value is a little unusual but it is thought to be due to limitations of the statistical software.

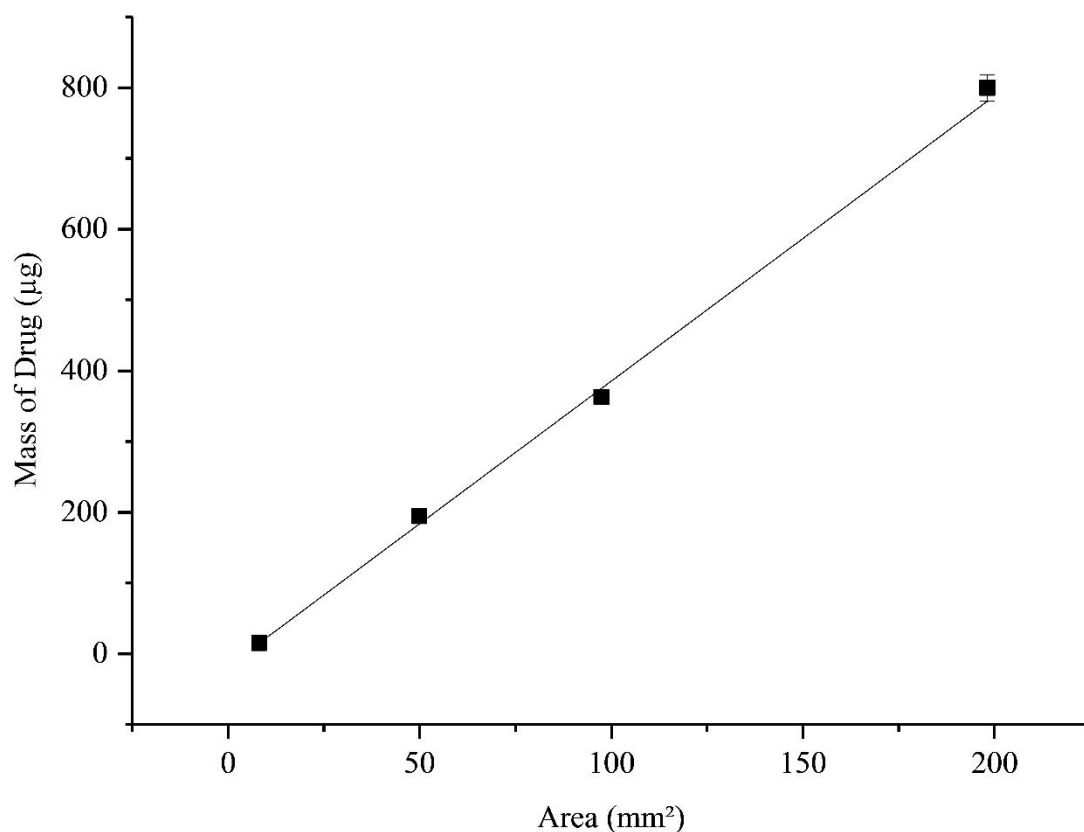


Figure 44: The effect of deposition size on mass of drug printed using a 1:1 fenofibrate:PVP K30 premixed ink with a 250 µm nozzle at 3 mm/s to print a 5mm diameter circle, where $r^2=0.99869$ and $n=6\pm$ standard error with 95% confidence intervals of 7.42 µm and 23.14 µm, 168.25 µm and 220.87 µm, 341.14 µm and 384.66 µm, and 752.81 µm and 846.53 µm for 8.13, 49.94, 97.44 and 198.13mm² respectively. N.B. Some error bars are so small they cannot be distinguished from the points. $P=0$ for all the relationships between samples. P of the slope= 6.57601×10^{-4} .

Deposition size was found to be more linear overall which may be due to the fact that depositions can be designed to the micrometre in AutoCAD. Changing the size of deposition to alter the dose has been employed previously by thermal inkjet printing warfarin using a Hewlett-Packard (HP) 5940 Deskjet. Printing 0.5cmx1-7cm rectangles was shown to result in a linear relationship between the length and drug mass with an r-squared value of 0.9999. (Vuddanda et al. 2018). Another paper using the same type of printer with levothyroxine sodium and liothyronine sodium, was utilised to print 1cmx6-12cm rectangles. This demonstrates a linear relationship between mass and length of rectangle printed, although not as linear as Vuddanda et

al. with a r-squared value of 0.9817 (Alomari et al. 2018). Lysozyme and ribonuclease-A were printed with sodium deoxycholate using a Hewlett Packard Deskjet 1000. Areas of 4, 9, 16, and 49 cm² were printed yielding r-squared values of 0.978 to 1, suggesting some samples were more linear than others which may be due to the nature of the material printed (Montenegro-Nicolini et al. 2017).

3.3.1.4 Layering

As can be seen in Figure 45, layering depositions to generate dosage forms results in good linearity being observed overall with an r-squared value of 0.99903. The average mass of drug deposited per layer is approximately 200µg each time. The results are also fairly reproducible in nature based on the size of the error bars. From the statistical analysis a P-value of 1.28876×10^{-5} was obtained suggesting a significant relationship between the layer number and the mass deposited. Additionally, on performing an ANOVA on the individual samples, a statistically significant relationship was shown between each of the layer changes.

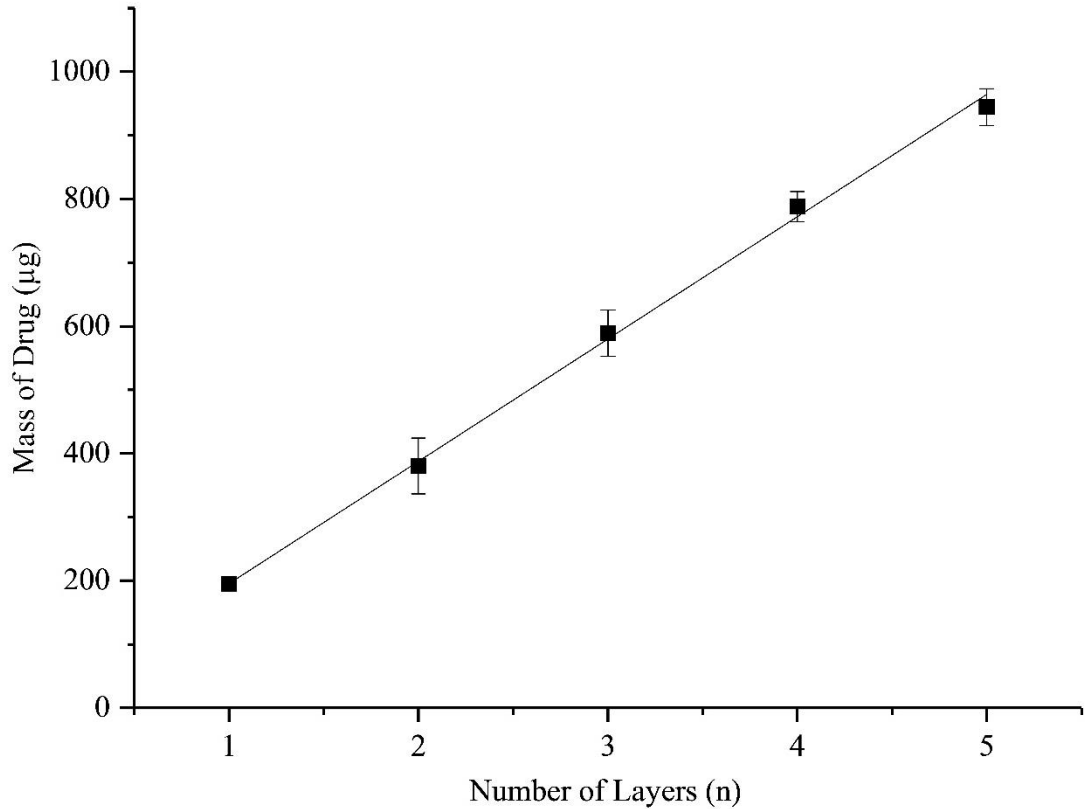


Figure 45: The effect of layer number on mass of drug printed using a 1:1 fenofibrate:PVP K30 premixed ink with a 250 µm nozzle at 3 mm/s to print 5mm diameter circles, where $r^2=0.99903$ and $n=6\pm$ standard error with 95% confidence intervals of 168.25 µm and 220.87 µm, 267.53 µm and 493.29 µm, 494.89 µm and 683.19 µm, 727.04 µm and 848.86 µm, and 870.21 µm and 1019.08 µm for 1, 2, 3, 4 and 5 layers respectively. $P=0.00243$ for 1 to 2 layers, $P=7.23072\times 10^{-4}$ for 2 to 3 layers, $P=0.00121$ for 3 to 4 layers and $P=0.01131$ for 4 to 5 layers. P of the slope= 1.28876×10^{-5} .

Layering was observed to be very linear, as exhibited previously in inkjet printing (Akagi et al. 2014, Vakili et al. 2015, Wickström et al. 2017). It is thought that this shows the best linearity overall as using the same AutoCAD drawing and the same speed throughout eliminates any program dependent issues and using the same nozzle size eliminates any manufacturer dependent variation. Unlike other studies (Wickström et al. 2015), material is not lost by using this method as the dragging action is eliminated by the free moving stage. Generally previous printing papers have

reported layering but have often failed to demonstrate linearity (Buanz et al. 2011, Akagi et al. 2014, Wickström et al. 2015). One exception to this is a paper by Vakili et al. using a Canon Pixma M495. This paper demonstrates a linear relationship between the number of layers of theophylline and glycerine printed by thermal inkjet printing and the resultant drug loading detected, with an r-squared value of 0.991 (Vakili et al. 2015). Another exception is a paper by Wickström et al, where the effect of printing paediatric doses of vitamins B₁, B₂, B₃ and B₆ on rice paper, sugar paper and standard home printer paper was compared using a Canon Pixma iP3600 thermal desktop inkjet printer, analysing samples by LC-MS. Due to the smoother thinner surface of standard home printer paper it was found to exhibit the highest degree of linearity for all but vitamin B₃ on comparing number of layers to mass detected. Rice paper showed very similar values only differing by between 1 and 3 r-squared values. Sugar paper showed less linearity overall as the surface was rougher and thicker in nature (Wickström et al. 2017). Standard printer paper was not used in the current study purely due to its higher cellulose content but this paper confirms that the effect of printing on rice paper results in little change to the relationship between mass and layers.

Layering exhibiting linearity has also been demonstrated using an aerosol jet printer previously. Examples of this include printing silver ink where thickness was compared between 1 and 4 layers (Kopola et al. 2012), printing silver ink and carbon nanotube inks comparing thickness on increasing layer number over a range of 10 to 30 layers (Goh et al. 2018) and printing barium titanate BTO based multilayer ceramic capacitors where thickness was compared between 1 and 5 layers (Folgar et al. 2011). However, it has never been demonstrated with API and thus investigation using the printer in this study is fairly novel.

3.3.1.5 Depth by Laser Triangulation

Laser triangulation allows determination of the thickness of depositions (Figure 46). As single layer thickness is incredibly difficult to separate from the substrate thickness,

5 layer samples were utilised. The thickness seems to increase with polymer content which the author theorises to be due to the changes in droplet size allowing better flow out of the instrument and changes in the packing of particles within the sample itself. An ANOVA demonstrates a significant difference between 33.33 and 50% drug but non-significant differences between other samples, supporting the exponential increase observed in Figure 46.

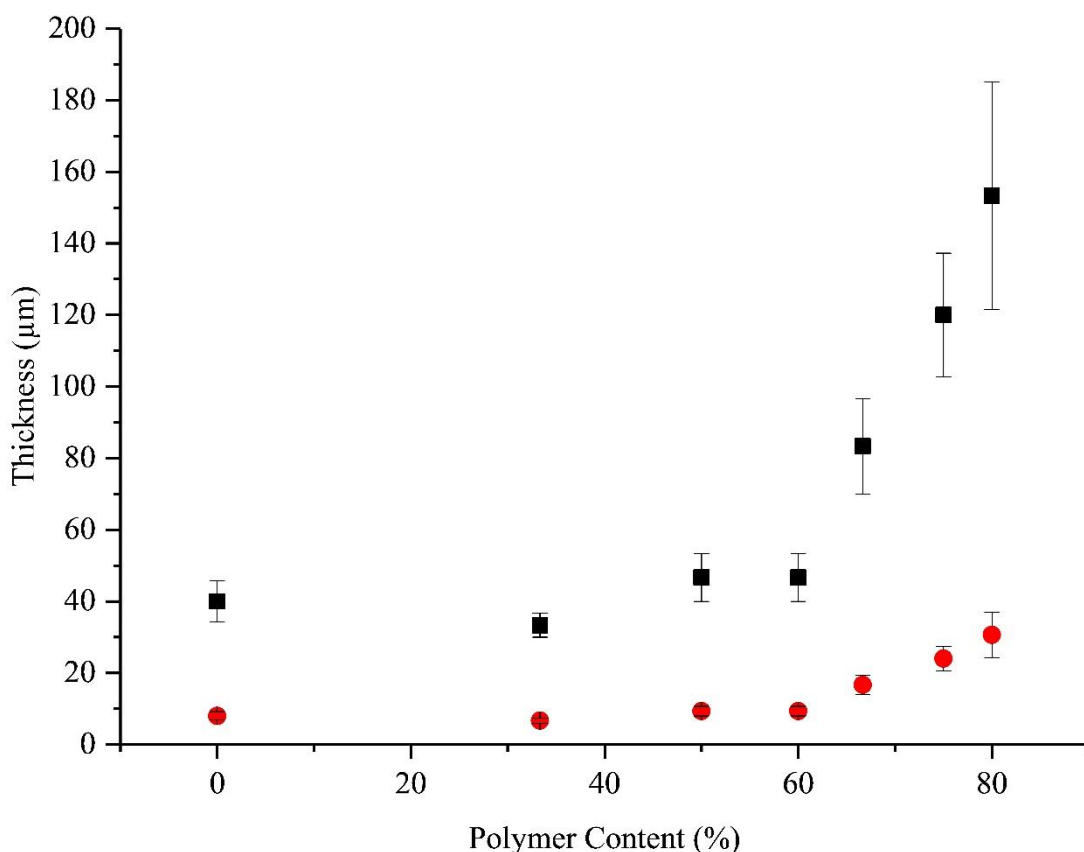


Figure 46: Thickness of depositions based on polymer content as detected by laser triangulation of 5 layer (black) and theoretical 1 layer (red) samples, $n=3 \pm$ standard error with 95% confidence intervals of 15.16 μm and 64.84 μm , 18.99 μm and 47.68 μm , 17.98 μm and 75.35 μm , 17.98 μm and 75.35 μm , 25.96 μm and 140.7 μm , 45.48 μm and 194.52 μm , and 16.52 μm and 290.15 μm for 0, 33.3, 50, 60, 66.67, 75 and 80% PVP ink content respectively. $P=0.22772$ for 0 to 33.33% drug, $P=0.01816$ for 33.33 to 50%, $P=1$ for 50 to 60%, $P=0.61907$ for 60 to 66.67%, $P=0.61907$ for 66.67 to 75% and $P=0.68062$ for 75 to 80% for 5 the layer samples.

Only one paper on laser triangulation for dosage form thickness could be found. This was limited in value as it describes the development of the technique rather than its use (Yawei et al. 2013). Therefore, the current study is fairly novel. In terms of comparison of the effect of printing different polymer concentrations on the thickness of the dosage form generated, there seems to be little literature evidence for previous studies.

3.3.2 Drug Distribution

3.3.2.1 3D-Raman Mapping

3D Raman mapping (Figures 47, 48 and 49) shows noticeable differences between 2:1, 1:1, 2:3 and the higher polymer ratios. The drug (red) goes from being the most prevalent component in the 2:1 sample to an even mixture with the polymer (blue) in the 1:1 and 2:3 samples. On comparison to the SEM and AutoCAD images, it can be concluded that the distinct areas can be attributed to crystalline drug areas and amorphous polymer areas. In the SEM of 2:1 it can be seen that the plate-like conformation shows some evidence of polymer particles but is largely crystalline (Figure 47). Likewise, in the SEM of 1:1, it can be observed that there are defined crystals throughout the dosage form (Figure 47). The 2:3 sample has more evidence of smaller amorphous particles coupled with larger crystalline ones (Figure 48). There is also some evidence in this sample of the so called coffee-ring effect with a concentration of particles in the outer ring. The 1:2 sample shows more polymer content with the drug only evidential in the spiral of the print head (Figure 48). The polymer eventually overshadows the drug in the 1:3 and 1:4 samples (Figure 49). This is believed to be due to the formation of amorphous material, as the instrument appeared to struggle to pick up the drug in this form. However, this would require analysis of the amorphous form of the drug as a reference to confirm. The mPAT has the ability to calculate pixel calculations and translate them into percentage content (Table 15). The more crystalline samples show a content which is similar to the expected value but the accuracy of this seems to fall as the crystalline content is lost supporting the theory the mPAT fails to process amorphous material as accurately. In the case of fenofibrate this may be due to the smoothing of peaks that occurs on

formation of amorphous material, potentially making them less defined. Additionally, the peak height exhibited by fenofibrate relative to that of the PVP peaks decreases with polymer content.

The limitation of this technique is that it needs to be able to pick up distinct peaks for each substance. The risk of printing on rice paper was that the Raman spectrometer could pick up the signal from this in addition to the drug and polymer. As can be observed in Figure 50, there is a chance that rice paper may be wrongly identified as PVP on the map and there is also a slight chance it may also be identified as fenofibrate as they share some functional groups. This would explain the blue areas and red areas observed outwith the deposition area.

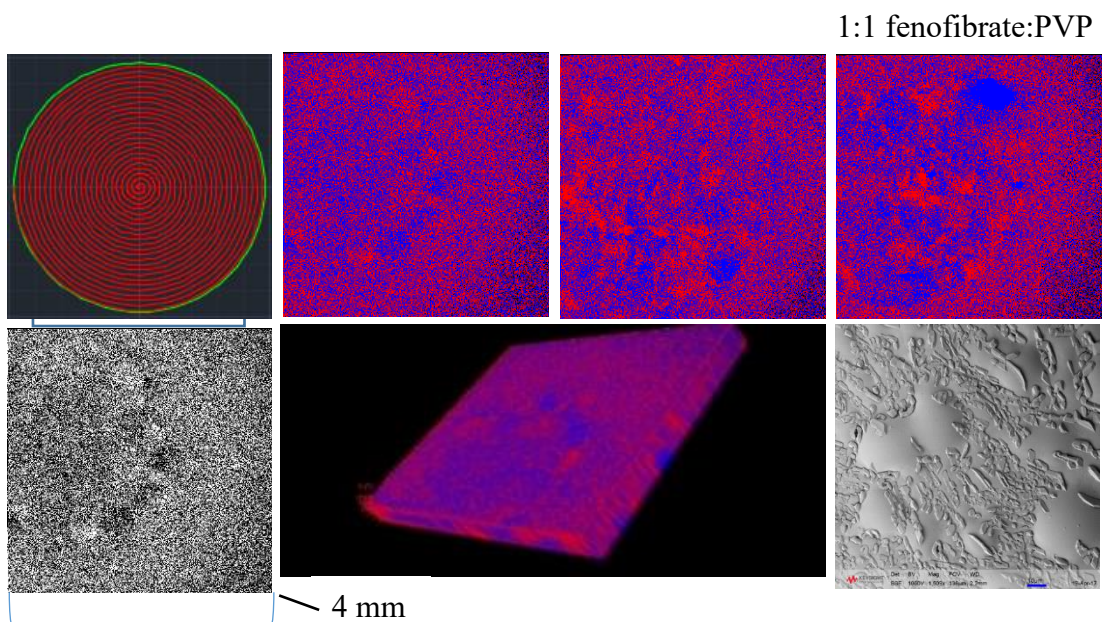
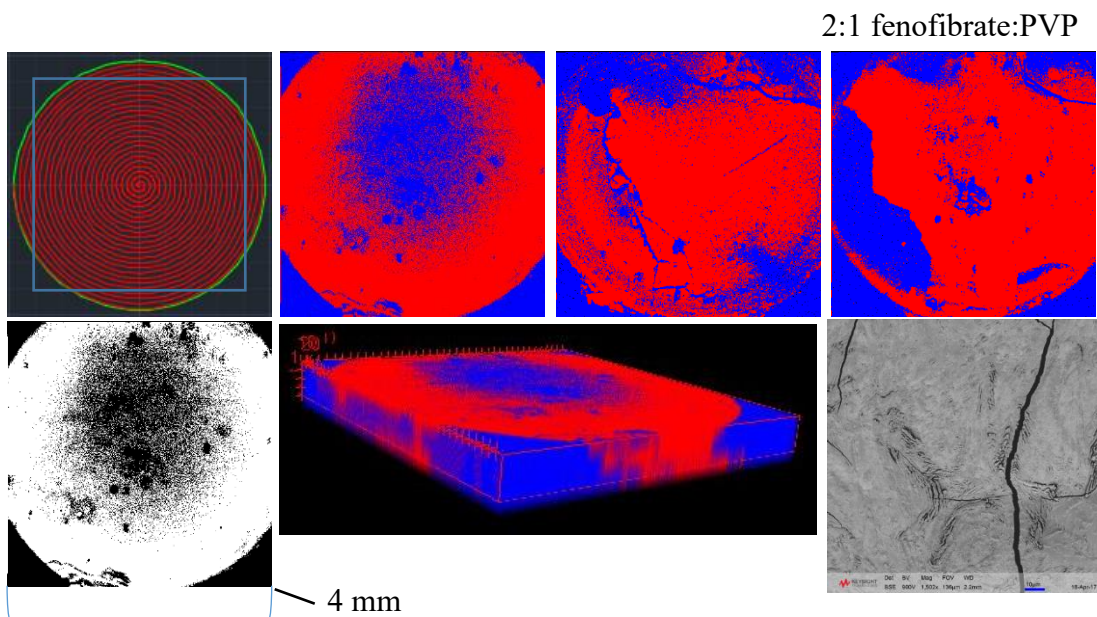
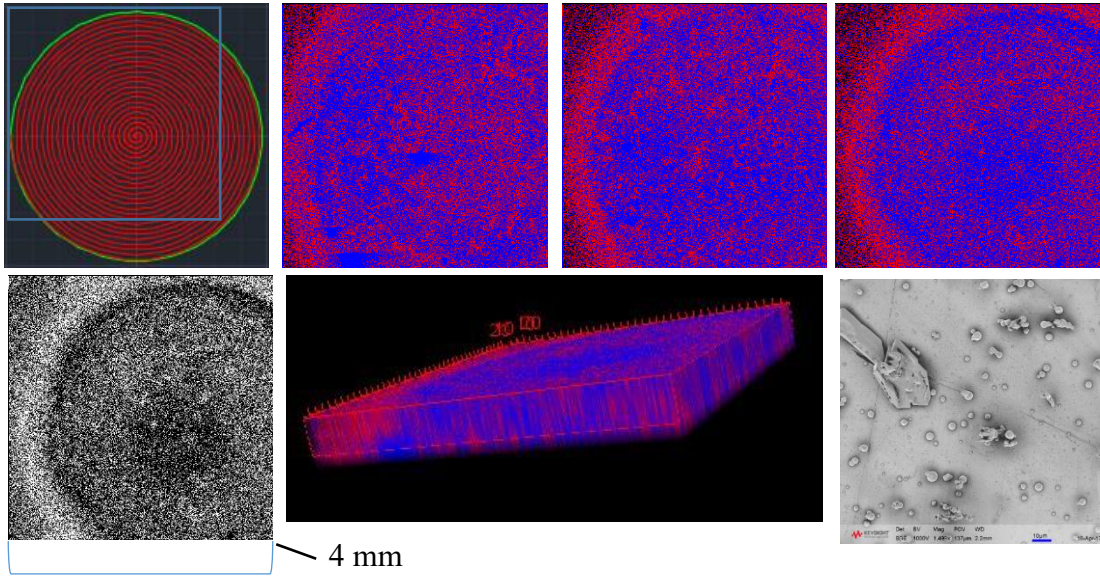


Figure 47: 3D Raman maps of dosage forms consisting of 2:1 and 1:1 fenofibrate:PVP compared to their deposition design and SEM images. Maps were taken using an H2Optx mPAT over an area of 4x4mm using a 754 nm laser. Images as follows: 5mm AutoCAD drawing with 4x4mm imaging area (top left), Raman maps of fenofibrate (red) and PVP (blue) outer tablet surface (left middle), slice 1 (right middle), slice 2 (right), and orthosubtracted image of fenofibrate (white) and PVP (black) (bottom left), 3D image combining maps (middle), and the associated SEM image (bottom right).

2:3 fenofibrate:PVP



1:2 fenofibrate:PVP

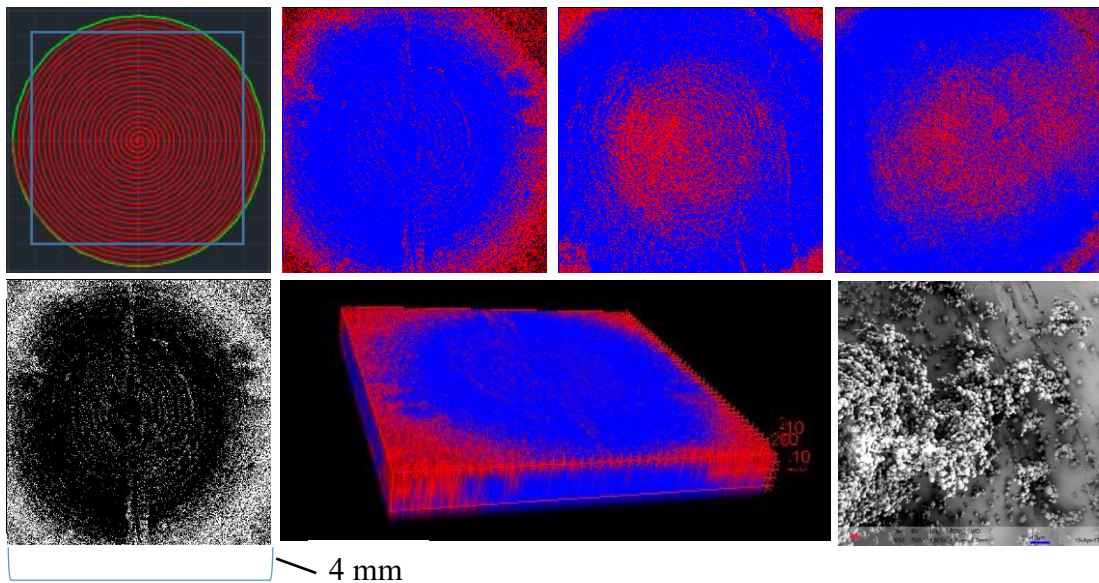


Figure 48: 3D Raman maps of dosage forms consisting of 2:3 and 1:2 fenofibrate:PVP compared to their deposition design and SEM images. Maps were taken using an H2Optx mPAT over an area of 4x4mm using a 754 nm laser. Images as follows: 5mm AutoCAD drawing with 4x4mm imaging area (top left), Raman maps of fenofibrate (red) and PVP (blue) outer tablet surface (left middle), slice 1 (right middle), slice 2 (right), and orthosubtracted image of fenofibrate (white) and PVP (black) (bottom left), 3D image combining maps (middle), and the associated SEM image (bottom right).

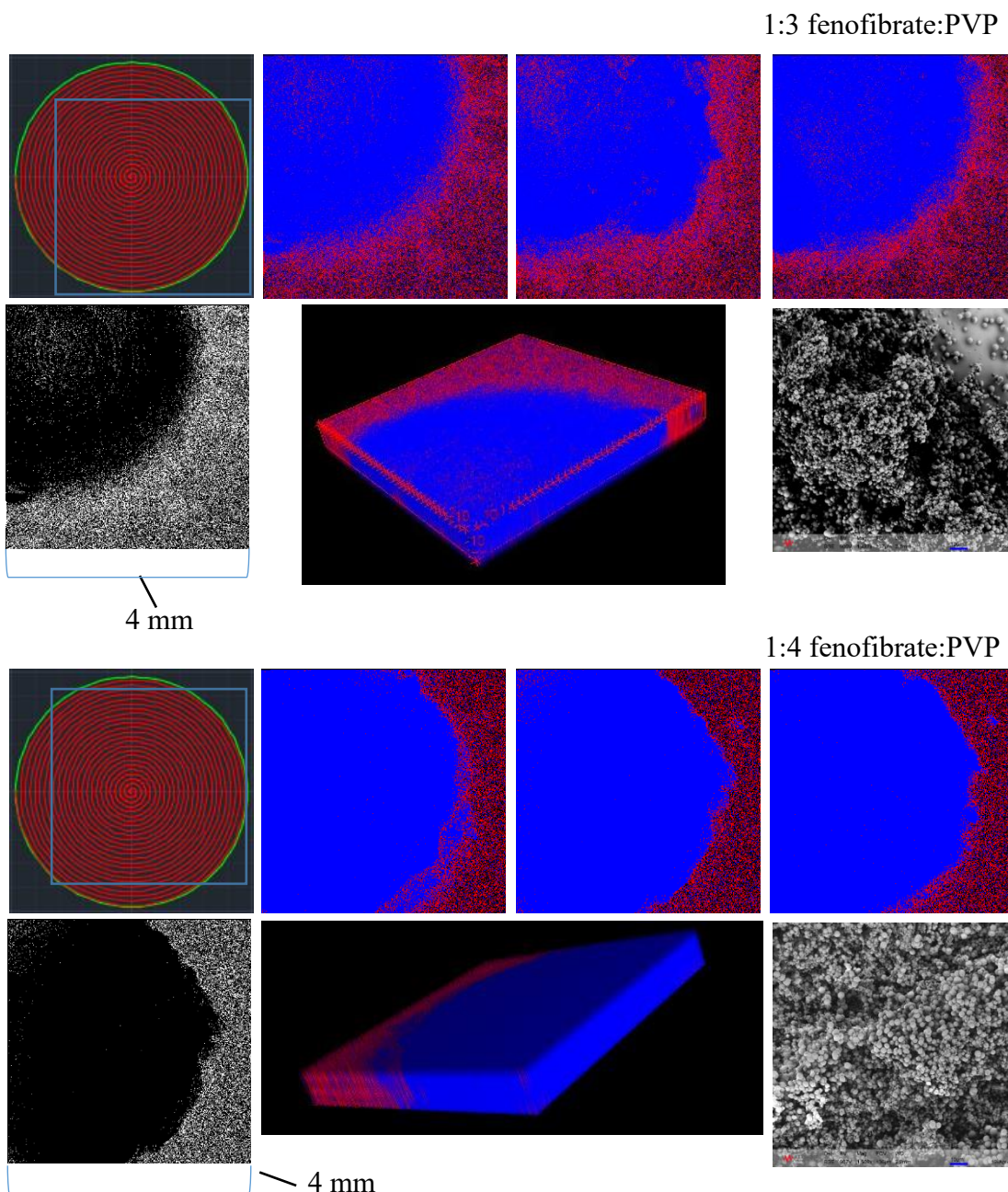


Figure 49: 3D Raman maps of dosage forms consisting of 1:3 and 1:4 fenofibrate:PVP compared to their deposition design and SEM images. Maps were taken using an H2Optx mPAT over an area of 4x4mm using a 754 nm laser. Images as follows: 5mm AutoCAD drawing with 4x4mm imaging area (top left), Raman maps of fenofibrate (red) and PVP (blue) outer tablet surface (left middle), slice 1 (right middle), slice 2 (right), and orthosubtracted image of fenofibrate (white) and PVP (black) (bottom left), 3D image combining maps (middle), and the associated SEM image (bottom right).

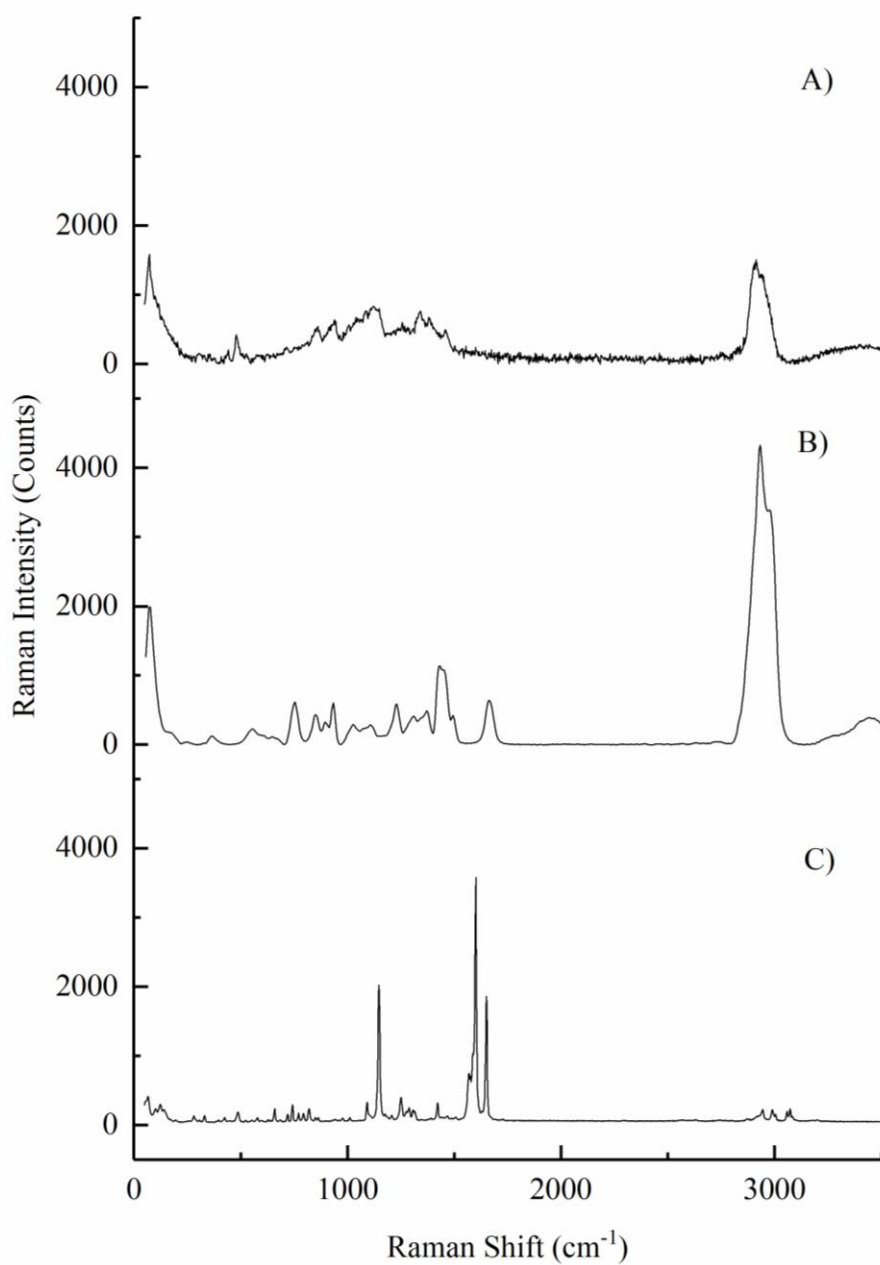


Figure 50: Raman spectra comparing the spectral regions of (A) rice paper, (B) PVP and (C) fenofibrate

Table 15: Percentage content detected by the H2Optix mPAT Python script from premixed samples

Formulation	Percentage Drug Added to the Starting Ink	Average Percentage Drug Content Detected (n=3, to 1 d.p.)
2:1	67%	67.3%
1:1	50%	48.2%
2:3	40%	38.0%
1:2	33%	22.8%
1:3	25%	23.74%
1:4	20%	10.0%

The effect of printing fenofibrate and PVP K30 separately on control over drug distribution was tested by printing as layers and as 3 tori with 0.5mm walls surrounding a 2mm core (Figure 51). Similar to the premixed samples, evidence of the deposition can be observed. On layering there is a suggestion of the separate layers but this is limited due to the crude nature of slicing with a diamond blade by hand. As such the layers are not 100% clean and the percentage calculated by the Python script in Table 16 reflects this. There is also some evidence of the coffee-ring effect with the lower layer of drug being visible as a ring around the polymer in the first layer. For the tori style system, both components can be clearly seen suggesting the printer is capable of controlling distribution to the micrometre scale. The slightly more ragged areas are a result of cutting open a tablet using a diamond blade manually and the brittle, porous nature of the polymer. Again, the layers (cut as shown in Figure 51) are not perfect as a result of the diamond blade and also the porous nature of the sample, which is reflected in Table 16. As the surface was damaged in transit the overall reading was lower for the initial surface of the tablet. The first slice into the centre of the tablet demonstrated a percentage very similar to the predicted content which suggests the torus gives a higher level of control over the content. The bottom slice again exhibits

a lower content than expected which may be again due to damage in cutting the sample. Overall, it is possible to observe the distinct areas of drug and polymer in the central and bottom layers indicating there is a definite level of precision possible. Again, it is possible there is some influence of the rice paper as there is evidence of ghosting in the initial sample layer but not there after which given the sample is cylindrical seems odd.

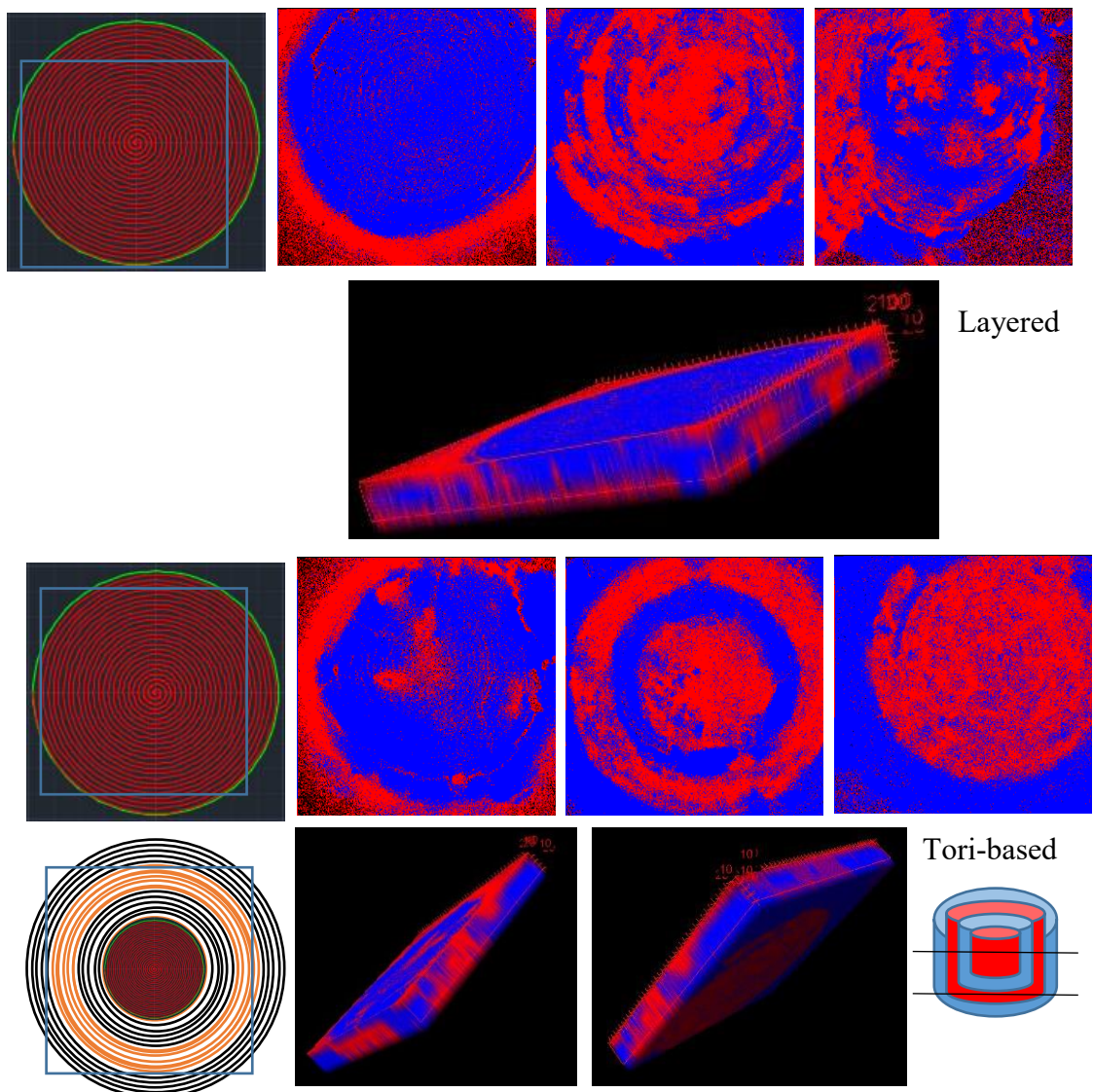


Figure 51: A 3D Raman mapping images of fenofibrate (red) and PVP K30 (blue) aerosol jet printed as separate layers (top) and tori-based regions (bottom) taken using an H2Optx mPAT over an area of 4x4mm using a 754 nm laser. The images show the initial 5mm diameter AutoCAD design with the 4x4mm imaging area (top left), the outer face of the dosage form (top middle left), the initial slice into the middle of the tablet (top middle right), the second slice into the tablet (right) and the 3 images stacked to form a 3D image (bottom). Additionally, the inner tori design (bottom left) and the overall design with approximate slice locations (bottom right) are shown for the tori based system.

Table 16: Percentage content detected by the H2Optix mPAT Python script

Formulation	Predicted Percentage Drug Content	Average Percentage Drug Content Detected
Layers (top)	100.0%	27.5%
Layers (middle)	0%	49.9%
Layers (bottom)	100.0%	43.8%
Torus (top)	100%	33.4%
Torus (middle)	53.3%	49.7%
Torus (bottom)	76.5%	49.6%

Only one paper exists using the H2Optix mPAT currently. Fauteux-lefebvre et al. analysed tablet surfaces in this manner to compare tablets of different particle sizes but the current work is believed to be the first to analyse solid dispersion-based dosage forms (Fauteux-lefebvre et al. 2018). There is however a previous study demonstrating 2D Raman mapping of cross section of core and matrix style dosage forms at 754nm. This demonstrates distinct areas of drug and polymer in the core style systems and more evenly mixed drug and polymer in the matrix style systems. However, this is not oral dosage forms but silicon vaginal rings using TMC120 for HIV treatment (Bell et al. 2007). There are also two papers demonstrating distinct areas of a tablet. For example Choi et al. demonstrated Raman images of a central active core of Tamsulosin HCl and hydrophilic excipients including polyethylene glycol and an outer barrier layer of polyox WSR (Choi, Kim, et al. 2013). Goyanes et al. also demonstrated layers and central cores of 3D printed tablets consisting of PVA, paracetamol and caffeine (Goyanes, Wang, et al. 2015). Additionally, there is extensive research into amorphous solid dispersions (Karavas et al. 2007, Furuyama et al. 2008, Luebbert et al. 2018). There is some previous evidence of examination of inkjet printed samples in this manner but previous research has mostly just highlighted the content of single drops (Scoutaris et al. 2011) or the effect of layering on the intensity of functional groups (Edinger et al. 2017). As the aerosol jet technology has

never been used for pharmaceutical products previously there is no prior evidence of Raman mapping of drugs and/or polymers in these systems.

3.3.2.2 TOF-SIMS

TOF-SIMS was utilised to establish if the effect of precision printing separate areas of drug and polymer observed in the 3D Raman images could be detected using a more established technique. TOF-SIMS demonstrates a similar effect to the 3D Raman data. A sample based on 3 tori designed in the same manner as the 3D Raman sample shows a similar pattern on the TOF-SIMS (Figure 52) with the crystalline fenofibrate being clearly separated from the distinct lines of PVP. The PVP lines are much sharper in nature than the fenofibrate lines which is potentially due to the nature of the particles generated on printing with the growth of crystalline particles disrupting the integrity of the printed line on drying. The drug areas seem to show some evidence of the lines but there are some areas where the crystals have fused resulting in more intensely red areas. The associated analysis images (Figures 53, 55 and 57) demonstrate the presence of no crystalline topography in the PVP only region and an interface in the PVP and fenofibrate containing region. 2 lines per tori and 1 line per tori samples were compared to the 5 line samples. It was found that 2 lines (Figure 54) results in more scattering potentially down to the thickness of the spray jet and thus more bleeding of drug into the polymer tori. Printing 6mm structures using single lines (Figure 56) results in more distinct areas of drug and polymer, thus proving that the drug distribution can be controlled to the micrometre.

Previous papers have demonstrated the ability of TOF-SIMS to identify components of inkjet printed samples. For example, Scoutaris et al tested inkjet samples of an HCT/PLGA drug formulation (Scoutaris et al. 2012), Filenkova et al. analysed inkjet samples of Igepal CA-720, glycerol, water, lithium chloride and crystal violet (Filenkova et al. 2011) and Vercammen and Luppen analysed inkjet printed samples of UV-curable ink based on dipropylene glycol diacrylate (DPGDA) and vinyloxyethoxyethyl acrylate (VEEA) monomers with magenta pigment dispersions

(Vercammen and Luppen 2013). However, there is no previous evidence of examining formulations with separate areas printed.

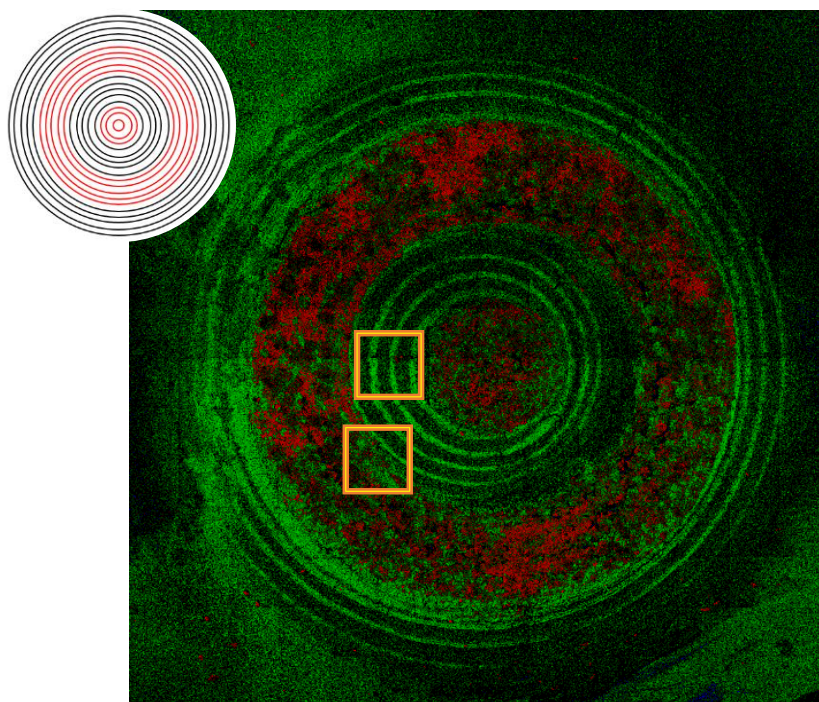


Figure 52: A TOF-SIMS image and its starting deposition design depicting a 6mm diameter deposition consisting of 2 distinct areas of fenofibrate (red) and 2 distinct areas of PVP K30 (green/black) of 5 printed lines each.

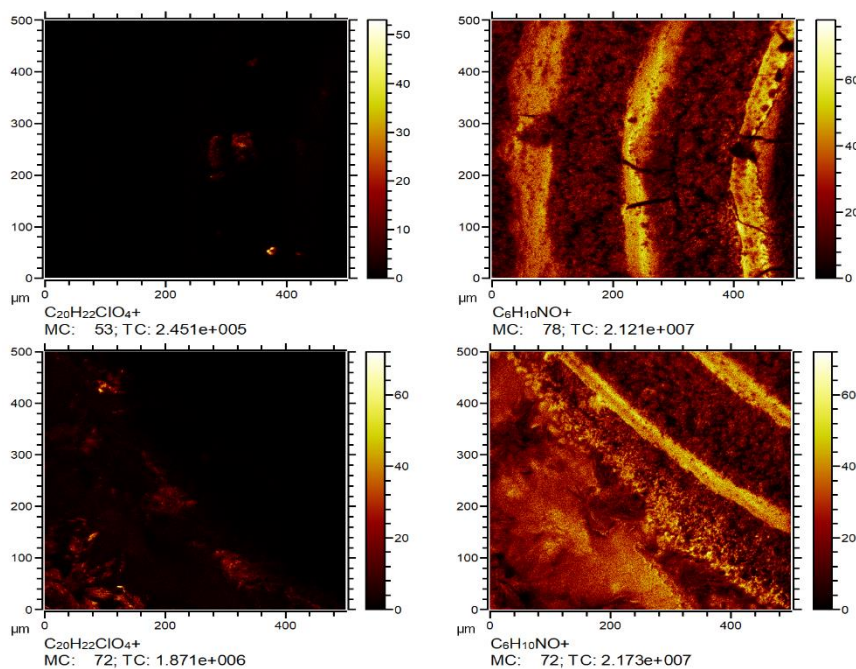


Figure 53: TOF-SIMS images taken of the 2 areas highlighted in Figure 52 with measurements for fenofibrate (left) and PVP K30 (right)

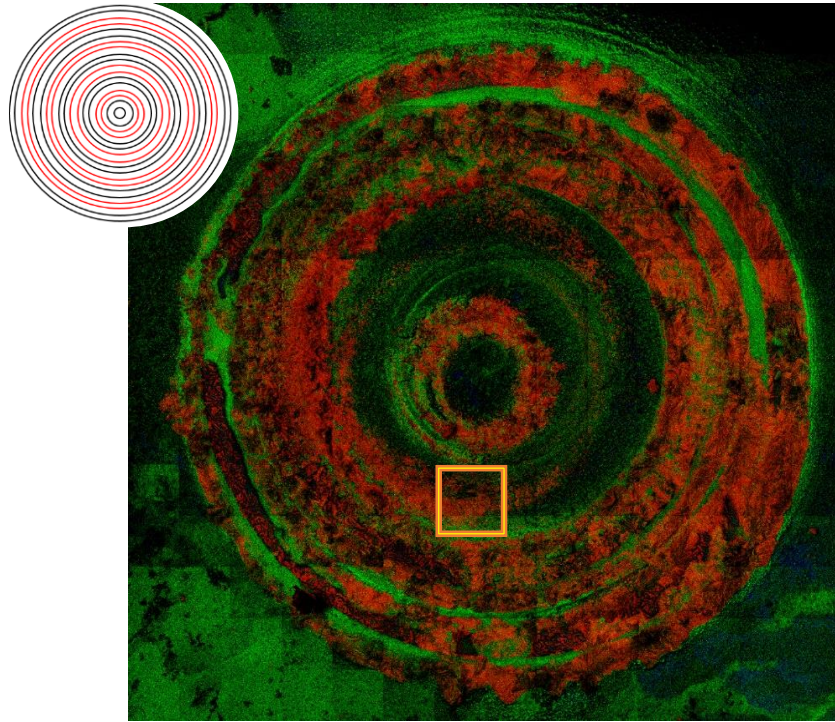


Figure 54: A TOF-SIMS image and its starting deposition design depicting a 6mm diameter deposition consisting of 4 distinct areas of fenofibrate (red) and 5 distinct areas of PVP K30 (green/black) of 2 printed lines each.

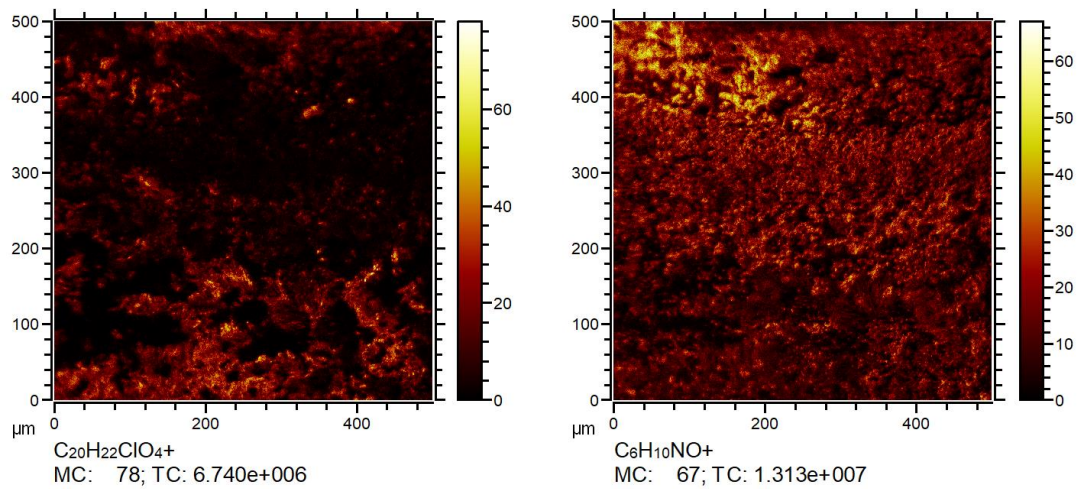


Figure 55: TOF-SIMS images taken of the area highlighted in Figure 54 with measurements for fenofibrate (left) and PVP K30 (right)

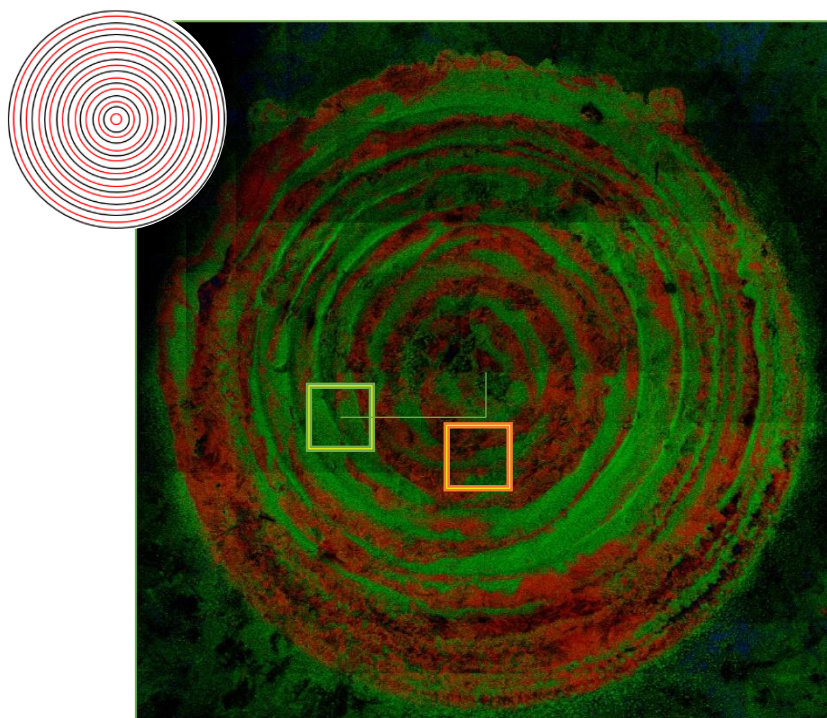


Figure 56: A TOF-SIMS image and its starting deposition design depicting a 6mm diameter deposition consisting of 9 distinct areas of fenofibrate (red) and 9 distinct areas of PVP K30 (green/black) of 1 printed line each.

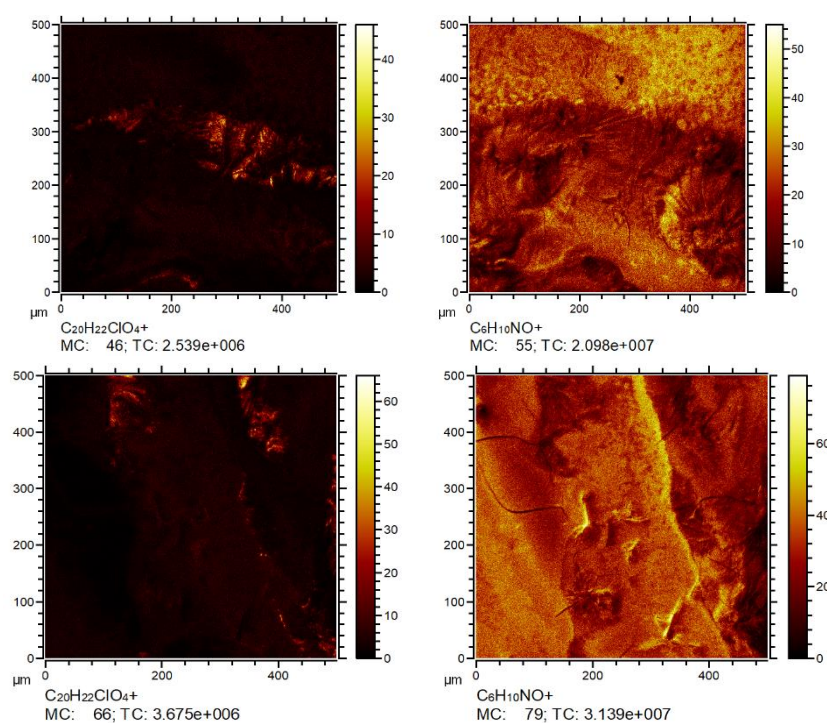


Figure 57: TOF-SIMS images taken of the 2 areas highlighted in Figure 56 with measurements for fenofibrate (left) and PVP K30 (right).

3.4 Conclusions

The use of the aerosol jet printer was analysed to establish if this technique was capable of scaling and high precision. Printing allows scaling by changing the number of layers, the area of deposition and the nozzle diameter. The most effective means was found to be layering as the same deposition was used consistently and there was no reliance on company specifications. The effect of changing the speed of deposition was also tested but it was found to be inadvisable as printing slowly resulted in more agglomeration and printing faster proved very unpredictable. Aerosol jet has never been used with pharmaceuticals previously. Ink materials including silver and carbon nanotubes have demonstrated the ability of the printer to generate focused lines with a range of different materials. The printer produces similarly linear relationships between nozzle size and layering, and similarly not so linear relationships with speed. As a result of this similar effect with different materials, there is evidence that the printer could be applied to additional materials and different drugs. Layering has previously shown a risk of material loss and nozzle size has previously been inflexible. The aerosol jet has eliminated this lack of movement and also the risk of tugging, which may damage the sample surface. Depth was shown to increase with polymer content which is thought to be related to the droplet size generated as demonstrated in Chapter 2. The level of control exhibited in the distribution testing is significantly higher than that of more conventional solid dosage form manufacturing processes. Drug distribution was also found to be controllable to the micrometre by printing drug and polymer separately with 3D Raman mapping and TOF-SIMS demonstrating distinct areas of drug and polymer. This is thought to be due to the ability to design samples using AutoCAD and thus bring a degree of control to the manufacturing process which standard manufacturing processes do not allow. The effect printing has on dissolution will be explored in Chapter 4.

Chapter 4: The Effect of Aerosol Jet Printing on Dissolution

4.1 Introduction

The current chapter is concerned with the effect of aerosol jet printing on dissolution. Drawing on the previous two chapters the effect of altering the solid state and producing precise dosage forms will be explored. Samples were once again printed as mixtures and as layered dosage forms. Samples were initially analysed by HPLC to determine their drug content. Dissolution was carried out by surface dissolution imaging, comparing the printed samples to direct compression controls. Samples were tested for drug release and intrinsic dissolution rate. The latter parameter was able to be related to wettability by utilising contact angle.

4.2 Materials and Methods

4.2.1 Materials

As detailed in Chapter 2 with the exception that the spin coated samples in this section were made at AstraZeneca, Macclesfield and as such the PVP K30 used was obtained from BASF (Ludwigshafen, Germany). This was directly compared to the Sigma PVP K30 and there was minimal difference.

4.2.2 Methods

4.2.2.1 Drug Content Analysis

Fenofibrate samples were analysed by UHPLC in manner detailed in Chapter 3. Based on the literature (Caviglioli et al. 2002, Farrar et al. 2002), mobile phases A (acidified water) and B (acetonitrile) used for fenofibrate were also applicable to ibuprofen but due to the nature of the UHPLC initial tests were required to confirm this. A method was developed for ibuprofen at 214nm as shown in Table 17. The validated calibration curve can be observed in Appendix 3. As with fenofibrate,

ibuprofen samples were printed on rice paper and dissolved in 10ml acetonitrile by sonication for 45 minutes and analysed in the manner detailed in Chapter 3.

Table 17: Method development for UHPLC of ibuprofen

Method	Mobile Phase (ACN: Acidified Water)	Observations
1	80:20	The baseline was relatively flat apart from an initial solvent front at 0.96 minutes, ibuprofen shows a retention time of 3.02 minutes
2	70:30	The baseline was a little noisy, an initial solvent front was observed at 0.727 minutes, ibuprofen shows a retention time of 4.553 minutes
3	60:40	The baseline was relatively flat apart from an initial solvent front at 0.707 minutes, ibuprofen shows a retention time of 7.7 minutes

4.2.2.2 Printing for Dissolution

Printing was carried out in the manner detailed in Chapter 2. All samples were prepared at 3mm/s using a 300µm nozzle and an ethanol-based ink and the details of preparation of individual formulations is given in Table 18. The samples were prepared by printing directly onto filled plastic sample cups obtained from Paraytec Ltd. (York, U.K.)

Initial printing work was very much focused on developing formulations to increase the overall release of fenofibrate relative to comparable physical mixtures. These formulations took 2 broad forms which were premixed ink-based formulations, and layers of drug alone and polymer alone. Latterly formulations took the form of ibuprofen-based premixed printed formulations as a comparison to the initial fenofibrate printed formulations. The complexities of each of these 3 formulations are given in Table 18 and a diagram demonstrating their differences is given in Figure 58.

Table 18: Formulations to increase dissolution of Class II Drugs

Dosage Form	CAD Drawing(s) to achieve	Components	Number of Layers (n)
Premix	2mm circle	Fenofibrate alone	25/5
		2:1 FNF:PVP premixed	
		1:1 FNF:PVP premixed	
		2:3 FNF:PVP premixed	
		1:2 FNF:PVP premixed	
		1:3 FNF:PVP premixed	
		1:4 FNF:PVP premixed	
Premix 2	2mm circle	Ibuprofen alone	5

		1:1 IBU:PVP premixed	
		1:2 IBU:PVP premixed	
		1:3 IBU:PVP premixed	
		1:4 IBU:PVP premixed	
Layered	2mm circle	FNF top layer, PVP bottom layer	20 for each layer
		PVP top layer, FNF bottom layer	
		FNF sandwiched between PVP in a 1:1 ratio	10 for each PVP layer, 20 for FNF layer
		As above in 1:2 ratio	20 for each PVP layer, 20 for FNF layer
		As above in 1:3 ratio	30 for each PVP layer, 20 for FNF layer
		As above in 1:4 ratio	40 for each PVP layer, 20 for FNF layer

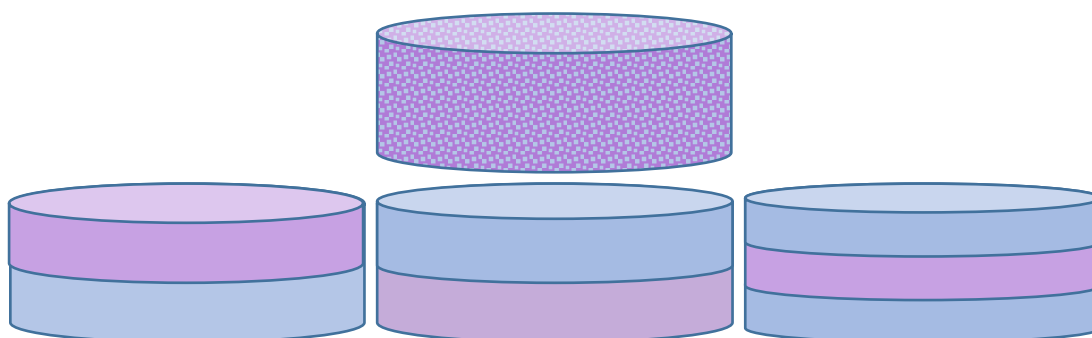


Figure 58: Designs of premixed (top), PVP first (left), fenofibrate first (middle) and sandwiched dosage forms.

4.2.2.3 *In Vitro* Dissolution Testing

Drug release was assessed using a Sirius Surface Dissolution Imager (SDI) (Sirius Analytical Instruments Ltd., Forrest Row, East Sussex, U.K.) (Figure 59).

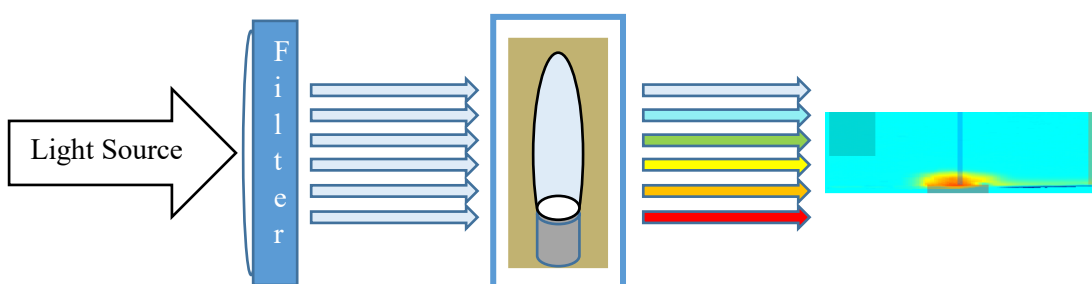


Figure 59: SDI process: UV light is shone through a UV filter into the quartz flow cell, which contains a sample cup. The UV absorbance is then fed into the Sirius Data Analyser.

Samples were tested in pH 6.8 simulated intestinal fluid (SIF) without enzymes (phosphate buffer) prepared following the standard British Pharmacopoeia method. 6.8g of potassium dihydrogen phosphate and 0.89g sodium hydroxide were dissolved in 1L deionised water, adjusting the pH with 0.1M sodium hydroxide as required (British Pharmacopoeia Commission, 2018).

Prior to dissolution testing a molar extinction coefficient value (MEC) had to be

obtained. This was achieved by dissolving the drug in methanol to form an initial stock solution. Then, for fenofibrate, this was diluted using methanol initially to make the total solvent content up to 10% and then filled up to the mark with SIF to give concentrations over a range of 1-10 μ g/ml. For ibuprofen this process was repeated but methanol was only used in the stock and not in the diluent. The resultant calibration standards were run in the SDI by initially adding an SIF:methanol blank for fenofibrate or SIF blank alone for ibuprofen to the syringe to generate a background reading. Then each standard was added to the flow cell by direct syringe infusion, measuring the UV absorbance of each at 0 ml/min over a period of 30 seconds. The SDI was run with a 280nm filter for fenofibrate samples and 214nm filter for ibuprofen samples. The molar concentration of the standards was multiplied by the path length (0.4 cm) (d) and plotted against absorbance using Microsoft Excel 2013 and Origin Pro 2017 (Appendix 3).

Compacts were prepared (using the standard Sirius Analytical Method) by adding physical mixtures to the sample cup within the micro compressor die and compressing to two clicks using a torque wrench at 60N for 10 minutes (using the standard Sirius Analytical Method, (Ward et al. 2017)). Samples were then added to the SDI flow cell chamber and SIF was passed over the surface of the sample cup for 1 minute at 1ml/min to remove any bubbles, 20 minutes at 0.2 ml/min and then flushed for 2 minutes at 1ml/min and allowed to diffuse for a further 1 minutes before flushing again.

Powdered controls were then compared to the formulations (Table 18) directly printed onto filled sample cups (obtained from Paraytec Ltd., York, U.K.). Release was observed using the Sirius program as a video, recording the absorbance over time. Samples were then analysed using the data analysis software with the appropriate MEC and molecular mass values for fenofibrate (14831 M/cm⁻¹ and 360.83 g/mol respectively) or ibuprofen (14806 M/cm⁻¹ and 206.29 g/mol respectively). Initial printed premixed drug and polymer tests took the form of 25 layer samples and comparisons were made to layered samples, however due to the need for development

as detailed in Chapters 5 and 6 and the constraints of the flow cell size, premixed samples were also tested with 5 layers and compared to ibuprofen. The drug release and intrinsic dissolution rate were plotted against time using Microsoft Excel 2013 and Origin Pro 2017.

4.2.2.4 Contact Angle

Samples were prepared for contact angle in two different ways. One set were printed using the Optomec as detailed in Chapter 2. The printer was run at 3mm/s using a 2cm diameter circle design to produce single layer samples. Glass microscope slides were used as substrates as glass was the most comparable to spin coating and also more compatible with contact angle measurement than rice paper. The other samples were prepared by spin coating using a Chemat Tech KW-4A Spin Coater (Chemat Scientific, Magnus, Tamworth, U.K.). The spin coater was run at 3000 rpm for 1 minute. A 50 μ l drop was added when the maximum speed was achieved, pipetting at a 90° angle to form an even coat. A more detailed list of samples prepared can be seen in Table 19.

Table 19: Samples prepared for contact angle

Sample Type	Components	“Ink” concentration in Ethanol
Spin coated	PVP only	15mg/ml, 30mg/ml, 45mg/ml, 60mg/ml, 90mg/ml and 120mg/ml
Spin coated	PVP and Fenofibrate	30mg/ml fenofibrate alone and with 15mg/ml (2:1), 30mg/ml (1:1), 45mg/ml (2:3), 60mg/ml (1:2), 90mg/ml (1:3) and 120mg/ml (1:4)
Inkjet Printed	PVP and Fenofibrate	30mg/ml fenofibrate alone and with 15mg/ml (2:1), 30mg/ml (1:1), 45mg/ml (2:3), 60mg/ml (1:2), 90mg/ml (1:3) and 120mg/ml (1:4)
Inkjet Printed 2	PVP and Ibuprofen	30mg/ml ibuprofen alone and with 30mg/ml (1:1), 60mg/ml (1:2), 90mg/ml (1:3) and 120mg/ml (1:4)

Samples were tested using a Krüss DSA 100 Contact Angle at AstraZeneca, Macclesfield and latterly a Krüss DSA 30 within the CMAC Hub (Krüss GmbH, Hamburg, Germany). 20 µl droplets of water were applied to the surface using a needle, using an autosampler on the Krüss DSA 100 and manually on the Krüss DSA 30. The instruments were both driven using the Drop Shape Analyser software and samples were analysed using the same software. The drop was initially created on the

needle surface and then the needle was lowered until it was just above the sample surface, as observed in the drop window. A video recording was started and then the needle was lowered until the droplet detached onto the sample surface. The changes in the sample were observed in real time on the video and once recorded the video was analysed using the video window. The point of initial contact was established and this was designated point zero. The baseline was then lined up with the point of surface contact and the contact angle was taken using the drop measurement tool. Care was taken to ensure the measurement reflected the shape of the actual droplet. The software was then allowed to run the remainder of the video to calculate the contact angle over time. Unfortunately, due to the nature of the samples utilised in this study this measurement proved less useful and thus the results were based on the initial contact angle taken at point zero.

4.3 Results & Discussion

4.3.1 Drug Content

4.3.1.1 Fenofibrate

It can be observed that fenofibrate and its premix formulations with PVP exhibit different drug content (Tables 20-21). Fenofibrate alone exhibits a high degree of error suggesting printing the drug alone is not very reproducible. Taking the standard error as a percentage of the average mass gives a value of 24.0%, which is the highest for all of the samples. The mass appears to increase with polymer content until 50% polymer content, following which the mass is observed to fall. It should be noted that the error between samples is also particularly high for the 50% samples, demonstrated by a standard error which is 20.4% of the average mass. This suggests printing this polymer to drug ratio is not very reproducible. The mass detected then falls which may be due to a combination of the viscosity resulting in larger droplets reducing the amount leaving the printer and the overall ratio of drug to polymer. On performing an ANOVA on the 25 layer samples, P-values of 0.73981 for fenofibrate and 2:1 fenofibrate:PVP, 0.01602 for 2:1 and 1:1 fenofibrate:PVP, 0.48568 for 1:1 and 2:3 fenofibrate:PVP, 0.98659 for 2:3 and 1:2 fenofibrate:PVP, 0.88768 for 1:2 and 1:3

fenofibrate:PVP, and 0.99969 for 1:3 and 1:4 fenofibrate:PVP. This supports the rise and fall in mass.

On comparison with the 5 layer samples (Table 21), a similar pattern in the results can be observed but with the highest content being observed at 2:3 fenofibrate:PVP. The variation between the average mass of each of the different ratios is statistically insignificant with P-values of 0.99774 for 2:1 and 1:1 fenofibrate:PVP, 0.32824 for 1:1 and 2:3 fenofibrate:PVP, 0.55606 for 2:3 and 1:2 fenofibrate:PVP, 0.99836 for 1:2 and 1:3 fenofibrate:PVP, and 0.9131 for 1:3 and 1:4 fenofibrate:PVP. It should be noted that the variation between 1:1 and 2:3 fenofibrate:PVP, and the variation between 2:3 and 1:2 is more significant, although statistically insignificant overall. This supports the difference in the drug: polymer exhibiting the highest mass.

The nature of the droplet formation may explain differences in mass between the different formulations as the higher the viscosity the larger the droplet formed and thus the more material carried. Fenofibrate is most prone to blockage as the drug readily crystallises on the metallic surfaces of the printer from its supersaturated atomisation state. As such the mass is quite low compared with the premixed drug and polymer samples. The mass increases until amorphous particles start to form and following this the mass starts to fall which may be due to a combination of viscosity and the resultant droplet morphology generated on atomisation.

Table 20: Drug content of printed fenofibrate alone and premixed with PVP as 25 layer x 0.9 mm² circle depositions, generated using a 300µm nozzle at 3 mm/s, measured at 280 nm by UHPLC.

Sample (FNF:PVP)	Average Drug Content (µg, n=10)	Standard Error (±µg, 2 d.p.)	95% LCL	95% UCL	Samples within BP specs for uniformity of content (%)
1:0	399.08	95.72	182.5 4	615.6 2	10
2:1	582.50	66.72	431.5 8	733.4 3	30
1:1	985.40	201.19	530.2 8	1440. 52	0
2:3	757.43	47.51	649.9 5	864.9 0	30
1:2	657.13	33.29	500.6 6	813.6 0	30
1:3	507.14	71.71	344.9 2	699.3 6	30
1:4	451.88	103.00	218.8 7	684.8 9	0

Table 21: Drug content of printed fenofibrate alone and premixed with PVP as 5 layer x 0.9 mm² circle depositions, generated using a 300µm nozzle at 3 mm/s, measured at 280 nm by UHPLC.

Sample (FNF:PVP)	Average Drug Content (µg, n=3, 2 d.p.)	Standard Error (±µg, 2 d.p.)	95% LCL	95% UCL	Samples within BP specs for uniformity of content (%)
2:1	91.96	20.55	3.55	180.38	33.33
1:1	98.28	11.24	49.93	146.63	33.33
2:3	130.75	15.32	76.92	184.58	66.67
1:2	105.19	16.61	33.70	176.68	33.33
1:3	111.089	28.18	-10.14	232.32	33.33
1:4	96.37	3.70	83.38	109.35	100

4.3.1.2 Ibuprofen

As can be observed in Table 22, like fenofibrate, ibuprofen printed alone is lower in terms of content compared to the samples printed with PVP, as demonstrated by a statistically significant P-value of 0.01534. However, once PVP is added the difference between the samples is considerably less than the fenofibrate samples with statistically insignificant P-values of 0.52595 on comparison of 1:1 and 1:2, 0.59093 on comparison of 1:2 and 1:3 and 0.30897 on comparison of 1:3 and 1:4 ibuprofen:PVP. The error for each of the different sample types is also considerably lower suggesting the samples are more reproducible overall. It should be noted that ibuprofen generally printed more efficiently than fenofibrate which may explain the more reproducible mass. Additionally, the particles produced on printing ibuprofen and PVP together are more similar in nature overall suggesting the droplets produced during atomisation are more similar than their fenofibrate counterparts. 1:4

ibuprofen:PVP may be slightly lower overall as the SEM suggests the material is more agglomerated.

Table 22: Drug content of printed ibuprofen alone and premixed with PVP as 5 layer x 0.9 mm² circle depositions, generated using a 300µm nozzle at 3 mm/s, measured at 214 nm by UHPLC.

Sample (IBU:PVP)	Average Drug Content (µg, n=3, 2 d.p.)	Standard Error (±µg, 2 d.p.)	95% LCL	95% UCL	Samples within BP specs for uniformity of content (%)
1:0	50.81	6.67	17.67	83.96	33.33
1:1	99.93	4.61	77.04	122.83	100
1:2	81.65	7.62	43.78	119.52	66.67
1:3	98.57	11.77	40.07	157.06	33.33
1:4	74.93	6.10	44.61	105.25	100

4.3.2 Dissolution

4.3.2.1 Fenofibrate

4.3.2.1.1 Molar Extinction Coefficient

The molar extinction coefficient (MEC) for fenofibrate was obtained from the mean result of 3 samples over a range of 1-10µg/ml. As can be observed in Appendix 3, the molar extinction coefficient obtained was 14831M/cm⁻¹, based on an r²-value of 0.9948. The r²-value is not as close to 1 as hoped but the low concentration range

limits this slightly. On statistical analysis the curve was found to be statistically non-significant supporting this. This curve is based on a 90:10 SIF:methanol solution as fenofibrate proved so poorly soluble that the use of a 10% methanol solution was necessary even at 1µg/ml to ensure the solution did not precipitate out in the syringe. This does limit the data slightly but unfortunately no other solution could be found to this issue. Previous studies (Dhabale and Gharge 2010, Gupta et al. 2010, Kondawar et al. 2011, Sevda et al. 2011, Mandwal et al. 2012, Hirave et al. 2013) carried out their entire calibration curve in methanol but it was felt this would yield too big a difference from the buffer solution.

4.3.2.1.2 Physical Mixtures vs. Printed Mixtures

4.3.2.1.2.1 Drug Release

Drug release achieved from control powder based compacts of fenofibrate and PVP K30 (Figure 60) results in an increase in drug release relative to drug alone, with the release increasing with polymer content. Ultimately on addition of 80% polymer the release increases by 10-fold relative to the drug alone. However, this increase is not very reproducible between the compacts and in fact does not increase in a linear fashion. For example, on addition of 33.3% polymer the release is lower than that of the drug alone, and samples with 60% polymer content exhibit a higher average release than those with 66.7% polymer content. On conducting an ANOVA, most of the samples do not exhibit a significant change from fenofibrate alone with the exception of those containing 80% polymer content which have a P-value of 0.04244.

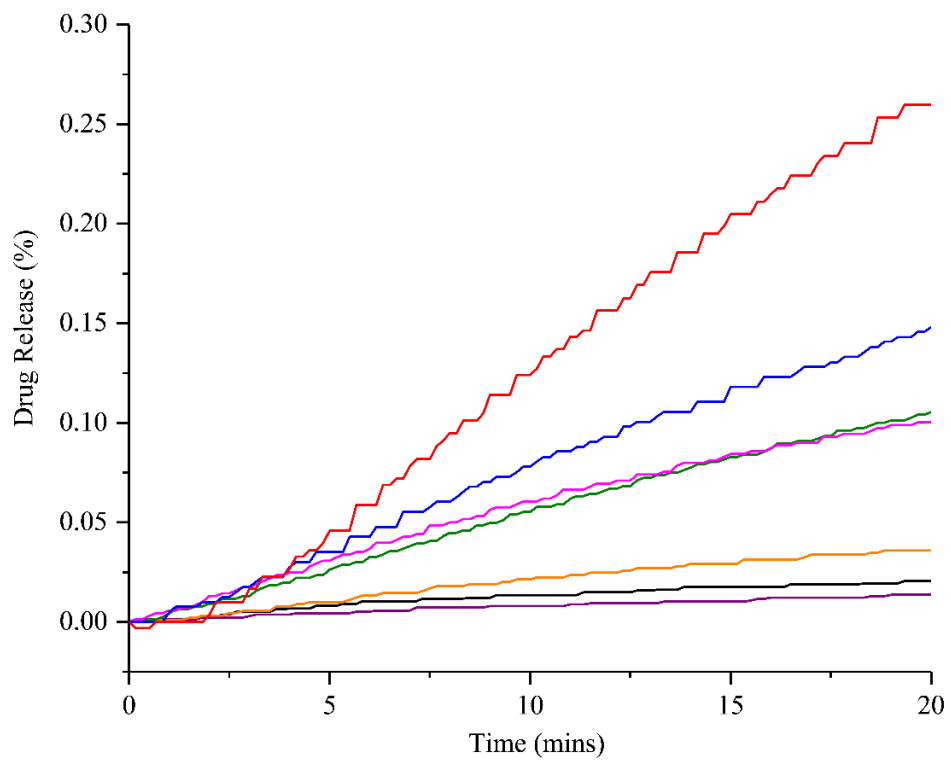
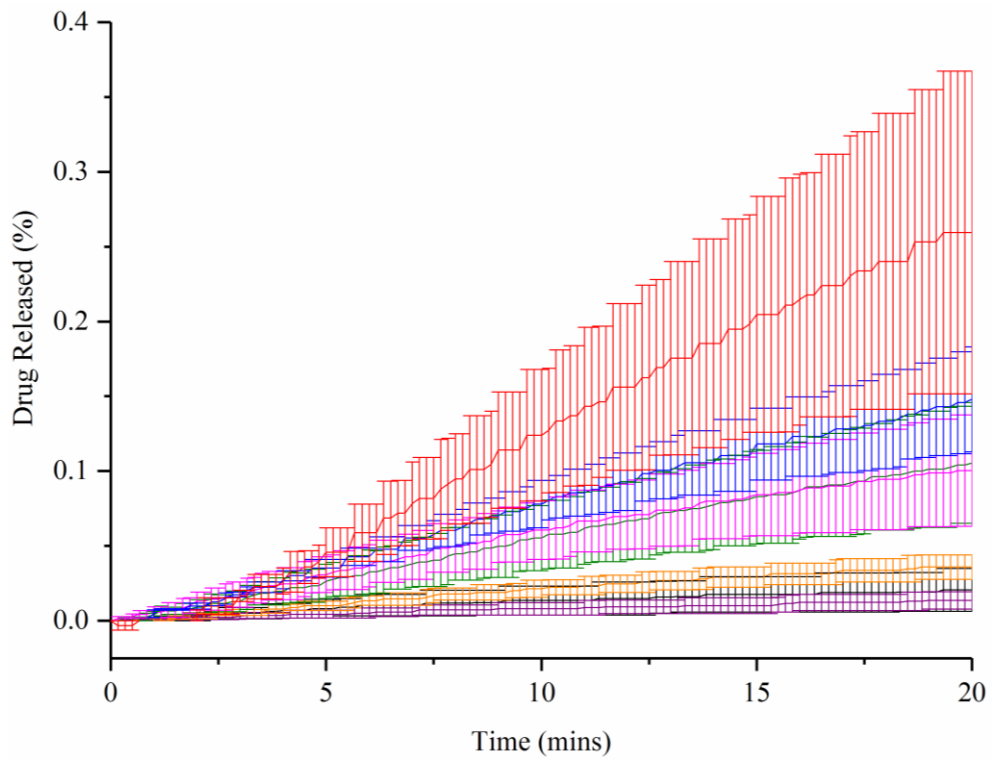


Figure 60: Percentage Drug Release from compacts of fenofibrate (100% crystalline) (black) and, 2:1 (88.7% crystalline) (purple), 1:1 (87.7% crystalline) (orange), 2:3 (85.9% crystalline) (green), 1:2 (85.9% crystalline) (magenta), 1:3 (87.3% crystalline)

(blue) and 1:4 (78.9% crystalline) (red) fenofibrate:PVP K30, $n=3 \pm$ standard error, with (top) and without (bottom) error bars. $P=1$ for FNF to 2:1, $P=0.99986$ for 2:1 to 1:1, $P=0.94029$ for 1:1 to 2:3, $P=1$ for 2:3 to 1:2, $P=0.99012$ for 1:2 to 1:3 and $P=0.66756$ for 1:3 to 1:4.

The printed samples (Figure 61), however, show a 10 to 30-fold higher drug release relative to the comparable powder-based compact samples. The greatest release is achieved by the samples exhibiting amorphous particles with 2:3 fenofibrate:PVP showing a substantial increase relative to 1:1 fenofibrate:PVP on initial amorphous particle formation, and 1:3 fenofibrate:PVP showing a substantial increase relative to 1:2 fenofibrate:PVP on the complete loss of crystallinity with the latter showing a statistically significant P-value of 0.004. 1:4 fenofibrate:PVP shows the greatest increase overall with up to 4.3% release in 20 minutes. This shows a 40-fold increase relative to printed drug alone. On conducting an ANOVA, the significant change relative to the drug alone is demonstrated by P-values of 0.00757, 1.647×10^{-7} and 3.62978×10^{-7} for 1:2 fenofibrate:PVP, 1:3 fenofibrate:PVP and 1:4 fenofibrate:PVP respectively. On direct comparison with the powdered samples these three samples also showed the most significant change relative to their powder counterparts with P-values of 0.00986, 2.09001×10^{-7} and 1.04387×10^{-7} for 1:2, 1:3 and 1:4 fenofibrate:PVP respectively. The samples are also generally more reproducible than the powder compacts as demonstrated by smaller error bars overall.

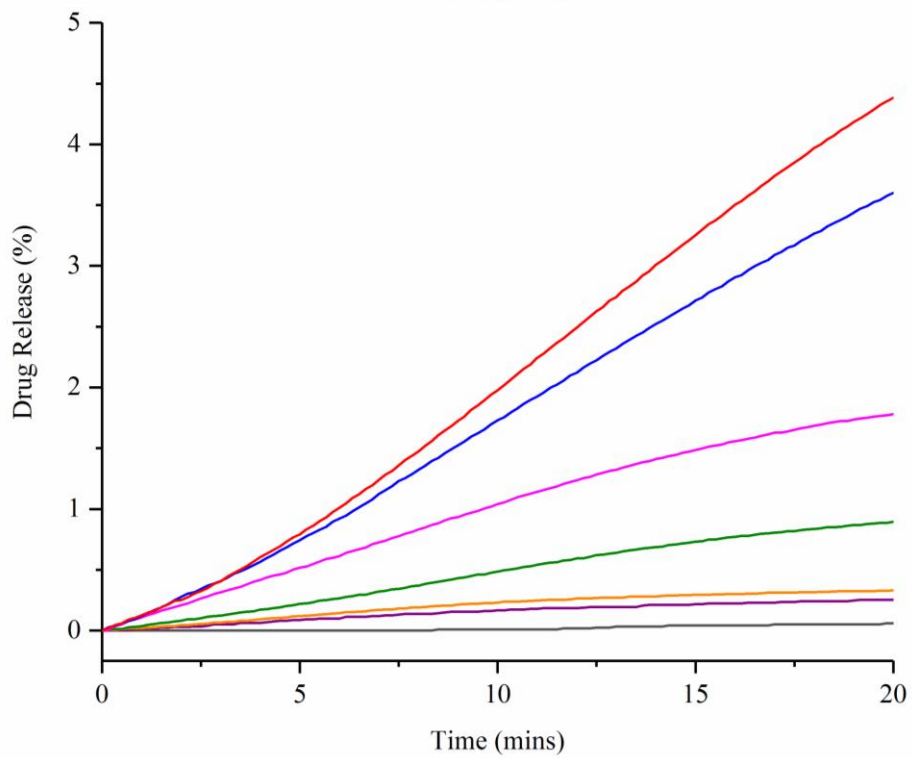
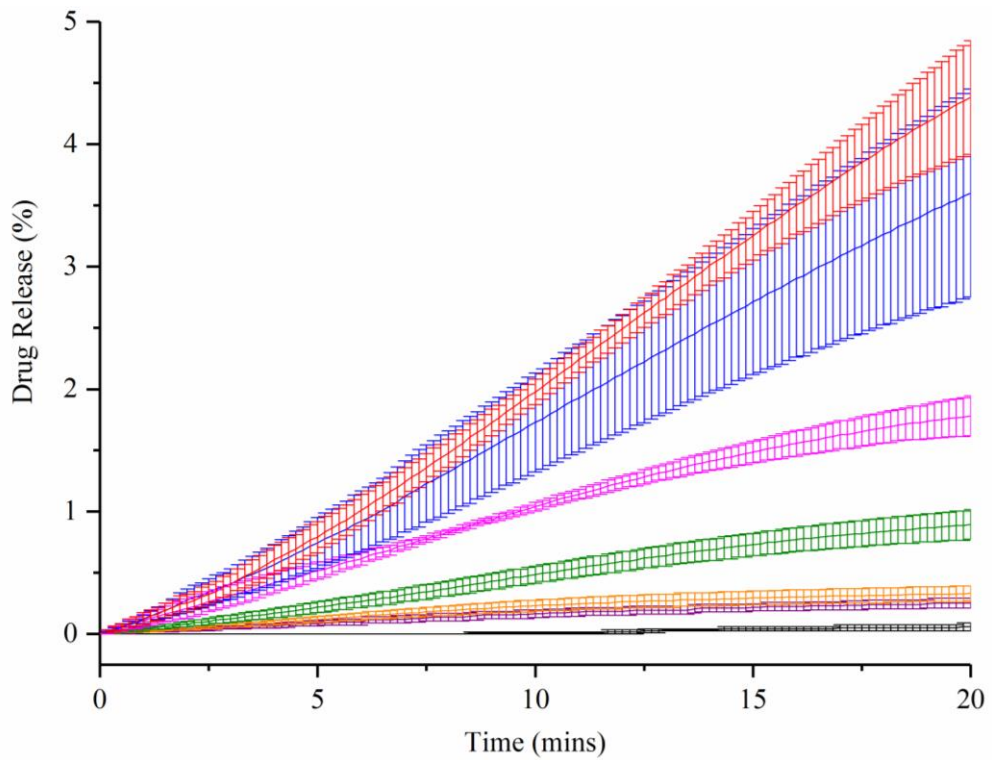


Figure 61: Percentage Drug Release from printed samples of fenofibrate (100% crystalline) (black) and, 2:1 (66% crystalline) (purple), 1:1 (59.5% crystalline) (orange), 2:3 (44.8% crystalline) (green), 1:2 (41.1% crystalline) (magenta), 1:3 (0% crystalline) (blue) and 1:4 (0% crystalline) (red) fenofibrate:PVP K30, $n=3 \pm$ standard error, with (top) and without (bottom) error bars. $P=1$ for FNF to 2:1, $P=1$ for 2:1 to

1:1, P=0.96255 for 1:1 to 2:3, P=0.5598 for 2:3 to 1:2, P=0.004 for 1:2 to 1:3, P=0.73471 for 1:3 to 1:4.

On comparison to the literature, the most similar papers which could be found investigated the effect of spray drying nanoparticles of fenofibrate and PVP. In a study by Hugo et al., fenofibrate was spray dried with PVP K25 in a 1:3 ratio in ethanol resulting in a 10-fold increase in dissolution similar to this study (Hugo et al. 2012). Another study by Choi et al. demonstrating preparation of fenofibrate: polymer 1:1 nanoparticles by spray drying compared the use of ethyl cellulose, Carbopol, HPMC and PVP on drug dissolution. PVP showed the greatest effect on dissolution with more than a 4-fold increase in dissolution compared to the drug alone (Choi, Lee, et al. 2013). An increase in drug release from inks using fenofibrate in ethanol (Vialpando et al. 2012, Hossen et al. 2014) have also been demonstrated previously but interestingly inkjet printing the combination of fenofibrate and PVP in ethanol has not been presented in the literature.

4.3.2.1.2.2 Intrinsic Dissolution Rate

There has been extensive research carried out into intrinsic dissolution rate using the SDI in the Østergaard group (Østergaard, Lenke, et al. 2014, Jensen et al. 2016, Sun and Østergaard 2017, Ward et al. 2017, Østergaard 2018). However, the current study is believed to be one of the first to use fenofibrate and as such is fairly novel. Like drug release intrinsic dissolution rate increases with polymer content in the control compacts but the increase is no more than $5\mu\text{g}/\text{min}/\text{cm}^2$ (Figure 62). However, on printing this increase is up to $40\mu\text{g}/\text{min}/\text{cm}^2$ (Figure 63), showing nearly a 10-fold increase. The 1:2, 1:3 and 1:4 fenofibrate:PVP samples show the most notable difference as shown by an exponential increase in Figure 64. This is supported by an ANOVA where 1:2, 1:3 and 1:4 are found to have a statistically significant difference from their powder counterparts. Additionally, 2:3, 1:2, 1:3 and 1:4 fenofibrate:PVP printed samples also show significant differences compared to printed drug alone, which may be due to the presence of amorphous particles. Whereas, the powdered

physical mixtures do not show statistically significant differences from the raw drug alone. Once again, the compacts are found to have sizeable error bars compared to the printed samples suggesting the latter is more reproducible overall. This may be due to the manner in which the compact erodes as well as the lack of control over drug distribution. This has been observed previously in compact based studies using the poorly soluble drug griseofulvin (Madelung et al. 2017). Additionally, it should be noted that the average intrinsic dissolution rates of the 2:3, 1:2, 1:3 and 1:4 fenofibrate:PVP compacts do not follow a logical pattern, with intrinsic dissolution rate increasing with polymer content. The curves for 2:3 and 1:2 fenofibrate:PVP are generally higher than that of 1:4 fenofibrate:PVP. Whereas, on printing intrinsic dissolution rate increases with polymer content. Additionally, the shape of intrinsic dissolution rate curves changes on printing. The compacts are observed to result in an initial sharp increase before a gradual decrease. This has been observed in the literature previously with this behaviour being attributed to heterogeneity in the blend and an initial release of loose powder (Østergaard, Lenke, et al. 2014, Madelung et al. 2017, Ward et al. 2017). On printing the intrinsic dissolution shows more of a gentle curvature which may be attributed to the gradual release from a matrix. This may be due to the improved dispersion of drug and the absence of loose powder.

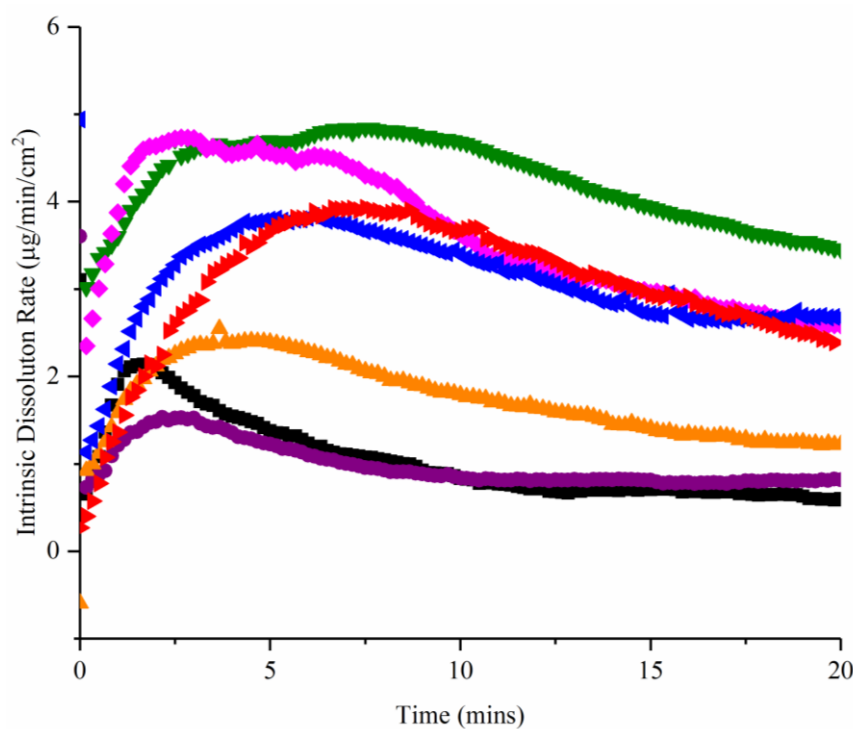
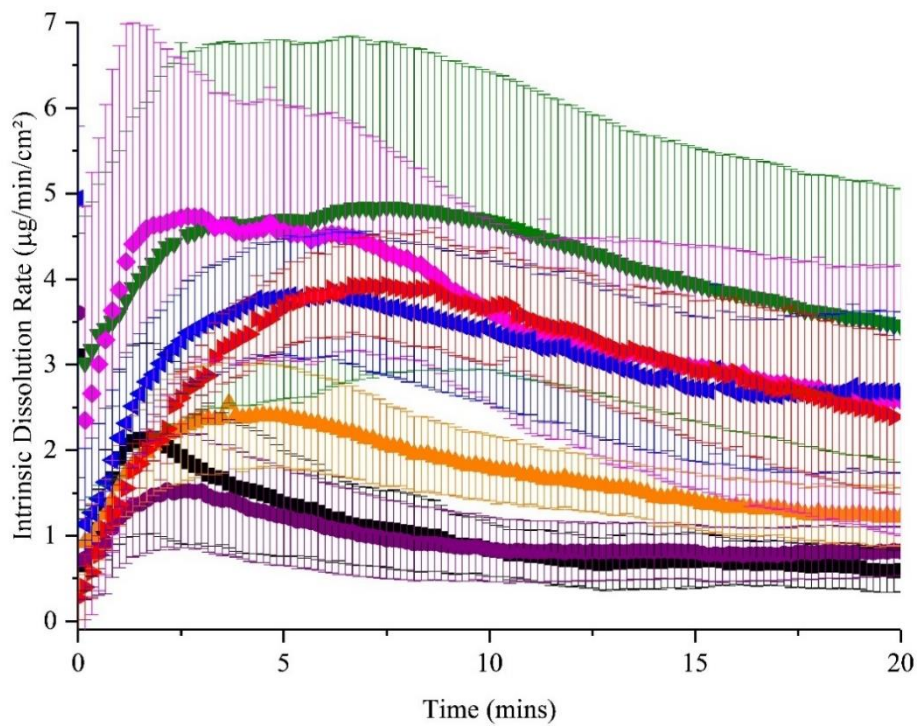


Figure 62: Intrinsic Dissolution Rate obtained from compacts of fenofibrate (black) and, 2:1 (purple), 1:1 (orange), 2:3 (green), 1:2 (magenta), 1:3 (blue) and 1:4 (red) fenofibrate:PVP K30, $n=3 \pm$ standard error, with (top) and without (bottom) error bars. $P=1$ for FNF to 2:1, $P=1$ for 2:1 to 1:1, $P=0.99999$ for 1:1 to 2:3, $P=1$ for 2:3 to 1:2, $P=1$ for 1:2 to 1:3 and $P=1$ for 1:3 to 1:4. $P=1$ for FNF and 1:1, $P=0.99995$ for FNF and 2:3, $P=0.99997$ for FNF and 1:2, $P=1$ for FNF and 1:3 and $P=1$ for FNF and 1:4.

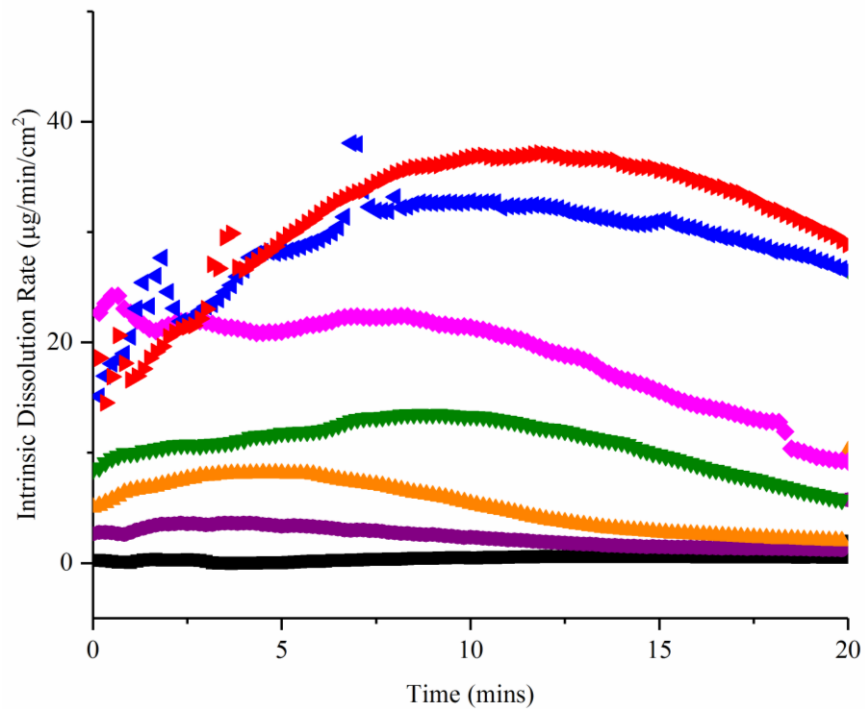
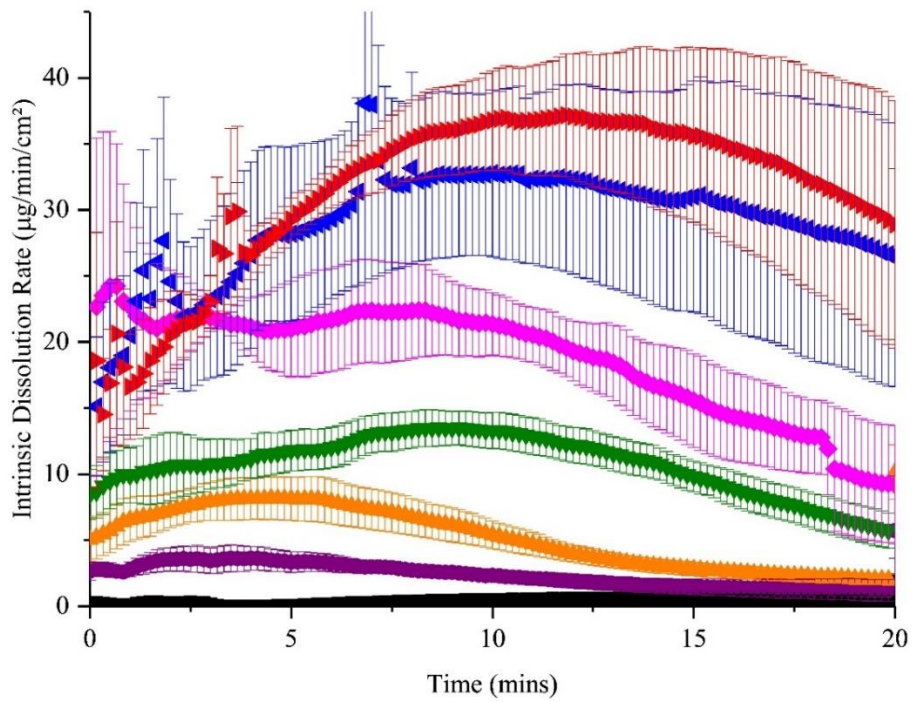


Figure 63: Intrinsic Dissolution Rate obtained from printed samples of fenofibrate (black) and, 2:1 (purple), 1:1 (orange), 2:3 (green), 1:2 (magenta), 1:3 (blue) and 1:4 (red) fenofibrate:PVP K30, $n=3 \pm$ standard error. $P=0.99982$ for FNF to 2:1, $P=0.95479$ for 2:1 to 1:1, $P=0.44234$ for 1:1 to 2:3, $P=0.55913$ for 2:3 to 1:2, $P=0.96696$ for 1:2 to 1:3 and $P=0.98319$ for 1:3 to 1:4. $P=0.55226$ for FNF and 1:1, $P=0.0033$ for FNF and 2:3, $P=1.04535 \times 10^{-5}$ for FNF and 1:2, $P=4.07014 \times 10^{-7}$ for FNF and 1:3, $P=1.17143 \times 10^{-7}$ for FNF and 1:4.

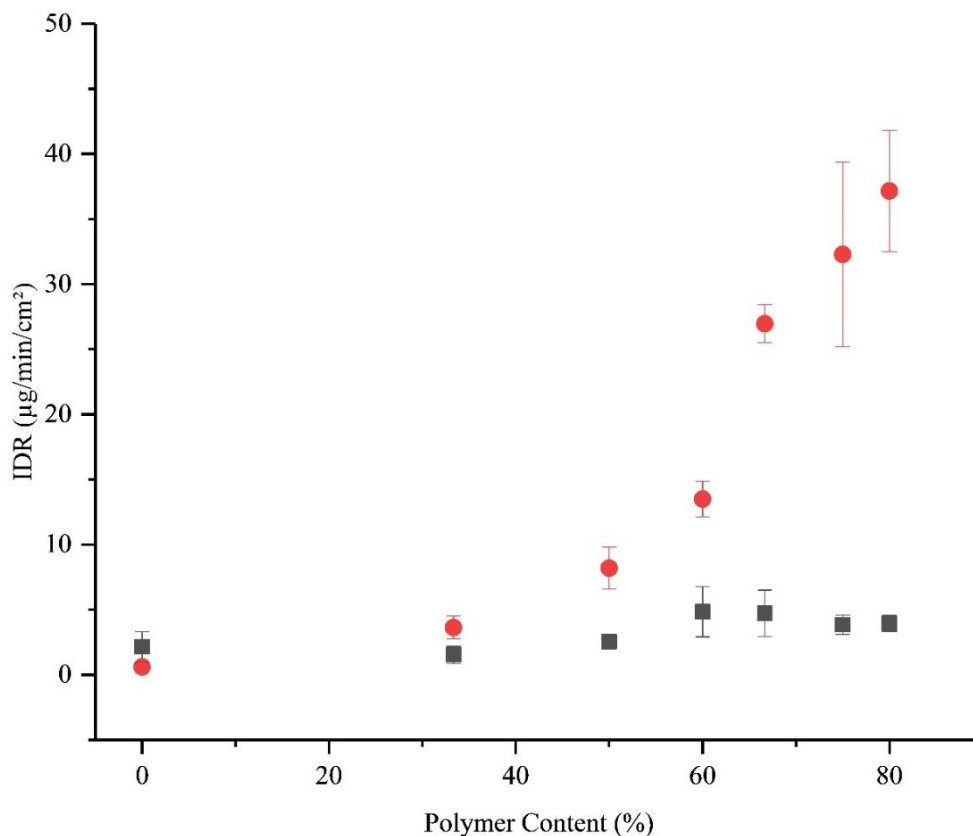


Figure 64: Comparison of intrinsic dissolution rate of powder (black) and printed (red) samples against percentage polymer content. $P=1$ for FNF, $P=1$ for 2:1, $P=0.85795$ for 1:1, $P=0.05068$ for 2:3, $P=1.65097 \times 10^{-4}$ for 1:2, $P=2.72202 \times 10^{-6}$ for 1:3 and $P=2.1033 \times 10^{-7}$ for 1:4.

On comparison of images taken from the SDI (Figure 65), it can be observed that the compacts behave very differently to the printed samples. Initially, fenofibrate shows little difference on printing which is consistent with the drug release and intrinsic dissolution rate. However, 2:1 and 1:1 fenofibrate:PVP show more of a tail on printing which is consistent with their higher drug release and intrinsic dissolution rate values. Although the tail increases with polymer content in the compact samples the printed samples continue to demonstrate more movement of material. On printing 2:3 fenofibrate:PVP, swelling of the sample and a broader tail can be observed which may be due to the amorphous particle induction. This effect becomes more pronounced with polymer content with 1:3 and 1:4 fenofibrate:PVP showing the greatest degree of

swelling and material flow overall, reflecting their higher intrinsic dissolution rate and drug release.

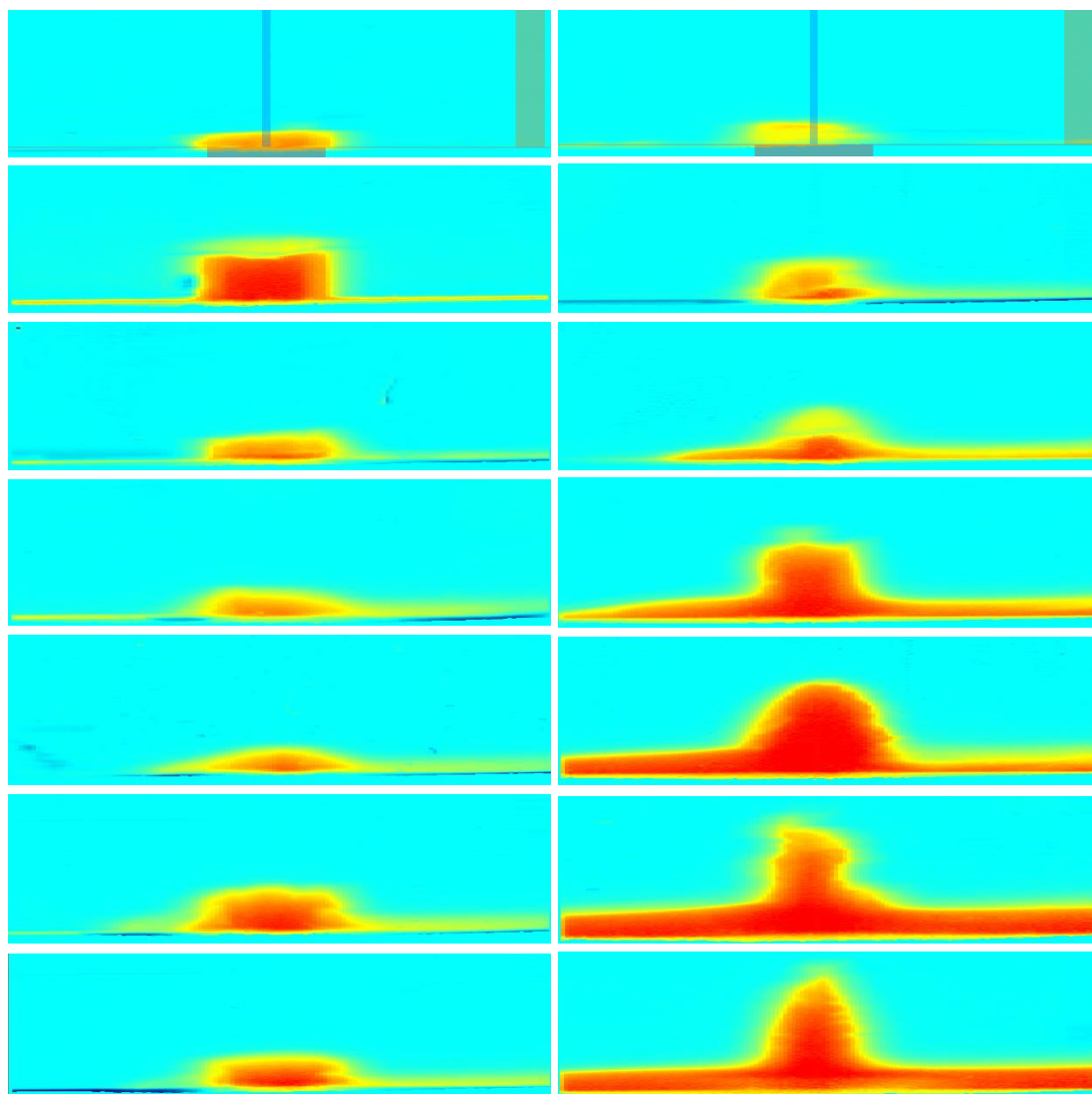


Figure 65: Images taken from the Sirius SDI Data Analysis software of fenofibrate and PVP powder compacts and printed samples at 5 minutes into the dissolution run - powdered samples (left) and printed samples (right) of (top to bottom) fenofibrate and fenofibrate:PVP 2:1, 1:1, 2:3, 1:2, 1:3, 1:4.

4.3.2.1.3 Layered Samples

No previous evidence could be found for using the SDI for this type of sample and as such this section is novel in nature. Layering samples (Figures 66-70) also shows a slight increase in drug release and intrinsic dissolution rate relative to the physical

mixtures, although not as dramatic as that of the premixed samples. It is thought this is due to the presence of PVP in a porous form which the drug can interact and diffuse through, but the drug retains its crystalline character and thus the overall release is inhibited. Samples are much less uniform overall, and this is primarily due to the fact that as the drug and polymer are not premixed the release is not as well controlled.

On performing an ANOVA, it can be observed that there is no significant difference between the drug release of the samples apart from that of 1:4 fenofibrate:PVP. These samples show a P-value of 4.83837×10^{-5} on comparison with 1:3 fenofibrate:PVP and a P-value of 6.26591×10^{-7} on comparison with a 1:4 fenofibrate:PVP physical mixture. However, there is no significant difference between the layered 1:4 fenofibrate:PVP samples and premixed printed samples. On comparison of the steady state intrinsic dissolution values it can be observed that there is no significant difference between the layered samples or on comparison to their physical mixture counterparts (Figure 67). However, there is a significant difference between some of the layered and premix samples as exhibited by P-values of 4.98885×10^{-6} , 3.89482×10^{-6} and 1.43103×10^{-5} for 1:2, 1:3 and 1:4 fenofibrate:PVP respectively.

On direct comparison of the 50% polymer samples it can be observed that drug location has minimal effect on the release (Figure 68). Additionally, on carrying out an ANOVA, there is no significant difference between intrinsic dissolution rates at steady state and the overall drug release as demonstrated by P-values of 1 (Figures 68 and 69).

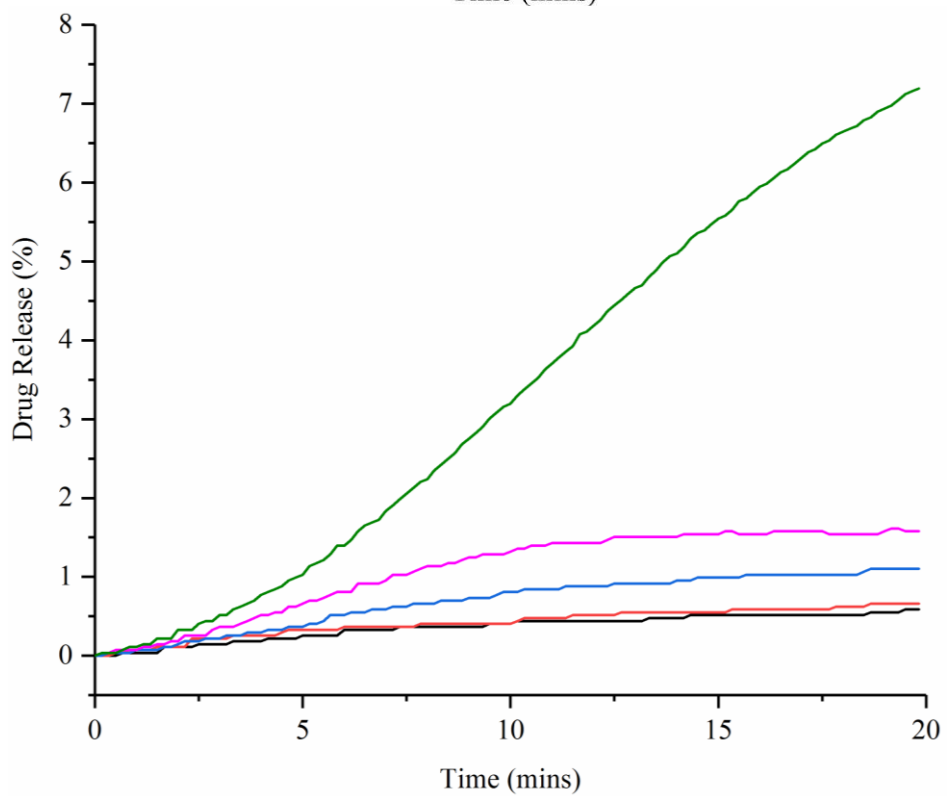
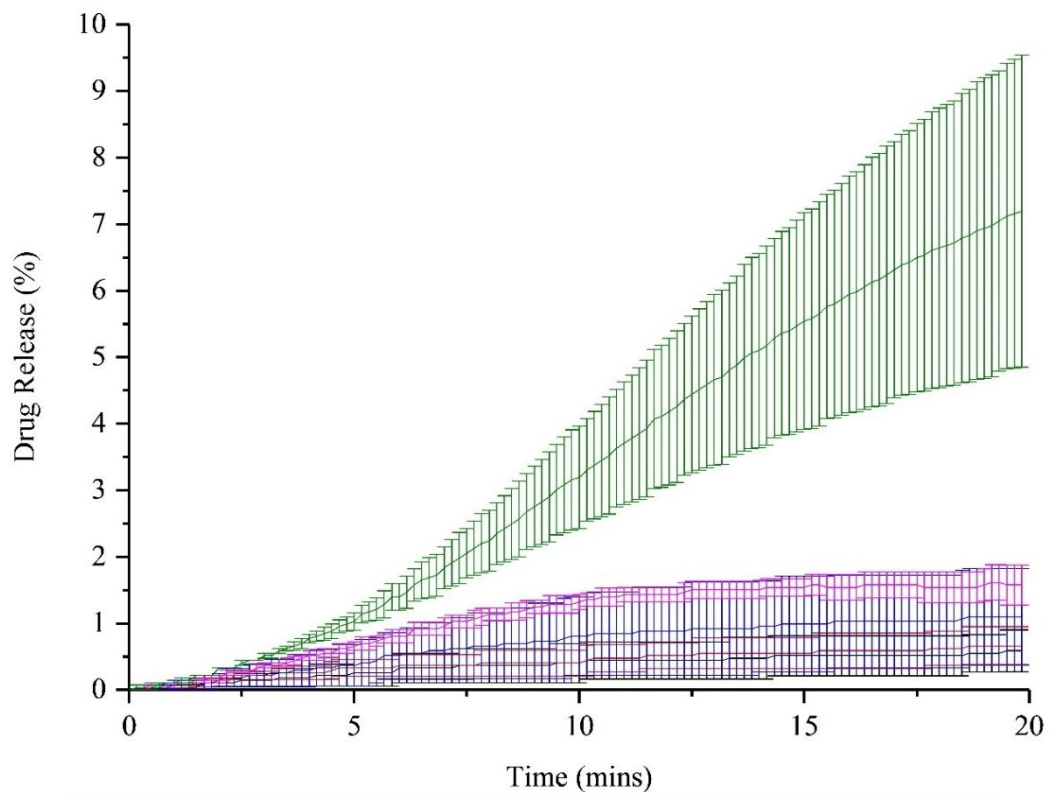


Figure 66: Percentage drug release of printed fenofibrate (black) compared to layered with PVP in 1:1 (red), 1:2 (blue), 1:3 (magenta) and 1:4 (green) ratios where $n=3\pm SE$, with (top) and without (bottom) error bars. $P=1$ for fenofibrate to 1:1, $P=1$ for 1:1 to 1:2, $P=1$ for 1:2 to 1:3 and $P=4.83837\times 10^{-5}$ for 1:3 for 1:4.

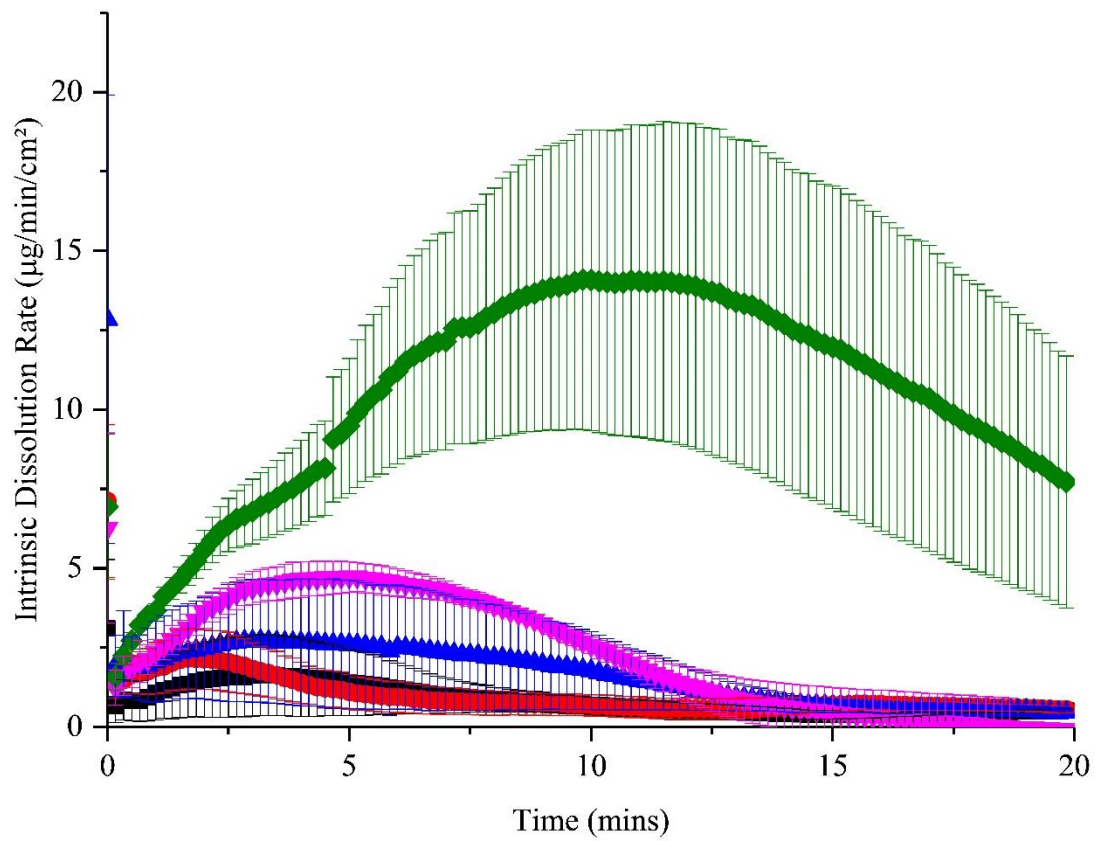


Figure 67: Intrinsic dissolution rate of printed fenofibrate (black) compared to layered with PVP in 1:1 (red), 1:2 (blue), 1:3 (magenta) and 1:4 (green) ratios where $n=3\pm SE$. $P=1$ for fenofibrate to 1:1, $P=1$ for 1:1 to 1:2, $P=1$ for 1:2 to 1:3 and $P=0.50254$ for 1:3 for 1:4.

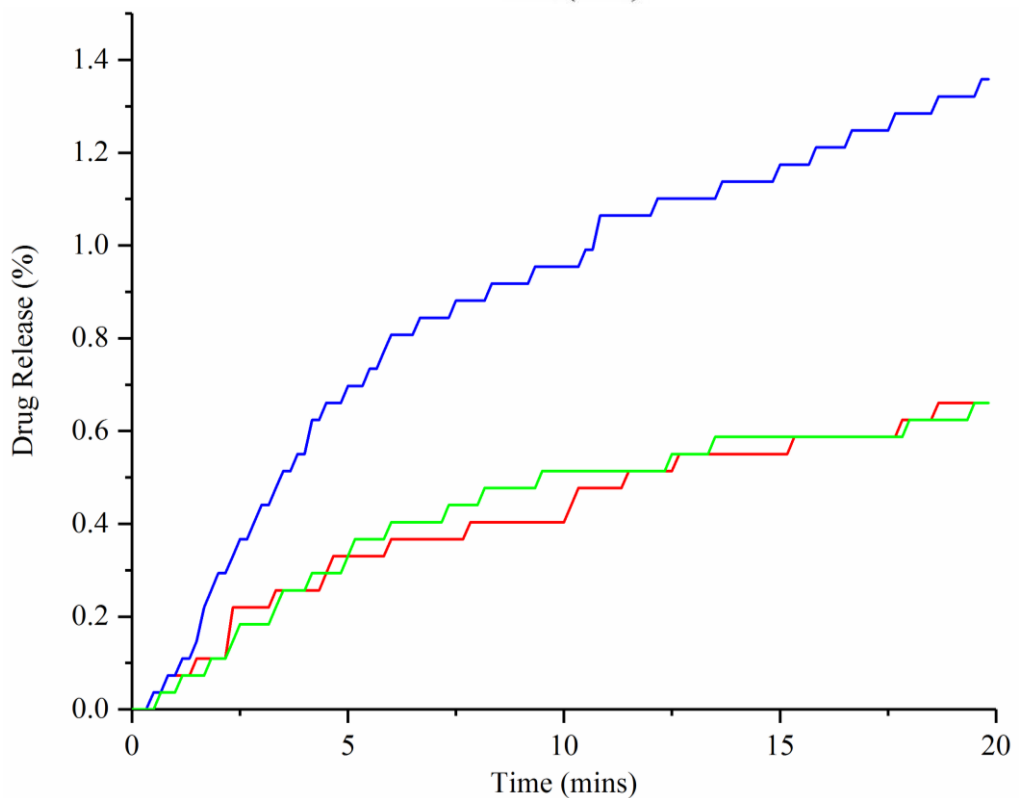
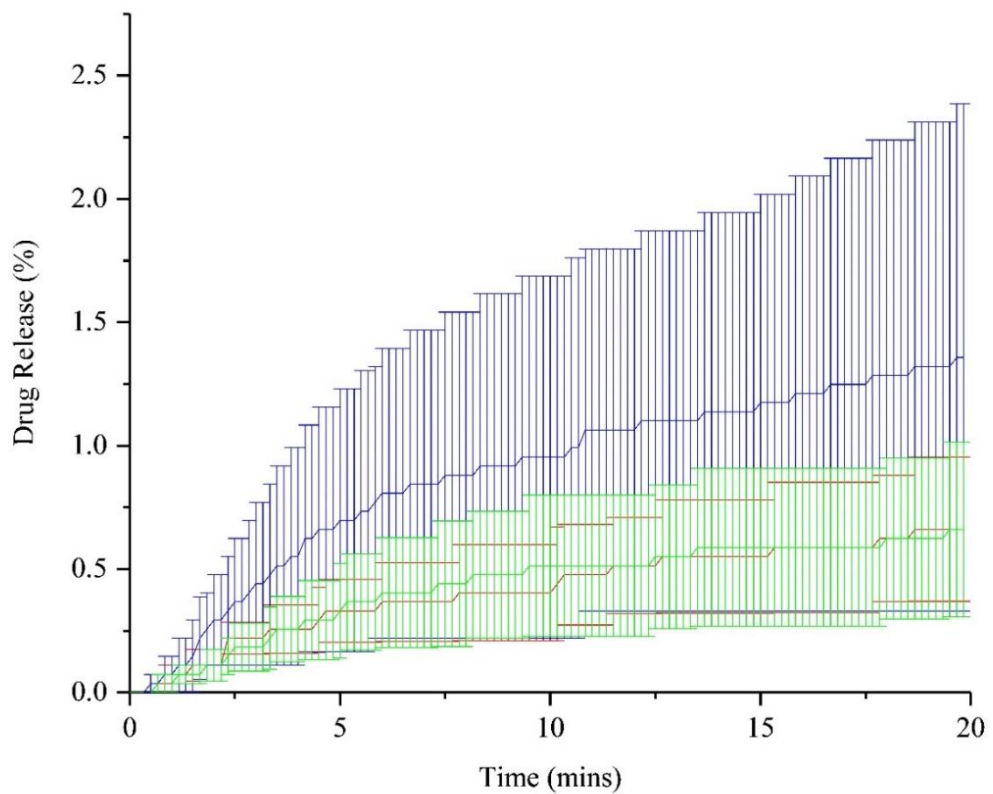


Figure 68: Comparison of percentage drug release of 1:1 layered samples, 1:1 PVP first (blue), 1:1 fenofibrate first (green) and 1:1 sandwiched (red) where $n=3\pm SE$, with (top) and without (bottom) error bars. $P=1$ for 1:1 sandwiched to 1:1 PVP first, $P=1$ for 1:1 sandwiched to 1:1 FNF first, $P=1$ for 1:1 PVP first to 1:1 FNF first.

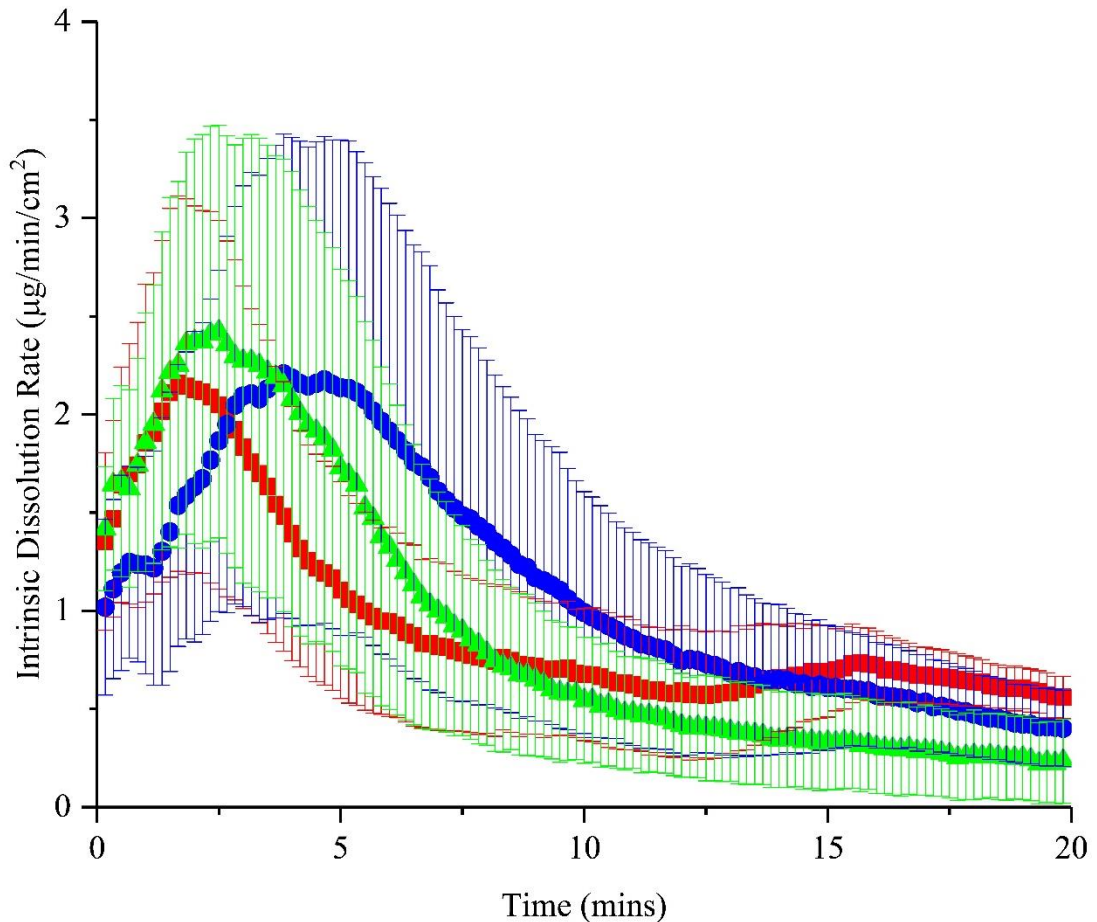


Figure 69: Comparison of intrinsic dissolution rate of 1:1 layered samples, 1:1 PVP first (blue), 1:1 fenofibrate first (green) and 1:1 sandwiched (red) where $n=3 \pm SE$. $P=1$ for 1:1 sandwiched to 1:1 PVP first, $P=1$ for 1:1 sandwiched to 1:1 FNF first, $P=1$ for 1:1 PVP first to 1:1 FNF first.

As can be observed in Figure 70, the flow of material changes with polymer content as it did on premixing but the effect is not as pronounced. 1:1 PVP first, 1:1 fenofibrate first and 1:1 sandwiched all show similar tails which is consistent with the fairly similar release and intrinsic dissolution rate. 1:2 and 1:3 have slightly more pronounced tails but not as pronounced as their premix counterparts. 1:4 shows evidence of swelling which may explain the higher release and intrinsic dissolution rate observed overall.

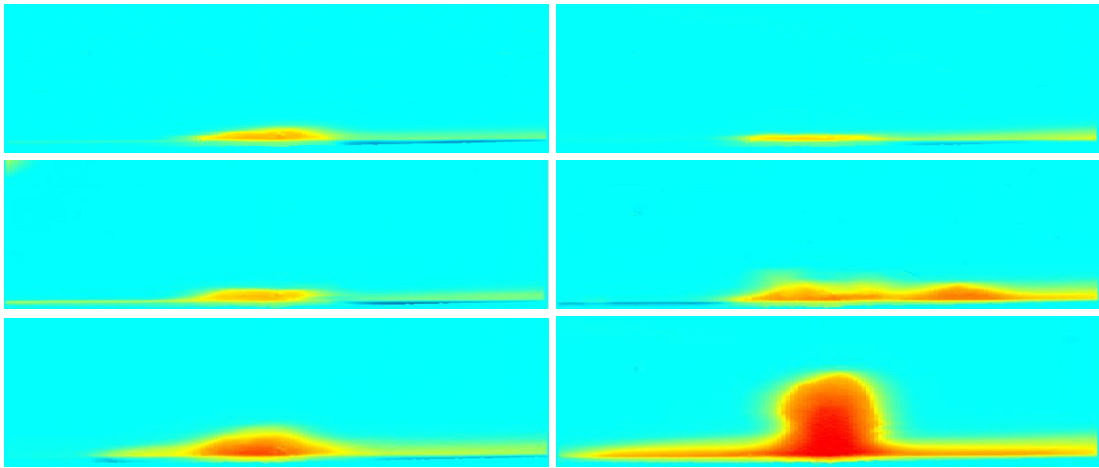


Figure 70: Images taken from the Sirius SDI Data Analysis software of fenofibrate and PVP layered samples at 5 minutes into the dissolution run: Layered printed samples of fenofibrate:PVP 1:1 PVP printed first (top left), 1:1 fenofibrate printed first (top right), 1:1 sandwiched (middle left), 1:2 sandwiched (middle right), 1:3 sandwiched (bottom left) and 1:4 sandwiched (bottom right)

4.3.2.1.4 Premix 5 Layers

On reducing the overall mass printed the drug release is still comparable with 25 layers but it would be expected that the overall percentage should increase which suggested that the fenofibrate had become a limiting factor to the study (Figure 71). This is supported by an ANOVA which showed no significant changes between the drug release values between the 25 layer and 5 layer samples. The intrinsic dissolution rate also drops considerably as a result of the change in layer number with 2:3 fenofibrate:PVP showing a P-value of 0.0061, 1:2 fenofibrate:PVP showing a P-value of 5.18738×10^{-5} , 1:3 fenofibrate:PVP showing a P-value of 4.32801×10^{-6} and 1:4 fenofibrate:PVP showing a P-value of 4.91635×10^{-7} (Figure 72). Due to the requirements of the work detailed in Chapters 5 and 6, the drug was changed in favour of ibuprofen, which has the advantage of being less poorly soluble in pH 6.8.

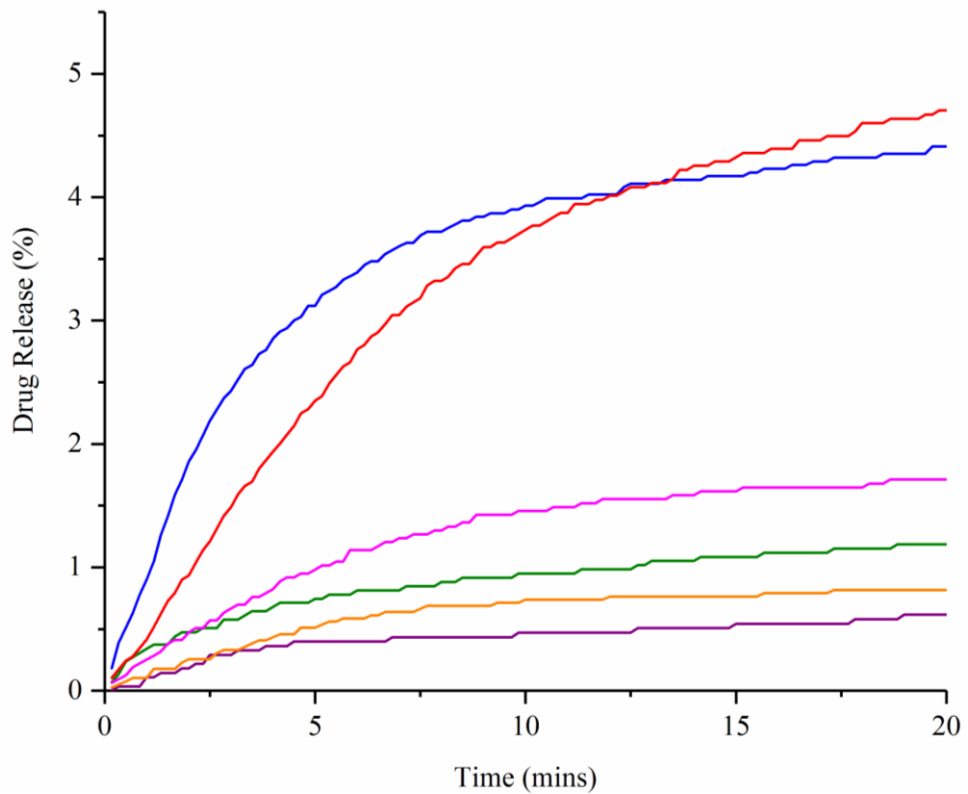
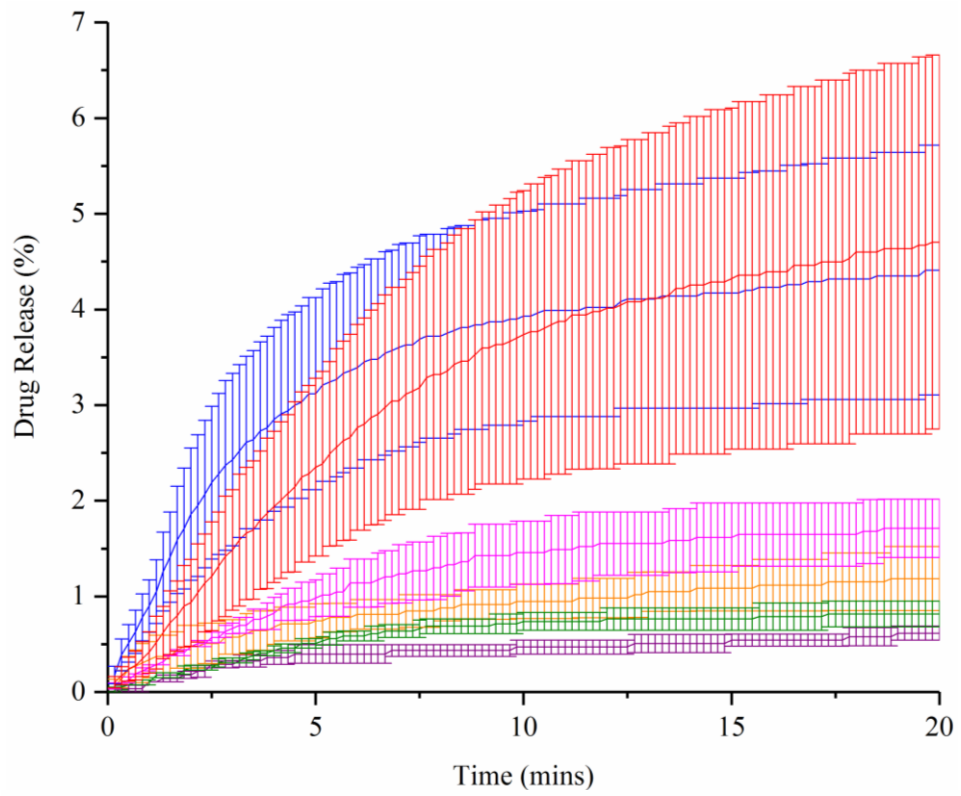


Figure 71: Percentage drug release of 5 layered printed premixed fenofibrate:PVP 2:1 (purple), 1:1 (orange), 2:3 (green), 1:2 (magenta), 1:3 (blue) and 1:4 (red), with (top) and without (bottom) error bars. $P=0.99999$ for 2:1 to 1:1, $P=1$ for 1:1 to 2:3, $P=0.99911$ for 2:3 to 1:2, $P=0.36718$ for 1:2 to 1:3 and $P=1$ for 1:3 to 1:4.

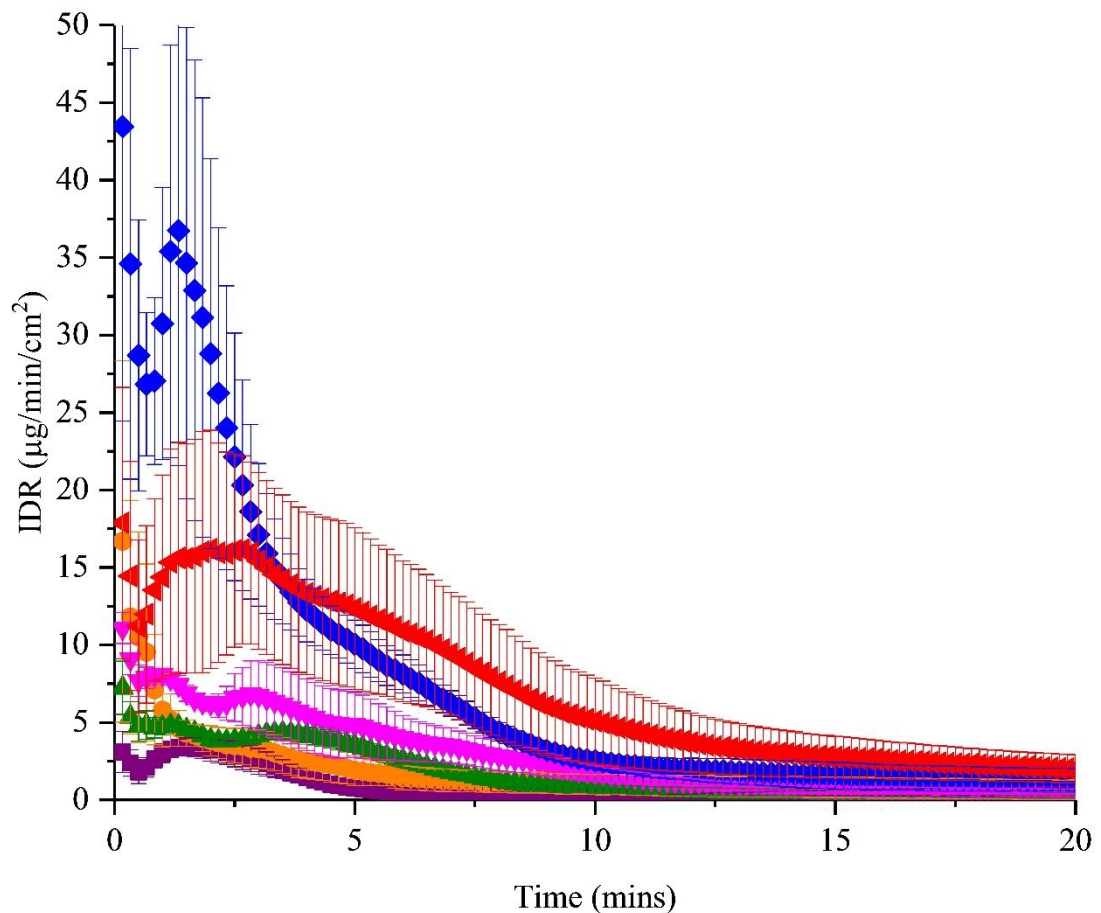


Figure 72: Intrinsic dissolution rate of 5 layered printed premixed fenofibrate:PVP 2:1 (purple), 1:1 (orange), 2:3 (green), 1:2 (magenta), 1:3 (blue) and 1:4 (red). P=1 for 2:1 to 1:1, P=1 for 1:1 to 2:3, P=1 for 2:3 to 1:2, P=1 for 1:2 to 1:3 and P=1 for 1:3 to 1:4.

4.3.2.2 *Ibuprofen*

4.3.2.2.1 *Molar Extinction Coefficient*

The molar extinction co-efficient was obtained from the mean result of 3 samples over a range of 1-10µg/ml (Appendix 3). The resultant molar extinction coefficient was observed to be 14806M/cm⁻¹ with an r²-value of 0.9915. The r²-value is a result of the low concentration range, which has limitations on accuracy and UV detection. This is supported by a statistically non-significant P-value. It should be noted these

solutions contained less than 1% methanol so the effect of its presence should be negligible.

4.3.2.2.2 Drug Release

On initial comparison of compacts of fenofibrate and ibuprofen it can be observed that, despite being a BCS Class II drug, ibuprofen results in a 10-fold higher release (Figure 73). On performing a paired T-test a significant difference between the drug release achieved by the two drugs was demonstrated.

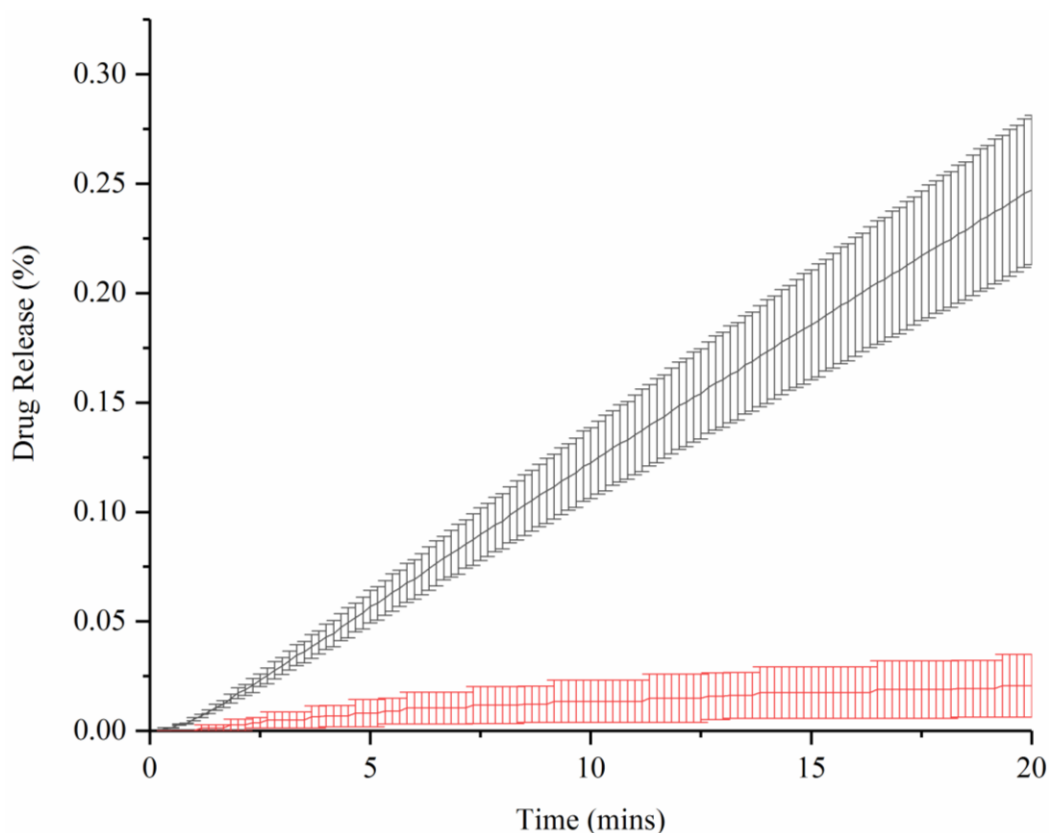


Figure 73: Comparison of the percentage drug release of fenofibrate (red) and ibuprofen (black) raw powder compacts. $P=0.03524$ for ibuprofen vs. fenofibrate.

On dissolution of ibuprofen based printed samples, it can be observed that greater release is achieved overall compared to fenofibrate, with up to a 3-fold higher drug release relative to that of a comparable fenofibrate:PVP premix (Figure 74). On

performing an ANOVA, the comparison of the 1:1 fenofibrate:PVP 5 layer samples with the 1:1 ibuprofen:PVP samples results in a P-value of 5.93412×10^{-4} , the comparison of the 1:2 API:PVP samples results in a P-value of 2.11928×10^{-4} and comparison of the 1:4 API:PVP samples results in a P-value of 0.0017. The difference between the 1:3 API:PVP samples was not significant. Ibuprofen alone does seem to result in high release but it should be noted that it is levelling off while the other samples are not suggesting that this is merely due to a lower drug content as shown in Table 21. Similar to fenofibrate, once PVP is introduced the drug release increases with polymer content, as demonstrated by an ANOVA. On comparison to the 5 layer samples of fenofibrate, it should be particularly noted that the release is more reproducible overall which may be due to the nature of the droplets produced. On comparison to the powdered sample between 30 and 60-fold higher release was achieved as demonstrated by ANOVA generated P-values of 9.76256×10^{-4} , 0.00162, 6.41262×10^{-4} , 0.00803 and 4.05941×10^{-4} on comparison of ibuprofen powder with ibuprofen printed, and ibuprofen:PVP 1:1, 1:2, 1:3 and 1:4 respectively.

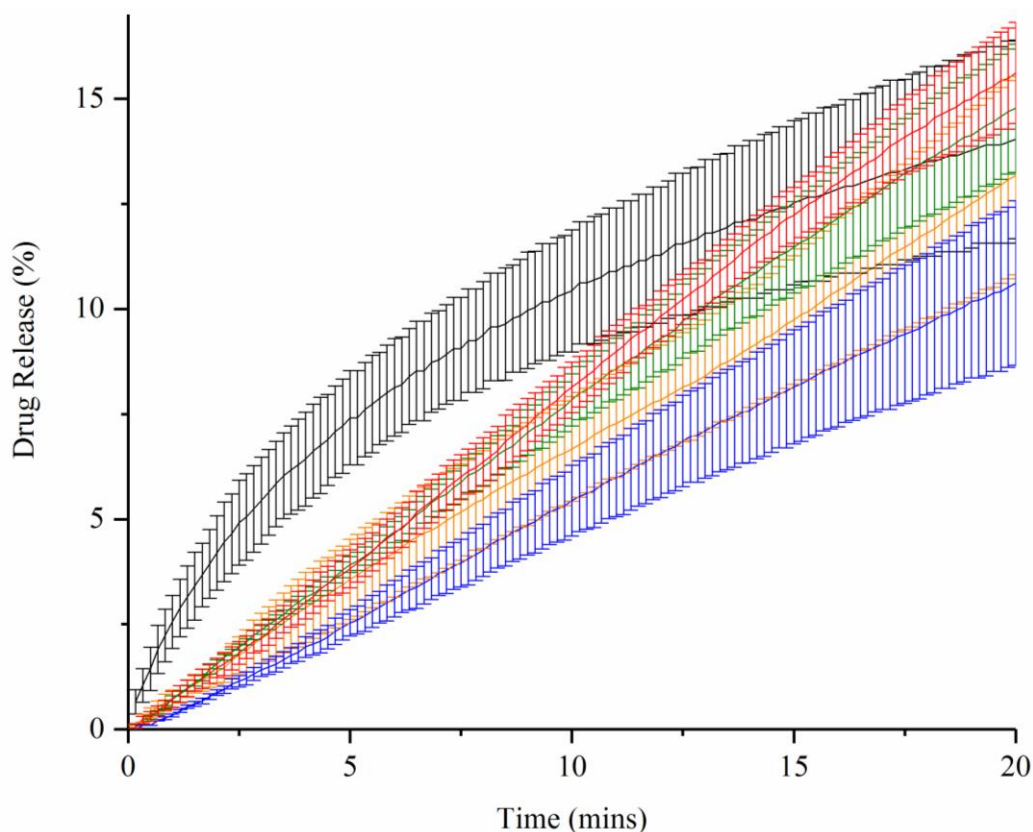


Figure 74: Percentage drug release of 5 layered printed ibuprofen (black) compared to printed premixed ibuprofen :PVP 1:1 (orange), 1:2 (green), 1:3 (blue) and 1:4 (red). $P=0.99999$ for IBU to 1:1, $P=0.99821$ for 1:1 to 1:2, $P=0.60893$ 1:2 to 1:3 and $P=0.37848$ for 1:3 to 1:4.

The effect of solid dispersion formation on the dissolution of ibuprofen has been well documented previously. Ibuprofen has also been previously used in spray drying with ethanol. As demonstrated by numerous previous studies, formation of amorphous particles in this manner also results in a considerable increase in release rate supporting the current data. For example Shen et al. achieved this effect co-spray drying with mesoporous silica, Melzig et al. achieved it through co-spray drying with polysorbate 80 and Li et al. achieved it through co-spray drying with gelatine and sodium lauryl sulphate (Li, Oh, et al. 2008, Shen et al. 2011, Melzig et al. 2018). There is also previous evidence for the use of ibuprofen in inkjet printing with a previous study combining it with PEG and PEGDA to increase solubility using a MicroFab

piezoelectric dispenser but there is no evidence for the solid state effects of this detailed in this paper (Acosta-Vélez et al. 2018).

4.3.2.2.3 *Intrinsic Dissolution Rate*

On comparison of the intrinsic dissolution rate of compacts of fenofibrate and ibuprofen it can be observed that ibuprofen results in more than a 10-fold increase in intrinsic dissolution rate (Figure 75). A paired T-test demonstrates the significant difference between the intrinsic dissolution rate achieved by the two drugs. This is believed to be due to the higher solubility exhibited by ibuprofen. It should be noted there is a very regular wave in the intrinsic dissolution rate curve. This is believed to be due to an issue with the pump.

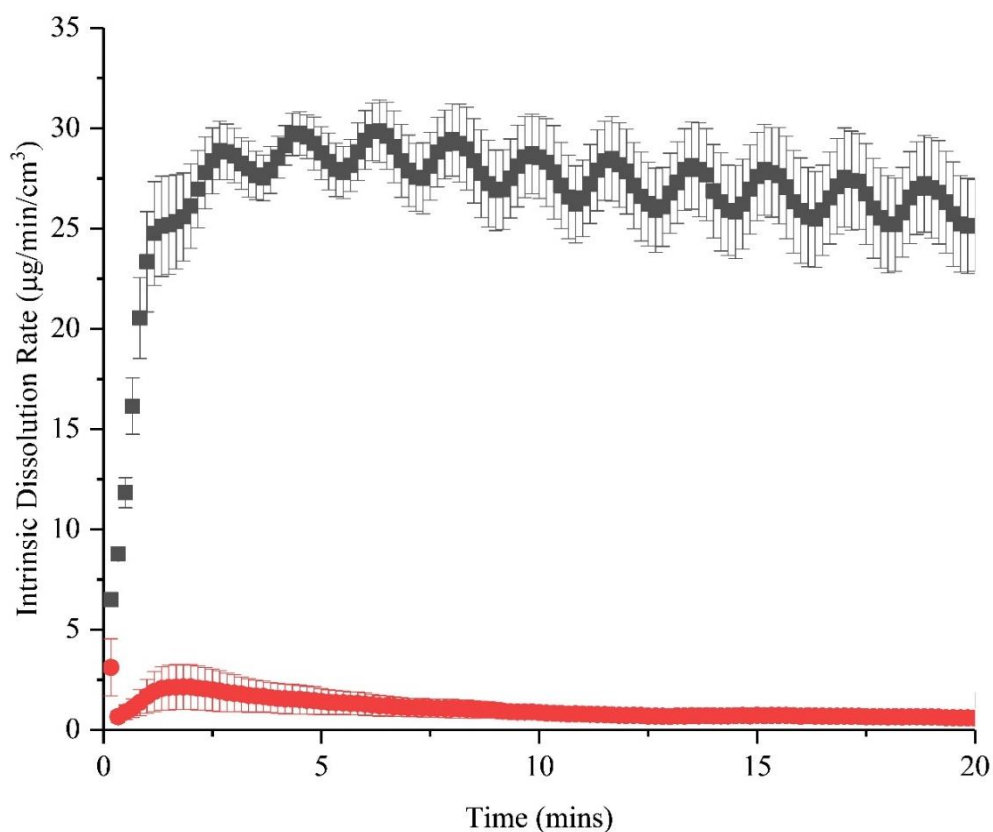


Figure 75: Comparison of the intrinsic dissolution rate of fenofibrate (red) and ibuprofen (black) raw powder compacts. $P=0.00347$ for ibuprofen vs. fenofibrate.

Measurement of the intrinsic dissolution rate of printed ibuprofen-based samples also shows a significant increase on use of ibuprofen over fenofibrate (Figure 76). On performing an ANOVA P-values of 3.49229×10^{-4} , 0.0047 and 0.04289 were obtained on comparison of 1:1, 1:2 and 1:3 API:polymer samples respectively. Ibuprofen alone has a significantly lower intrinsic dissolution rate than that of the polymer containing samples supporting the hypothesis that the drug release is high due to the drug content of the sample rather than its dissolution capacity. An ANOVA shows a significant change in the data on addition of polymer. On comparison of the polymer containing samples to each other, however, a significant difference in intrinsic dissolution rates is not observed and is not statistically significant. This may be a result of the fully amorphous nature of the particles generated on printing ibuprofen and 50% polymer or more. On comparison to the powder alone the printed samples do exhibit a slightly lower intrinsic dissolution rate but this may be due to the overall mass of material present. Unlike the drug release, the only significant difference on performing an ANOVA is from the comparison between the printed and powdered ibuprofen with a P-value of 0.00777. However, on comparison of the powdered ibuprofen to printed ibuprofen:PVP 1:1, 1:2, 1:3 and 1:4 P-values of 0.94395, 0.44948, 0.18998 and 0.18114 were obtained suggesting the difference does reduce with PVP.

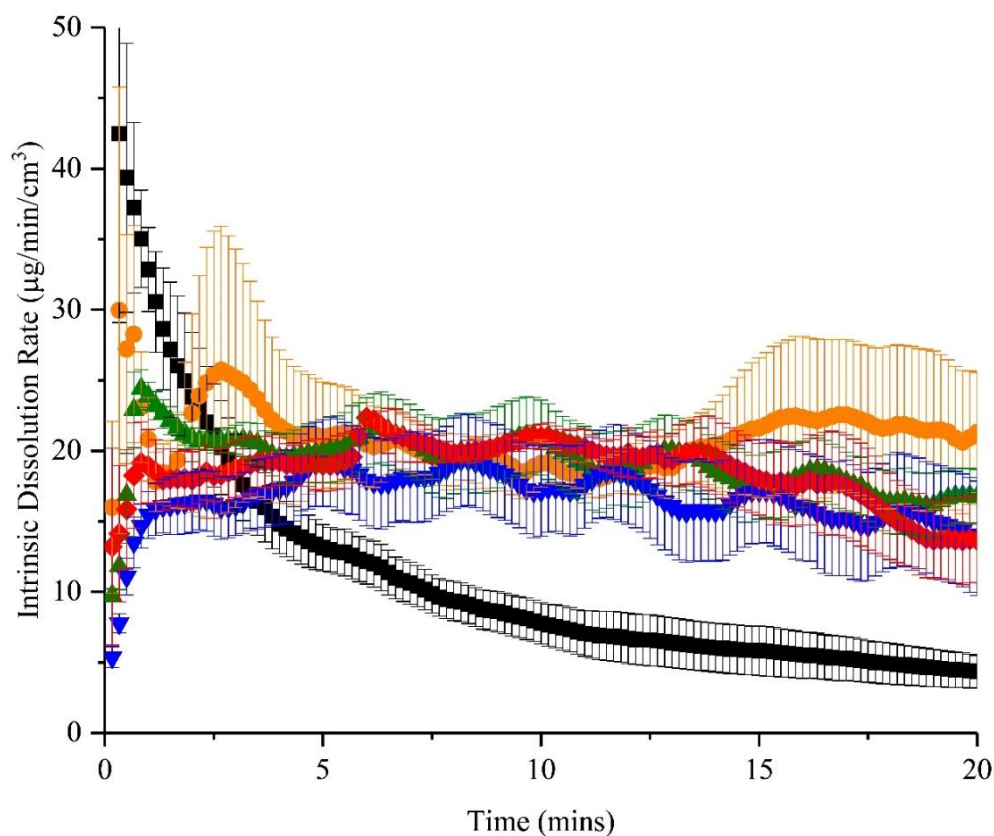


Figure 76: Intrinsic dissolution rate of 5 layered printed ibuprofen (black) compared to printed premixed ibuprofen :PVP 1:1 (orange), 1:2 (green), 1:3 (blue) and 1:4 (red). $P=0.00225$ for IBU to 1:1, $P=0.86309$ for 1:1 to 1:2, $P=0.34675$ for 1:2 to 1:3 and $P=0.33195$ for 1:3 to 1:4. $P=8.24574 \times 10^{-4}$ for IBU and 1:2, $P=0.00739$ for IBU and 1:3, $P=7.95473 \times 10^{-4}$ for IBU and 1:4.

As can be observed in Figure 77, ibuprofen consistently shows a considerable tail on SDI analysis. The printed ibuprofen shows a lesser tail than the raw powder sample which is consistent with the intrinsic dissolution rate and confirms the theory that it is due to the mass of material present. As with fenofibrate, adding PVP increases the size of the tail and the surface of the printed sample begins to swell. Consistent with the intrinsic dissolution rate the PVP containing samples exhibit very similar tails of material.

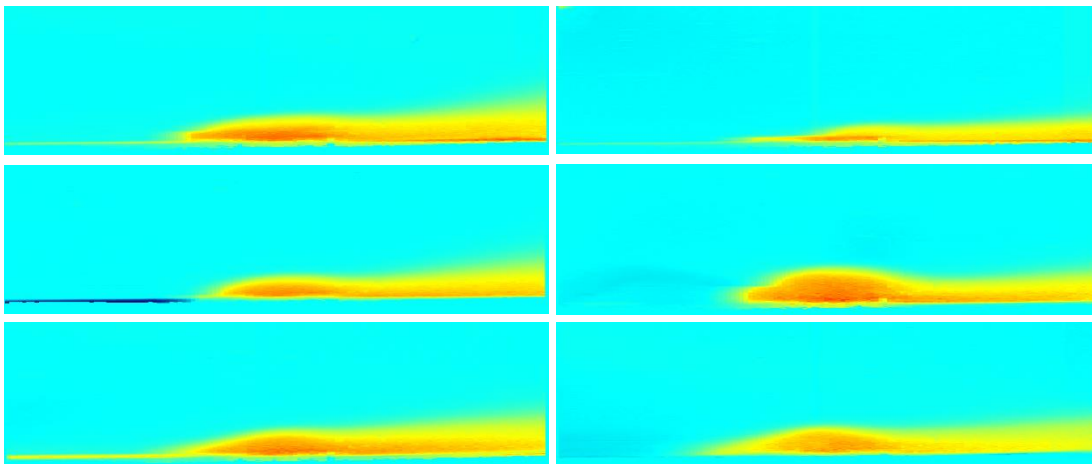


Figure 77: Images taken from the Sirius SDI Data Analysis software of ibuprofen and PVP samples at 5 minutes into the dissolution run: Ibuprofen powder (top left), printed ibuprofen (top right), and printed ibuprofen:PVP 1:1 (middle left), 1:2 (middle right), 1:3 (bottom left) and 1:4.(bottom right)

Considering the literature, although inkjet printed samples have not been tested using the SDI, the intrinsic dissolution rate of compacted ibuprofen has been tested previously. Samples were run as in the current study at 0.2ml/min using a wavelength of 214nm but using 1% SDS instead of pH 6.8 buffer. The IDR was found to rise to over $40\mu\text{g}/\text{min}/\text{cm}^3$ before falling back to $20\mu\text{g}/\text{min}/\text{cm}^3$ similar to how the printed samples behave. It should be noted the error is greatest in the initial few points where there is the increase, this may be due to the rapid removal of surface particles, initial erosion of the surface by lamination or disruption of the laminar flow (Ward et al. 2017).

4.3.3 Contact Angle

4.3.3.1 PVP Alone

The results were initially taken for the whole video for each sample however it was found the camera was not coping with the topography of the samples, particularly the more soluble ones where the droplet was falling below the horizon as it spread (for data see Appendix 4). As such the decision was made to take just the initial contact point. The PVP contact angle showed little change with polymer concentration which

is supported by an ANOVA which demonstrated consistent P-values of 1. This may be due to the low viscosity of the ink. Figure 78 shows minimal variation between the contact angle values obtained and the images in Figure 79 support this as the appearance of the droplets are very similar overall.

PVP contact angle has been previously reported in the literature. Hayama et al. demonstrated a very similar set of contact angle values for PVP K30 although the material was prepared by thermal film casting rather than spin coating (Hayama et al. 2004). Ultimately little change was seen in the contact angle with polymer concentration, which is potentially due to the relatively low viscosity of starting solutions.

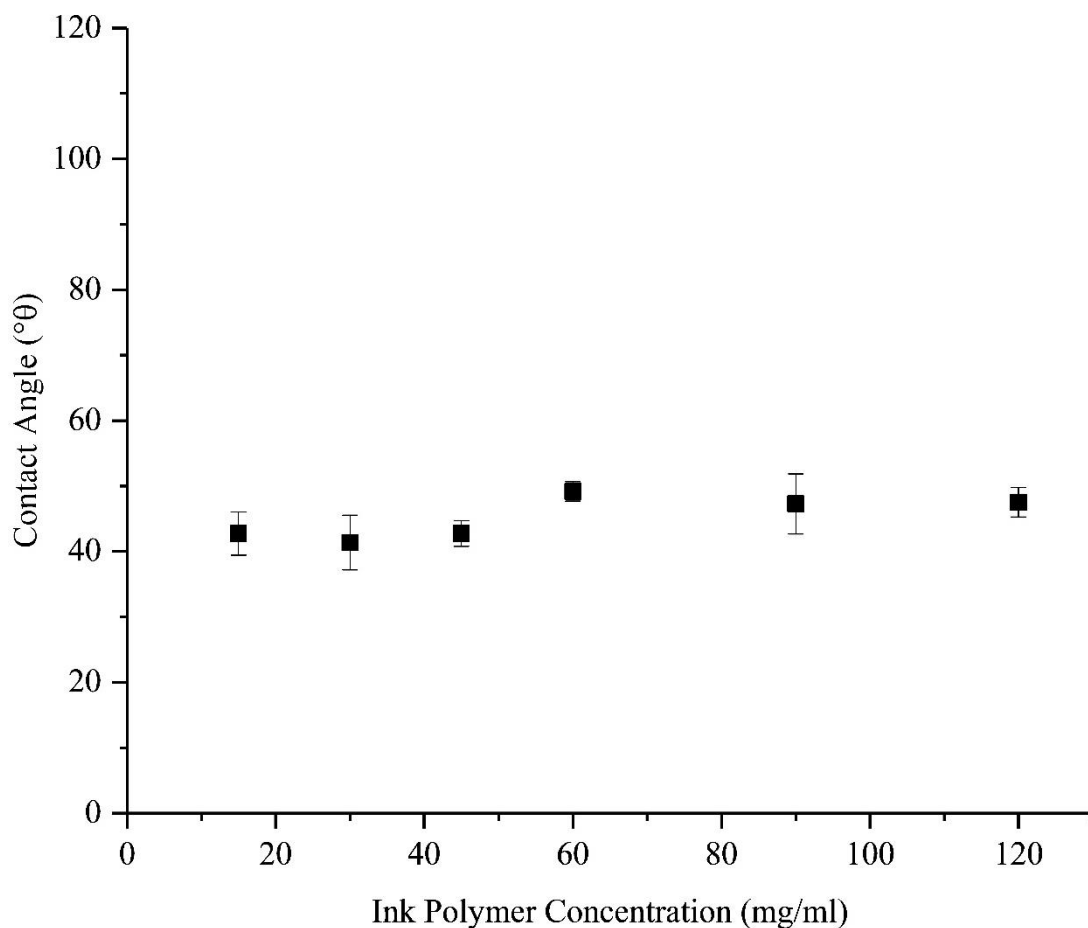


Figure 78: The effect of polymer ink concentration on the contact angle of PVP spin coated samples measured at point zero, where $n=9 \pm$ standard error with 95% confidence intervals of $35.12^\circ\theta$ and $50.33^\circ\theta$, $31.76^\circ\theta$ and $50.98^\circ\theta$, $38.21^\circ\theta$ and $47.31^\circ\theta$, $45.75^\circ\theta$ and $52.60^\circ\theta$, $36.66^\circ\theta$ and $57.87^\circ\theta$, and $42.34^\circ\theta$ and $52.73^\circ\theta$ for 15, 30, 45, 60, 90 and 120mg/ml PVP K30 in ethanol. $P=1$ for 15mg/ml to 30mg/ml, $P=1$ for 30mg/ml to 45mg/ml, $P=0.99996$ for 45mg/ml to 60mg/ml, $P=1$ for 60mg/ml to 90mg/ml and $P=1$ for 90mg/ml to 120mg/ml.

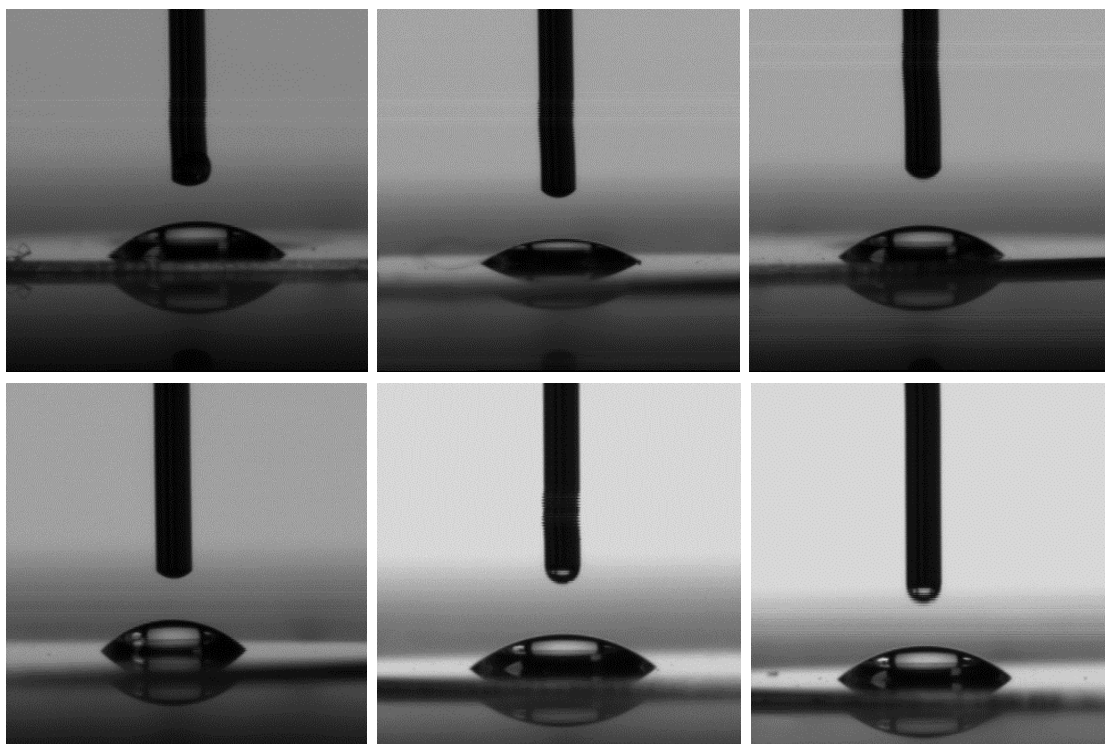


Figure 79: Comparison of initial contact angle images of spin coated PVP samples - (from top to bottom and left to right for each row) PVP concentrations 15mg/ml, 30mg/ml, 45mg/ml, 60mg/ml, 90mg/ml and 120mg/ml.

4.3.3.2 Spin Coated PVP and Fenofibrate Mixtures

As with the PVP spin coated samples only the contact angle at point zero is displayed, with the other data given in Appendix 4. The results are displayed in Table 23, as graphs (Figure 80) and as images (Figure 81) below. Spin coating fenofibrate in ethanol alone resulted in a relatively high contact angle and thus poor wettability which was to be expected as fenofibrate is virtually insoluble in water. The wettability increased considerably on addition of polymer with a 2:1 drug: polymer ratio causing the contact angle to fall from an average of 80.5 to 46.2° θ , supported by a P-value of 1.01056x10⁻⁵ on taking an ANOVA. The contact angle does not seem to change massively from that of the polymer after this until the 1:3 and 1:4 fenofibrate:PVP samples. This increase in contact angle may be attributed to fenofibrate precipitation which began to occur as water was applied. However, an ANOVA did not show a significant change between the points after 2:1 fenofibrate:PVP or on comparison to the PVP samples with a comparable polymer concentration.

Table 23: The effect of concentration of polymer used to prepare spin coated samples on the contact angle measured at point zero

Drug: Polymer Ratio	Drug Content (mg/ml)	Polymer Content (mg/ml)	Average Contact Angle (°) n=9, 2d.p.
1:0	30	0	80.51
2:1	30	15	46.29
1:1	30	30	54.59
2:3	30	45	39.06
1:2	30	60	41.51
1:3	30	90	61.03
1:4	30	120	60.62
0:1	0	30	45.03

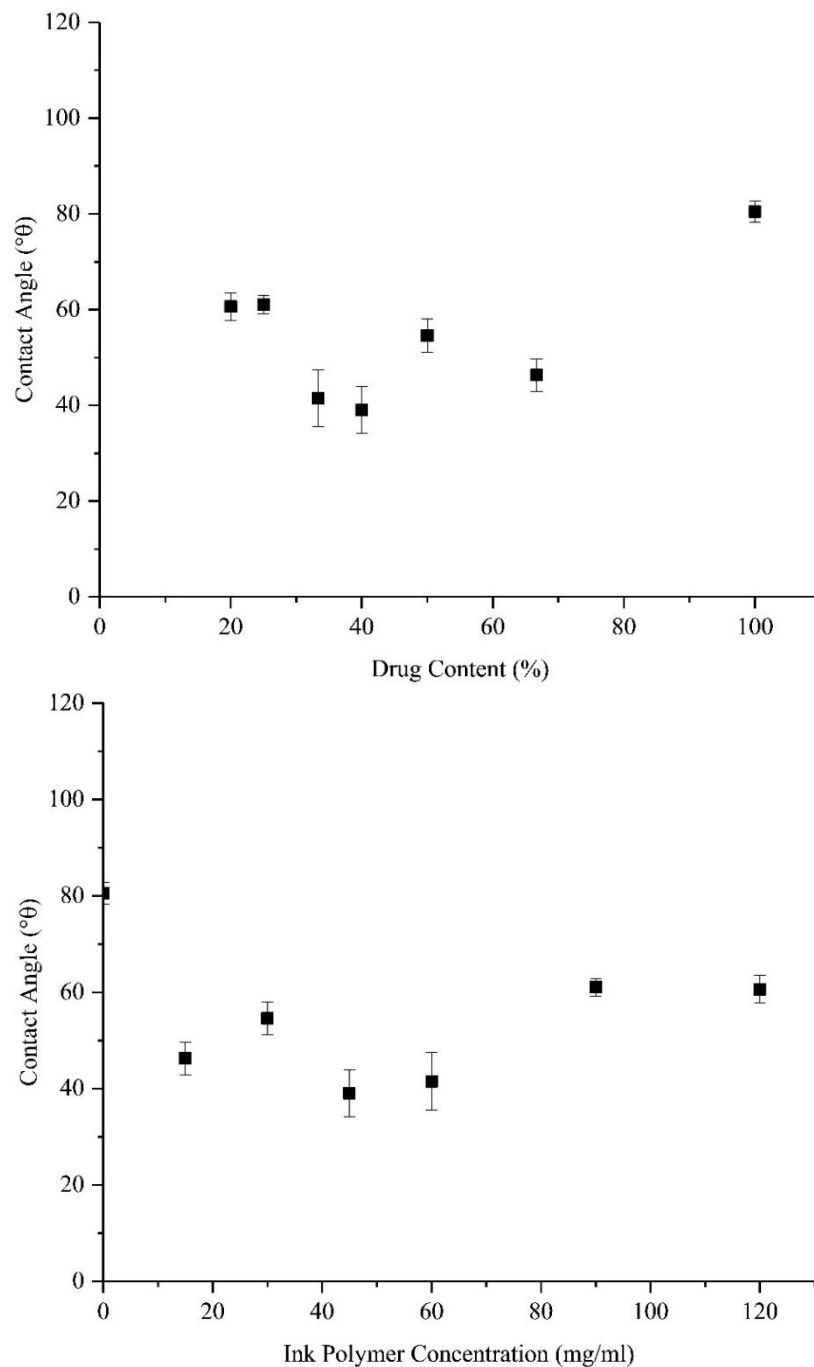


Figure 80: The effect of polymer concentration on the contact angle of fenofibrate and PVP spin coated samples measured at point zero, against drug content (top), and ink polymer concentration (bottom), where $n=9 \pm$ standard error with 95% confidence intervals of $75.31^\circ\theta$ and $85.71^\circ\theta$, $38.44^\circ\theta$ and $54.14^\circ\theta$, $46.66^\circ\theta$ and $62.52^\circ\theta$, $27.96^\circ\theta$ and $50.15^\circ\theta$, $27.73^\circ\theta$ and $55.29^\circ\theta$, $48.30^\circ\theta$ and $73.77^\circ\theta$, and $56.66^\circ\theta$ and $64.58^\circ\theta$ for 1:0, 2:1, 1:1, 2:3, 1:2, 1:3 and 1:4 FNF:PVP respectively. $P=1.01056 \times 10^{-5}$ for FNF to 2:1, $P=0.99841$ for 2:1 to 1:1, $P=0.53467$ for 1:1 to 2:3, $P=1$ for 2:3 to 1:2, $P=0.13969$ for 1:2 to 1:3 and $P=1$ for 1:3 to 1:4.

Samples were compared to their comparable spin coated polymer samples to establish the effect of drug loading on the contact angle. An ANOVA demonstrated a non-significant difference between the spin coated polymer samples and the drug containing spin coated samples with P-values of 1, 0.80878, 1, 0.99947, 0.75157 and 0.82168 for 15mg/ml, 30mg/ml, 45mg/ml, 60mg/ml, 90mg/ml and 120mg/ml PVP K30 containing samples respectively. However, with the exception of 60 and 66% polymer content (45 and 90mg/ml), the drug loaded samples appeared less wettable as expected.

The images of the initial contact point (Figure 81) visually illustrate the difference between the drug alone compared with samples with the polymer present. There is very little visual difference between the polymer containing samples however. PVP alone is very distinct however.

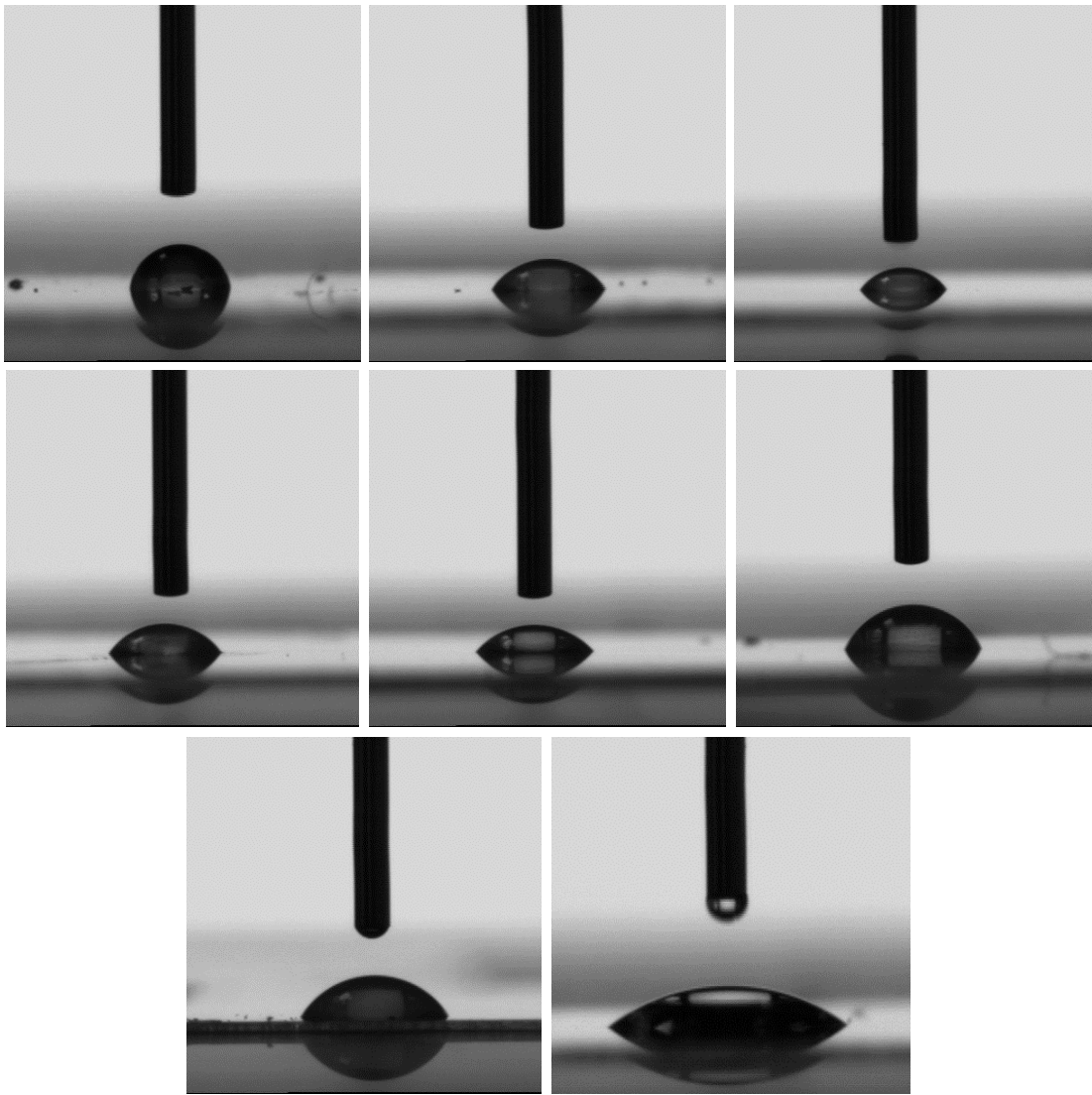


Figure 81: Comparison of initial contact angle images of fenofibrate and PVP spin coated samples – (from top to bottom and left to right) spin coated samples consisting of fenofibrate alone, fenofibrate:PVP K30 2:1, 1:1, 2:3, 1:2, 1:3, 1:4 and PVP alone

There is no previous evidence of contact angle on fenofibrate and PVP together but as stated in the previous section the effect on PVP has been observed in other studies. Additionally, wettability of fenofibrate has been analysed in the literature previously. The contact angle established by Buch et al. is nearly identical despite using a different system, a DataPhysics Contact Angle System OCA 20 (Buch et al. 2011).

Ultimately, the wettability is observed to increase with polymer content relative to the drug alone but at the highest polymer concentrations the contact angle seems to break

the trend and increase slightly which may be due to precipitation of the drug.

4.3.3.3 Printed PVP and Fenofibrate Mixtures

As described in Section 4.2.3.1, only the contact angle at point zero is displayed with all additional data given in Appendix 4. The results are displayed as a table and graphs below (Table 24 and Figures 82 and 83). Printing fenofibrate in ethanol alone resulted in a relatively high contact angle and thus poor wettability which was to be expected as fenofibrate is virtually insoluble in water. The wettability of printed fenofibrate may be lower than that of spin coated samples due to a combination of the crystal growth which occurs from the supersaturated atomised ink and the chance that some residual ethanol may remain in the spin coated samples as they were prepared on the day of analysis rather than weeks prior. This is supported by an ANOVA yielding a P-value of 2.2922×10^{-4} on comparison of the spin coated and printed samples.

The wettability increased considerably on addition of polymer with a 2:1 drug: polymer ratio causing the contact angle to fall from an average of 110.7° to 65.02° . This is supported by an ANOVA as the difference between this point and that of the fenofibrate has a P-value of 1.51711×10^{-8} . The contact angle falls with increasing polymer content until 2:3 at an average of 43.24° , after which the graph is observed to level off with values of 45.67° , 30.52° and 40.87° for the 1:2, 1:3 and 1:4 fenofibrate:PVP samples respectively. This is supported by statistically insignificant P-values. This may be attributed to formation of amorphous drug particles, increasing the overall wettability of the drug. Thus, the wettability may be considered solely a function of the polymer until 2:3 fenofibrate:PVP, where the amorphous particles begin to play a part with the fully amorphous 1:3 and 1:4 fenofibrate:PVP samples ultimately showing the greatest wettability overall. This is unlike the spin coated samples prepared with comparable ink solutions, which suggests the phase change occurring on atomisation and printing is thus vital to the wettability and thus the change in intrinsic dissolution seen previously. This is supported by a statistically significant change between the printed and spin coated 1:3 fenofibrate:PVP on performing an ANOVA. On comparison to the PVP spin coated samples with comparable starting polymer concentrations, an ANOVA demonstrated a significantly

higher contact angle for 2:1 fenofibrate:PVP compared to 15mg/ml PVP with a P-value of 0.03665. As the polymer content is increased the P-value ceases to be significant with values of 0.80104, 1, 1, 0.38585 and 0.99993 for 1:1 and 30mg/ml, 2:3 and 45mg/ml, 1:2 and 60mg/ml, 1:3 and 90mg/ml, and 1:4 and 120mg/ml respectively. This demonstrates the wettability becoming more akin to that of the polymer alone.

Table 24: Average contact angle for each type of printed sample taken at point zero from lowest to highest polymer content

Drug: Polymer Ratio	Drug Content (mg/ml)	Polymer Content (mg/ml)	Average Contact Angle (°) n=9, 2d.p.	Variation from Equivalent Average Contact Angle from Spin Coated Samples (°)
1:0	30	0	110.70	+30.19
2:1	30	15	65.02	+18.73
1:1	30	30	54.67	+0.08
2:3	30	45	43.24	+4.18
1:2	30	60	45.67	+4.16
1:3	30	90	30.52	-30.51
1:4	30	120	40.87	-19.75

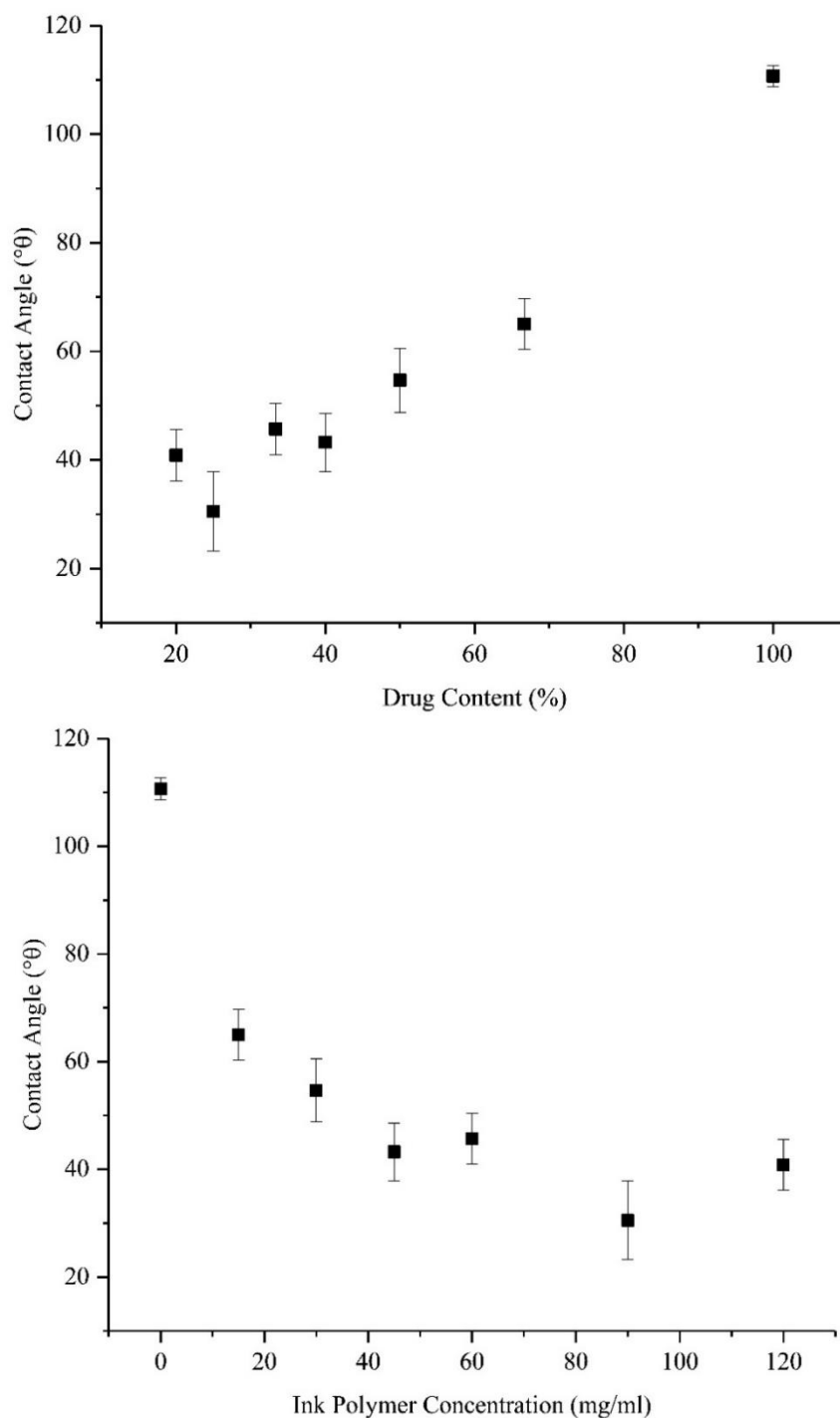


Figure 82: Average contact angle values of printed fenofibrate and PVP samples taken at point zero against (top) percentage drug content and (bottom) polymer concentration of the starting ink, where $n=9 \pm$ standard error with 95% confidence intervals of $106.11^\circ\theta$ and $115.29^\circ\theta$, $54.23^\circ\theta$ and $75.81^\circ\theta$, $41.15^\circ\theta$ and $68.19^\circ\theta$, $30.90^\circ\theta$ and $55.59^\circ\theta$, $34.70^\circ\theta$ and $56.63^\circ\theta$, $13.64^\circ\theta$ and $47.41^\circ\theta$, and $29.90^\circ\theta$ and $51.84^\circ\theta$ for 1:0, 2:1, 1:1, 2:3, 1:2, 1:3 and 1:4 fenofibrate:PVP K30 respectively. $P=1.51711 \times 10^{-8}$ for

FNF to 2:1, $P=97735$ for 2:1 to 1:1, $P=0.9405$ for 1:1 to 2:3, $P=1$ for 2:3 to 1:2, $P=0.58429$ for 1:2 to 1:3 and $P=0.9776$ for 1:3 to 1:4. $P=3.29942 \times 10^{-8}$ for FNF and 1:1, $P=0$ for FNF and 2:3, $P=0$ for FNF and 1:2, $P=0$ for FNF and 1:3, $P=0$ for FNF and 1:4.

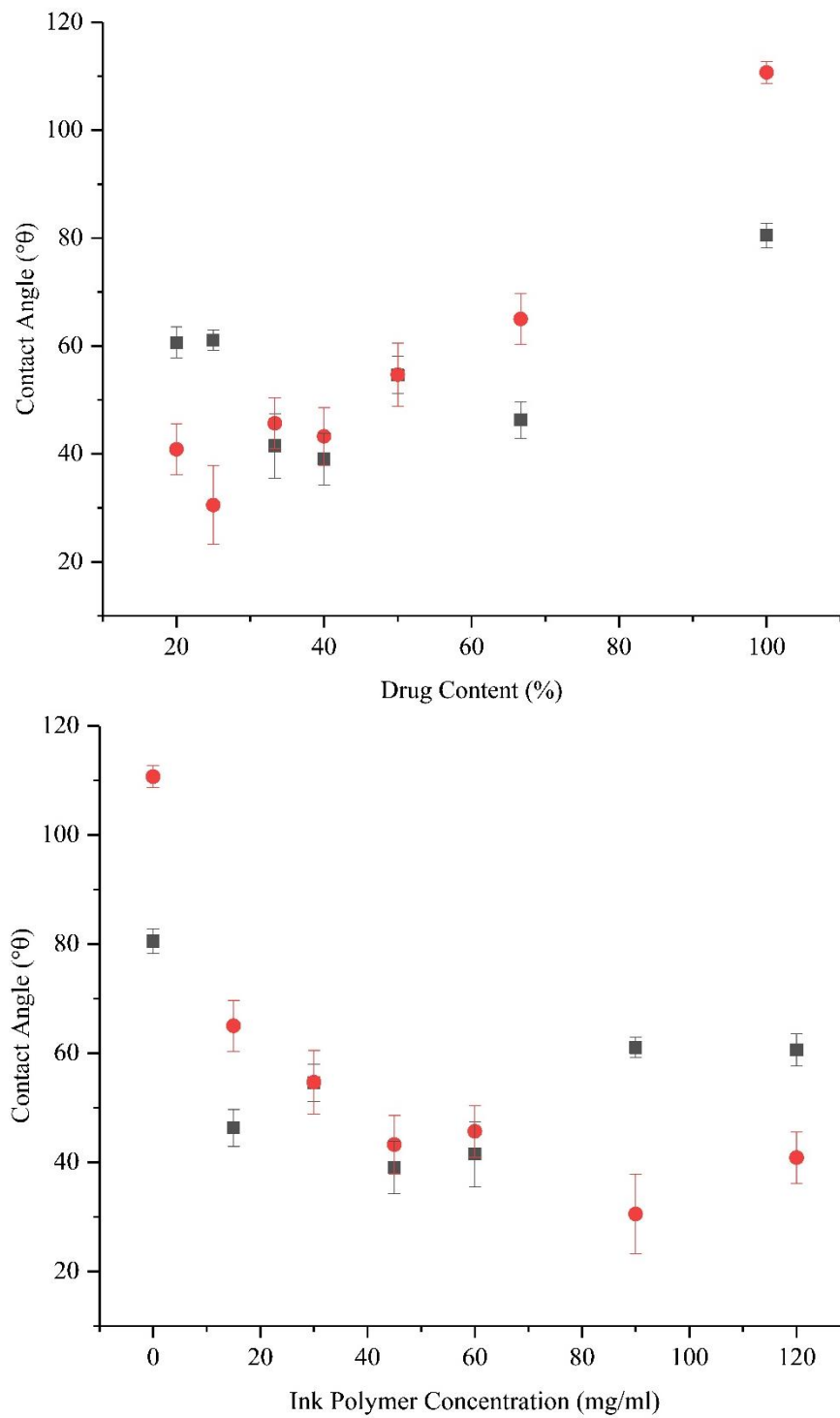


Figure 83: Comparison of printed samples (red) to spin coated samples (black) based on contact angle values taken at point zero against (top) percentage drug content and (bottom) polymer concentration of the starting ink, where $n=9 \pm$ standard error. $P=2.2922 \times 10^{-4}$ for FNF, $P=0.19317$ for 2:1, $P=1$ for 1:1, $P=1$ for 2:3, $P=1$ for 1:2, $P=1.80601 \times 10^{-4}$ for 1:3, $P=0.12628$ for 1:4.

Samples were also compared visually (Figure 84) with a noticeable change being observed between the fenofibrate alone (top left) and the 2:1 fenofibrate:PVP sample (top right). The degree to which the droplet was convex to the surface can be observed to decrease with increasing polymer content. 1:3 fenofibrate PVP has been displayed as 3 different images as it was found 2 out of the 3 films proved more powdery and liquid absorbent than the third more gel like film. Interestingly for these two films the water spread much more quickly and dropped below the camera view just after the image was taken. As a result of this the resultant contact angle value for the 1:3 fenofibrate:PVP samples is slightly lower than that of the 1:4 fenofibrate:PVP samples although 1:4 was quite similar in behaviour to the latter 1:3 sample.

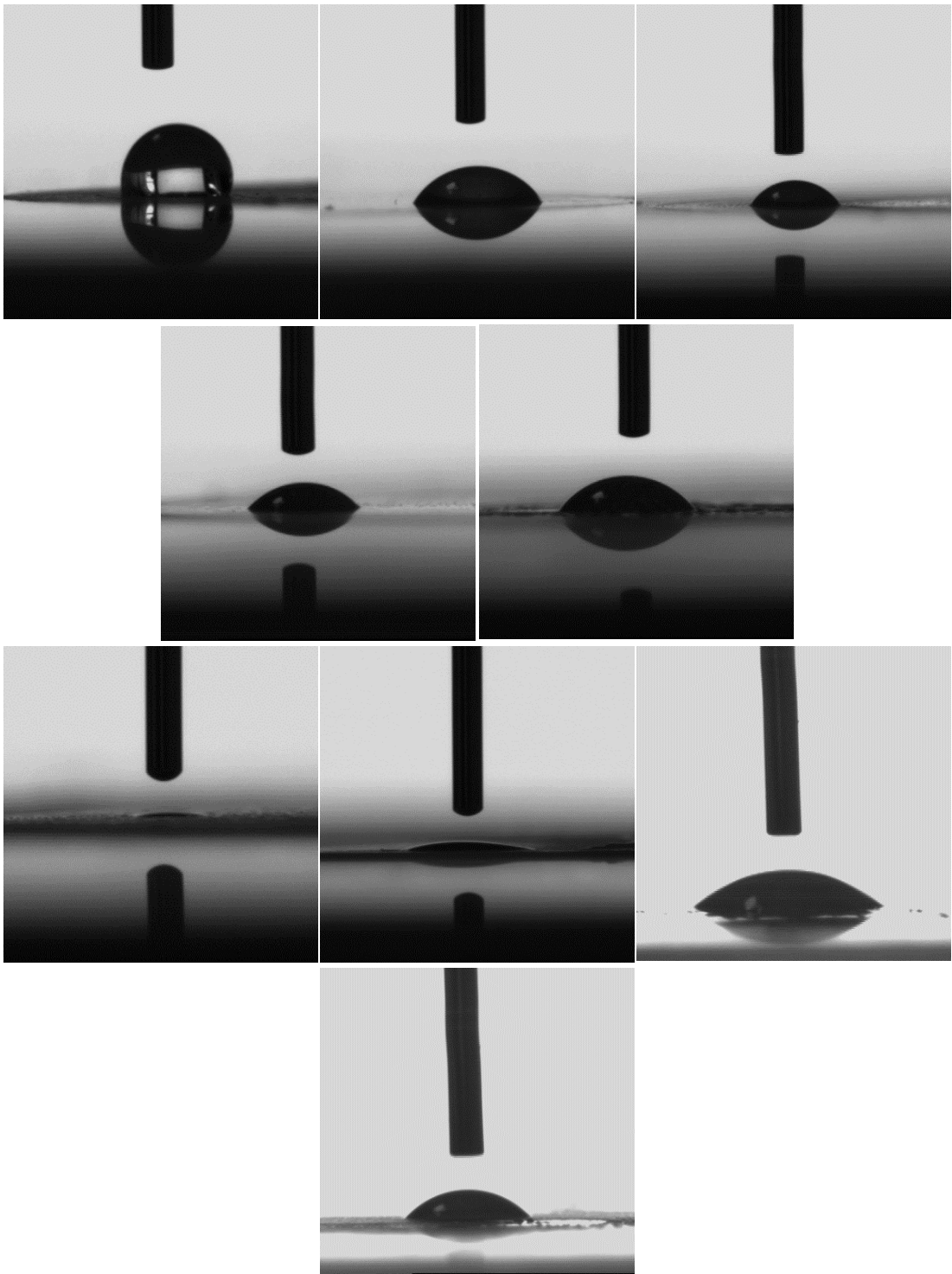


Figure 84: Comparison of initial contact angle images of fenofibrate and PVP printed samples – (from top to bottom and left to right) fenofibrate and premixed samples consisting of fenofibrate:PVP K30 2:1, 1:1, 2:3, 1:2, 1:3 (x3), and 1:4

The results can be compared to previous intrinsic dissolution and drug release data (Figures 59 and 61). In both cases a considerable change can be seen between the 1:1 and 2:3 fenofibrate:PVP samples, while less dramatic changes are seen from then on which mirrors the levelling off affect seen in the contact angle data suggesting at this point the amorphous content is very much what dictates the wetting and dissolution of the API. The relationship between contact angle and dissolution has been explored previously investigating simvastatin and PVP by fluid bed coating in a paper by Lu et al. The exponential rise in dissolution is also observed in this study supporting the wetting behaviour seen in the current study (Lu, Tang, et al. 2014).

Ultimately, the printed samples were found to increase in wettability with polymer concentration until 60% polymer content following which the contact angle values were observed to begin to level off. This may be attributed to formation of amorphous particles. This supports previous work into intrinsic dissolution rate. This is unlike the spin coated samples produced from comparable solutions which does suggest that the formation of amorphous particles is key to this degree of wettability.

4.3.3.4 Ibuprofen

On changing the drug, a slightly different effect was observed than previously (Figure 85). Ibuprofen shows a lower contact angle overall, suggesting it is more wettable than fenofibrate, which supports both the intrinsic dissolution and drug release data previously presented (Figures 74-77). On performing an ANOVA on fenofibrate and ibuprofen alone a P-value of 0.0605 was obtained confirming a significant change. On addition of polymer the wettability increases considerably as exemplified by a decrease in contact angle as shown in Table 25 and Figure 85. Although, not considered statistically significant with a P-value of 0.26917, ibuprofen and 1:1 ibuprofen:PVP K30 shows the greatest change overall as after this the P-values obtained are all between 0.9 and 1 suggesting the graph has levelled off. Ibuprofen was observed to have a very similar contact angle value in a previous study by Varghese and Ghoroi. Additionally, on blending and co-grinding with microcrystalline cellulose to generate solid dispersion-like properties, a very similar

drop in contact angle and a considerable increase in dissolution was observed on comparison to the raw drug (Varghese and Ghoroi 2017).

On comparison of these samples to their fenofibrate containing counterparts P-values of 0.47266, 1, 0.48104 and 0.96996 were obtained for the 1:1, 1:2, 1:3 and 1:4 ibuprofen:PVP samples respectively, which is not considered statistically significant. This may be due to the limiting factor for fenofibrate being release of the drug into solution rather than the initial wetting. As such the difference in dissolution performance between fenofibrate and ibuprofen is demonstrated better after the initial wetting.

Table 25: Average contact angle values obtained for printed ibuprofen and ibuprofen:PVP printed mixtures

Drug: Polymer Ratio	Drug Content (mg/ml)	Polymer Content (mg/ml)	Average Contact Angle (°) n=3, 2d.p.
1:0	30	0	68.90923
1:1	30	30	36.24594
1:2	30	60	44.71649
1:3	30	90	55.04058
1:4	30	120	49.02805

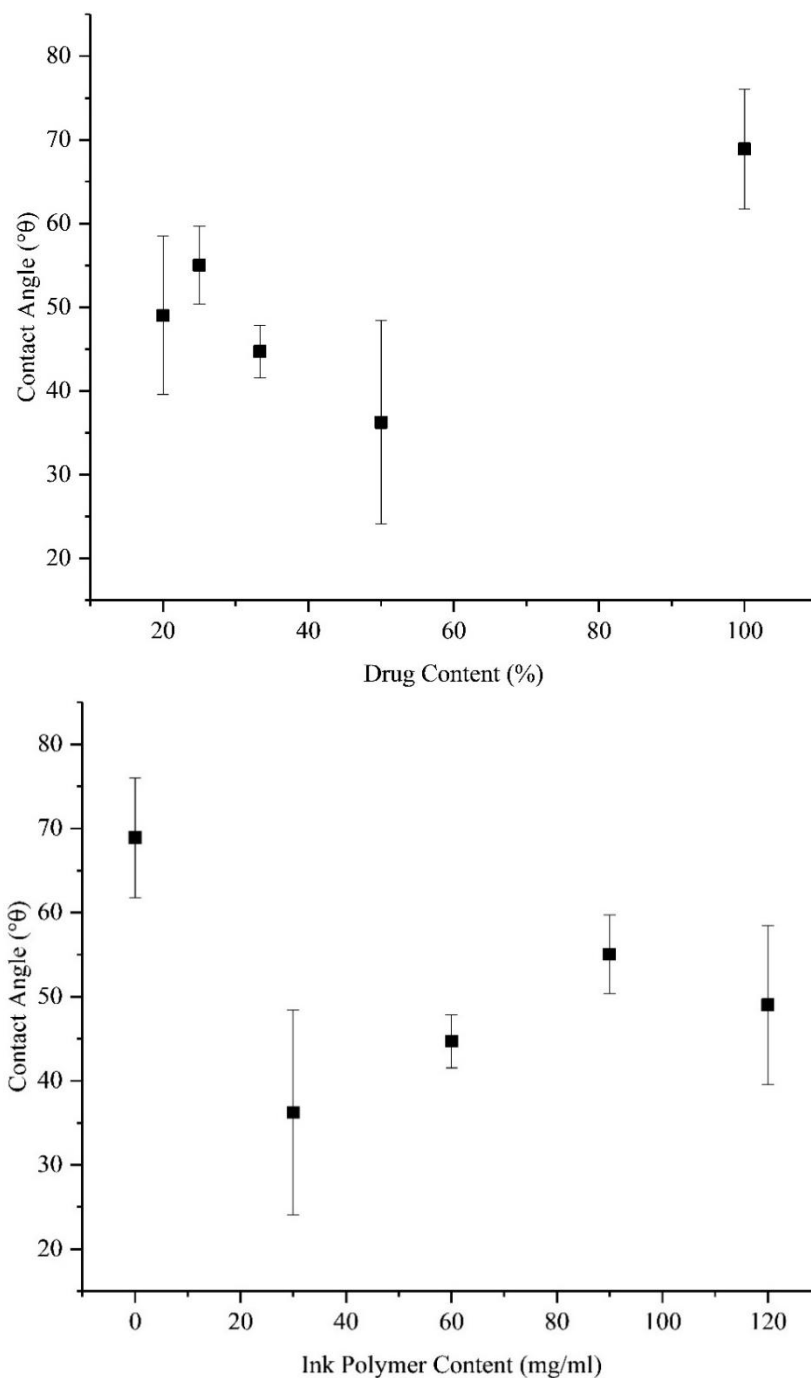


Figure 85: Average contact angle of ibuprofen and PVP printed samples measured at point zero against drug content (top) and starting ink polymer content (bottom), where $n=3 \pm$ standard error with 95% confidence intervals of $38.26^\circ\theta$ and $99.56^\circ\theta$, $-16.07^\circ\theta$ and $88.56^\circ\theta$, $31.13^\circ\theta$ and $58.31^\circ\theta$, $34.91^\circ\theta$ and $75.17^\circ\theta$, and $8.30^\circ\theta$ and $89.76^\circ\theta$ for 1:0, 1:1, 1:2, 1:3 and 1:4 ibuprofen:PVP K30 respectively. $P=0.26917$ for IBU to 1:1, $P=0.99929$ for 1:1 to 1:2, $P=0.99681$ for 1:2 to 1:3 and $P=0.99996$ for 1:3 to 1:4. $P=0.63764$ for IBU to 1:2, $P=0.97583$ for IBU to 1:3 and $P=0.8297$ for IBU to 1:4.

4.4 Conclusions

Initially the drug content of samples was analysed. Fenofibrate samples showed an increase in mass with polymer content up to 50% polymer content. Following this the mass decreased. This is thought to be the effect of the rheology and droplet size changes occurring on atomisation. On comparison to ibuprofen, fenofibrate showed greater variation between samples which may be due to the overall droplet size and solubility. Ibuprofen showed more consistent mass of drug produced in the presence of PVP overall and more predictable content.

The effect of printing fenofibrate and ibuprofen alone and with PVP on dissolution was analysed over time. On printing premixes of fenofibrate and PVP, use of the aerosol causes a 10-fold increase in drug release and intrinsic dissolution rate. Printing layered samples causes an increase but to a lesser extent, suggesting the combining of drug and polymer at the solution stage is vital for this increase. On printing ibuprofen, the release and intrinsic dissolution rate is 3-fold and 4-fold higher than fenofibrate. The intrinsic dissolution rate increases considerably on addition of PVP but there is little difference between the PVP containing ibuprofen samples. However, on comparison of the drug release addition of 80% polymer results in the highest drug release overall.

On comparison of contact angle, the fenofibrate formulations were found to increase in wettability with polymer content until the formation of amorphous particles which have a contact angle very similar to PVP alone. However, ibuprofen showed an increase in wettability from the drug alone but changed little after this as 50% polymer was enough to result in fully amorphous samples. As a result, it was established that the lower intrinsic dissolution rate of fenofibrate overall was a result of the washing away of the PVP exposing the drug. The development of the technology for use in pulsatile systems will be detailed in Chapters 5 and 6.

Chapter 5: Aerosol Inkjet Printing Pulsatile Release Systems Utilising Fenofibrate

5.1 Introduction

After developing the initial dosage form manufacturing technique, the decision was made to develop the technology to allow more complex dosage forms. As a result of the flexibility of the technique pulsatile release systems were developed. Pulsatile release systems are defined by bursts of immediate release after a lag in the profile. Pulsatile systems may have one or more pulses depending on the requirements of the drug utilised. Uses include navigation of the gastrointestinal tract intact, which is particularly important for drugs which are vulnerable to acid hydrolysis, irritate the gastric mucosa or are emetic in nature, control over the dose for drugs with narrow therapeutic indexes, ensuring the drugs with action sites in the lower gastrointestinal tract reach these undamaged. Additionally it may be used for drugs which are vulnerable to first pass metabolism. (Tangri and Khurana 2011, Prasanth et al. 2012). This type of controlled release can be used as a means of matching circadian rhythms such as hormone secretion, gastric emptying and other metabolic processes. As such diseases and conditions currently targeted in this manner include peptic ulcers, asthma, cardiovascular conditions, arthritis, diabetes mellitus, ADHD, some forms of cancer, neurological disorders (Tangri and Khurana 2011, Tajane et al. 2012).

Advantages of pulsatile technology include reduced dosing frequency improving patient compliance, reducing API wastage and overall cost. Additionally, pulsatile technology allows night time dosing, which is particularly beneficial for conditions such as insomnia where the patient requires a dose to enable sleep and a further dose to keep them asleep. Dosing prior to waking can also be used for treating conditions such as hypertension and rheumatoid arthritis which can be worse first thing in the morning. The control pulsatile systems can also reduce the overall dose required reducing the chance of toxicity (Tangri and Khurana 2011).

Existing methods of pulsatile include time controlled systems such as capsular systems controlled by a plug which is removed by swelling or erosion, systems based around semipermeable membranes, osmotic pressure based systems, reservoir based systems, rupturable coating systems and time controlled explosion systems (Bussemer et al. 2003, Dashevsky and Mohamad 2006, Mohamad and Dashevsky 2006, Stevenson et al. 2012, Yang and Pierstorff 2012, Li et al. 2018). Additional forms of previous pulsatile technology have included thermo-responsive systems, chemical induced systems, for example, glucose induced, inflammation induced hydroxyl radicals and pH sensitive systems, electrically responsive systems consisting of polyelectrolytes such as xanthan gum, calcium arginate and acrylate and magnetically induced systems (Bussemer et al. 2003, Kashyap et al. 2007, Roy and Shahiwala 2009, Jessy et al. 2011, Tangri and Khurana 2011, Prasanth et al. 2012). This has never been attempted using aerosol jet technology previously.

This chapter explores the initial attempts to generate pulsatile release systems utilising the initial model drug fenofibrate. The effect of sandwiching the 1:4 fenofibrate:PVP amorphous solid dispersion generated in previous chapters between PVP layers is explored. This chapter demonstrates the potential of this technique for generating pulsatile release but also reveals the reason for changing the drug in the latter stages of the project.

5.2 Materials and Methods

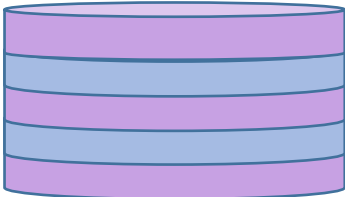
5.2.1 Materials

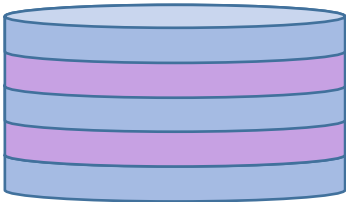
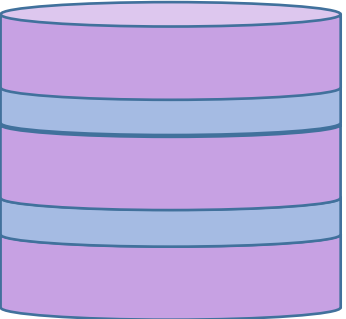
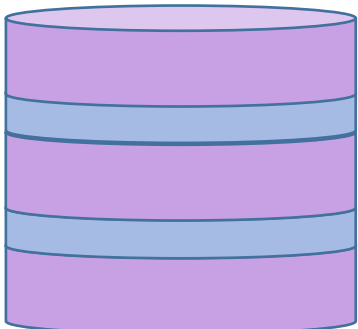
As in Chapter 2.

5.2.2 Methods

Printing was carried out in the manner detailed in Chapter 2. All samples were prepared at 3mm/s using a 300µm nozzle and an ethanol-based ink. With the exception of the sandwich-style pulsatile formulations, all samples were prepared by printing directly onto filled plastic sample cups obtained from Paraytec Ltd. The sandwich-style samples were prepared in standard Sirius SDI cups filled to halfway with 3D printed PLA secured with super glue. Following on from the premix and separate component work, more complex formulations with more complex release profiles were sought. As such pulsatile systems were developed initially printing 1:4 fenofibrate:PVP with PVP alone layers (Table 26).

Table 26: Fenofibrate formulations to achieve pulsatile release

Dosage Form	Number of Layers	Content of Layers	Thickness of Layers	Schematic
Sandwiched 2mm circles	5	1:4 FNFPVP, PVP, 1:4 FNFPVP, PVP, 1:4 FNFPVP	5 printed layers per component layer	

Sandwiched 2mm circles	5	PVP, 1:4 FNFPVP, PVP, 1:4 FNFPVP, PVP	5 printed layers per component layer	
Sandwiched 2mm circles	5	PVP, 1:4 FNFPVP, PVP, 1:4 FNFPVP, PVP	10:5:10:5:10	
Sandwiched 2mm circles	5	PVP, 1:4 FNFPVP, PVP, 1:4 FNFPVP, PVP	5:2:5:2:5	

Samples were analysed using the SDI as described in Chapter 4 but running samples for up to 1.5 hours at 0.2ml/min.

5.3 Results & Discussion

As can be observed in Figures 86 and 87, samples generally showed a very slight initial pulse but failed to show a second resulting in a minor pulse followed by sustained release. The only exception to this is one 5x5 layer sample with PVP printed first. The other two samples in this study do not show this so it is suggested that this minor increase is down to the release of a slightly bigger particle as the solution passed over the surface rather than a significant increase in release. The sustained release effect is thought to be due to a combination of fenofibrate's inherent poor solubility and changes to the formulation as the SIF penetrates it over time, resulting in a washing away of the polymer and potentially an antisolvent effect on the drug as the aqueous solution comes in to contact with the drug. Additionally, within the initial pulse only a fraction of the expected release occurred. On analysis of the pulse layers alone, as demonstrated in Chapter 4, it was established that the drug was not released to the same degree as in previous samples which may be due to the differing surface area. Increasing the polymer content of the buffer layers also seemed to have the opposite effect from the expected with less drug being released overall. On reducing the overall drug content, the drug release increased, however this was a reflection of the overall drug content rather than the mass released as demonstrated by the intrinsic dissolution rate remaining very similar to that of the other samples. With the exception of the afore mentioned latter pulse the configuration of the dosage forms appears to have minimal effect on the intrinsic dissolution rate.

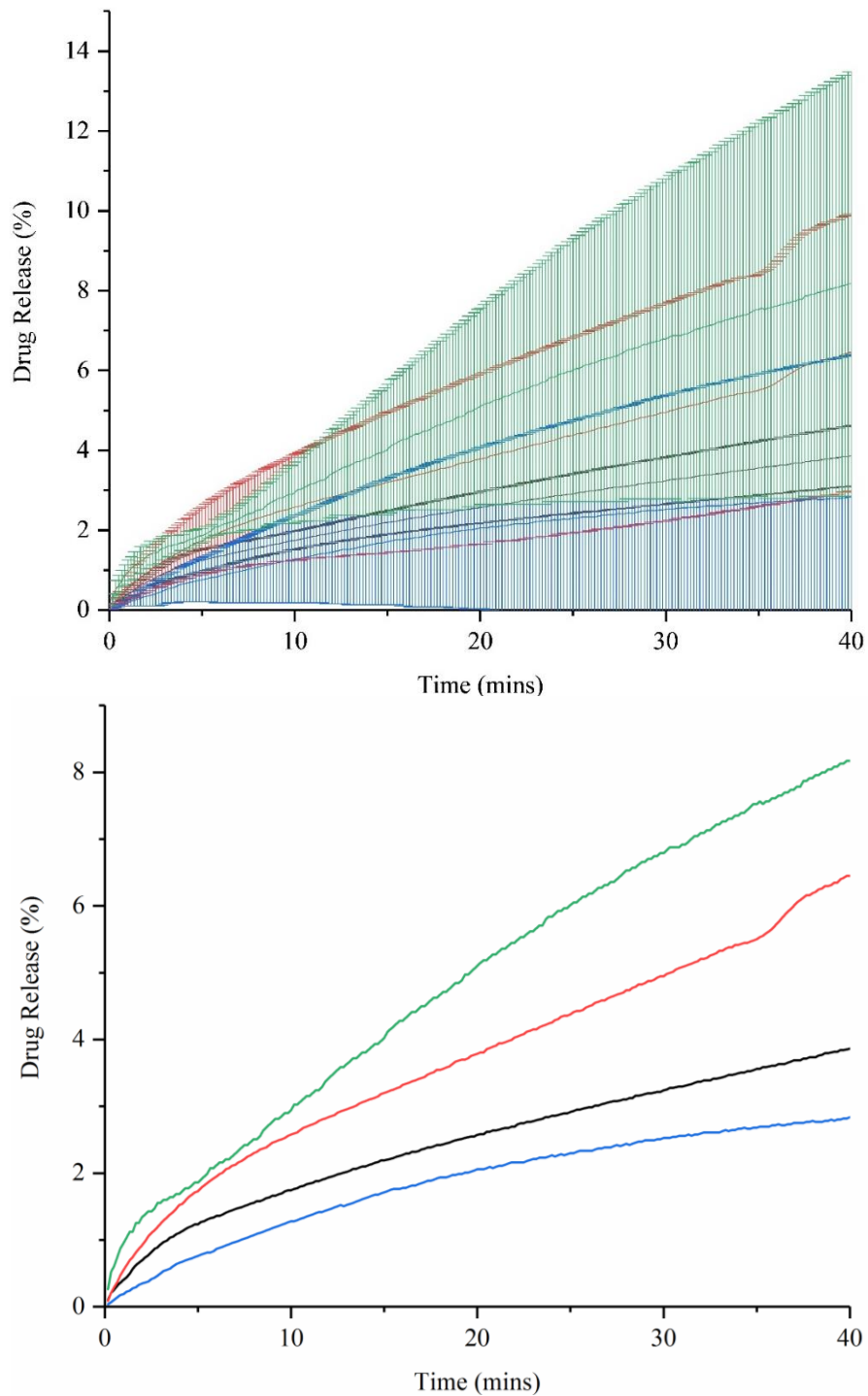


Figure 86: Drug Release from fenofibrate containing sandwich-style systems with 1:4 fenofibrate:PVP as 3x5 layer pulse layers between 2x5 layer PVP buffer layers (black), 2x5 layer pulse layers between 3x5 layer PVP buffer layers (red), 2x5 layer pulse layers between 3x10 layer PVP buffer layers (blue) and 2x2 layer pulse layers between 3x5 layer PVP buffer layers (green), where $n=3\pm$ standard error, with (top) and without (bottom) error bars.

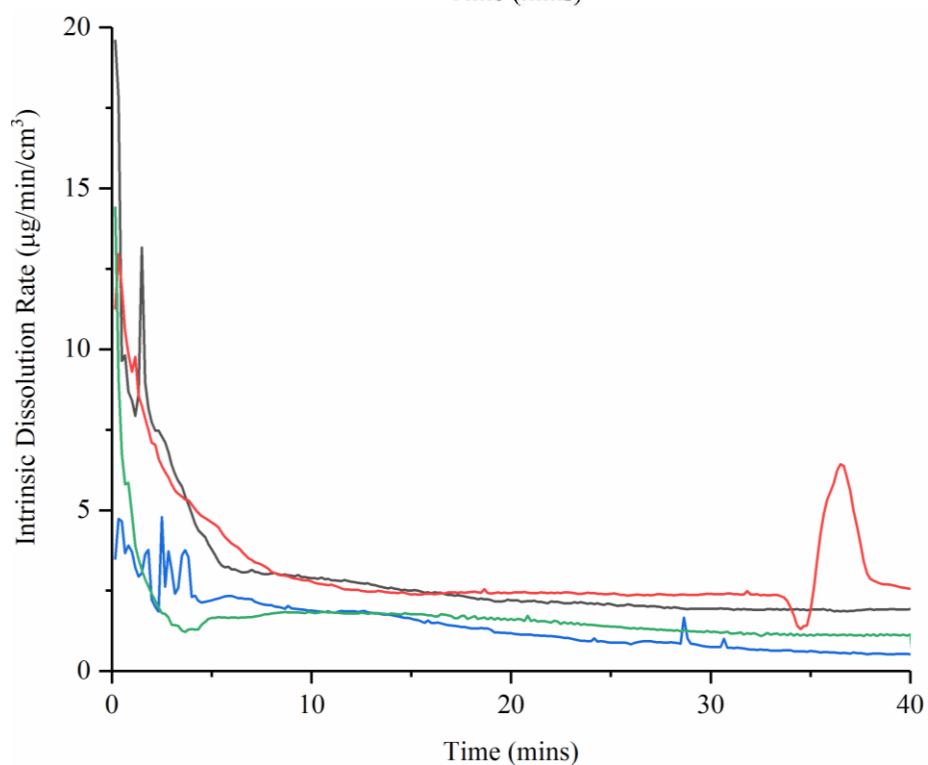
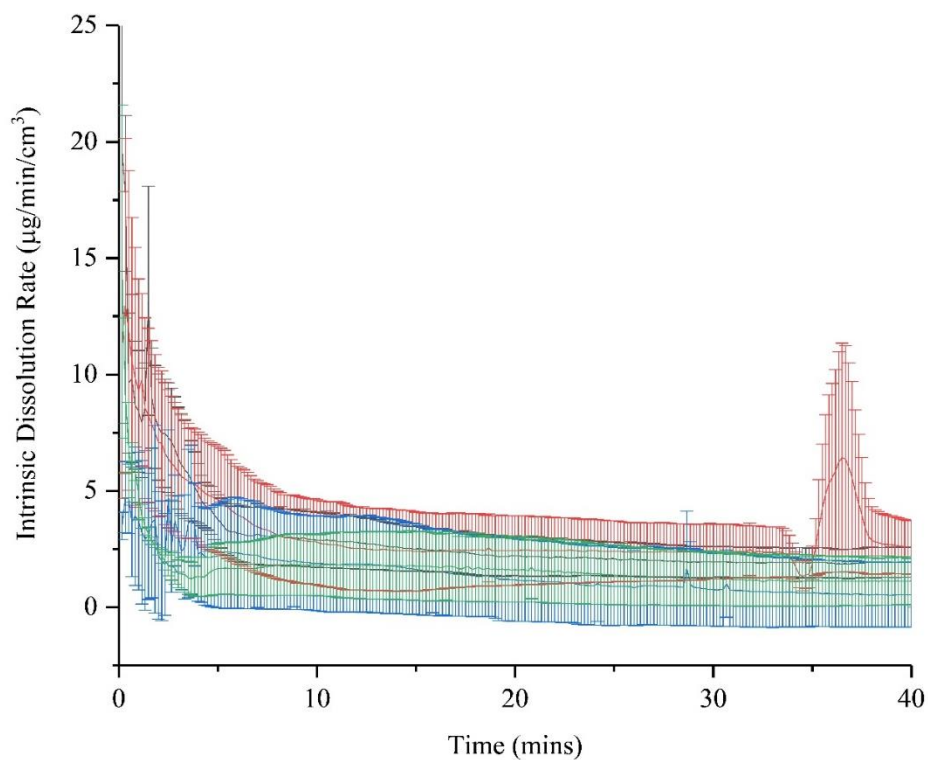


Figure 87: Intrinsic dissolution rate from fenofibrate containing sandwich-style systems with 1:4 fenofibrate:PVP as 3x5 layer pulse layers between 2x5 layer PVP buffer layers (black), 2x5 layer pulse layers between 3x5 layer PVP buffer layers (red), 2x5 layer pulse layers between 3x10 layer PVP buffer layers (blue) and 2x2 layer pulse layers between 3x5 layer PVP buffer layers (green), where $n=3 \pm$ standard error.

5.4 Conclusions

Initial attempts to achieve pulsatile release showed some evidence of an initial pulse and a sustained release profile. However, all but one sample failed to show any evidence of a second pulse and the overall drug release remained low. Furthermore, the intrinsic dissolution rate was observed to fall over time as a result of the exposure of the drug to the dissolution media. Ultimately, fenofibrate was concluded to be unsuitable for use in an aerosol jet printed pulsatile system.

Chapter 6: Aerosol Inkjet Printing Pulsatile Release Systems Utilising Ibuprofen

6.1 Introduction

This chapter explores the development of the pulsatile platform with the slightly less poorly soluble drug ibuprofen. As ibuprofen was inclined to release more quickly than fenofibrate, the chances of observing a pulsed profile rather than a sustained release profile were considerably higher. In this chapter, the effect of configuration, layer thickness, drug core thickness and layer number were explored with a view to demonstrating the capacity of the printer to produce different release profiles. The initial aim was to produce 2 or more pulses within 1 to 2 hours.

Once this was established to be possible, the next step was to see if it was possible to scale this effect up. Printing was scaled up from 2mm diameter to 1cm diameter with a view to testing the effect of scale up by USP IV. The additional advantage of scale up was it allowed analysis of a printed, multicomponent dosage form by Nano CT. This allowed conclusions to be drawn about precision, scale and quality of the print.

6.2 Materials and Methods

6.2.1 Materials

As in Chapter 2.

6.2.2 Methods

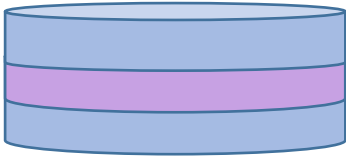
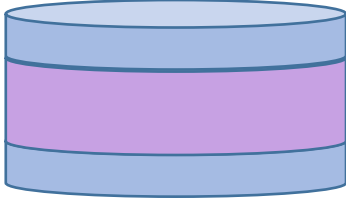
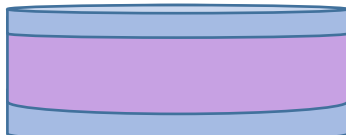
6.2.2.1 SDI Samples

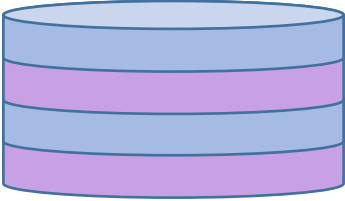
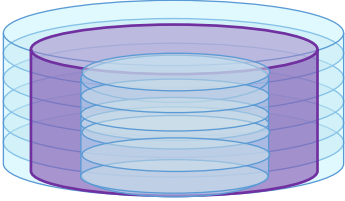
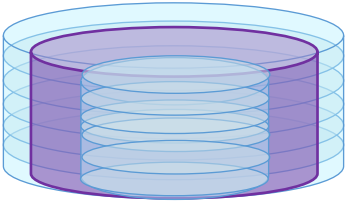
Printing was carried out in the manner detailed in Chapter 2. All samples were prepared at 3mm/s using a 300µm nozzle and an ethanol-based ink. With the

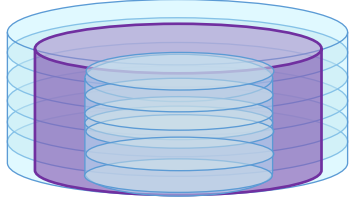
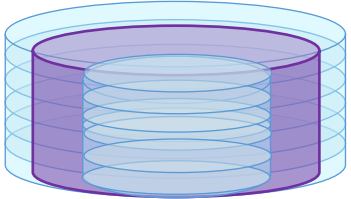
exception of the sandwich-style pulsatile formulations, all samples were prepared by printing directly onto filled plastic sample cups obtained from Paraytec Ltd.

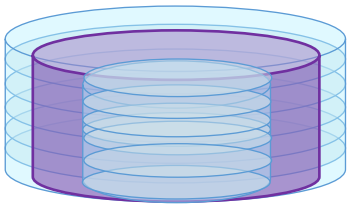
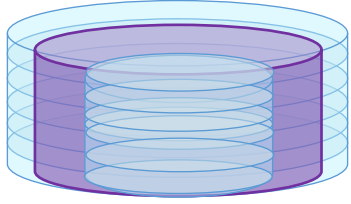
Samples were prepared with 1:4 ibuprofen:PVP with PVP alone layers. These dosage forms fall into 2 categories which are sandwich-style and tori-style (Table 27). The former is based on printing 2mm circles in a stack and exposing only the top surface by using sample cups with an edge. The latter is based on concentric circles and lids which provides a dome which releases from the flat sample cup surface. The complexities of the individual formulations are given in Table 27.

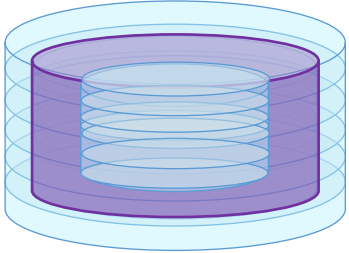
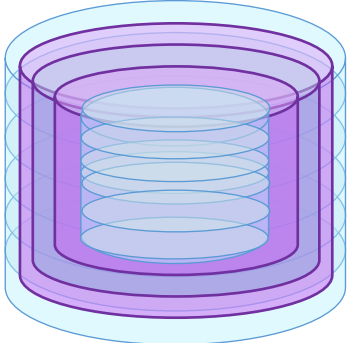
Table 27: Ibuprofen formulations to achieve pulsatile release

Dosage Form	Number of Layers	Content of Layers	Thickness of Layers	Schematic
Sandwiched 2mm circles	3	1:4 IBU:PVP, PVP, 1:4 IBU:PVP	5:5:5	
Sandwiched 2mm circles	3	1:4 IBU:PVP, PVP, 1:4 IBU:PVP	5:10:5	
Sandwiched 2mm circles	3	1:4 IBU:PVP, PVP, 1:4 IBU:PVP	2:10:2	

Sandwiched 2mm circles	4	PVP, 1:4 IBU:PVP, PVP, 1:4 IBU:PVP	5:5:5	
Tori-style	3	1:4 IBU:PVP, PVP, 1:4 IBU:PVP	10 layers thick: 0.8mm core, 0.6mm torus and 1.4mm circle buffer, 0.6mm torus and 2mm drug circle exterior	
Tori-style	3	1:4 IBU:PVP, PVP, 1:4 IBU:PVP	10 layers thick: 0.8mm core, 0.3mm torus and 1.1mm circle buffer, 0.9mm torus and 2mm drug	

			circle exterior	
Tori-style	3	1:4 IBU:PVP, PVP, 1:4 IBU:PVP	10 layers thick: 0.8mm core, 0.9mm torus and 1.7mm circle buffer, 0.3mm torus and 2mm drug circle exterior	
Tori-style	3	1:4 IBU:PVP, PVP, 1:4 IBU:PVP	5 layers thick: 0.8mm core, 0.6mm torus and 1.4mm circle buffer, 0.6mm torus and 2mm drug circle exterior	

<p>Tori-style</p>	<p>3</p>	<p>1:4 IBU:PVP, PVP, 1:4 IBU:PVP</p>	<p>5 layers thick with 10 layer core: 0.8mm core, 0.6mm torus and 1.4mm circle buffer, 0.6mm torus and 2mm drug circle exterior</p>	
<p>Tori-style</p>	<p>3</p>	<p>1:4 IBU:PVP, PVP, 1:4 IBU:PVP</p>	<p>10 layer thick with 20 layer core: 0.8mm core, 0.6mm torus and 1.4mm circle 2mm drug circle exterior</p>	

<p>Encapsulated Tori-style</p>	<p>3</p>	<p>1:4 IBU:PVP, PVP, 1:4 IBU:PVP, PVP, 1:4 IBU:PVP</p>	<p>5 layers thick: 0.8mm core, 0.3mm torus and 1.1 mm circle buffer, 0.3mm torus and 1.4mm circle drug layer, 0.3mm torus and 1.7mm circle buffer layer and 0.3mm torus and 2mm drug circle exterior</p>	
<p>Encapsulated Tori-style</p>	<p>5</p>	<p>1:4 IBU:PVP, PVP, 1:4 IBU:PVP, PVP, 1:4 IBU:PVP</p>	<p>10 layers thick: 0.8mm core, 0.3mm torus and 1.1 mm</p>	

			circle buffer, 0.3mm torus and 1.4mm circle drug layer, 0.3mm torus and 1.7mm circle buffer layer and 0.3mm torus and 2mm drug circle exterior	
--	--	--	--	--

Samples were analysed using the SDI as described in Chapter 4 but running samples for up to 1.5 hours at 0.2ml/min.

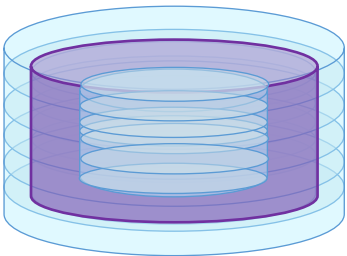
6.2.2.2 Full-size Tablet

6.2.2.2.1 Printing

A single full-size tablet sample was printed in the same manner as detailed in Chapter 2. The reason this was not carried out in triplicate is due to the size of the tablet and the time taken to print a single layer. It took 20 hours to print one tablet, not including cleaning between inks. The sample was prepared as detailed in Table 28, to yield a larger version of the design given in Table 27. The sample was built from the bottom up in 5 steps. This started with the bottom drug-containing layer, then the bottom

buffer layer, then the drug-containing core, then the surrounding buffer collar and top layer and finally the outer drug-containing collar and top layer.

Table 28: Full Size Tablet Design

Tablet section	Design components	Ink utilised	Schematic
Outer layer	Bottom: 50x 1 cm circles Collar: 150x 1.5 mm width tori Top: 50x 1 cm circles	1:4 ibuprofen:PVP K30 (based on 30mg/ml IBU in ethanol)	
Buffer layer	Bottom: 50x 7 mm circles Collar: 50x 1.5 mm width tori Top: 50x 7 mm circles	PVP K30 30mg/ml in ethanol	
Core	50x 4 mm circles	1:4 ibuprofen:PVP K30	

6.2.2.2.2 Nano CT

Samples were run using a Bruker SkyScan 2211 v2.0 Nano CT at 9.05 μ m pixels, a source voltage of 35kV and a source current of 500uA. Sampling was carried out over 3 hours and 14 minutes at a distance of 57.84mm from the source. The data was analysed using the SkyScan software (v.2.5.0) to generate 2D and 3D images of the interior of the tablet.

6.2.2.2.3 *Drug Content Analysis*

Drug content analysis was carried out by UHPLC as in Chapter 3 using the ibuprofen method detailed in Chapter 4. Single layer individual torus and circle component parts (Table 28) were printed on rice paper and characterised by dissolving in acetonitrile.

6.2.2.2.4 *Dissolution*

Dissolution was carried out using an ERWEKA HKP 720 Flow-cell USP IV (Erweka GmbH, Heusenstamm, Germany) with an ALS SP700 UV Spectrophotometer (Automated Lab Systems Ltd., Wokingham, Berkshire, U.K.) as this was thought to be the most comparable to the SDI method utilised previously in this chapter and in Chapter 4. Initially a calibration was carried out by dissolving ibuprofen in methanol and diluting down using SIF to generate standards as in Chapter 4. 1µg/ml, 2µg/ml, 5µg/ml, 10µg/ml and 20µg/ml standards were generated. Standards were analysed by UV spectrometry at 222 nm and the calibration curve was generated on UV Win and plotted using Origin Pro 2017 (Appendix 5).

After taking a blank media reading, the tablet was added to the flow cell chamber. The USP IV lines were connected to the UV spectrometer and the media was pumped over the samples at 37°C based on a rate of 16 ml/min and a pump rotation of 120rpm. Readings were taken in an automated fashion at one minute intervals using the automated USP II software IDIS (Automated Lab Systems Ltd., Wokingham, Berkshire, U.K.). The data was then exported to Microsoft Excel and plotted using Origin Pro 2017.

6.3 Results & Discussion

6.3.1 SDI Samples

Ibuprofen was employed as an alternative to fenofibrate as, despite being a Class II drug, it had previously shown good release on the SDI. As can be observed in Chapter 4, a 3-fold higher drug release and 4-fold higher intrinsic dissolution rate resulted from printed 1:4 ibuprofen:PVP compared to printed 1:4 fenofibrate:PVP. As such it was hoped this would enable the desired 2 or 3 pulse pulsatile formulation.

6.3.1.1 Sandwich-Style

A sandwich-style pulsatile configuration was explored initially preparing samples as in Table 27. Initial samples (Figures 88 and 89) showed evidence of pulsing in the first 10 minutes of the dissolution run. The drug release (Figure 88) shows evidence of the characteristic lag phase and wave like conformation of a pulsatile curve. It almost forms a step-like profile in the 10 layers PVP to 10 layers fenofibrate configurations. The intrinsic dissolution rate (Figure 89) of all the formulations rises and falls. However, both the drug release and the intrinsic dissolution rate lacked definition. Due to time constraints this experiment was only carried out once, as it was favoured to proceed to more viable options.

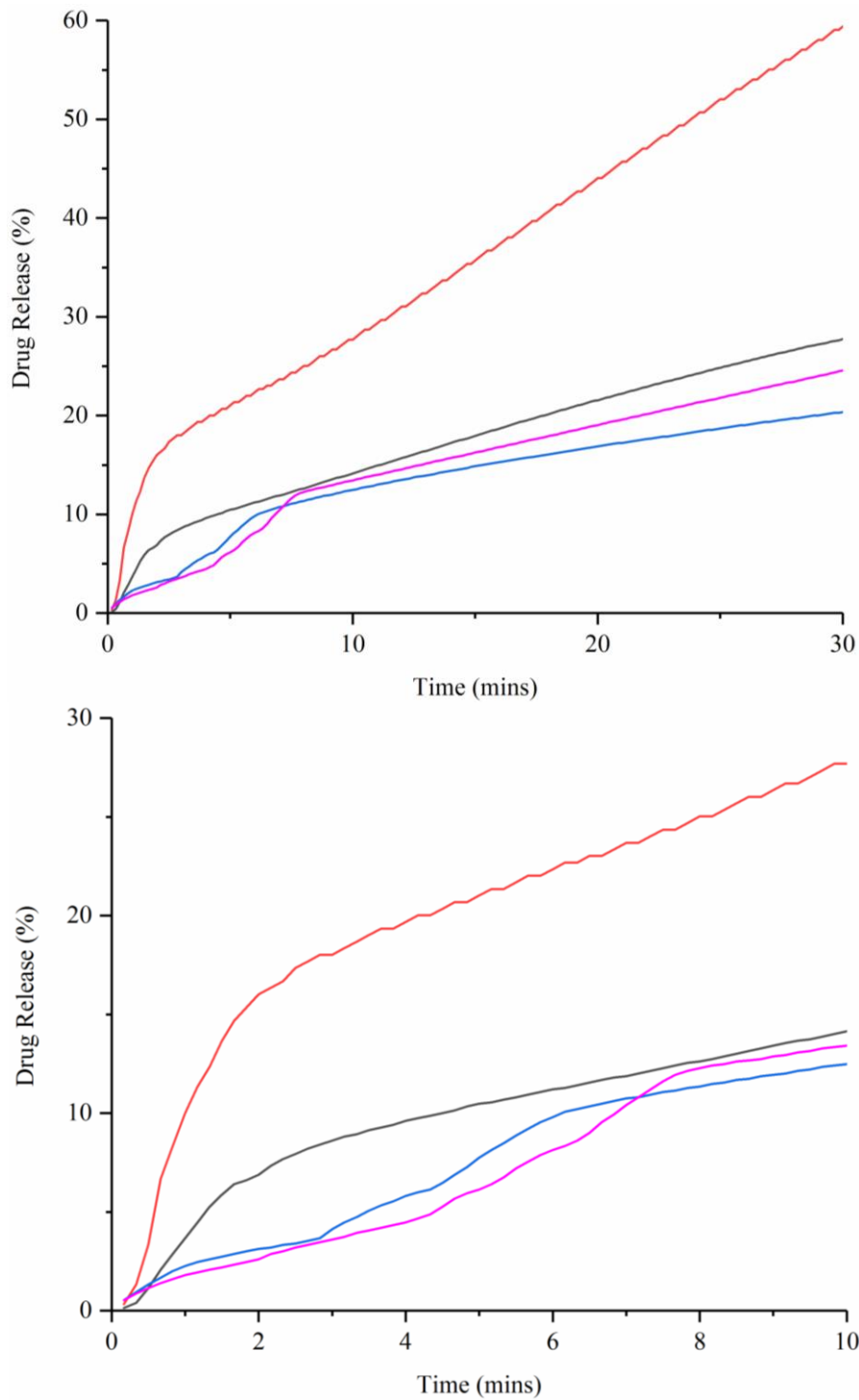


Figure 88: Drug release from sandwich-style prototype pulsatile dosage forms consisting of 2.5 layer 1:4 ibuprofen:PVP layers to 1.5 layer PVP buffer layers (black), 2.2 layer 1:4 ibuprofen:PVP layers to 1.10 layer PVP buffer layer (red), 2.5 layer 1:4 ibuprofen:PVP layers to 1.10 layer PVP buffer layer (blue) and 2.5 layer 1:4 ibuprofen:PVP layers to 2.5 layer PVP buffer layers (magenta), where $n=1$. The drug release is shown over 30 minutes (top) and zooming into the first 10 minutes (bottom).

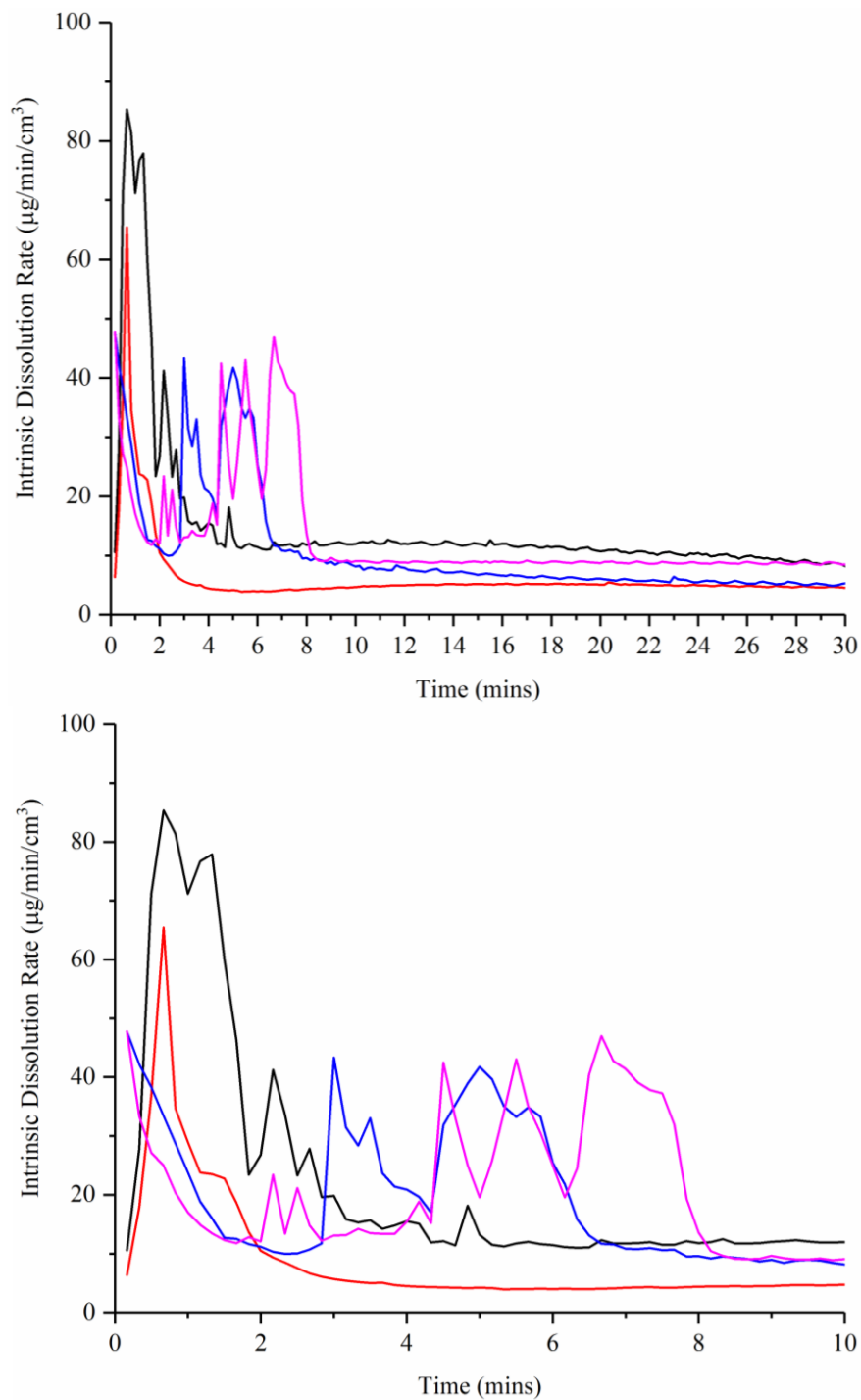


Figure 89: Intrinsic Dissolution Rate from sandwich-style prototype pulsatile dosage forms consisting of 2.5 layer 1:4 ibuprofen:PVP layers to 1.5 layer PVP buffer layer (black), 2.2 layer 1:4 ibuprofen:PVP layers to 1.10 layer PVP buffer layer (red), 2.5 layer 1:4 ibuprofen:PVP layers to 1.10 layer PVP buffer layers (blue) and 2.5 layer 1:4 ibuprofen:PVP layers to 2.5 layer PVP buffer layers (magenta), where $n=1$. The intrinsic dissolution rate is shown over 30 minutes (top) and zooming into the first 10 minutes (bottom).

The sandwich style samples are supported by a number of previous studies. Interestingly most studies on layered tablets feature a sandwich configuration but with barrier layers either side of the drug loaded layer rather than the other way around. For example, a study by Gohel and Bariya demonstrated three layered tablets with a matrix core of venlafaxine hydrochlorate, Hypromellose K100M and Avicel PH 101 and barrier layers of Hypromellose K100M, Pharmatose DCL 11 and magnesium stearate. This yielded an initial burst and then sustained release (Gohel and Bariya 2009). Another study demonstrates a sandwich-style gastroretentive with diltiazem hydroxide and polyethylene oxide with sodium bicarbonate resulting in either immediate or sustained release (Raut Desai and Rohera 2014). Sandwich style samples were prepared previously using granulation and compression of guar gum alone base layer, guar gum and metoprolol tartrate central layer, and guar gum alone top layer resulting in release in 2 hours (Al-Saidan et al. 2004). Additionally, three layered tablets were demonstrated in another study consisting of an upper barrier layer of polyox WSR 303 and magnesium stearate, a central active layer of Tamsulosin HCl dihydrate, Pearlitol 160C, macrogol 6000, sodium hydroxide and magnesium stearate, and a lower barrier layer of polyox WSR 303 and magnesium stearate (Choi, Kim, et al. 2013). The use of a solid dispersion in a 3-layer matrix style tablet has been demonstrated previously with solid dispersions of acetaminophen with PVP K30 by solvent evaporation using HPMC outer layers resulting in two bursts of sustained release (Qi et al. 2015).

6.3.1.2 Tori Style

Tori based dome-like samples were prepared as detailed in Table 27. As can be observed in Figures 90 and 91, a similar initial pulse to the sandwich-style samples is generated on printing samples in a dome-like fashion. However, with the exception of 1 of the 5 layer samples, this initial pulse occurs fully within the first 5 minutes. There is also a potential second pulse within this first 5 minutes. The sample which showed a lesser first pulse may be explained by a release which is more like a typical

matrix tablet. Interestingly this sample also shows a latter pulse but later. As a result, the effect of fully encasing the layers was explored.

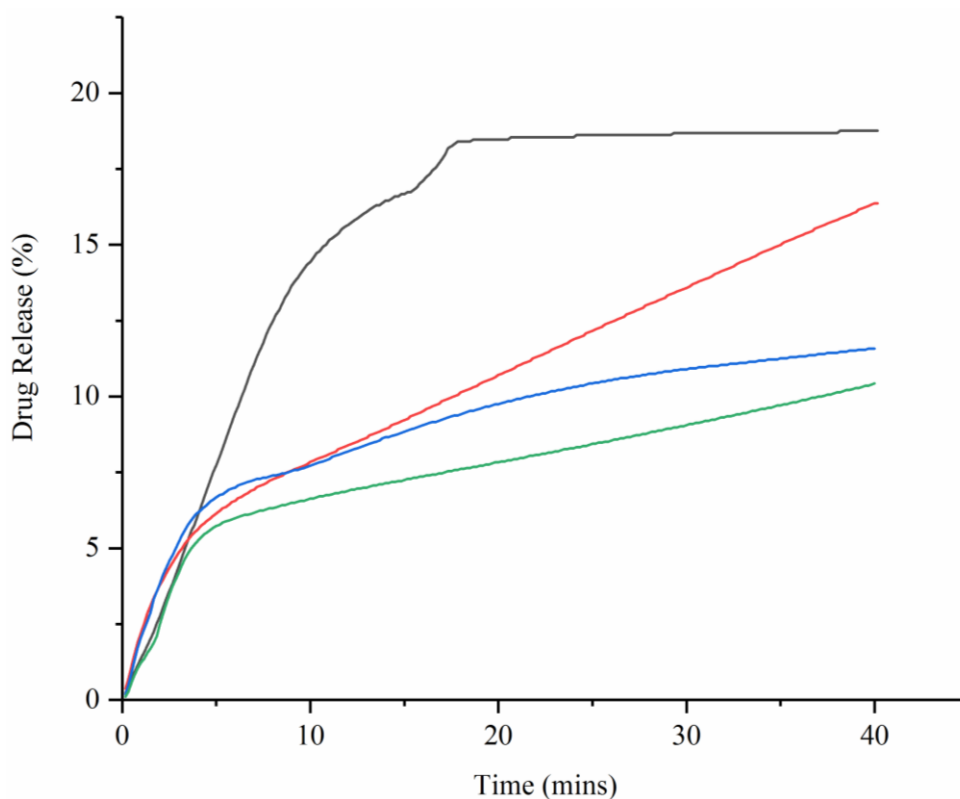


Figure 90: Drug release from tori based dome-style prototype pulsatile dosage forms consisting of 2 5 layer 1:4 ibuprofen:PVP layers to 1 5 layer PVP buffer layer (black and red) and 2 10 layer 1:4 ibuprofen:PVP layers to 1 10 layer PVP buffer layers (blue and green), where $n=1$.

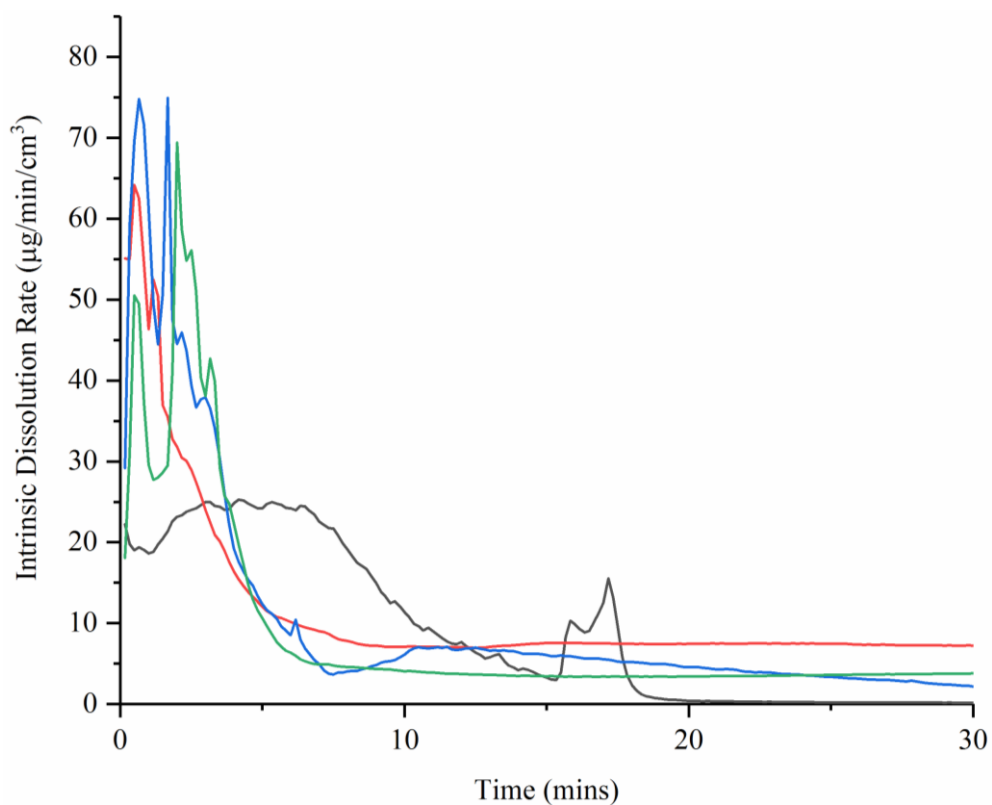


Figure 91: Intrinsic dissolution rate from tori based dome-style prototype pulsatile dosage forms consisting of 2 5 layer 1:4 ibuprofen:PVP layers to 1 5 layer PVP buffer layer (black and red) and 2 10 layer 1:4 ibuprofen:PVP layers to 1 10 layer PVP buffer layers (blue and green), where $n=1$.

6.3.1.3 Encapsulated Tori

Following on from the dome-style tori-based samples, bases were added to the individual layers creating a fully encapsulated effect.

6.3.1.3.1 2 Pulse Attempts

6.3.1.3.1.1 5 vs. 10 layers

Initially 2 pulses were attempted using a basic 5 and 10 layer structure based on a drug containing core separated from an outer drug containing layer by a polymer buffer layer. As can be observed in Figures 92 and 93, printing 5 or 10 layers results in an initial pulse followed by a sustained period and a second pulse. The pulsing effect can be seen in a more pronounced manner in Figures 94 and 95. For 10 layers, the intrinsic dissolution rate demonstrates 2 distinct peaks within an hour. There is

potential evidence of a third peak but due to the initial flush it is difficult to confirm if this is a true peak. For 5 layers, the pulsing effect is present but not all of the samples exhibit the same definite peaks that 10 layers show. This may be due to the nature of the SDI rather than the dosage form as the manner in which the solution passes over the surface may be washing away the drug before an effective UV signal can be taken.

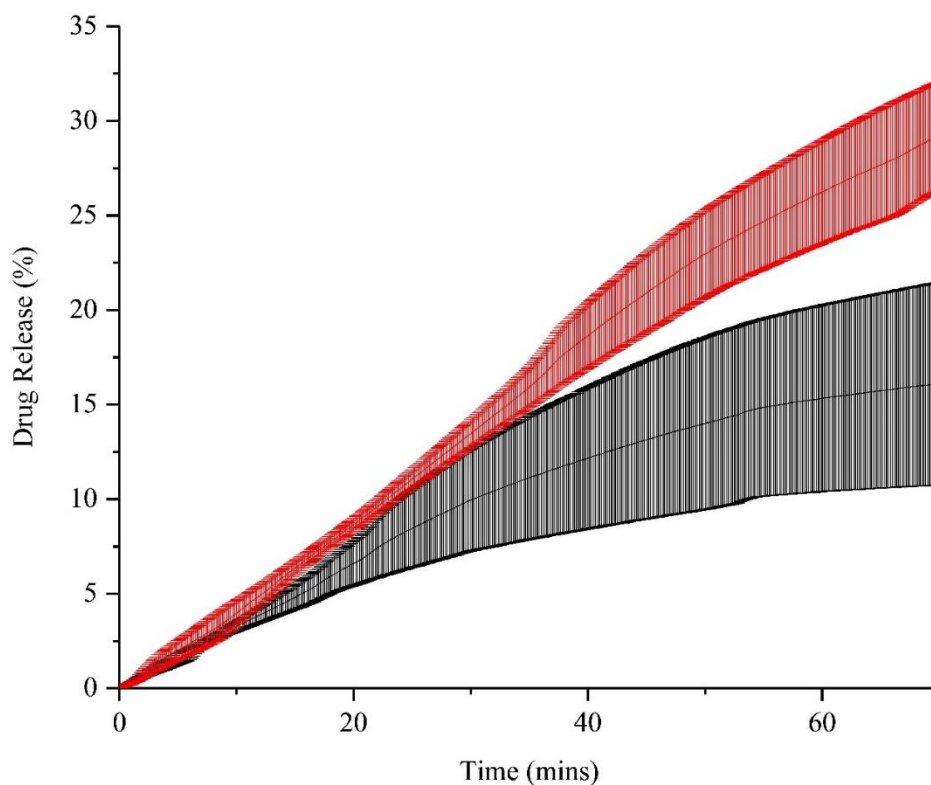


Figure 92: Drug release from encapsulated prototype pulsatile dosage forms consisting of 2 5 layer 1:4 ibuprofen:PVP layers to 1 5 layer PVP buffer layer (red) and 2 10 layer 1:4 ibuprofen:PVP layers to 1 10 layer PVP buffer layers (black), where $n=3 \pm$ standard error.

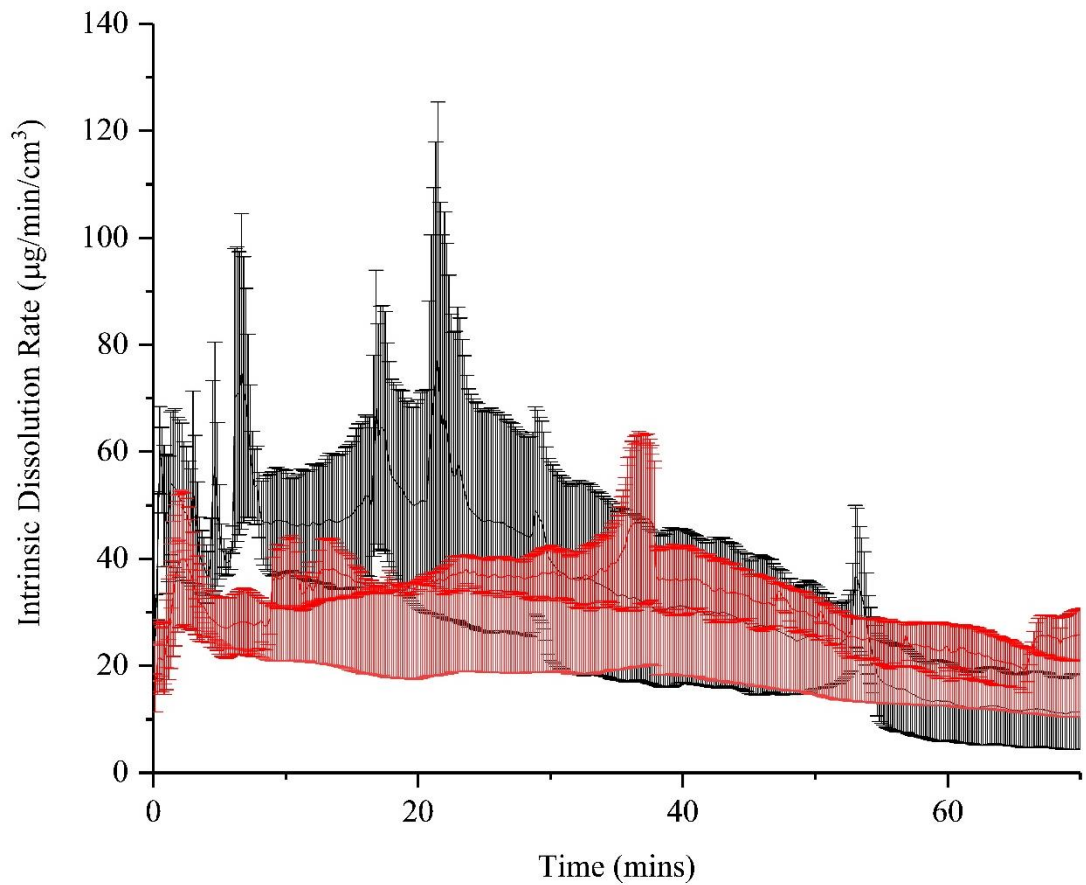


Figure 93: Intrinsic dissolution rate from encapsulated prototype pulsatile dosage forms consisting of 2.5 layer 1:4 ibuprofen:PVP layers to 1.5 layer PVP buffer layer (red) and 2.10 layer 1:4 ibuprofen:PVP layers to 1.10 layer PVP buffer layers (black), where $n=3 \pm$ standard error.

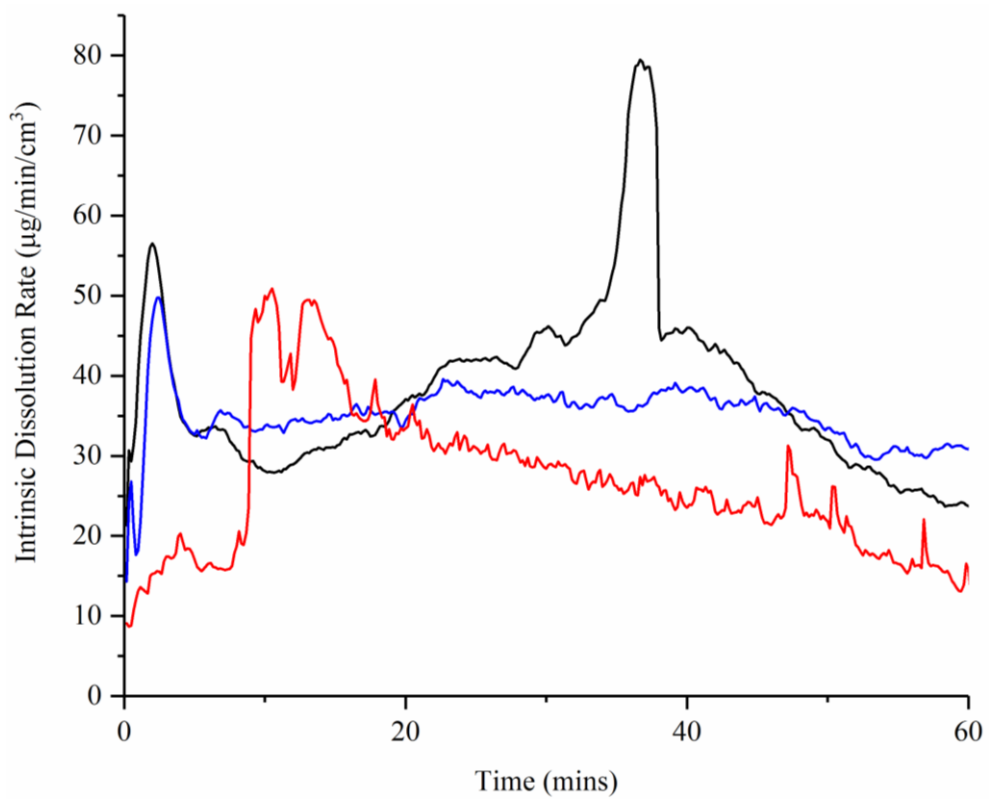


Figure 94: Intrinsic dissolution rate from encapsulated prototype pulsatile dosage forms consisting of 2.5 layer 1:4 ibuprofen:PVP layers to 1.5 layer PVP buffer layer, where $n=1$.

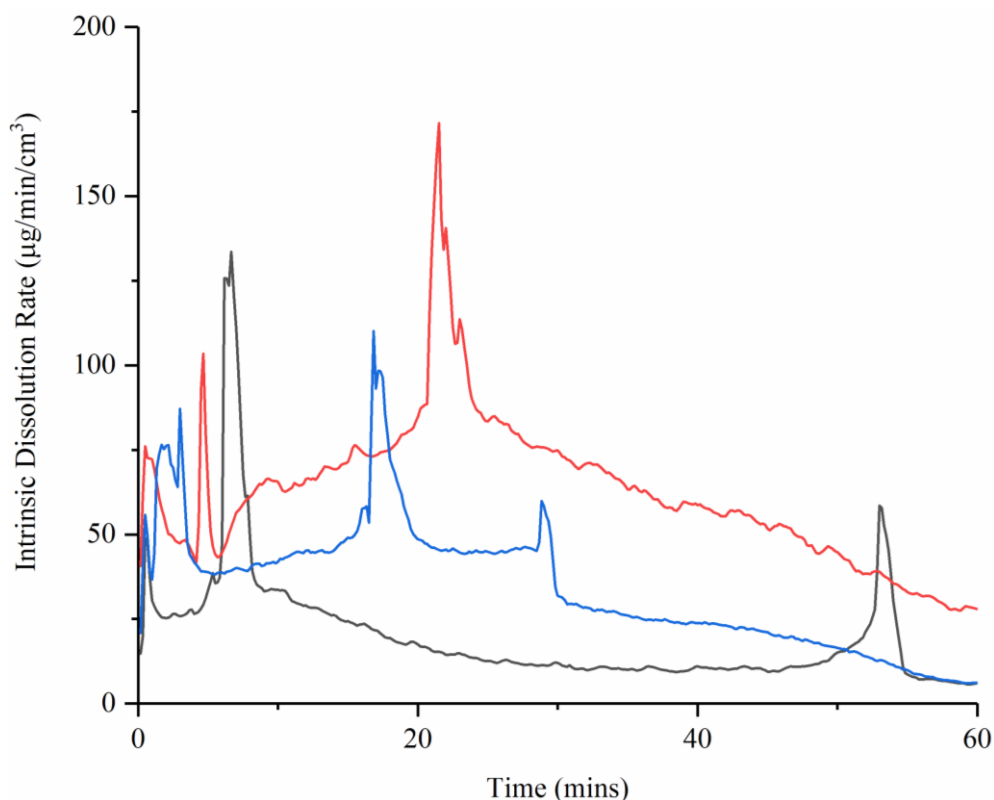


Figure 95: Intrinsic dissolution rate from encapsulated prototype pulsatile dosage forms consisting of 2 10 layer 1:4 ibuprofen:PVP layers to 1 10 layer PVP buffer layers, where n=1.

On comparison to the literature there is very little previous evidence for this. For example, samples with a drug-loaded outer coating and a matrix layer also have been prepared previously but these tablets lacked a barrier layer (Elzayat et al. 2017). Additionally, a very similar drug release rate pattern was observed over a longer period from a layered tablet within a capsule. The tablets consisted of diclofenac sodium with a modulating barrier and a lactose between two immediate release layers and a modulating barrier and an immediate release layer. This resulted in an initial burst in the first hour followed by a second burst at 5 to 6 hours and a final burst at 10 to 11 hours (Li, Zhu, et al. 2008). There are also a number of patents on multicomponent tablet designs but none on inkjet printing in this manner (Arndt et al. 2001, Plachetka et al. 2002, Petereit et al. 2004, Nutalapati 2012, Yeoman et al. 2016).

6.3.1.3.1.2 Changing the Buffer Layer

On changing the buffer layer thickness, it can be observed that not only does the overall release reduce (Figures 96, 98 and 100), it is not guaranteed that both intrinsic dissolution rate (Figures 97, 99 and 101) pulses are achieved. For the thicker 1.7mm buffer layer, is possible that the initial outer layer is lost before the measurement run starts. One substantial drawback of the SDI is a need to flush the flow cell after the sample is added to prevent bubbles interfering with the UV signal. This requires a 10-30 second flush at 2ml/min and thus the fiercer flow rate may damage or dissolve the initial layer. The thinner 1.1mm buffer may result in a loss of the second peak as the buffer layer is not thick enough to fully separate the 2 drug containing layers once the SIF diffusion into the system begins.

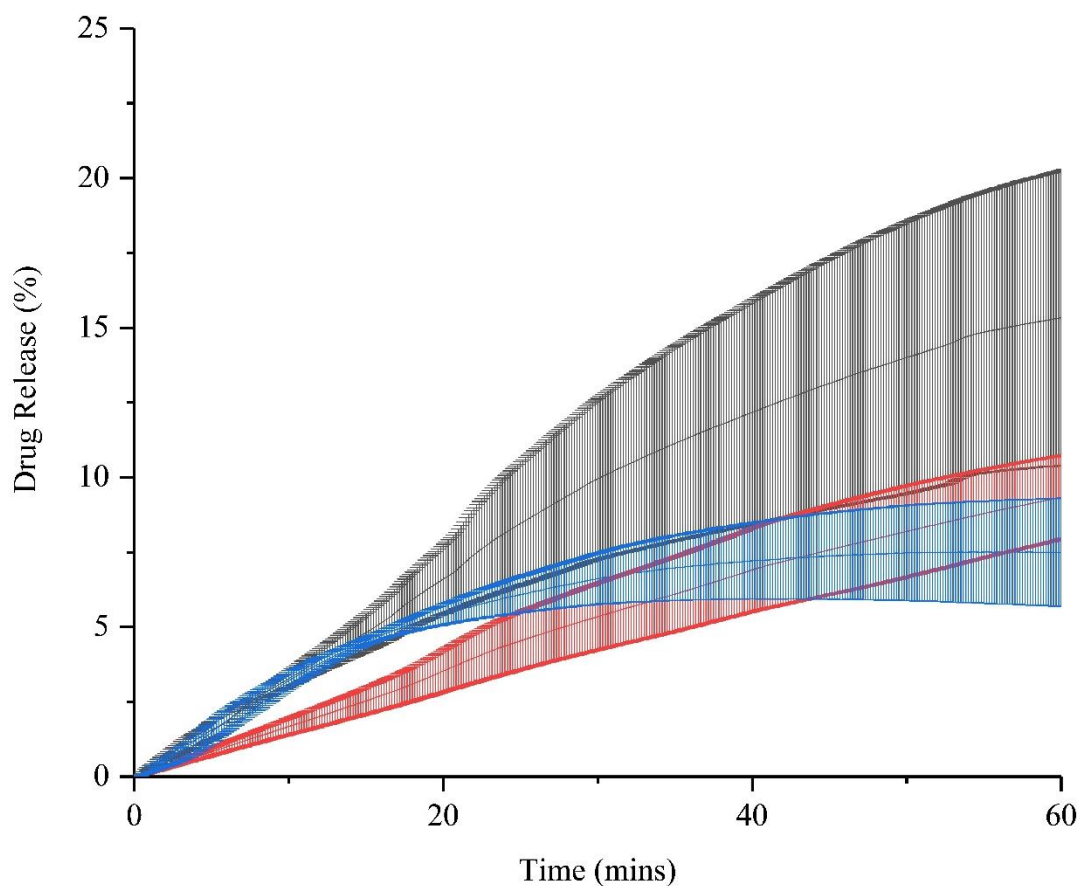


Figure 96: Drug release from encapsulated prototype pulsatile dosage forms consisting of 2 5 layer 1:4 ibuprofen:PVP layers to 1 5 1.1mm layer PVP buffer layer (red), 1.4mm buffer layer (black) and 1.7mm buffer layer (blue), where $n=3\pm$ standard error.

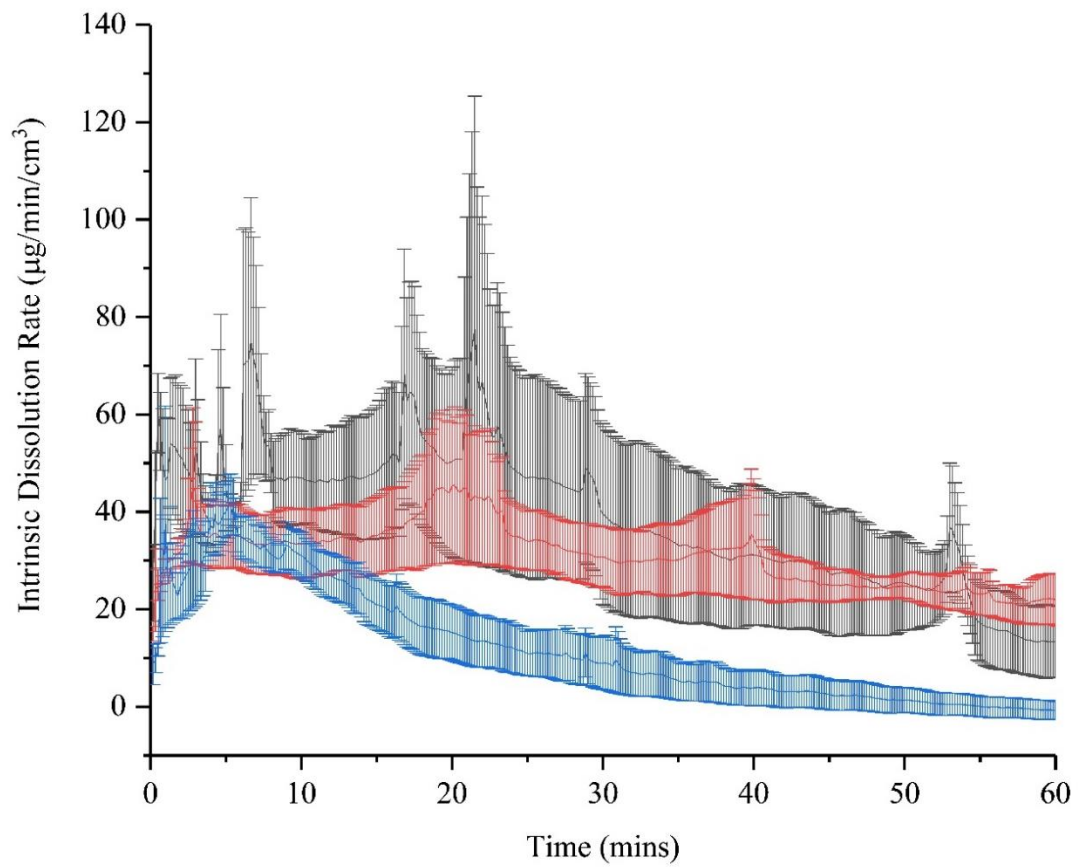


Figure 97: Intrinsic dissolution rate from encapsulated prototype pulsatile dosage forms consisting of 2.5 layer 1:4 ibuprofen:PVP layers to 1.5 1.1mm layer PVP buffer layer (red), 1.4mm buffer layer (black) and 1.7mm buffer layer (blue), where $n=3 \pm$ standard error.

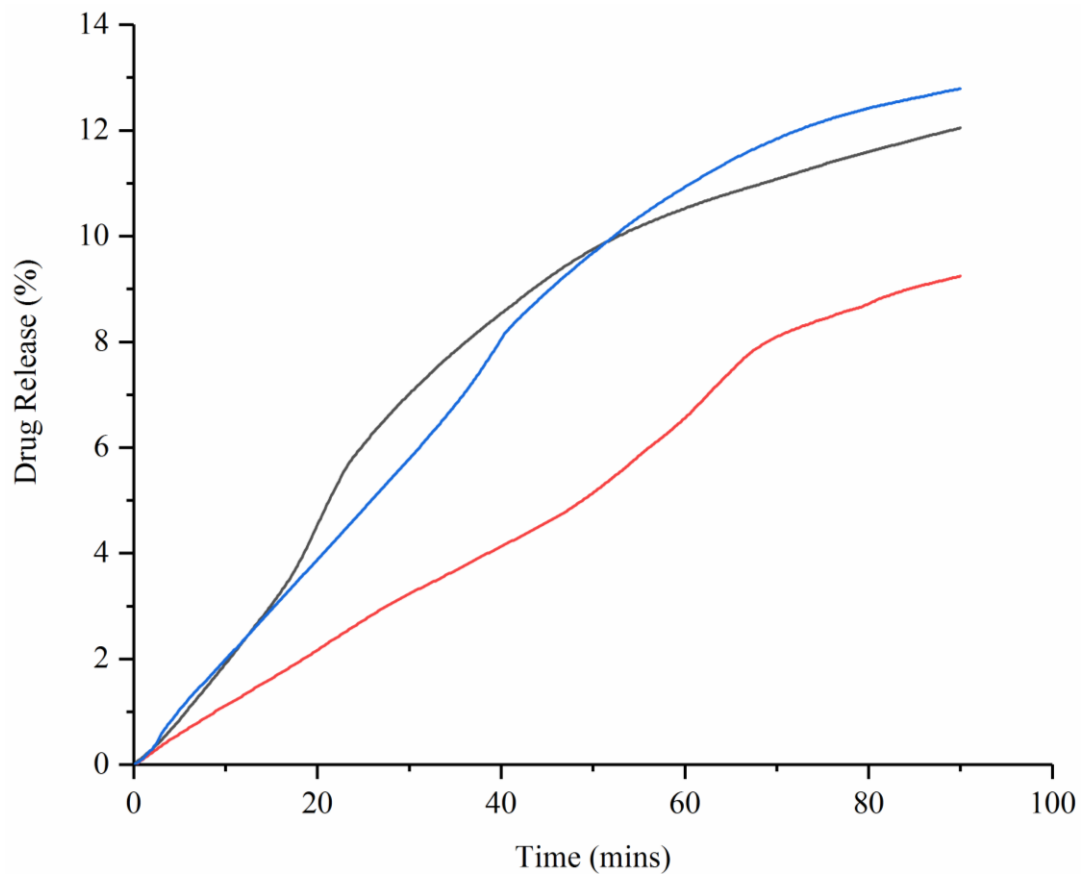


Figure 98: Drug release from encapsulated prototype pulsatile dosage forms consisting of 2.5 layer 1:4 ibuprofen:PVP layers to 1.5 1.1mm layer PVP buffer layer, where $n=1$.

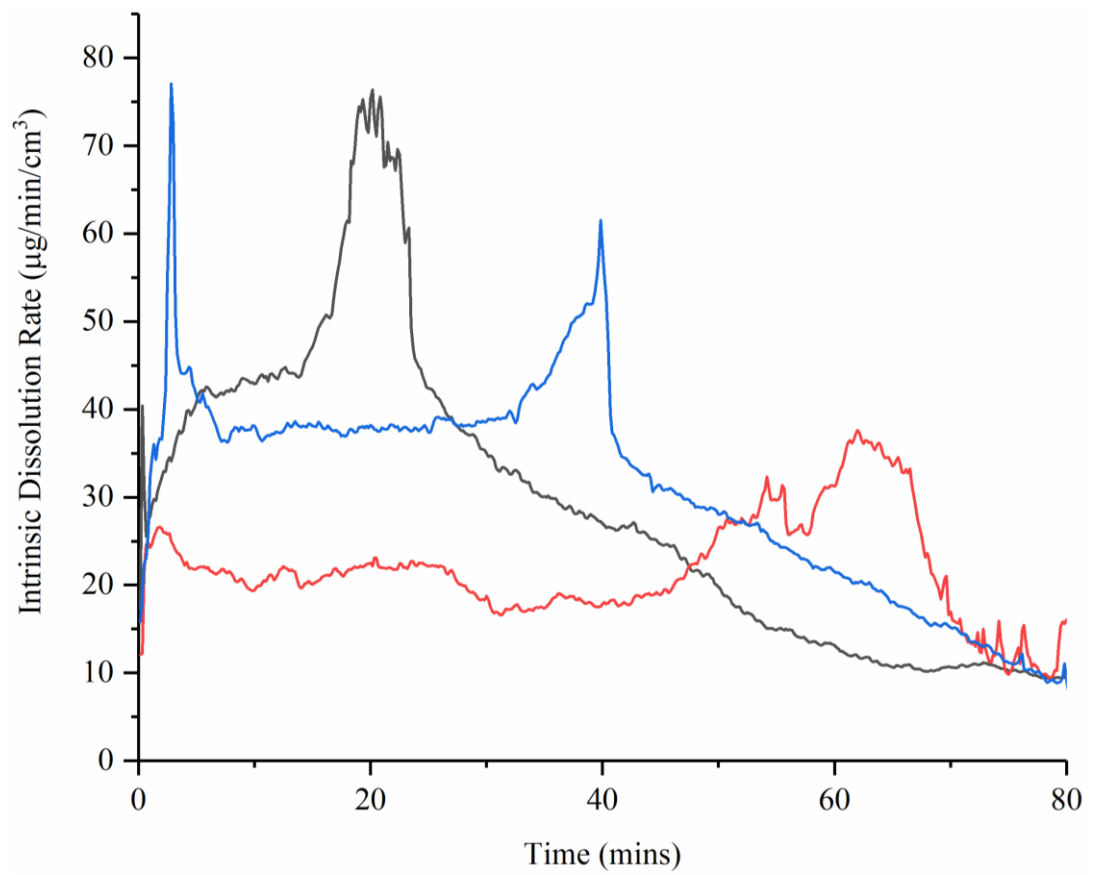


Figure 99: Intrinsic dissolution rate from encapsulated prototype pulsatile dosage forms consisting of 2.5 layer 1:4 ibuprofen:PVP layers to 1.5 1.1mm layer PVP buffer layer, where n=1.

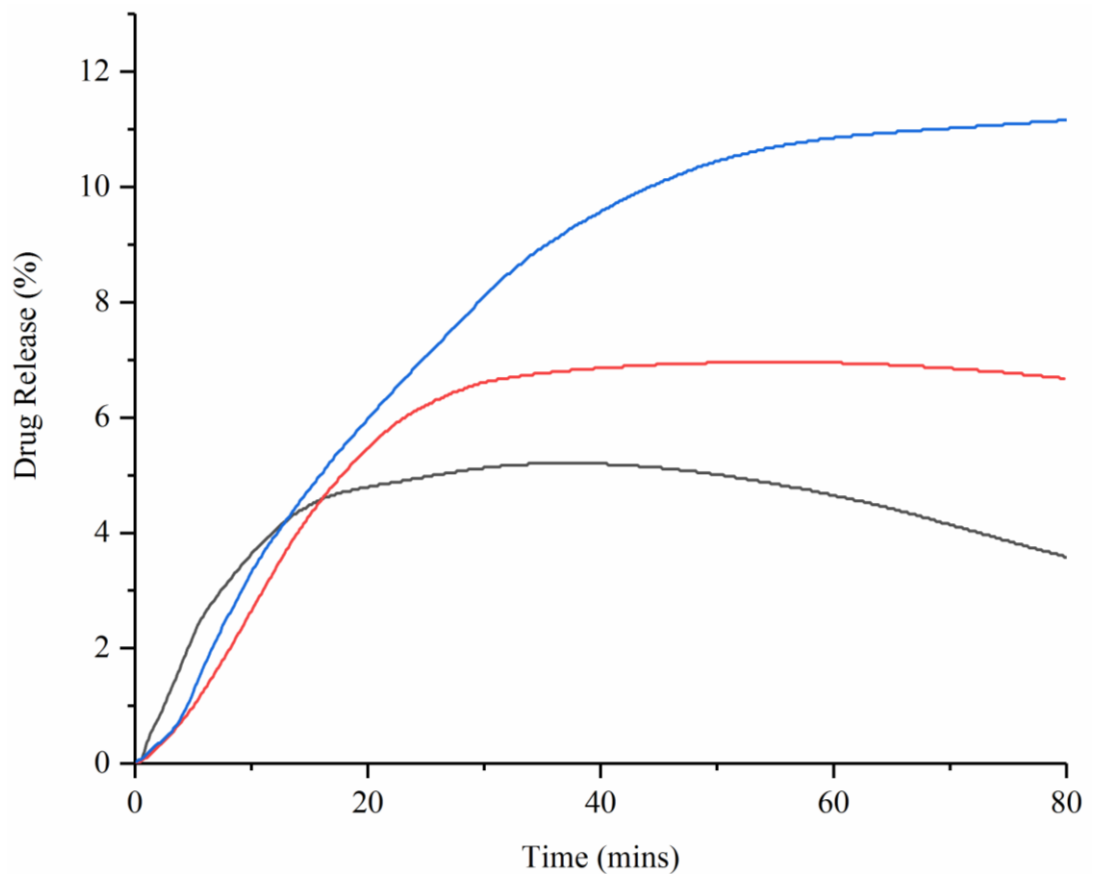


Figure 100: Drug release from encapsulated prototype pulsatile dosage forms consisting of 2.5 layer 1:4 ibuprofen:PVP layers to 1.5 1.7mm layer PVP buffer layer, where $n=1$.

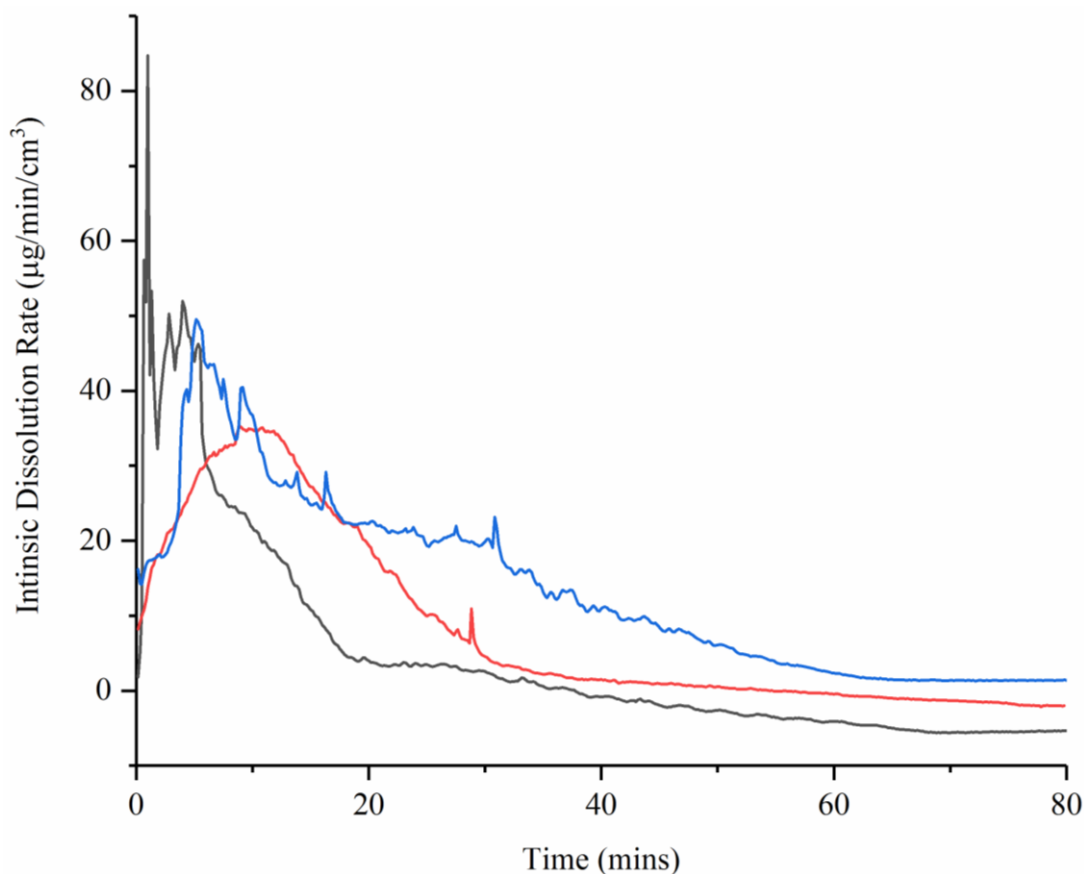


Figure 101: Intrinsic dissolution rate from encapsulated prototype pulsatile dosage forms consisting of 2.5 layer 1:4 ibuprofen:PVP layers to 1.5 1.7mm layer PVP buffer layer, where $n=1$.

6.3.1.3.1.3 Changing the Core

The effect of changing the core can be observed in Figures 102 and 103. On changing the thickness of the drug-containing core to 10 layers to the outer layers' 5, the second pulse is found to occur more quickly overall (Figures 104 and 105). On average it occurs 20 minutes sooner than when the core thickness matches the outer layer. The effect is more muted on changing the core to 20 layers to the outer layers' 10 (Figures 106 and 107). Interestingly, this seems to result in a more matrix-like release as shown by the more curved intrinsic dissolution rate profile.

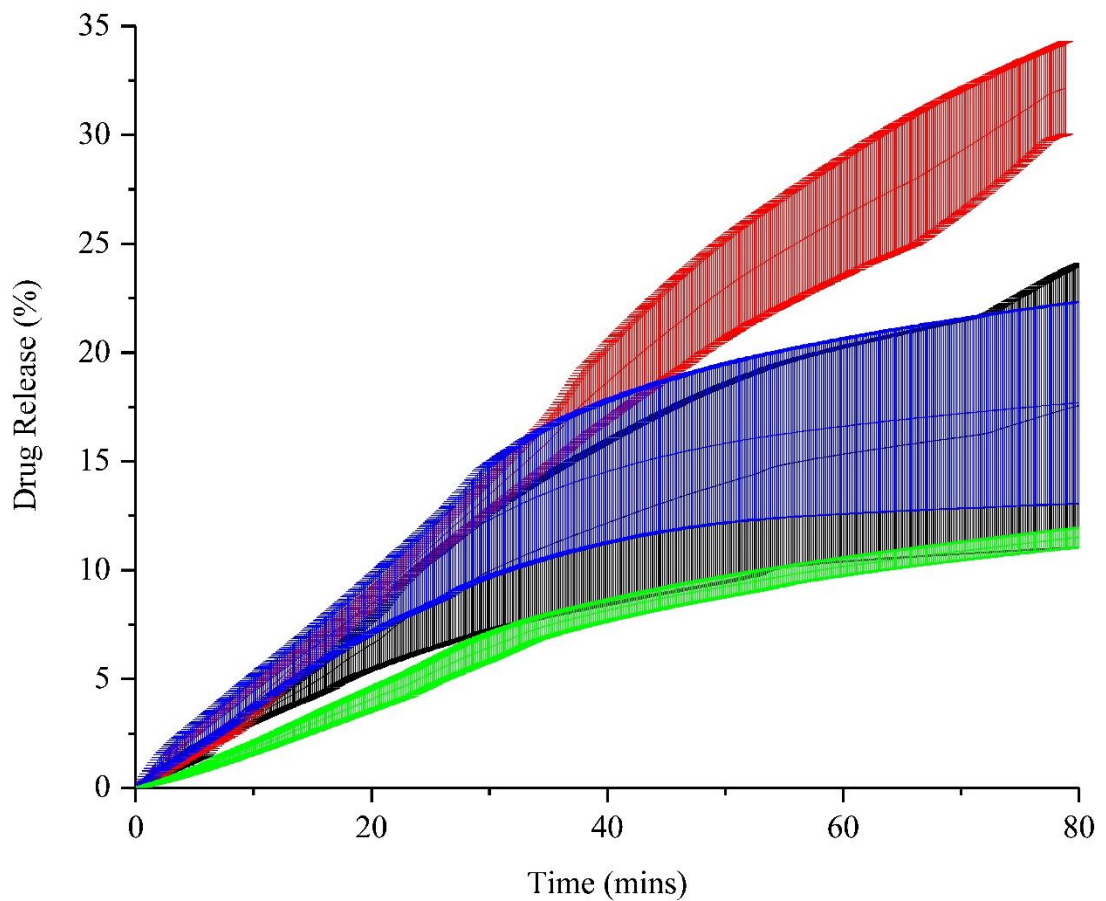


Figure 102: Drug release from encapsulated prototype pulsatile dosage forms consisting of 2 10 layer 1:4 ibuprofen:PVP layers to 1 10 1.4mm layer PVP buffer layer (red), 2 5 layer 1:4 ibuprofen:PVP layers to 1 5 1.4mm layer PVP buffer layer (black), 1 5 layer 1:4 ibuprofen:PVP outer layer and 1 10 layer 1:4 ibuprofen:PVP core to 1 5 1.4mm layer PVP buffer layer (blue) and 1 10 layer 1:4 ibuprofen:PVP outer layer and 1 20 layer 1:4 ibuprofen:PVP core to 1 10 1.4mm layer PVP buffer layer (green), where $n=3 \pm$ standard error.

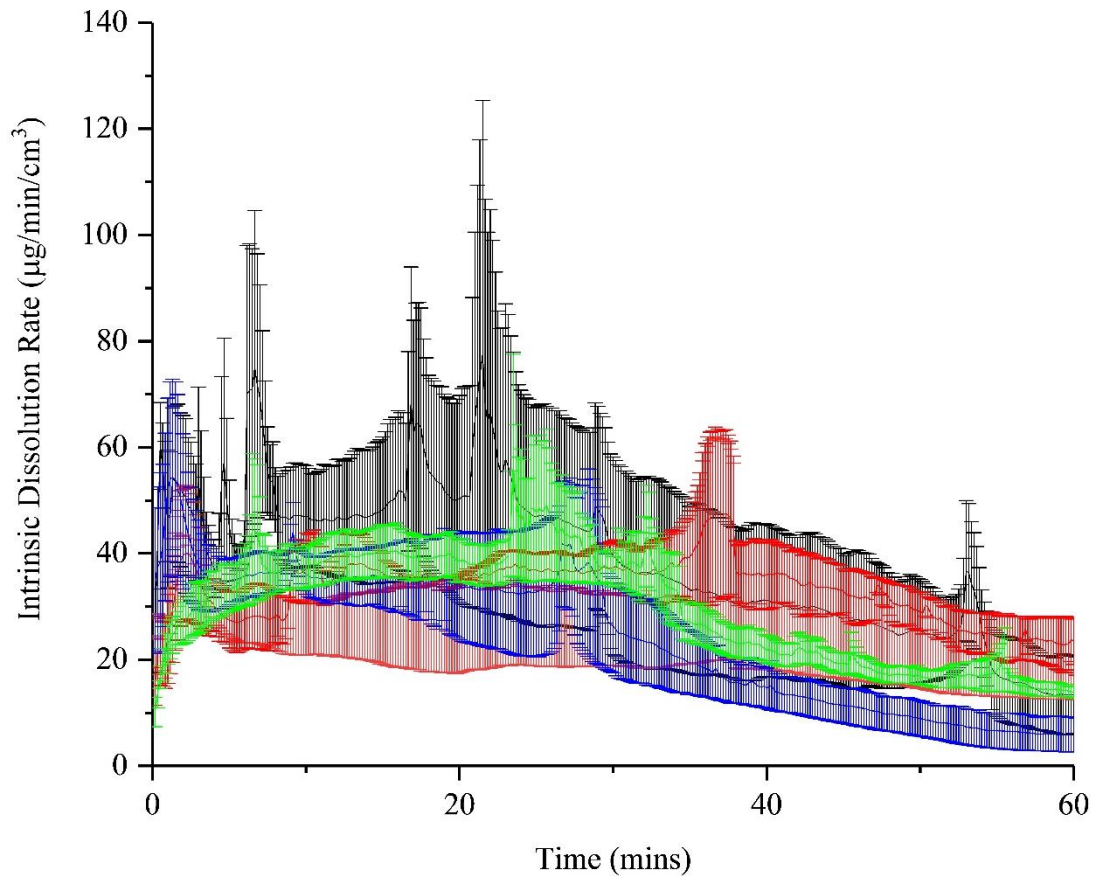


Figure 103: Intrinsic Dissolution Rate from encapsulated prototype pulsatile dosage forms consisting of 2 10 layer 1:4 ibuprofen:PVP layers to 1 10 1.4mm layer PVP buffer layer (red), 2 5 layer 1:4 ibuprofen:PVP layers to 1 5 1.4mm layer PVP buffer layer (black), 1 5 layer 1:4 ibuprofen:PVP outer layer and 1 10 layer 1:4 ibuprofen:PVP core to 1 5 1.4mm layer PVP buffer layer (blue) and 1 10 layer 1:4 ibuprofen:PVP outer layer and 1 20 layer 1:4 ibuprofen:PVP core to 1 10 1.4mm layer PVP buffer layer (green), where $n=3 \pm$ standard error.

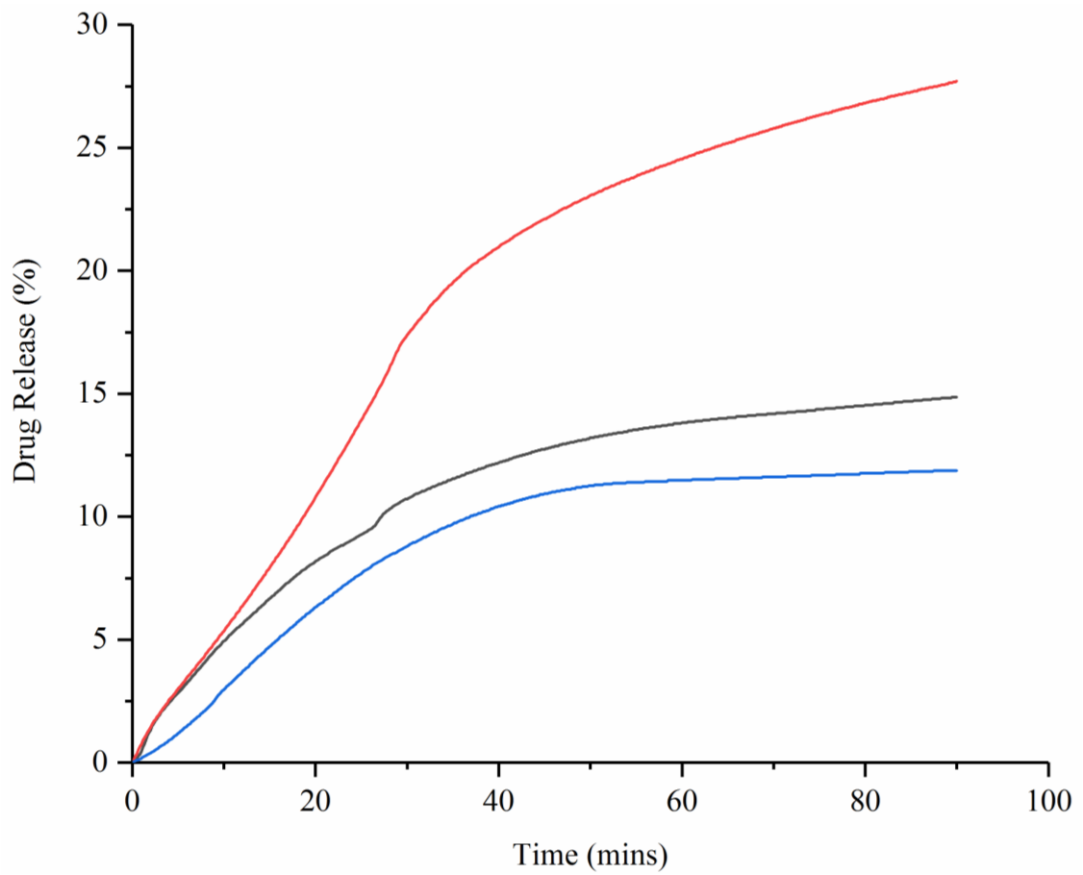


Figure 104: Drug release from encapsulated prototype pulsatile dosage forms consisting of 1.5 layer 1:4 ibuprofen:PVP outer layer and 1.10 layer 1:4 ibuprofen:PVP core to 1.5 1.4mm layer PVP buffer layer, where n=1.

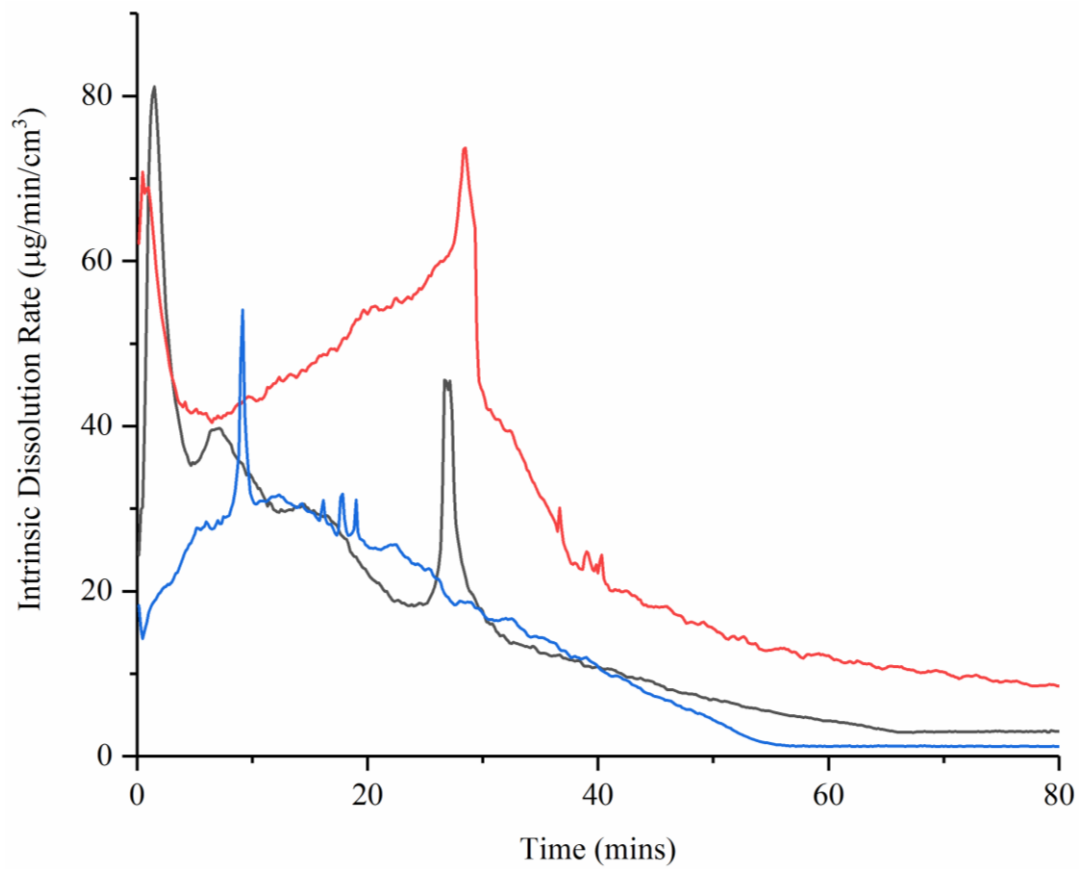


Figure 105: Intrinsic dissolution rate from encapsulated prototype pulsatile dosage forms consisting of 1 5 layer 1:4 ibuprofen:PVP outer layer and 1 10 layer 1:4 ibuprofen:PVP core to 1 5 1.4mm layer PVP buffer layer, where $n=1$.

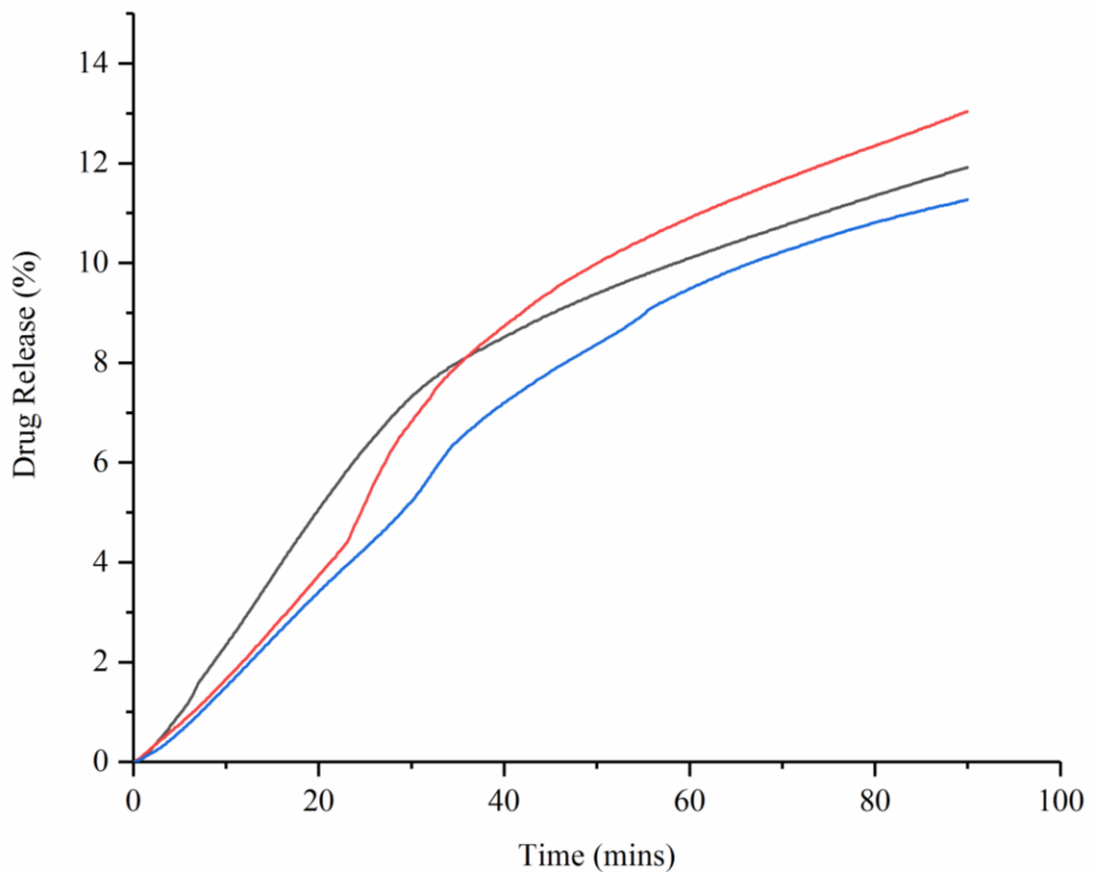


Figure 106: Drug release from encapsulated prototype pulsatile dosage forms consisting of 1 10 layer 1:4 ibuprofen:PVP outer layer and 1 20 layer 1:4 ibuprofen:PVP core to 1 10 1.4mm layer PVP buffer layer, where n=1.

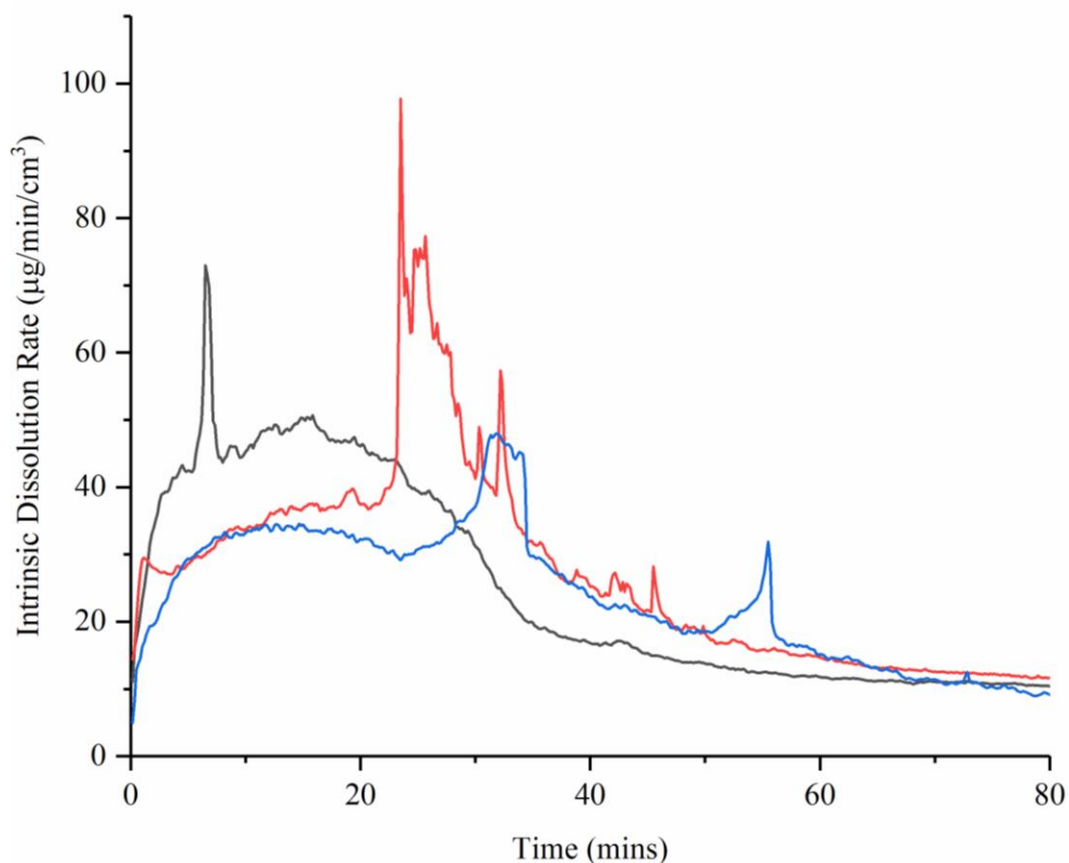


Figure 107: Intrinsic dissolution rate from encapsulated prototype pulsatile dosage forms consisting of 1 10 layer 1:4 ibuprofen:PVP outer layer and 1 20 layer 1:4 ibuprofen:PVP core to 1 10 1.4mm layer PVP buffer layer, where $n=1$.

6.3.1.3.2 3 Pulse Attempts

On increasing the number of distinct drug-containing layers and buffer layers in an attempt to increase the number of pulses, a more rapid initial increase in release occurs (Figure 108). However, on examination of the intrinsic dissolution rate (Figure 109), it can be observed that, although the initial pulsatile peak is retained, the latter peaks are more flat resulting in a more matrix-like release. This suggests there is a limit to the thickness of layers to separate the individual layers. This is particularly important as the SIF starts to diffuse through the porous dosage form. It is suggested that the limits of the SDI have been reached and thus to achieve more pulses, the dosage form would have to be scaled up and a different form of dissolution set up utilised.

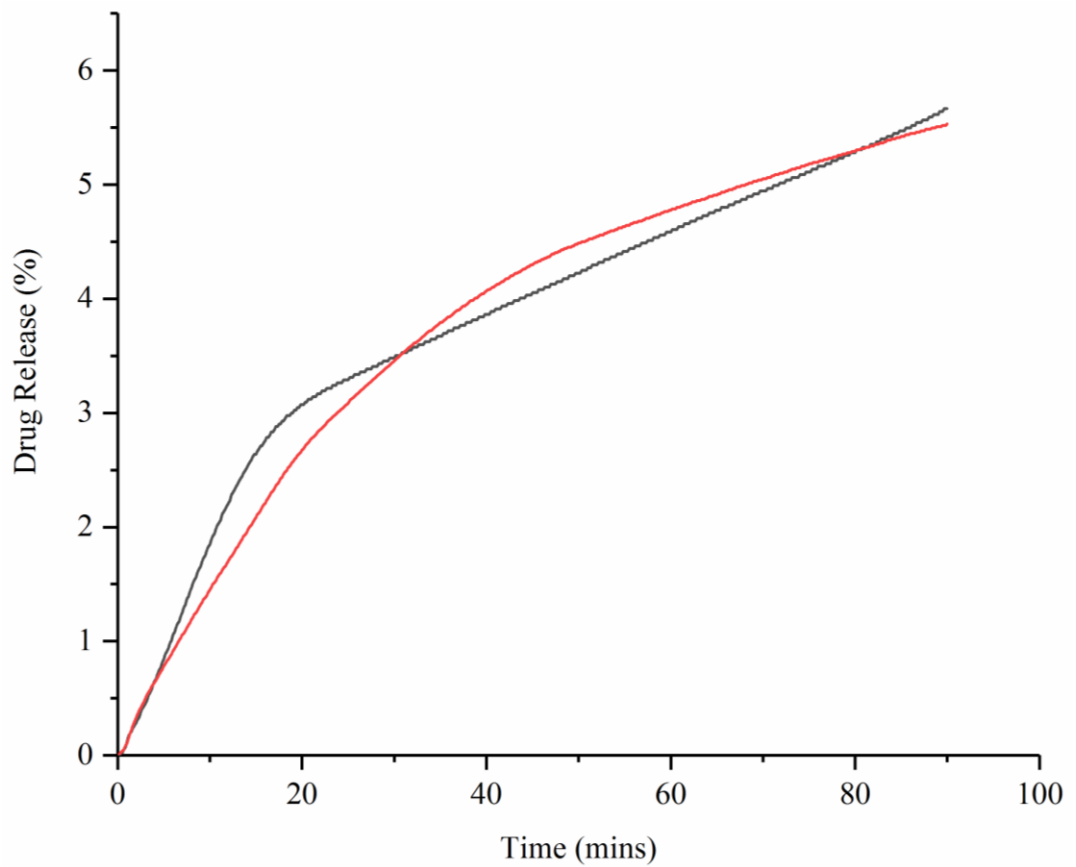


Figure 108: Drug release from encapsulated prototype pulsatile dosage forms consisting of 3.5 layer 1:4 ibuprofen:PVP layers to 2.5 1.4mm layer PVP buffer layers (black) and 3.10 layer 1:4 ibuprofen:PVP layers to 2.10 1.4mm layer PVP buffer layers (red), where $n=1$.

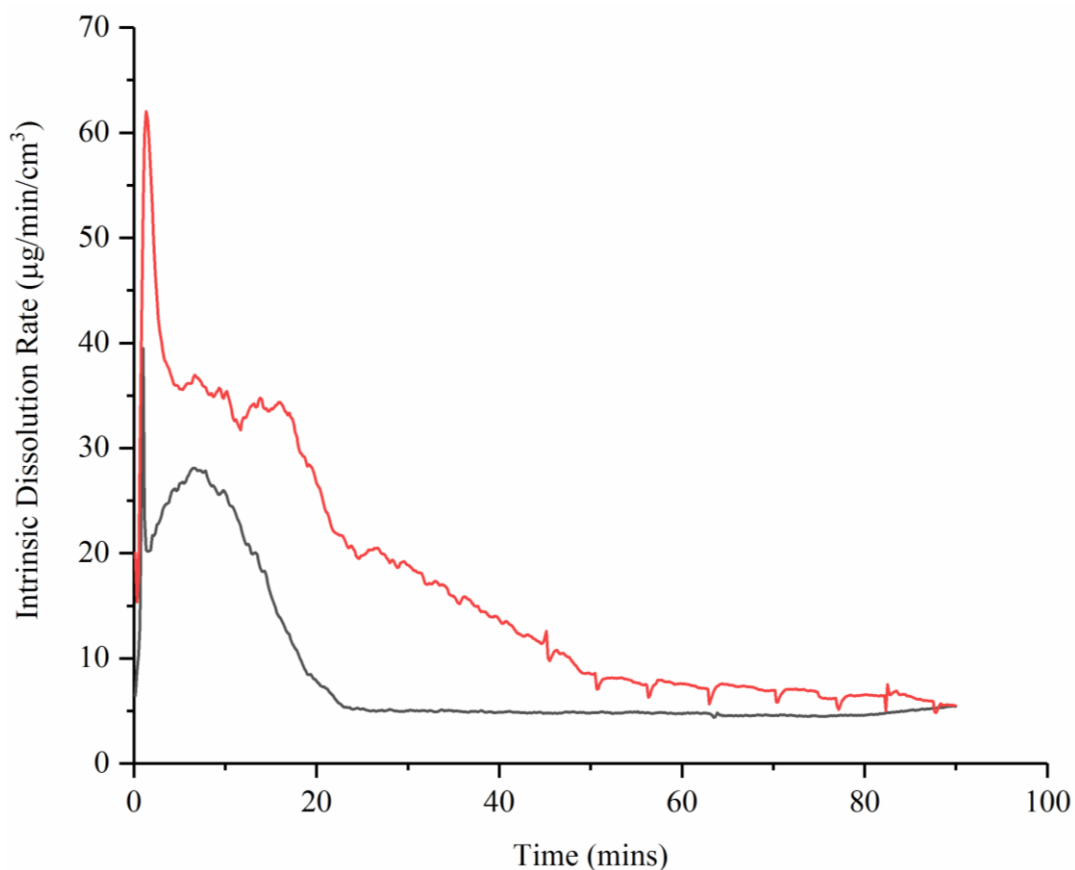


Figure 109: Intrinsic dissolution rate from encapsulated prototype pulsatile dosage forms consisting of 3 5 layer 1:4 ibuprofen:PVP layers to 2 5 1.4mm layer PVP buffer layers (black) and 3 10 layer 1:4 ibuprofen:PVP layers to 2 10 1.4mm layer PVP buffer layers (red), where n=1.

6.3.2 Full-Size Tablet

6.3.2.1 Nano CT

Nano CT allows identification of the drug containing areas of the tablet as described in Table 28. Unfortunately, the rice paper was unable to be detached from the tablet as ibuprofen and PVP seemed to have a much greater adhesive quality and resisted delamination. However, as it is fairly distinct in all images it does not have a detrimental effect on the data quality. Initially looking at the outer surface of the tablet (Figure 110), there is evidence of the printed layers with the definition being particularly clear on stripping back the image. There is some evidence of the effect

of spraying using a jet with a ghosting effect around the exterior of the tablet which supports some of the images seen previously in 3D Raman work (Chapter 3).

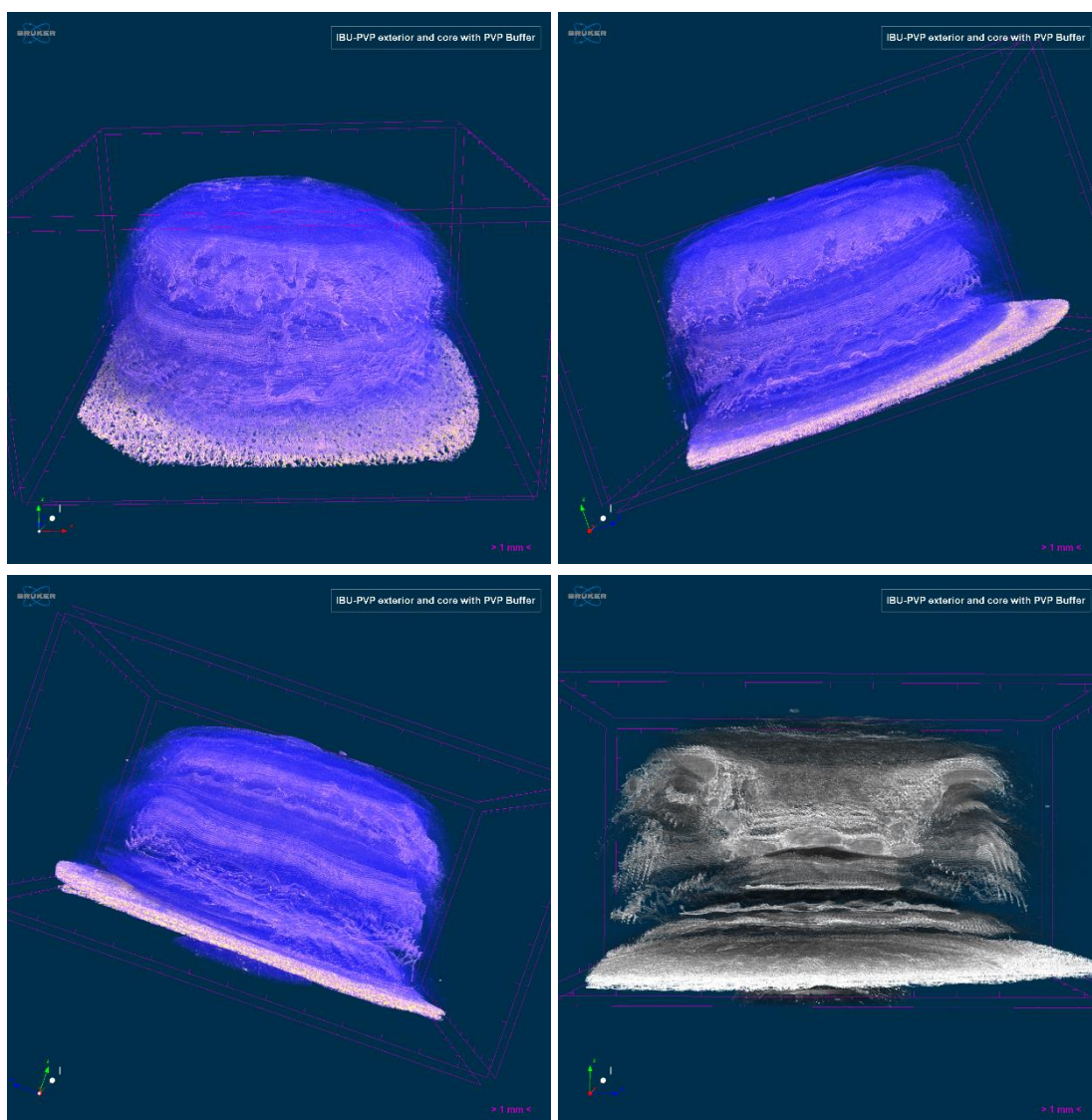


Figure 110: Nano CT image of the full size ibuprofen (purple) and PVP K30 (blue) tablet at different angles and stripped back in black and white.

Figures 111 and 112 show slices through the tablet horizontally, looking down from above. The rings of drug containing layer and polymer only can be clearly seen defined from the drug containing core. The porosity of the tablet can be observed with slightly ragged edges in Figure 111, but the distribution appears to be largely as expected supporting the previous TOF-SIMS and 3D Raman data (Chapter 3).

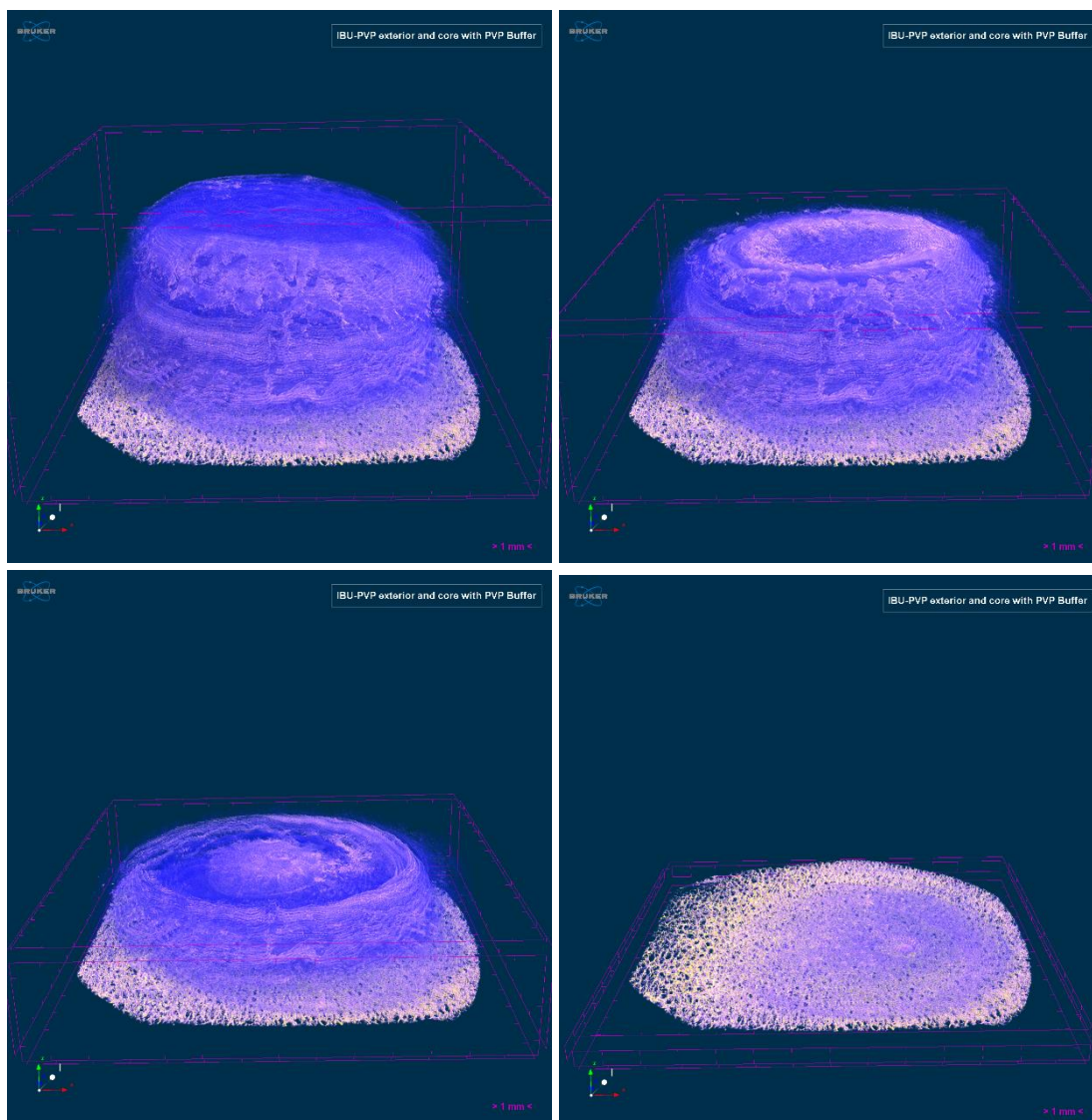


Figure 111: Nano CT image of the full size tablet sliced horizontally from above with the full tablet (top left) being sliced a third of the way down to show the start of the PVP buffer (top right), then another third to show the drug containing core (bottom left) and right down to the substrate (bottom right).

In Figure 112, it can be observed that the top layer shows an oil-like, marbled distribution of drug and polymer, with ragged edges. The mid-section shows evidence of porosity in the PVP layer, which may be due to agglomeration of the particles on drying or a potential printer issue. The lines made by the printer can be seen in this layer, as well as more ghosting from the spray of the printer. The bottom slice shows more

evidence of the printer lines, ghosting and potential coffee ring effects. The latter effect is something often observed in the literature (Yun, Kim, Lee, Cho, et al. 2009b, Yun, Kim, Lee, Yoo, et al. 2009, Singh et al. 2010, Scoutaris 2010, Fu et al. 2015, Sun et al. 2015, Talbot et al. 2015, Jabari and Toyserkani 2015, 2016, Seifert, Baum, et al. 2015, Seifert, Sowade, et al. 2015, Soleimani-Gorgani 2016, Jonathan and Karim 2016, Liu et al. 2016, Luan et al. 2016, Guo et al. 2017).

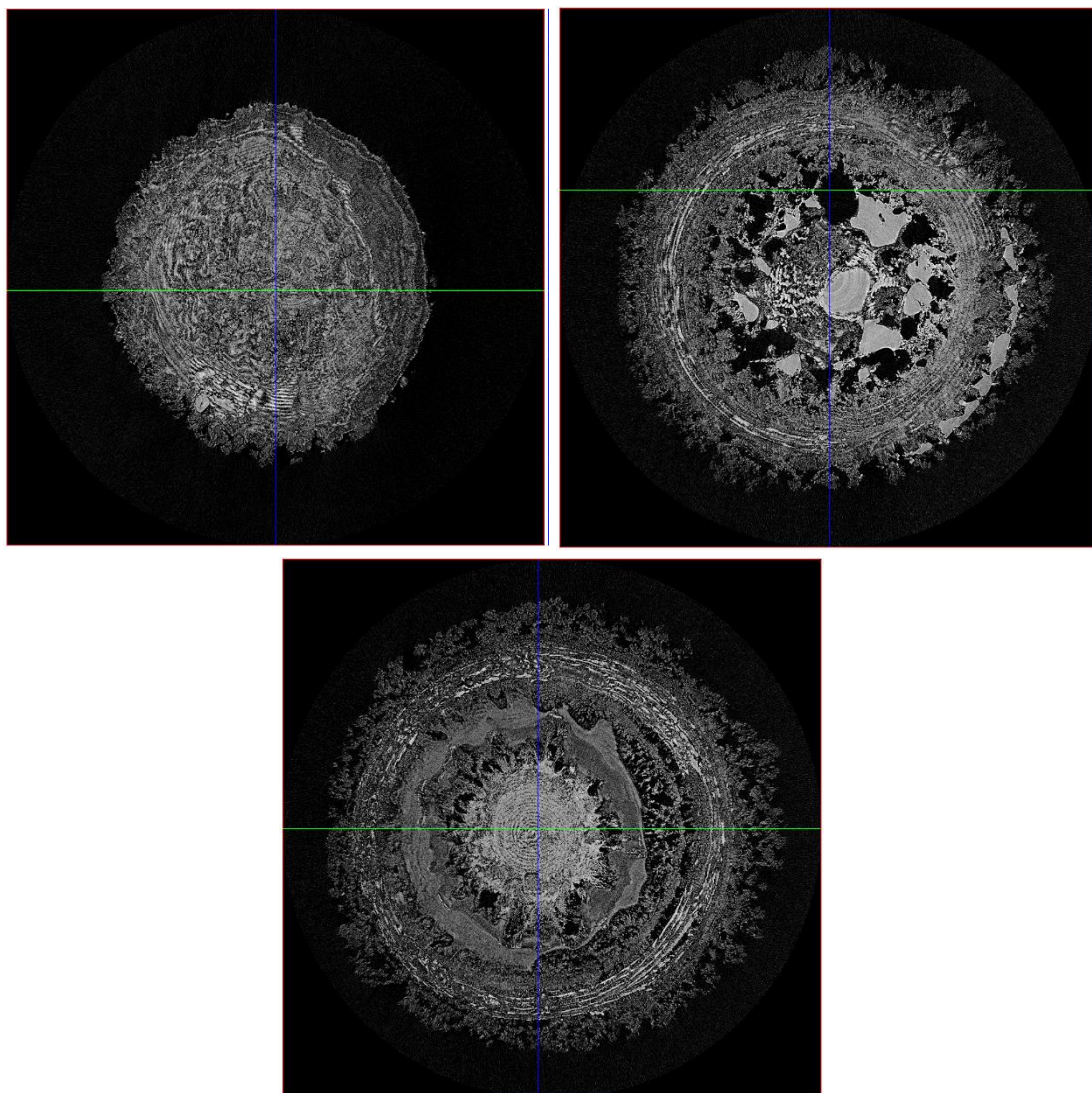


Figure 112: Nano CT image of the full size tablet sliced horizontally from above as 2D cutaway images of the tablet uncut (top left), a third removed (top right) and 2 thirds removed (bottom).

Figure 113 demonstrates the effect of slicing through the tablet horizontally, looking up from below. The first layer shows evidence of the rings of polymer alone and polymer and drug. There is some evidence of a slight shift and ghosting in the print which may be due to the dependence on a vacuum to hold the substrate in position. This was reinforced with Sellotape in the latter stages. The second slice shows the rings and the core more clearly and some evidence of spray ghosting. The third slice shows the core more closely. It appears off centre as the tablet was mounted on a pin and unfortunately was not completely straight. The fourth slice shows the top of the PVP layer and the fifth slice shows the beginning of the outer drug containing layer. These both exhibit an oily, porous appearance with ragged edges, which may be due to the spherical particles and agglomerates produced on printing in combination with the effect of spraying. Ultimately, the last image shows the top layer, which again shows a slight angle due to the mounting of the sample.

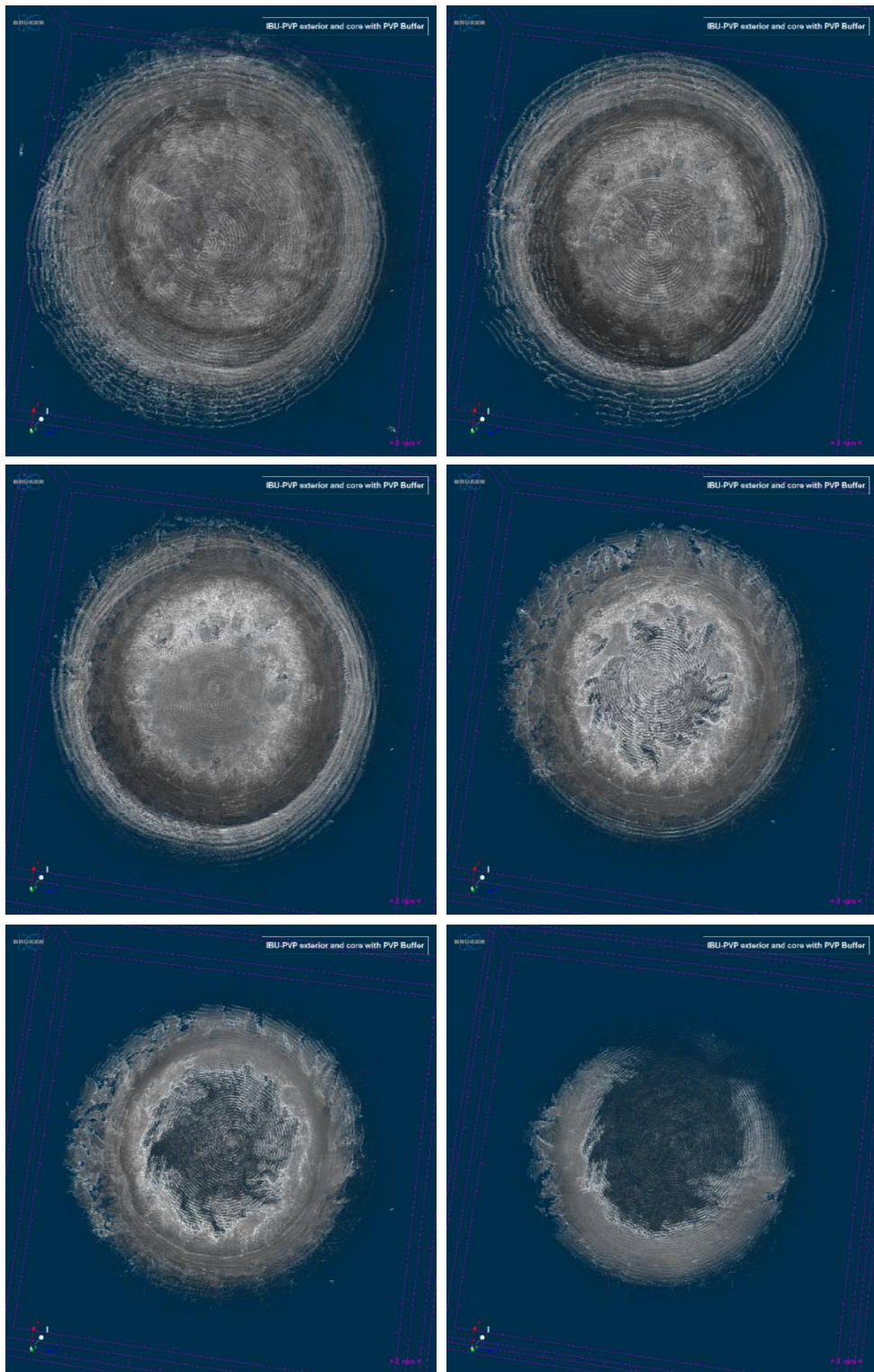


Figure 113: Nano CT image of the full size tablet sliced horizontally from below with the rice paper removed (top left), less than a quarter removed (top right), about half removed (middle left), about 3 quarters removed (middle right), about 7 eighths removed (bottom left) and nearly all removed (bottom right).

Figure 114 demonstrates the effect of slicing through the tablet vertically from 2 different angles. The initial tablet images (top left and middle right) consistently show the drug and polymer layers generated by the printer around the curved face of the tablet as seen in the previous figures. On the initial slice of both samples (top right and bottom left), the domed inner layers begin to appear with evidence of the layering becoming more prominent. On slicing further into the tablet (middle left and bottom right), the images exhibit an interesting effect. Due to the prolonged spray period and cone like nature of the jet there is a build-up of material in areas outwith the intended deposition. A U-shaped dip can be observed in both the drug containing layer and the polymer only layer which may be due to scattering of the buffer material more than intended causing a lip around the edge of the tablet.

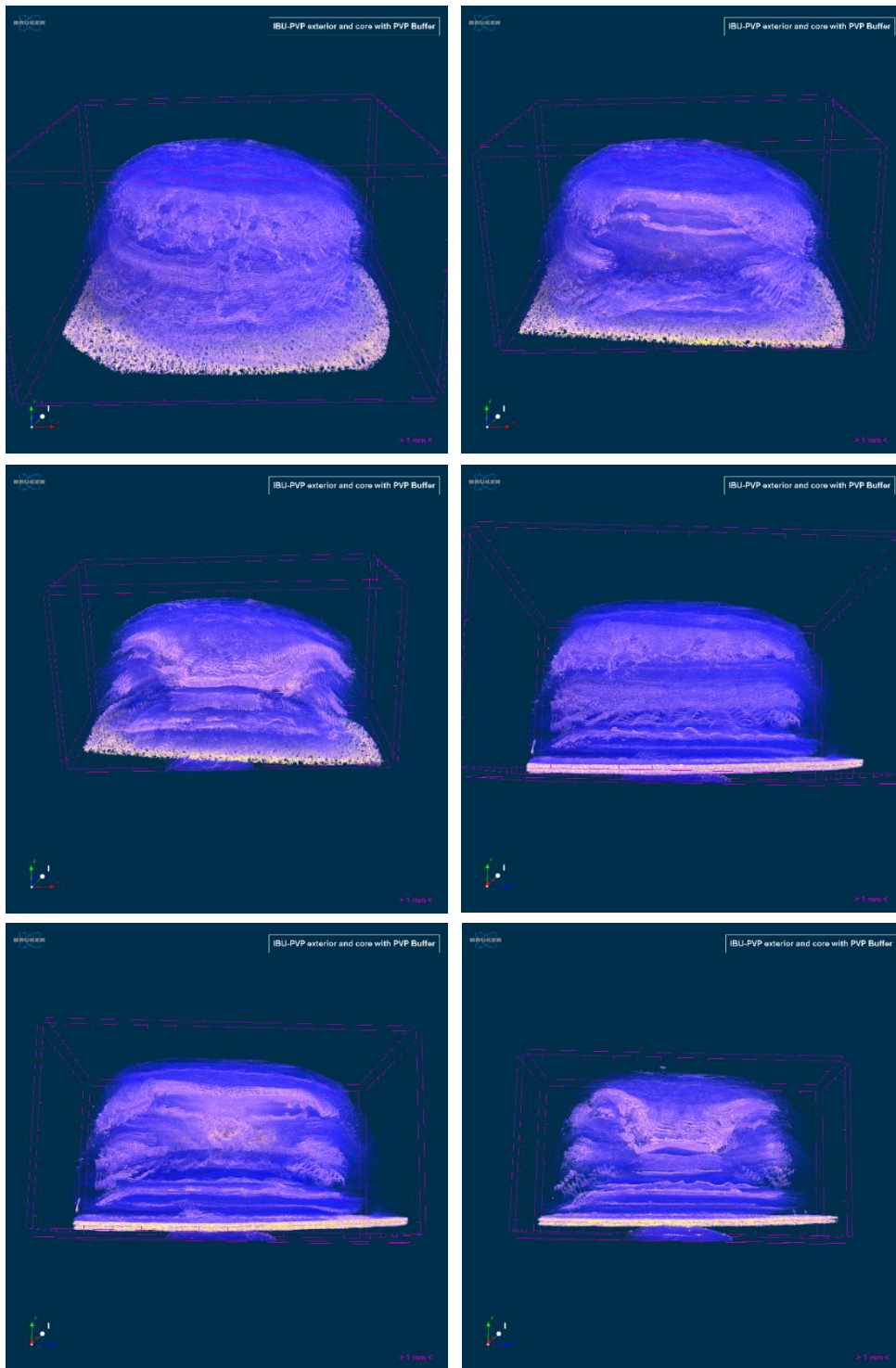


Figure 114: Nano CT image of the full size tablet sliced vertically gradually revealing the tablet core from two angles: angle 1: complete tablet (top left) and slice 1 (top right) and slice 2 (middle left), and angle 2: complete tablet (middle right), slice 1 (bottom left) and slice 2 (bottom right).

On comparison to the literature there is no prior evidence of examination of pulsatile or inkjet printed tablets using x-ray CT of any kind. However, there is prior evidence of analysis of tablets for the component density. For example microcrystalline cellulose tablets were analysed using x-ray CT this manner to demonstrate the effect of granulation and compression (Sinka et al. 2004, Busignies et al. 2006). Micro CT has been used previously to analyse coating thickness which supports the layering effect. For example Kollicoat IR, talc, titanium dioxide, and iron oxide red tablets coated with Walocel HM5 PA2910 and polyethylene glycol 1500 were analysed in this manner (Russe et al. 2012).

6.3.2.2 Drug Content

On UHPLC analysis, the estimated drug content of the tablet was found to be approximately 92mg as demonstrated in Table 29. The variation between samples is observed to be relatively low which is consistent with previous printing of ibuprofen samples (Table 22).

Table 29: Drug content of full size tablet components

Tablet Component	Average Drug Content (µg, n=3)	Standard Error (µg ±)	95% LCL	95% UCL
Outer Layer Torus (1 cm-7.3 mm) x1	205.69	23.2	90.42	320.96
Outer layer Top/Bottom (1 cm) x1	562.33	47.9	324.46	800.20
Core (4 mm) x1	113.8	13.2	48.09	179.55
Entire Tablet (50x layer core, 50x layer outer top, 50x layer outer bottom and 150x layer outer torus)	92777.89	N/A	N/A	N/A

6.3.2.3 Dissolution

Figure 115 demonstrates the drug release achieved from the full size tablet. It can be observed that the graph finishes after 2 minutes. This is as a result of the UV detector saturating and the IDIS software aborting as a result. Although this meant that a full dissolution run was unable to be analysed, evidence of the initial pulse can still be observed. The issue may have been that the overall concentration was too high to be measured using the flow cell set up. Therefore, any future studies would have to be either carried out in a USP II set up or the overall tablet size or layer thickness would have to be reduced to prevent UV saturation.

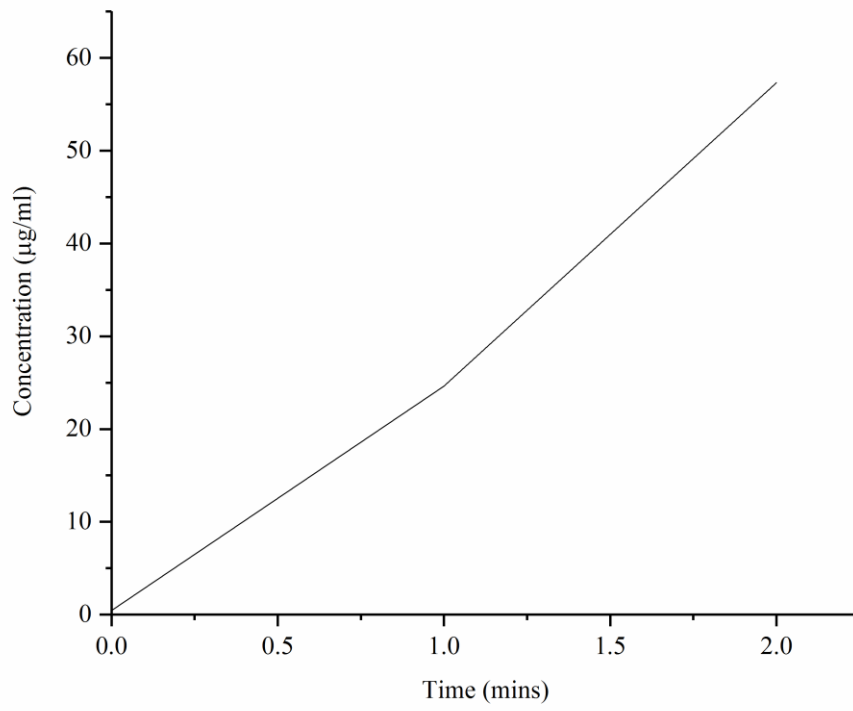


Figure 115: Drug release from a full size pulsatile ibuprofen and PVP prototype.

6.4 Conclusions

Initially samples were produced in a sandwich-style but media penetration resulted in loss of the second pulse, therefore a torus approach was employed and then ultimately a fully encapsulated approach enabling 2 pulses in 50 minutes to be achieved. Samples were modified by changing the core and buffer layers. On changing the buffer layer, it was found that the peaks became less defined and often the latter peak was lost. On changing the formulation to a 5:10 outer layers: core structure the pulses were found to come more quickly. On changing the formulation to a 10:20 outer layers: core structure the pulses were found to be less defined and a more matrix like dissolution rate was observed. On changing the layer number in pursuit of 3 pulses it was found the pulses became less defined suggesting the technology had reached its limits on the SDI.

On scale up, it was observed through the Nano CT images that the distinct areas of drug and polymer were retained. Rings of polymer and drug containing layers could be observed suggesting there is potential in scale up. However, the jet did begin to have ghosting and weight interfering effects as the prolonged print period continued which may limit the aerosol jet printer's use in this manner. The drug content was found to be relatively consistent on printing and thus relatively predictable. The sample was run on the USP IV but unfortunately the initial release pulse was found to be too large and thus the high concentration saturated the detector preventing further analysis.

Chapter 7: Conclusions, Challenges and Future Work

7.1 Conclusions

Aerosol jet printing has never been used in the field of pharmaceutical manufacturing previously. As such the capabilities of the printer for use in dosage form manufacture were initially tested. The printer exhibited a high degree of flexibility and precision as demonstrated by analysis of scalability and distribution. The printer proved itself capable of easily changing the dose of samples without changing the starting ink in a reproducible manner by changing the number of layers and size of deposition pattern utilised. Nozzle size may also be used but its reproducibility is limited slightly by the specifications of the manufacturer. Speed was also tested but failed to prove sufficiently linear and reproducible to be used as a viable method of scaling. Distribution was found to be controllable both in terms of the distribution throughout a solid dispersion and in terms of being able to produce distinct areas of drug and polymer.

Printing fenofibrate or ibuprofen alone resulted in a fully crystalline product. On addition of PVP the solid state changed dramatically. On printing fenofibrate with PVP the crystallinity was gradually reduced with polymer content until a fully amorphous product was formed at 75% or higher. By contrast, on printing ibuprofen with PVP the crystallinity was fully lost at 50% polymer content. Both drugs eventually formed spherical particles in a similar manner to spray drying. The particle formation is very much dictated by the droplets formed on atomisation which can be considered a function of the rheological properties which suggest the higher the polymer content the higher the viscosity and the larger the droplet. This also has an impact on the mass of drug detected with the polymer content dictating the ability to transverse the tubing and print head.

The formation of amorphous material has a considerable impact on dissolution and wettability. Dissolution increases considerably on comparison to physical mixtures in the same ratios as a result of greater control over the drug content and distribution. Additionally, the changes to particle morphology and solid state result in greater dissolution overall. With regards to fenofibrate, initially the dissolution and wettability increased in a gradual manner with PVP content until the amorphous particle formation. At this point the dissolution increased considerably and the wettability became very similar to that of PVP. With regards to ibuprofen, the wettability increases with the amorphous particle formation on addition of PVP and then remains relatively constant. As a result of this, the intrinsic dissolution rate is fairly constant, however the drug release is more of a function of the polymer content and the overall drug content.

Fenofibrate and PVP were also printed separately to observe the effect of polymer and drug interfaces. On analysis of samples by SEM and TOF-SIMS interfaces were observed and these are believed to result in a reduction in the overall crystallinity. As a result, the dissolution is improved but not as much as premixed formulations and not as reproducibly.

On development of the technology to generate pulsatile profiles the existing solid dispersions were utilised with PVP alone layers with a view to generating the characteristic lag-pulse profile. Fenofibrate proved inadvisable as the solubility became a rate limiting step as the media started to penetrate the dosage form washing away the PVP. Ibuprofen however proved much more effective with initial “sandwich-style” studies showing minute evidence of pulsing. By changing the manner of encasing the drug, the pulsing was refined to give up to two distinct pulses. Ultimately, it was possible to obtain an intrinsic dissolution rate profile rarely seen the literature previously. The two pulses effectively formed two distinct peaks within an hour. On scale up, it was possible to observe the tablet using nano CT. Samples demonstrated evidence of layering and of the distinct areas of drug and polymer suggesting scale up is possible. However, the prolonged period of printing did result

in more risk of ghosting and weight bearing issues. Additionally, dissolution studies using this tablet proved unsuccessful as the initial pulse was found to saturate the UV detector.

Overall it has been concluded that aerosol jet printing is a viable method of manufacturing dosage forms. It has allowed a higher degree of precision than seen previously, enabling scaling and control over the location of the drug within a dosage form. As such it has potential for either preparing low dose dosage forms for use in personalised medicine or paediatric treatments, or as part of a larger dosage form for example as an infill or coating technique. It has demonstrated an ability to produce dosage forms capable of increasing the dissolution of BCS Class II drugs in a manner akin to a miniaturised spray dryer with multiple drugs. Typically printing the drug alone results in a crystalline product but in the case of both drugs tested on the addition of sufficient polymer a wettable amorphous product was formed. Interestingly, for fenofibrate the dissolution was a function of PVP content until the amorphous product was formed, whereas for ibuprofen the PVP content proved more important after amorphous particle formation. The printer also has proven itself capable of generating more complex dosage forms with an intrinsic dissolution rate profile rarely seen previously. Scale up was found to be possible, however dissolution of the resultant tablet failed.

Thus, referring back to the research questions presented at the beginning of this thesis aerosol jet is capable of producing an oral dosage form which could at least supplement standard methods of tablet manufacturing. Additionally, this system could be used to increase control over drug and excipient location within a dosage form and thus could be used for personalised medicine or controlled release. Moreover, class II drugs can be effectively solubilised in this manner mostly by generating a solid dispersion through amorphous material formation.

7.2 Challenges

7.2.1 Limitations of the Instrument

7.2.1.1 Mechanical Limitations

The Optomec AJ200 unfortunately struggles with right-angled turns. However, it performs well on more obtuse angles such as those in hexagons and also performs well on circles, which in the context of pharma are the most applicable shapes. The closest thing to squares and rectangles can be achieved on application of fillet commands on AutoCAD so if necessary these shapes can be utilised without the presence of sharp angles.

Another major issue with the Optomec is that it has a single print head and a single pneumatic atomisation vessel and thus for production of controlled release formulations it is limited. Ideally it could be improved by adding an additional print head which could be interchanged with the existing one with ease and an additional vessel (Figure 116). The idea of a multiple nozzle print head is something that Optomec has patented for use in other types of printers so it is possible that the current one could be easily modified (King 2014).

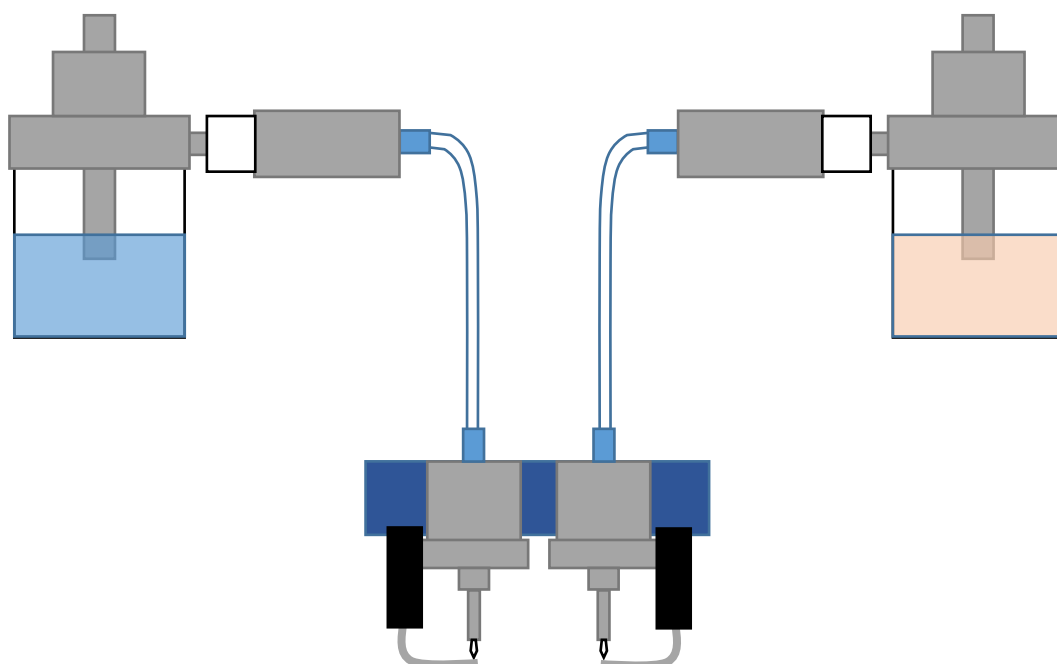


Figure 116: Theoretical design of a dual atomiser and print head system.

Additionally, the printer cannot be considered fully continuous. Currently the printer is continuous from drug and excipient mixing to product, but the mixer cannot be fed continuously limiting integration into the continuous line. This could be remedied by modifying the instrument to include a feeder. However, due to the need for complete nitrogen leak sealing of the instrument to allow sufficient pressure this would require the design of a feeder with valves which would prevent pressure loss.

7.2.1.2 Limitations of the Software

Another major limitation to integration into a continuous line is the fact that the Optomec AJ200 Inkjet 3D Printer is not fully automated. As this aerosol jet printer comes with the standard Optomec Aerosol Jet KEWA software provided by the company for use in constructing very fine metal components, it is not really designed for layering or more complex tablet designs. As such to achieve a layered formulation the operator must continuously restart the process. This has pros and cons. The pros are that it allows the operator to check for any issues with ink flow or pressure between layers. However, the printer is not able to be fully automated as a result of this and

thus requires full supervision which may be taxing to the operator. Additionally, if the formulation encompasses an infill element for delayed or pulsatile release, a minimum of 3 different CAD scripts are required rather than the normal single CAD script. Thus, improvements to this could involve development of a script to instruct the instrument to perform repeats and read more complex CAD outputs.

Furthermore, the instrument software has a flaw in that although the instrument has a risk of damage should the nitrogen pressure get too high, there is no means of cutting the gas flow automatically. The application of a script could allow control over the pressure by instructing the software to switch off the atomiser flow should the pressure exceed the normal ranges.

7.2.1.3 Instrument Blockages due to Precipitation

As the Optomec AJ200 was not designed for use in pharma there were a number of challenges associated with using APIs in the system. Pure fenofibrate was particularly difficult as due to its poor solubility and the volatile nature of ethanol, it had a tendency to precipitate out in the narrow orifices of the printer, most notably in the virtual impactor and the ceramic nozzle tips. Risk of crystallisation and precipitation within the lines and pneumatic atomisation vessel was also an issue, with larger particles increasing the chance of blockages. Attempts were made to reduce the risk of this by reducing the concentration of drug from 40 mg/ml to 30 mg/ml to keep the drug in solution. This still blocked the printer and thus the concentration was reduced further to 20 and then 10 mg/ml, however neither of these provided an advantage over 30 mg/ml. Thus, the higher concentration was retained as the benefits of drug loading outweighed the drawbacks of the need for more frequent sonication or multiple nozzle tips.

On application of pure polymer, it was found that PVP 10,000 and PVP K30 could be easily printed. However, the printer struggled with PVP K90 at 30 mg/ml and thus the concentration had to be reduced by 3-fold to reduce the viscosity enough to allow

effective printing. On application of HPMC the printer struggled even further, even at a reduced concentration and thus this polymer was discounted from the current study. When fenofibrate and PVP K30 were premixed it was found that deposition was considerably easier to achieve than pure drug as the polymer enabled better flow and reduced the overall risk of precipitation. Additionally, keeping the ink for a maximum of 3 days, cleaning the print head with a needle and changing the tubing regularly seemed to improve flow overall. Interestingly ibuprofen did not as readily block the printer which may be due to the slightly higher solubility possessed by this compound.

Additionally, the printer has a tendency to block at the print head as a result of build-up of material in the shutter. The printer has a continuous flow but in order to allow generation of patterns the flow must be controlled by a shutter head. This shutter head however is not self-cleaning as previous work with the printer has not required such viscous substances or such considerable volumes. As such the shutter can cause issues such as spray and blocking. The addition of a vacuum to remove excess ink could be easily achieved as the stage already has one. This would enable less blockage and less risk of contamination.

7.2.2 Challenges due to the Nature of the Manufacturing Technique

As inkjet printing requires some form of substrate, a number of issues were encountered in analysis. For XRD, initial samples were printed on standard printer paper and Kapton film. Printer paper was found to result in extra peaks which are believed to be due to the cellulose content (Foner and Adan 1983). Although the Kapton film gave a better signal than printer paper, on comparison to rice paper the latter was found to produce more prominent API crystalline peaks overall. From this point on in the study, printing was to be carried out on rice paper and then the rice paper was subtracted using the diffraction software. UHPLC was also carried out on rice paper as it was found with sufficient sonication and filtration the rice paper had no detrimental effect. Due to the risk of signal disruption, DSC and SEM were carried

out by printing directly on to the pans and plates utilised. Additionally, TOF-SIMS was printed directly on to silica to avoid signal disruption or surface effects.

Dissolution was perhaps the most challenging as due to the relatively small mass of drug and overall surface area utilised initially. Thus, the Sirius SDI, which is conventionally used to test surface dissolution of powder and granular systems, was utilised (Ward et al. 2017). However, the depth of the standard sample cups meant the time taken to produce individual samples was too long. As such modified sample cups were made initially by 3D printing plastic insets which could be glued in position within the existing sample cups. Unfortunately, the plastic could not withstand the solvents required to clean the drug from the sample cups. Thus, plastic purpose made cups capable of withstanding solvent use were procured from Paraytec Ltd. The SDI itself also proved challenging because the presence of a single bubble in the media could completely ruin the UV absorbance recorded. However, it was established that heating the media to 37°C prior to addition to the instrument and insulating the syringe with aluminium foil seemed to prevent bubbles. This has been observed previously in other SDI studies (Madelung et al. 2017).

Samples exhibited varying degrees of fragility. Pure PVP samples were only stable up to a concentration of 60 mg/ml and as such some samples were lost to cracking and delamination. Some of the 1:3 and 1:4 fenofibrate:PVP samples suffered a similar fate but it was found the larger the area printed and the thicker the sample, the more stable they were. The effect of cracking and delamination has been observed in a number of studies previously (Podczeck et al. 2006, Podczeck and Al-Muti 2010, Podczeck 2011, Choi et al. 2014, Papós et al. 2015, Demiri et al. 2018). Samples would have to be protected in the packaging stage primarily however other excipients may need to be added to increase stability as it was occasionally found that samples cracked during production too. Transport to Macclesfield and New Jersey proved challenging as a result of the fragility and required heat sealing in foil/polymer bags.

Interestingly the presence of the drug in the formulation seemed to result in more robust samples relative to the polymer alone as 30 mg/ml fenofibrate to 120 mg/ml PVP K30 resulted in a relatively strong formulation compared to 120 mg/ml PVP K30 alone which was found to be highly prone to cracking. This plasticizing effect has been observed in a number of studies previously and as such could be cultivated to improve stability (Forster, Hempenstall, and Rades 2001, Huang et al. 2006, Li et al. 2014, Wiranidchamong et al. 2015).

7.2.3 Challenges Arising from the Drugs Utilised

7.2.3.1 Issues of Content Uniformity

Initially the content detected within the fenofibrate samples was observed to be very irregular and thus it was thought to be an issue with the printer. There was better dissolution in the samples containing polymer with increasing content of polymer correlating with higher drug concentrations detected. Thus, it was concluded the drug may be failing to dissolve fully in the solvent. It was established latterly this was due to a failure for the rice paper to fully release the drug, as sonication seemed to achieve better content uniformity, and thus this would need to be considered if rice paper was incorporated into future formulations.

Some formulations continued to have some issues with content uniformity latterly, however it is believed this is due to the differences in morphology exhibited on the SEM, and thus differences in the manner in which they transverse the tubing, virtual impactor and print head. For example, 2:1 fenofibrate:PVP ink was found to result in larger plate-like particles and 2:3 fenofibrate:PVP ink was found to result in bigger agglomerates, both of which caused varying mass, while 1:1, 1:2, 1:3 and 1:4 had smaller, smoother, more uniform particles overall. The dosage forms with lower polymer content interestingly resulted in smoother tablets which it is believed may be due to the manner in which the drug and polymer interacted as the polymer appeared to coat the flatter drug particles allowing them to bind more closely at lower concentrations, rather than forming more porous formulations when the particles were

spherical. Ibuprofen proved to be much more reproducible overall which may be due to the more constant morphology of the particles.

7.2.3.2 UHPLC Method Choice

Initially the BP HPLC method using 70:30 acetonitrile:acidified water mobile phase and sample dissolution media was employed (British Pharmacopoeia Commission, 2018). However, this proved to result in incorrect readings, low retention times, some potential degradation and similar retention times for both the drug and its potential degradation product. This may be due to the BP method being designed for a standard HPLC rather than a UHPLC (Elkady et al. 2017, 2017). Thus, method testing was carried out to test for the effect of temperature, flow rate, gradient testing, altering the mobile phase ratio and the use of acetonitrile alone for sample preparation. The primary objectives of this were to achieve longer retention times, distinct peaks for the drug and the metabolite, linear calibration curves and minimal noise interference on the baseline. Flow rate and temperature appeared to have no effect on the calibration curve relative to the original method. Dissolving in acetonitrile alone for these samples and the original method seemed to result in a more linear calibration curve. There was noise observed in the baseline of these samples. However, on application of an 80:20 acetonitrile:acidified water mobile phase minimal noisiness was observed, single peaks were observed and an r-squared value of 1 was observed for both the samples dissolved in mobile phase and those dissolved in acetonitrile. Likewise, an r-squared value of 1 was observed for the gradient samples, however these were all very noisy in nature, which may be attributed to the initial exposure to 70% acidified water potentially causing degradation to the samples. As such the 80:20 method was selected. For ibuprofen it was found that a very similar method could be used on consulting the literature (Caviglioli et al. 2002, Farrar et al. 2002). On running tests on 80:20, 70:30 and 60:40 acetonitrile:acidified water, 60:40 was found to have the least noisy baseline and a clean peak distinct from any solvent fronts.

7.2.3.3 Molar Extinction Coefficient

Determination of the molar extinction coefficient proved challenging as fenofibrate is so poorly soluble with an aqueous solubility of 0.000707 mg/ml as reported on Drugbank (Drugbank, 2018). Calibration samples were initially attempted in SIF with PVP present, this proved unsuccessful, then in a mix of methanol and SIF, which also proved unsuccessful. Then samples were prepared by generating a stock solution in methanol and diluting with SIF but this resulted in a very low value being obtained from the SDI and it is believed this may be why fenofibrate has never been used in this technology previously. Then polymer was added to the standards but even then, all standards exhibited some precipitation resulting in an unreliable set of MEC values. It was also considered to use data from other Sirius equipment such as the T3 but as fenofibrate is non-ionisable this proved inadvisable as this technique is very pH dependent. After consulting the literature (Dhabale and Gharge 2010, Gupta et al. 2010, Kondawar et al. 2011, Sevda et al. 2011, Mandwal et al. 2012, Hirave et al. 2013), the decision was made to use methanol to generate an initial stock solution and then this was diluted using SIF to ensure the calibration standards were as close as possible to the test media. However, the drug was still precipitating out so the content was increased to 10% in the diluted samples by adding the stock and then making the volume up to 10% with methanol before diluting with SIF. Ibuprofen was more soluble overall as demonstrated by an experimental solubility of 0.021 mg/ml on Drugbank (Drugbank, 2018). Although dissolving in pure SIF proved inadvisable, the use of a methanol stock and an SIF only diluent proved effective. This allowed more accurate determination of the molar extinction coefficient than fenofibrate as less than 1% methanol was required in this case.

7.2.3.4 Pulsatile

Initial attempts at pulsatile work featured fenofibrate as this was the original candidate drug but it was found that fenofibrate failed to pulse effectively out of a formulation. This is thought to be due to a combination of the relatively low solubility of the drug even in the solid dispersion, the porosity of the PVP and the flow cell design of the SDI. It is thought, based on the contact angle, what is likely to have happened is that

the SIF has penetrated the solid dispersion washing away much of the PVP and then the fenofibrate has precipitated out in the aqueous solution. Fenofibrate was then replaced by ibuprofen as due to its ionisable nature this drug performed far better in SIF than fenofibrate overall, despite its BCS Class II properties.

7.3 Future Work

7.3.1 Alterations to the method

As the aerosol jet has never been used in pharmaceutical manufacturing prior to the current study, the possibilities of future work are infinite. For example, the process could be tested using different drugs, solvents and polymers to examine the effect of each on the crystalline properties of the dosage form generated. The effect of printing film forming polymers previously used in spin coating or inkjet printing would be particularly interesting. As the study features both neutral and acidic BCS Class II compounds, it would be fitting to also analyse a basic compound such as carvedilol and compare the effects on dissolution. Additionally, it would be interesting to see how the instrument performs using other inks such as lipid-based inks and nanoparticulate inks. The latter would be particularly interesting as the aerosol jet has previously been used to deliver silver nanoparticulate ink and as such may be able to deliver drug nanoparticles without damaging them (Salary et al. 2016, Agarwala et al. 2017). It would also be interesting to see what the implications of the addition of other excipients such as disintegrants are on the ink generated, the particles produced and the resultant dissolution. Furthermore, this study has primarily focused on the use of circles to generate dosage forms but the printer is capable of creating other non-square shapes such as hexagons so theoretically the drug release could be modified using different shapes within the dosage form as demonstrated in previous inkjet printing papers (Kyobula et al. 2009, 2017, Yun, Kim, Lee, Yoo, et al. 2009).

One major requirement of future work is the use of on-line and in-line monitoring. This monitoring could be employed in two places in the study, at the initial manufacturing stage and at the flow cell dissolution stage. The printing process

ideally would be monitored at the jetting stage and initial atomisation. Previous aerosol jet printing studies have used cameras and shape from shading image analysis to collect data of silver ink lines (Salary et al. 2016, 2017). Optomec KEWA also has a built-in imaging system to observe printed samples on the stage but this was designed for metal inks and is dependent on their inherent colour and shiny nature. Thus, unfortunately pharmaceutical materials, which are largely white or colourless and matte in nature, cannot be seen effectively using this software. Ideally an infrared camera or a Raman probe would be required due to the size and particulate nature of the printed samples. Within the instrument itself, it may be more difficult to integrate PAT as the whole instrument is sealed to prevent nitrogen pressure drop. Although it is possible to attach a probe to the atomisation vessel to measure temperature it is merely a millimetre in diameter and thus considerably thinner than most PAT probes. Ideally NIR and Raman could be used in combination to analyse distribution and polymorphic state but locating a probe small enough may be problematic so changes to the design of the atomisation lid may be required to accommodate this (De Beer et al. 2011, Saerens et al. 2011, Vanarase et al. 2013). In terms of monitoring the dissolution, the SDI already contains on-line monitoring in the form of an integrated UV spectrometer, but this only allows detection of drug content and distribution. Due to the poorly soluble nature of the drugs used in the current study in-line monitoring of the polymorphic state is required, which may be conducted by use of a Raman probe (Østergaard, Wu, et al. 2014). Due to time constraints this unfortunately was not attempted in the current study.

In terms of progressing the work into scale up, a number of approaches could be taken to avoid the UV saturation issues. The overall dose of the tablet could be reduced by decreasing the deposition area or decreasing the drug content of the drug layers' starting ink. The former option may be preferable as this would reduce the overall manufacturing time, enabling more rapid production of multiple tablets. Additionally, the USP IV could be replaced with a standard USP II method decreasing the maximum concentration available and reducing the chance of saturating the UV detector.

7.3.2 Applications

The high precision nature of the technology has a number of potential uses. For example, it could be used to create a range of release profiles. Immediate and

sustained release layers may be delivered in this manner as shown previously in direct compression studies with immediate release lactose and nystatin and sustained release carbomer, HPMC and nystatin (Llabot et al. 2002). The ability to print distinct areas also means drugs and excipients with different properties could be used in conjunction within the same dosage form. For example, chemically incompatible drugs could be formulated together with a barrier layer, using two APIs or two layers of the same API with different release profiles, reduced dosing frequency and increased efficacy of the drugs via a synergistic effect (Abebe et al. 2014).

The scalable nature of the technology also has a number of potential uses. The primary use would be as a personalised medicine mechanism. Patients vary considerably in terms of their dose requirements as individuals can be different ages, genders, races and weights. Additionally, patients can have different levels of drug resistance which reduces the efficacy of the drug. It has also been demonstrated previously that the dose requirements of patients can vary by as much as 50-fold depending on how quickly and efficiently the body metabolises the API (Xie and Frueh 2005). Scaling is particularly applicable for use in paediatrics and elderly patients. The dose required for the former is so variable, is generally determined by weight and is often only a fraction of the adult dose. The latter group often requires a “cocktail” of drugs so dosing is even more important to avoid adverse effects.

The pulsatile systems could also be developed to match the requirements of particular drugs and disease states. For example, pH sensitive layers could be included to ensure release in the correct area of the gastrointestinal tract for the most efficient absorption (Blatnik et al. 2015). Here too, there is also the possibility of multiple configurations such as incorporating different release rate profiles within the same dosage form (Llabot et al. 2002, Malewar et al. 2015). Rowe demonstrated the ability for different regions of a printed sample to be utilised to generate different release profiles with pulsatile, immediate and extended release demonstrated in combinations. This was 3D printing but there is potential to do this on a higher precision level. (Rowe et al. 2000).

Additionally, the aerosol jet technology could be used in conjunction with other techniques to produce dosage forms. For example, it could be used to print an immediate release layer on the outer surface of a tablet for a burst release before a sustained release. Alternatively, it could be used as an infill technique to fill 3D printed tablets with a hollow core to either generate a different release profile within an outer matrix system (Marizza et al. 2013, Solanki et al. 2018, Verstraete et al. 2018). Additionally, this infill could be used as a means of generating a system for weaning patients off addictive drugs as the outer 3D printed tablet could even be a placebo.

Ultimately, the use of the instrument need not be limited to oral solid dosage forms. For example, previous research into inkjet printing has featured production of several different types of dosage forms. Previous research has included production of transdermal drug delivery systems such as microneedles and patches (Ross et al. 2015, Uddin et al. 2015, Xie et al. 2015, Economidou et al. 2018), implants (Mau et al. 2016, Scoutaris, Chai, et al. 2016, Scoutaris, Ross, et al. 2016) and hydrogels (Pataky et al. 2012, Wei et al. 2015, Nakagawa et al. 2017). Therefore, aerosol jet printing could potentially be developed as a method for producing patches, implants, stent coatings and ocular hydrogel based delivery systems.

References

- Aakeröy, C. B., Grommet, A. B., and Desper, J., 2011. Co-crystal screening of diclofenac. *Pharmaceutics*, 3 (3), 601–614.
- Abebe, A., Akseli, I., Sprockel, O., Kottala, N., and Cuitiño, A. M., 2014. Review of bilayer tablet technology. *International Journal of Pharmaceutics*, 461 (1–2), 549–558.
- Abt, M., Roch, A., Qayyum, J. A., Pestotnik, S., Stepien, L., Abu-Ageel, A., Wright, B., Ulusoy, A. C., Albrecht, J., Harle, L., Papapolymerou, J., and Schuelke, T., 2018. Aerosol printed highly conductive Ag transmission lines for flexible electronic devices. *IEEE Transactions on Components, Packaging and Manufacturing Technology*, 8 (10), 1838–1844.
- Acosta-Vélez, G. F., Zhu, T. Z., Linsley, C. S., and Wu, B. M., 2018. Photocurable poly(ethylene glycol) as a bioink for the inkjet 3D pharming of hydrophobic drugs. *International Journal of Pharmaceutics* [online], 546 (1–2), 145–153. Available from: <https://doi.org/10.1016/j.ijpharm.2018.04.056>.
- Agarwala, S., Goh, G. L., and Yeong, W. Y., 2017. Optimizing aerosol jet printing process of silver ink for printed electronics. *IOP Conference Series: Materials Science and Engineering*, 191 (1).
- Agarwala, S., Goh, G. L., and Yeong, W. Y., 2018. Aerosol Jet Printed Strain Sensor: Simulation Studies Analyzing the Effect of Dimension and Design on Performance (September 2018). *IEEE Access* [online], 6, 1–1. Available from: <https://ieeexplore.ieee.org/document/8496770/>.
- Agnihotri, S. A., Mallikarjuna, N. N., and Aminabhavi, T. M., 2004. Recent advances on chitosan-based micro- and nanoparticles in drug delivery. *Journal of Controlled Release* [online], 100 (1), 5–28. Available from: <http://linkinghub.elsevier.com/retrieve/pii/S0168365904003803>.
- Akagi, T., Fujiwara, T., and Akashi, M., 2014. Inkjet printing of layer-by-layer assembled poly(lactide) stereocomplex with encapsulated proteins. *Langmuir*,

30 (6), 1669–1676.

- Al-Hilal, T. a, Alam, F., and Byun, Y., 2013. Oral drug delivery systems using chemical conjugates or physical complexes. *Advanced drug delivery reviews* [online], 65 (6), 845–64. Available from: <http://www.ncbi.nlm.nih.gov/pubmed/23220326> [Accessed 6 Oct 2014].
- Al-Saidan, S. M., Krishnaiah, Y. S. R., Satyanarayana, V., Bhaskar, P., and Karthikeyan, R. S., 2004. Pharmacokinetic evaluation of guar gum-based three-layer matrix tablets for oral controlled delivery of highly soluble metoprolol tartrate as a model drug. *European Journal of Pharmaceutics and Biopharmaceutics*, 58 (3), 697–703.
- Alexy, P., Lacík, I., Šimková, B., Bakoš, D., Prónayová, N., Liptaj, T., Hanzelová, S., and Várošová, M., 2004. Effect of melt processing on thermo-mechanical degradation of poly(vinyl alcohol)s. *Polymer Degradation and Stability*, 85 (2), 823–830.
- Alomari, M., Mohamed, F. H., Basit, A. W., and Gaisford, S., 2015. Personalised dosing: Printing a dose of one's own medicine. *International Journal of Pharmaceutics* [online], 494 (2), 568–577. Available from: <http://dx.doi.org/10.1016/j.ijpharm.2014.12.006>.
- Alomari, M., Vuddanda, P. R., Trenfield, S. J., Dodoo, C. C., Velaga, S., Basit, A. W., and Gaisford, S., 2018. Inkjet Printing of T 3 and T 4 Oral Drug Combinations as a Novel Strategy for Hypothyroidism. *International Journal of Pharmaceutics* [online]. Available from: <https://doi.org/10.1016/j.ijpharm.2018.07.062>.
- Amidon, G. L., Lennernäs, H., Shah, V. P., and Crison, J. R., 1995. A Theoretical Basis for a Biopharmaceutic Drug Classification: The Correlation of in Vitro Drug Product Dissolution and in Vivo Bioavailability. *Pharmaceutical Research: An Official Journal of the American Association of Pharmaceutical Scientists*.
- Andrews, G. P., 2007. Advances in solid dosage form manufacturing technology. *Philosophical transactions. Series A, Mathematical, physical, and engineering*

sciences [online], 365 (1861), 2935–49. Available from:
<http://www.ncbi.nlm.nih.gov/pubmed/17855217> [Accessed 6 Nov 2014].

Arndt, U., Heinrich, T., Hinzpeter, J., Jacob, T., Luneburg, P., Stellmach, G., and Zeuschner, U., 2001. US2001/0046527A1: Tablet Rotary Compressing Press for the Manufacture of Multi-layered Tablets.

Atipamula S., Banerjee R., Bansal A.K., Biradha K., Cheney M.L., Choudhury A.R., Desiraju G.R., Dikundwar A.G., Dubey R., Duggirala N., Ghogale P.P., Ghosh S., Kumar Goswami P., Goud N.R., Jetty R.R.K.R., Karpinski P., Kaushik P., Kumar D., Kumar V., Moulton B., Mukherjee A., Mukherjee G., Myerson A.S., Puri V., Ramanan A., Rajamannar T., Reddy C.M., Rodriguez-Hornedo N., Rogers R.D, Guru Row N.T., Sanphui P., Shete N.S.G., Singh A., Sun C.C., Swift J.A., Thaimattam R., Thakur T.S., Thaper R.K., Thomas S.P., Tothadi S., Vangala V.R., Variankaval N., Vishweshwar P., Weyna D.R. and Zaworotko M.J., 2012, Polymorphs, Salts and Cocrystals: What's in a Name?, *Crystal Growth & Design*, 12(5):2147-2152

Baghel, S., Cathcart, H., and O'Reilly, N. J., 2016. Polymeric Amorphous Solid Dispersions: A Review of Amorphization, Crystallization, Stabilization, Solid-State Characterization, and Aqueous Solubilization of Biopharmaceutical Classification System Class II Drugs. *Journal of pharmaceutical sciences* [online]. Available from:
<http://www.sciencedirect.com/science/article/pii/S002235491500009X>.

Balint, G. a., 2001. Artemisinin and its derivatives: an important new class of antimalarial agents. *Pharmacology & Therapeutics* [online], 90 (2–3), 261–265. Available from:
<http://linkinghub.elsevier.com/retrieve/pii/S0163725801001401>.

Barui, S., Mandal, S., and Basu, B., 2017. ScienceDirect Thermal inkjet 3D powder printing of metals and alloys : Current status and challenges. *Current Opinion in Biomedical Engineering* [online], 2, 116–123. Available from:
<http://dx.doi.org/10.1016/j.cobme.2017.05.010>.

De Beer, T., Burggraeve, a., Fonteyne, M., Saerens, L., Remon, J. P., and Vervaet,

- C., 2011. Near infrared and Raman spectroscopy for the in-process monitoring of pharmaceutical production processes. *International Journal of Pharmaceutics* [online], 417 (1–2), 32–47. Available from: <http://dx.doi.org/10.1016/j.ijpharm.2010.12.012>.
- Bell, S. E. J., Dennis, A. C., Fido, L. A., Malcolm, R. K., Sirimuthu, N. M. S., Toner, C. F., and Woolfson, A. D., 2007. Characterization of silicone elastomer vaginal rings containing HIV microbicide TMC120 by Raman spectroscopy. *Journal of Pharmacy and Pharmacology* [online], 59 (2), 203–207. Available from: <http://doi.wiley.com/10.1211/jpp.59.2.0007>.
- Blagden, N., de Matas, M., Gavan, P. T., and York, P., 2007. Crystal engineering of active pharmaceutical ingredients to improve solubility and dissolution rates. *Advanced drug delivery reviews* [online], 59 (7), 617–30. Available from: <http://www.ncbi.nlm.nih.gov/pubmed/17597252> [Accessed 15 Nov 2013].
- Blatnik, S. U., Dreu, R., and Srčić, S., 2015. Influence of pH modifiers on the dissolution and stability of hydrochlorothiazide in the bi- and three-layer tablets. *Acta Pharmaceutica*, 65 (4), 383–397.
- Bou-Chacra, N., Melo, K. J. C., Morales, I. A. C., Stippler, E. S., Kesisoglou, F., Yazdani, M., and Löbenberg, R., 2017. Evolution of Choice of Solubility and Dissolution Media After Two Decades of Biopharmaceutical Classification System. *The AAPS Journal* [online], 19 (4), 989–1001. Available from: <http://link.springer.com/10.1208/s12248-017-0085-5>.
- Bouman, J., Belton, P., Venema, P., van der Linden, E., de Vries, R., and Qi, S., 2015. The Development of Direct Extrusion-Injection Moulded Zein Matrices as Novel Oral Controlled Drug Delivery Systems. *Pharmaceutical Research* [online], 32, 2775–2786. Available from: <http://link.springer.com/10.1007/s11095-015-1663-9>.
- British Pharmacopoeia Commission., British Pharmacopoeia 2018: Appendix XII: Recommendations on Dissolution Testing, London: TSO; 2018.
- British Pharmacopoeia Commission. British Pharmacopoeia 2018: Appendix XII C. Consistency of Formulated Preparations, London: TSO; 2018.

- Buanz, A. B. M., Saunders, M. H., Basit, A. W., and Gaisford, S., 2011. Preparation of personalized-dose salbutamol sulphate oral films with thermal ink-jet printing. *Pharmaceutical Research*, 28 (10), 2386–2392.
- Buch, P., Meyer, C., and Langguth, P., 2011. Improvement of the wettability and dissolution of fenofibrate compacts by plasma treatment. *International Journal of Pharmaceutics* [online], 416 (1), 49–54. Available from: <http://dx.doi.org/10.1016/j.ijpharm.2011.05.074>.
- Buckley, S. T., Frank, K. J., Fricker, G., and Brandl, M., 2013. Biopharmaceutical classification of poorly soluble drugs with respect to ‘enabling formulations’. *European journal of pharmaceutical sciences* [online], 50 (1), 8–16. Available from: <http://www.ncbi.nlm.nih.gov/pubmed/23583787> [Accessed 28 Oct 2014].
- Busignies, V., Leclerc, B., Porion, P., Evesque, P., Couarraze, G., and Tchoreloff, P., 2006. Quantitative measurements of localized density variations in cylindrical tablets using X-ray microtomography. *European Journal of Pharmaceutics and Biopharmaceutics*, 64 (1), 38–50.
- Bussemer, T., Dashevsky, a., and Bodmeier, R., 2003. A pulsatile drug delivery system based on rupturable coated hard gelatin capsules. *Journal of Controlled Release* [online], 93 (3), 331–339. Available from: <http://linkinghub.elsevier.com/retrieve/pii/S0168365903004085> [Accessed 1 Apr 2014].
- Calabrese, G. S. and Pissavini, S., 2011. Chemicals Manufacturing. *American Institute of Chemical Engineers*, 57 (4), 828–834.
- Caviglioli, G., Valeria, P., Brunella, P., Sergio, C., Attilia, A., and Gaetano, B., 2002. Identification of degradation products of Ibuprofen arising from oxidative and thermal treatments. *Journal of Pharmaceutical and Biomedical Analysis*, 30 (3), 499–509.
- Cervera-Padrell, A. E., Skovby, T., Kiil, S., Gani, R., and Gernaey, K. V., 2012. Active pharmaceutical ingredient (API) production involving continuous processes--a process system engineering (PSE)-assisted design framework. *European journal of pharmaceutics and biopharmaceutics* [online], 82 (2),

437–56. Available from: <http://www.ncbi.nlm.nih.gov/pubmed/22820647>
[Accessed 7 Nov 2014].

- Chachad, S. S., Gole, M., Malhotra, G., and Naidu, R., 2014. Comparison of Pharmacokinetics of Two Fenofibrate Tablet Formulations in Healthy Human Subjects. *Clinical Therapeutics* [online], 36 (6), 967–973. Available from: <http://linkinghub.elsevier.com/retrieve/pii/S014929181400215X>.
- Cheow, W. S., Kiew, T. Y., and Hadinoto, K., 2015. Combining inkjet printing and amorphous nanonization to prepare personalized dosage forms of poorly-soluble drugs. *European Journal of Pharmaceutics and Biopharmaceutics* [online], 96, 314–321. Available from: <http://linkinghub.elsevier.com/retrieve/pii/S0939641115003458>.
- Cho, K., Wang, X., Nie, S., Chen, Z. G., and Shin, D. M., 2008. Therapeutic nanoparticles for drug delivery in cancer. *Clinical cancer research : an official journal of the American Association for Cancer Research* [online], 14 (5), 1310–6. Available from: <http://www.ncbi.nlm.nih.gov/pubmed/18316549>.
- Choi, D. H., Kim, K. H., Park, J. S., Jeong, S. H., and Park, K., 2013. Evaluation of drug delivery profiles in geometric three-layered tablets with various mechanical properties, in vitro-in vivo drug release, and Raman imaging. *Journal of Controlled Release* [online], 172 (3), 763–772. Available from: <http://dx.doi.org/10.1016/j.jconrel.2013.08.301>.
- Choi, D. H., Lim, D. G., Son, H. M., and Jeong, S. H., 2014. Comprehensive evaluation of layer separation tendency of novel three-layered tablets with geometric and mechanical properties. *International Journal of Pharmaceutics* [online], 465 (1–2), 347–359. Available from: <http://dx.doi.org/10.1016/j.ijpharm.2014.02.014>.
- Choi, J. H., Lee, K., Hong, S., Lee, S. K., Oh, Y.-K., Choi, S. K., and Choi, H.-G., 2013. Effect of biocompatible polymers on the physicochemical and dissolution properties of fenofibrate in nanoparticle system. *Journal of Pharmaceutical Investigation* [online], 43 (6), 507–512. Available from: <http://link.springer.com/10.1007/s40005-013-0100-5>.

- Chuangchote, Surawut Sagawa, T. and Yoshikawa, S., 2009. Electrospinning of Poly(vinyl pyrrolidone): Effects of Solvents on Electrospinnability for the Fabrication of Poly(p-phenylene vinylene) and TiO₂ Nanofibers. *Journal of Applied Polymer Science*, 114, 2777–2791.
- Clark, E. A., Alexander, M. R., Irvine, D. J., Roberts, C. J., Wallace, M. J., Sharpe, S., Yoo, J., Hague, R. J. M., Tuck, C. J., and Wildman, R. D., 2017. 3D printing of tablets using inkjet with UV photoinitiation. *International Journal of Pharmaceutics* [online], 529 (1–2), 523–530. Available from: <http://dx.doi.org/10.1016/j.ijpharm.2017.06.085>.
- Clifford, B., Beynon, D., Phillips, C., and Deganello, D., 2018. Printed-Sensor-on-Chip devices – Aerosol jet deposition of thin film relative humidity sensors onto packaged integrated circuits. *Sensors and Actuators, B: Chemical* [online], 255, 1031–1038. Available from: <http://dx.doi.org/10.1016/j.snb.2017.08.086>.
- Daly, R., Harrington, T. S., Martin, G. D., and Hutchings, I. M., 2015. Inkjet printing for pharmaceuticals – A review of research and manufacturing. *International Journal of Pharmaceutics* [online], [Epub in a. Available from: <http://linkinghub.elsevier.com/retrieve/pii/S0378517315002331>.
- Dashevsky, A. and Mohamad, A., 2006. Development of pulsatile multiparticulate drug delivery system coated with aqueous dispersion Aquacoat ECD. *International journal of pharmaceutics* [online], 318 (1–2), 124–31. Available from: <http://www.ncbi.nlm.nih.gov/pubmed/16759827> [Accessed 6 Nov 2014].
- Deiner, L. J. and Reitz, T. L., 2017. Inkjet and Aerosol Jet Printing of Electrochemical Devices for Energy Conversion and Storage. *Advanced Engineering Materials*, 19 (7), 1–18.
- Demiri, V., Stranzinger, S., Rinner, P., Piller, M., Sacher, S., Lingitz, J., Khinast, J., and Salar-Behzadi, S., 2018. Gluing Pills Technology: A novel route to multilayer tablet manufacturing. *International Journal of Pharmaceutics* [online], 548 (1), 672–681. Available from: <https://doi.org/10.1016/j.ijpharm.2018.07.004>.
- Deng, H., Song, J., Elom, A. K., Xu, J., Fan, Z., Zheng, C., Xing, Y., and Deng, K.,

2016. Synthesis and Controlled Release Behavior of Biodegradable Polymers with Pendant Ibuprofen Group, 2016.

Dhabale, P. N. and Gharge, D. S., 2010. Simultaneous spectrophotometric estimation of atorvastatin and fenofibrate in bulk drug and dosage form by using simultaneous equation method. *International Journal of ChemTech Research*, 2 (1), 325–328.

Dressman, J. B. and Reppas, C., 2000. In vitro–in vivo correlations for lipophilic, poorly water-soluble drugs. *European Journal of Pharmaceutical Sciences* [online], 11 (S2), S73–S80. Available from: <http://linkinghub.elsevier.com/retrieve/pii/S0928098700001810>.

Drugbank, 2018, accessed September 2014 and January 2018, <<https://www.drugbank.ca/>

Eckstein, R., 2016. Aerosol Jet Printed Electronic Devices and Systems.

Eckstein, R., Hernandez-Sosa, G., Lemmer, U., and Mechau, N., 2014. Aerosol jet printed top grids for organic optoelectronic devices. *Organic Electronics: physics, materials, applications* [online], 15 (9), 2135–2140. Available from: <http://dx.doi.org/10.1016/j.orgel.2014.05.031>.

Economidou, S. N., Lamprou, D. A., and Douroumis, D., 2018. 3D printing applications for transdermal drug delivery. *International Journal of Pharmaceutics* [online], 544 (2), 415–424. Available from: <https://doi.org/10.1016/j.ijpharm.2018.01.031>.

Edinger, M., Bar-Shalom, D., Rantanen, J., and Genina, N., 2017. Visualization and Non-Destructive Quantification of Inkjet-Printed Pharmaceuticals on Different Substrates Using Raman Spectroscopy and Raman Chemical Imaging. *Pharmaceutical Research*, 34 (5), 1023–1036.

Elgart, A., Cherniakov, I., Aldouby, Y., Domb, A. J., and Hoffman, A., 2013. Improved oral bioavailability of BCS class 2 compounds by self nano-emulsifying drug delivery systems (SNEDDS): the underlying mechanisms for amiodarone and talinolol. *Pharmaceutical research* [online], 30 (12), 3029–44. Available from: <http://www.ncbi.nlm.nih.gov/pubmed/23686373> [Accessed 6

Nov 2014].

- Elkady, E. F., Tammam, M. H., and Abo Elmaaty, A., 2017. HPLC-UV vs. UPLC-DAD for Estimation of Tinidazole, Benzyl Alcohol and Hydrocortisone Acetate Simultaneously with Tioconazole and Its Related Impurities in Bulk and Pharmaceutical Formulations. *Analytical Chemistry Letters*, 7 (2), 153–169.
- Elmogi, A., Soenen, W., Ramon, H., Yin, X., Missinne, J., Spiga, S., Amann, M. C., Srinivasan, S. A., De Heyn, P., Van Campenhout, J., Bauwelinck, J., and Van Steenberge, G., 2018. Aerosol-Jet Printed Interconnects for 2.5D Electronic and Photonic Integration. *Journal of Lightwave Technology*, 36 (16), 3528–3533.
- Elzayat, E. M., Abdel-Rahman, A. A., Ahmed, S. M., Alanazi, F. K., Habib, W. A., Abou-Auda, H. S., and Sakr, A., 2017. Formulation and pharmacokinetics of multi-layered matrix tablets: Biphasic delivery of diclofenac. *Saudi Pharmaceutical Journal* [online], 25 (5), 688–695. Available from: <http://dx.doi.org/10.1016/j.jsps.2016.10.004>.
- Emami, J., 2006. In vitro - In vivo Correlation : From Theory to Applications. *Journal of Pharmacy and Pharmaceutical Sciences*, 9 (2), 31–51.
- Fabbiani, F. P. a and Pulham, C. R., 2006. High-pressure studies of pharmaceutical compounds and energetic materials. *Chemical Society reviews*, 35 (10), 932–942.
- Farrar, H., Letzig, L., and Gill, M., 2002. Validation of a liquid chromatographic method for the determination of ibuprofen in human plasma. *Journal of Chromatography B* [online], 780 (2), 341–348. Available from: <http://www.sciencedirect.com/science/article/B6X0P-46MT65H-1/2/11ee188d266edaac30d576a3798cbfa3>.
- Fauteux-lefebvre, C., Lavoie, F. B., Colbert, M., and Guay, J., 2018. Determining the Number of Components for Multivariate Curve Resolution : Case Study Using Raman Mapping of Pharmaceutical Tablets, 23 (Suppl 1), 2017–2018.
- Feng, J. Q., 2018. Mist Flow Visualization for Round Jets in Aerosol Jet ® Printing. *Aerosol Science and Technology* [online], 0 (0), 1–8. Available from: <https://arxiv.org/ftp/arxiv/papers/1805/1805.11015.pdf>.

- Fields, J. D., Pach, G., Horowitz, K. A. W., Stockert, T. R., Woodhouse, M., and van Hest, M. F. A. M., 2017. Printed interconnects for photovoltaic modules. *Solar Energy Materials and Solar Cells* [online], 159 (October 2016), 536–545. Available from: <http://dx.doi.org/10.1016/j.solmat.2016.09.024>.
- Filenkova, A., Acosta, E., Brodersen, P. M., Sodhi, R. N. S., and Farnood, R., 2011. Distribution of inkjet ink components via ToF-SIMS imaging, (February 2010), 576–581.
- Folgar, C. E., Suchicital, C., and Priya, S., 2011. Solution-based aerosol deposition process for synthesis of multilayer structures. *Materials Letters* [online], 65 (9), 1302–1307. Available from: <http://dx.doi.org/10.1016/j.matlet.2011.01.069>.
- Foner, H. A. and Adan, N., 1983. The Characterization of Papers by X-Ray Diffraction (XRD): Measurement of Cellulose Crystallinity and Determination of Mineral Composition. *Journal of the Forensic Science Society*, 23 (4), 313–321.
- Forster, A., Hempenstall, J., and Rades, T., 2001. Characterization of glass solutions of poorly water-soluble drugs produced by melt extrusion with hydrophilic amorphous polymers. *Journal of Pharmacy and Pharmacology* [online], 53 (3), 303–315. Available from: <http://doi.wiley.com/10.1211/0022357011775532>.
- Forster, A., Hempenstall, J., Tucker, I., and Rades, T., 2001. Selection of excipients for melt extrusion with two poorly water-soluble drugs by solubility parameter calculation and thermal analysis. *International Journal of Pharmaceutics* [online], 226 (1–2), 147–161. Available from: <http://linkinghub.elsevier.com/retrieve/pii/S0378517301008018>.
- Fortier, A., Liu, Y., Ghamarian, I., Collins, P. C., and Chason, E., 2017. Investigation of Tin (Sn) Film Using an Aerosol Jet Additive Manufacturing Deposition Process. *Journal of Electronic Materials*, 46 (8), 5174–5182.
- Fricke, G., Kromp, T., Wendel, A., Blume, A., Zirkel, J., Rebmann, H., Setzer, C., Quinkert, R.-O., Martin, F., and Müller-Goymann, C., 2010. Phospholipids and lipid-based formulations in oral drug delivery. *Pharmaceutical research* [online], 27 (8), 1469–86. Available from:

<http://www.ncbi.nlm.nih.gov/pubmed/20411409> [Accessed 21 Oct 2014].

- Fu, Y.-M., Liang, Y. R., Cheng, Y.-T., and Wu, P.-W., 2015. A combined process of liftoff and printing for the fabrication of scalable inkjet printed microstructures on a flexible substrate. *IEEE Transactions on Electron Devices* [online], 62 (4), 1248–1254. Available from: <http://ieeexplore.ieee.org/lpdocs/epic03/wrapper.htm?arnumber=7047690>.
- Furuyama, N., Hasegawa, S., Hamaura, T., Yada, S., Nakagami, H., Yonemochi, E., and Terada, K., 2008. Evaluation of solid dispersions on a molecular level by the Raman mapping technique. *International Journal of Pharmaceutics*, 361 (1–2), 12–18.
- Gao, W., Zhang, Y., Ramanujan, D., Ramani, K., Chen, Y., Williams, C. B., Wang, C. C. L., Shin, Y. C., Zhang, S., and Zavattieri, P. D., 2015. The status, challenges, and future of additive manufacturing in engineering. *Computer-Aided Design* [online], DOI: 10.10 ([Epub ahead of print]). Available from: <http://www.sciencedirect.com/science/article/pii/S0010448515000469>.
- Genina, N., Fors, D., Palo, M., Peltonen, J., and Sandler, N., 2013. Behavior of printable formulations of loperamide and caffeine on different substrates—Effect of print density in inkjet printing. *International Journal of Pharmaceutics* [online], 453 (2), 488–497. Available from: <http://linkinghub.elsevier.com/retrieve/pii/S0378517313004924>.
- Genina, N., Fors, D., Vakili, H., Ihalainen, P., Pohjala, L., Ehlers, H., Kassamakov, I., Haeggström, E., Vuorela, P., Peltonen, J., and Sandler, N., 2012. Tailoring controlled-release oral dosage forms by combining inkjet and flexographic printing techniques. *European Journal of Pharmaceutical Sciences* [online], 47 (3), 615–623. Available from: <http://dx.doi.org/10.1016/j.ejps.2012.07.020>.
- Giridhar, A., Gupta, A., Louvier, M., Joglekar, G., Nagy, Z. K., and Reklaitis, G. V., 2014. *Intelligent Process Management for Continuous Operations in Pharmaceutical Manufacturing*. Proceedings of the 24th European Symposium on Computer Aided Process Engineering Part A. Amsterdam: Elsevier.
- Goh, G. L., Agarwala, S., Tan, Y. J., and Yeong, W. Y., 2018. A low cost and

- flexible carbon nanotube pH sensor fabricated using aerosol jet technology for live cell applications. *Sensors and Actuators, B: Chemical* [online], 260, 227–235. Available from: <http://dx.doi.org/10.1016/j.snb.2017.12.127>.
- Gohel, M. and Bariya, S. H., 2009. Advanced formulation design of venlafaxine hydrochloride coated and triple-layer tablets containing hypromellose formulation design of venlafaxine HCl tablets M. Gohel and S.H. Bariya. *Pharmaceutical Development and Technology*, 14 (6), 650–658.
- Golovenko, N. Y. and Borisyuk, I. Y., 2008. The biopharmaceutical classification system-experimental model of prediction of drug bioavailability. *Biochemistry (Moscow) Supplement Series B: Biomedical Chemistry* [online], 2 (3), 235–244. Available from: <http://link.springer.com/10.1134/S1990750808030037> [Accessed 7 Oct 2014].
- Goyanes, A., Buanz, A. B. M., Basit, A. W., and Gaisford, S., 2014. Fused-filament 3D printing (3DP) for fabrication of tablets. *International Journal of Pharmaceutics* [online], 476 (1–2), 88–92. Available from: <http://linkinghub.elsevier.com/retrieve/pii/S0378517314006991>.
- Goyanes, A., Robles Martinez, P., Buanz, A., Basit, A. W., and Gaisford, S., 2015. Effect of geometry on drug release from 3D printed tablets. *International Journal of Pharmaceutics* [online], DOI: 10.10 ([Epub ahead of print]). Available from: <http://linkinghub.elsevier.com/retrieve/pii/S0378517315003890>.
- Goyanes, A., Wang, J., Buanz, A., Martinez-Pacheco, R., Telford, R., Gaisford, S., and Basit, A. W., 2015. 3D printing of medicines: Engineering novel oral devices with unique design and drug release characteristics. *Molecular Pharmaceutics* [online], 151009113832009. Available from: <http://pubsdc3.acs.org/doi/10.1021/acs.molpharmaceut.5b00510>.
- Grimling, B., Górnjak, A., Meler, J., and Pluta, J., 2012. EVALUATION OF PHYSICOCHEMICAL PROPERTIES OF SOLID DISPERSIONS OF BCS CLASS II SUBSTANCES WITH CHITOSAN Bożena Grimling , Agata Górnjak *, Jan Meler , Janusz Pluta. *Progress in the Chemistry and Application*

- Grimling, B., Górnjak, A., Meler, J., and Pluta, J., 2013. Influence of the physicochemical factors on dissolution of the substance of class II BCS from solid dispersions with chitosan. *Progress on Chemistry and Application of Chitin and its Derivatives*, 18, 157–166.
- Guo, Y., Patanwala, H. S., Bognet, B., and Ma, A. W. K., 2017. Inkjet and inkjet-based 3D printing: connecting fluid properties and printing performance. *Rapid Prototyping Journal* [online], 23 (3), 562–576. Available from: <http://www.emeraldinsight.com/doi/10.1108/RPJ-05-2016-0076>.
- Guo, Y., Wang, X., Shu, X., Shen, Z., and Sun, R., 2012. Self-Assembly and Paclitaxel Loading Capacity of Cellulose- graft t - poly(lactide) Nanomicelles. *Journal of Agricultural and Food Chemistry*, 60, 3900–3908.
- Gupta, K. R., Askarkar, S. S., Rathod, P. R., and Wadodkar, S. G., 2010. Validated spectrophotometric determination of Fenofibrate in formulation. *Pelagia Research Library*, 1 (1), 173–178.
- Guzman, H. R., Tawa, M., Zhang, Z., Ratanabanangkoon, P., Shaw, P., Gardner, C. R., Chen, H., Moreau, J.-P., Almarsson, O., and Remenar, J. F., 2007. Combined Use of Crystalline Salt Forms and Precipitation Inhibitors to Improve Oral Absorption of Celecoxib from Solid Oral Formulations. *Journal of pharmaceutical sciences*, 96 (10), 2686–2702.
- Hampton, T., 2005. Gene Variants Explain Patient Differences in Antiepileptic Drug Responses, 293 (18), 2199–2199.
- Hartman, A. R. and Helft, P., 2007. The ethics of CYP2D6 testing for patients considering tamoxifen. *Breast Cancer Research*, 9 (2), 6–7.
- Hayama, M., Yamamoto, K. I., Kohori, F., Uesaka, T., Ueno, Y., Sugaya, H., Itagaki, I., and Sakai, K., 2004. Nanoscopic behavior of polyvinylpyrrolidone particles on polysulfone/polyvinylpyrrolidone film. *Biomaterials*, 25 (6), 1019–1028.
- Heinz, A., Gordon, K. C., McGoverin, C. M., Rades, T., and Strachan, C. J., 2009. Understanding the solid-state forms of fenofibrate - A spectroscopic and

computational study. *European Journal of Pharmaceutics and Biopharmaceutics* [online], 71 (1), 100–108. Available from: <http://dx.doi.org/10.1016/j.ejpb.2008.05.030>.

Hirave, R. V., Ravindra., B. D., Maniyar, M. G., Kondawar, M. S., and Patil, S. B., 2013. Spectrophotometric method for Simultaneous estimation of Atorvastatin Calcium & Fenofibrate in tablet Dosage Form. *International Journal of Drug Development & Research*, 5 (1), 38–42.

Holthaus, M. G., Treccani, L., and Rezwan, K., 2011. Comparison of micropatterning methods for ceramic surfaces. *Journal of the European Ceramic Society* [online], 31 (15), 2809–2817. Available from: <http://dx.doi.org/10.1016/j.jeurceramsoc.2011.07.020>.

Hong, K., Kim, S. H., Mahajan, A., and Frisbie, C. D., 2014. Aerosol jet printed p- and n-type electrolyte-gated transistors with a variety of electrode materials: Exploring practical routes to printed electronics. *ACS Applied Materials and Interfaces*, 6 (21), 18704–18711.

Hong, K., Kim, Y. H., Kim, S. H., Xie, W., Xu, W. D., Kim, C. H., and Frisbie, C. D., 2014. Aerosol jet printed, Sub-2 v complementary circuits constructed from P-and N-type electrolyte gated transistors. *Advanced Materials*, 26 (41), 7032–7037.

Hossen, S. M. M., Sarkar, R., Towhid, H. A., Sultan, T., and Aziz, N. M. A., 2014. Study on the effect of different polymers on in-vitro dissolution profile of Fenofibrate by solid dispersion technique. *Journal of Applied Pharmaceutical Science* [online], 4 (06), 56–60. Available from: <http://japsonline.com/counter.php?aid=1265>.

Hu, L., Wu, H., Niu, F., Yan, C., Yang, X., and Jia, Y., 2011. Design of fenofibrate microemulsion for improved bioavailability. *International Journal of Pharmaceutics* [online], 420 (2), 251–255. Available from: <http://dx.doi.org/10.1016/j.ijpharm.2011.08.043>.

Huang, J., Wigent, R. J., Bentzley, C. M., and Schwartz, J. B., 2006. Nifedipine solid dispersion in microparticles of ammonio methacrylate copolymer and

- ethylcellulose binary blend for controlled drug delivery. Effect of drug loading on release kinetics. *International Journal of Pharmaceutics*, 319 (1–2), 44–54.
- Huang, S. H., Liu, P., Mokasdar, A., and Hou, L., 2013. Additive manufacturing and its societal impact: A literature review. *International Journal of Advanced Manufacturing Technology*, 67 (5–8), 1191–1203.
- Huang, Y. and Dai, W.-G., 2014. Fundamental aspects of solid dispersion technology for poorly soluble drugs. *Acta Pharmaceutica Sinica B* [online], 4 (1), 18–25. Available from: <http://linkinghub.elsevier.com/retrieve/pii/S2211383513000968> [Accessed 11 Jan 2015].
- Hugo, M., Kunath, K., and Dressman, J., 2012. Selection of excipient, solvent and packaging to optimize the performance of spray-dried formulations: case example fenofibrate. *Drug Development and Industrial Pharmacy*, 39 (November 2011), 1–11.
- Huh, K. M., Lee, S. C., Cho, Y. W., Lee, J., Jeong, J. H., and Park, K., 2005. Hydrotropic polymer micelle system for delivery of paclitaxel. *Journal of Controlled Release* [online], 101 (1–3), 59–68. Available from: <http://linkinghub.elsevier.com/retrieve/pii/S0168365904003128>.
- Hyun, W. J., Secor, E. B., Rojas, G. A., Hersam, M. C., Francis, L. F., and Frisbie, C. D., 2015. All-Printed, Foldable Organic Thin-Film Transistors on Glassine Paper. *Advanced Materials*, 27 (44), 7058–7064.
- Jabari, E. and Toyserkani, E., 2015. Micro-scale aerosol-jet printing of graphene interconnects. *Carbon* [online], 91, 321–329. Available from: <http://www.sciencedirect.com/science/article/pii/S0008622315003966>.
- Jabari, E. and Toyserkani, E., 2016. Aerosol-Jet printing of highly flexible and conductive graphene / silver patterns. *Materials Letters* [online], 174, 40–43. Available from: <http://dx.doi.org/10.1016/j.matlet.2016.03.082>.
- Jensen, S. S., Jensen, H., Goodall, D. M., and Østergaard, J., 2016. Performance characteristics of UV imaging instrumentation for diffusion, dissolution and release testing studies. *Journal of Pharmaceutical and Biomedical Analysis* [online], 131, 113–123. Available from:

<http://dx.doi.org/10.1016/j.jpba.2016.08.018>.

- Jessy, S., B, S. A., and Feb, I., 2011. ISSN 2230 – 8407 ORAL MULTIPARTICULATE PULSATILE DRUG DELIVERY SYSTEMS : A REVIEW Page 22-27 IRJP 2 (2) Feb 2011, 2 (2), 22–27.
- Jonathan, G. and Karim, A., 2016. 3D printing in pharmaceuticals: A new tool for designing customized drug delivery systems. *International Journal of Pharmaceutics* [online], 499 (1–2), 376–394. Available from: <http://www.sciencedirect.com/science/article/pii/S0378517315304622>.
- Jung, M.-S., Kim, J.-S., Kim, M.-S., Alhalaweh, A., Cho, W., Hwang, S.-J., and Velaga, S. P., 2010. Bioavailability of indomethacin-saccharin cocrystals. *The Journal of pharmacy and pharmacology* [online], 62 (11), 1560–1568. Available from: <http://www.ncbi.nlm.nih.gov/pubmed/21039541> [Accessed 27 Nov 2014].
- Karavas, E., Georganakis, M., Docoslis, A., and Bikiaris, D., 2007. Combining SEM, TEM, and micro-Raman techniques to differentiate between the amorphous molecular level dispersions and nanodispersions of a poorly water-soluble drug within a polymer matrix. *International Journal of Pharmaceutics*, 340 (1–2), 76–83.
- Kashyap, N., Viswanad, B., Sharma, G., Bhardwaj, V., Ramarao, P., and Ravi Kumar, M. N. V, 2007. Design and evaluation of biodegradable, biosensitive in situ gelling system for pulsatile delivery of insulin. *Biomaterials* [online], 28 (11), 2051–60. Available from: <http://www.ncbi.nlm.nih.gov/pubmed/17240443> [Accessed 21 Jan 2014].
- Kawabata, Y., Wada, K., Nakatani, M., Yamada, S., and Onoue, S., 2011. Formulation design for poorly water-soluble drugs based on biopharmaceutics classification system: basic approaches and practical applications. *International journal of pharmaceutics* [online], 420 (1), 1–10. Available from: <http://www.ncbi.nlm.nih.gov/pubmed/21884771> [Accessed 11 Nov 2013].
- Kawakami, K., 2012. Modification of physicochemical characteristics of active pharmaceutical ingredients and application of supersaturatable dosage forms for

improving bioavailability of poorly absorbed drugs. *Advanced drug delivery reviews* [online], 64, 480–95. Available from:
<http://www.ncbi.nlm.nih.gov/pubmed/22265844> [Accessed 11 Nov 2013].

Kazarian, S. G. and Martirosyan, G. G., 2002. Spectroscopy of polymer / drug formulations processed with supercritical fluids : in situ ATR – IR and Raman study of impregnation of ibuprofen into PVP, 232, 81–90.

Keleb, E. I., Vermeire, a, Vervaet, C., and Remon, J. P., 2004. Twin screw granulation as a simple and efficient tool for continuous wet granulation. *International journal of pharmaceutics* [online], 273 (1–2), 183–94. Available from: <http://www.ncbi.nlm.nih.gov/pubmed/15010142> [Accessed 7 Nov 2014].

Kennedy, M., Hu, J., Gao, P., Li, L., Ali-reynolds, A., Chal, B., Gupta, V., Ma, C., Mahajan, N., Akrami, A., and Surapaneni, S., 2008. Enhanced Bioavailability of a Poorly Soluble VR1 Antagonist Using an Amorphous Solid Dispersion Approach : A Case Study. *Molecular Pharmaceutics*, 5 (6), 981–993.

Khandare J. and Haag R., 2010 *Pharmaceutically Used Polymers: Principles Structures and Applications of Pharmaceutical Delivery Systems*, Schäfer-Korting M. (Ed.), *Handbook of Experimental Pharmacology*, Volume 197, pp 246, Heidelberg, Dordrecht, London and New York: Springer

Kim, C. H. and Frisbie, C. D., 2014. Determination of quantum capacitance and band filling potential in graphene transistors with dual electrochemical and field-effect gates. *Journal of Physical Chemistry C*, 118 (36), 21160–21169.

Kim, J. Y., Kim, S., Pinal, R., and Park, K., 2011. Hydrotropic polymer micelles as versatile vehicles for delivery of poorly water-soluble drugs. *Journal of controlled release* [online], 152, 13–20. Available from:
<http://www.ncbi.nlm.nih.gov/pubmed/21352878> [Accessed 13 Nov 2013].

Kim, S., Kim, J.-H., Jeon, O., Kwon, I. C., and Park, K., 2009. Engineered polymers for advanced drug delivery. *European journal of pharmaceutics and biopharmaceutics* [online], 71, 420–30. Available from:
<http://www.pubmedcentral.nih.gov/articlerender.fcgi?artid=2794279&tool=pmc-entrez&rendertype=abstract> [Accessed 7 Nov 2013].

- King, B. H., 2014. US Patent 8,640,975 B2: Miniature Aerosol Jet and Aerosol Jet Array. *United States Patent*.
- King, B. H. and Renn, M. J., 2008. Aerosol Jet® Direct Write Printing for Mil-Aero Electronic Applications. *WHITEPAPER - Optomec* [online]. Available from: <http://166.21.32.80/data/assets/ssc/atc/2009-04-09article.pdf>⁹http://www.optomec.com/downloads/Optomec_Aerosol_Jet_Direct_Write_Printing_for_Mil_Aero_Electronic_Apps.pdf.
- Kondawar, M. S., Kamble, K. G., Maharshi, K. H., and Khandare, M. M., 2011. UV Spectrophotometric estimation of Ezetimibe and Fenofibrate in Bulk drug and Dosage form using Simultaneous Equation Method. *International Journal*, 3 (2), 749–754.
- Kopola, P., Zimmermann, B., Filipovic, A., Schleiermacher, H. F., Greulich, J., Rousu, S., Hast, J., Myllylä, R., and Würfel, U., 2012. Aerosol jet printed grid for ITO-free inverted organic solar cells. *Solar Energy Materials and Solar Cells*, 107, 252–258.
- Krull, S. M., Moreno, J., Li, M., Bilgili, E., and Davé, R. N., 2017. Critical material attributes (CMAs) of strip films loaded with poorly water-soluble drug nanoparticles: III. Impact of drug nanoparticle loading. *International Journal of Pharmaceutics*, 523 (1), 33–41.
- Ku, M. S. and Dulin, W., 2012. A biopharmaceutical classification-based Right-First-Time formulation approach to reduce human pharmacokinetic variability and project cycle time from First-In-Human to clinical Proof-Of-Concept. *Pharmaceutical Development and Technology*, 17 (3), 285–302.
- Kumar, B. P., Chandiran, I. S., Bhavya, B., and Sindhuri, M., 2011. MICROPARTICULATE DRUG DELIVERY SYSTEM : A REVIEW. *Indian Journal of Pharmaceutical Science & Research*, 1 (1), 19–37.
- Kyobula, M., Adedeji, A., Alexander, M. R., Saleh, E., Wildman, R., Ashcroft, I., Gellert, P. R., and Roberts, C. J., 2017. 3D inkjet printing of tablets exploiting bespoke complex geometries for controlled and tuneable drug release. *Journal of Controlled Release* [online], 261 (March), 207–215. Available from:

<http://dx.doi.org/10.1016/j.jconrel.2017.06.025>.

- Kyobula, M., Alexander, M. R., Gellert, R. W. P. R., and Roberts, C. J., 2009. 3D Inkjet Printing of Solid Dosage Forms with Controlled Geometry, 1 (2006), 4877.
- Labuschagne, P. W., Kazarian, S. G., and Sadiku, R. E., 2011. Supercritical CO₂-assisted preparation of ibuprofen-loaded PEG-PVP complexes. *Journal of Supercritical Fluids* [online], 57 (2), 190–197. Available from: <http://dx.doi.org/10.1016/j.supflu.2011.03.001>.
- Lan, X., Lu, X., Chen, M. Y., Scherrer, D., Chung, T., Nguyen, E., Lai, R., and Tice, J., 2017. Direct On-Chip 3-D Aerosol Jet Printing With High Reliability. *IEEE Transactions on Components, Packaging and Manufacturing Technology*, 7 (8), 1369–1376.
- Lao, L. L., Venkatraman, S. S., and Peppas, N. A., 2008. A novel model and experimental analysis of hydrophilic and hydrophobic agent release from biodegradable polymers. *Journal of biomedical materials research. Part A* [online], 90 (4), 1054–65. Available from: <http://www.ncbi.nlm.nih.gov/pubmed/18671269> [Accessed 27 Nov 2013].
- Lauschke, V. M. and Ingelman-Sundberg, M., 2016. The importance of patient-specific factors for hepatic drug response and toxicity. *International Journal of Molecular Sciences*, 17 (10), 1–27.
- Leane, M., Pitt, K., Reynolds, G., Anwar, J., Charlton, S., Crean, A., Creekmore, R., Davies, C., DeBeer, T., De-Matas, M., Djemai, A., Douroumis, D., Gaisford, S., Gamble, J., Stone, E. H., Kavanagh, A., Khimiyak, Y., Kleinebudde, P., Moreton, C., Paudel, A., Storey, R., Toschkoff, G., and Vyas, K., 2015. A proposal for a drug product Manufacturing Classification System (MCS) for oral solid dosage forms. *Pharmaceutical Development and Technology*, 20 (1), 12–21.
- Lee, M. K., Kim, S., Ahn, C.-H., and Lee, J., 2010. Hydrophilic and hydrophobic amino acid copolymers for nano-comminution of poorly soluble drugs. *International journal of pharmaceutics* [online], 384 (1–2), 173–80. Available

from: <http://www.ncbi.nlm.nih.gov/pubmed/19788919> [Accessed 28 Nov 2013].

- Legato, M. J., Johnson, P. A., and Manson, J. E., 2016. Consideration of sex differences in medicine to improve health care and patient outcomes. *JAMA - Journal of the American Medical Association*, 316 (18), 1865–1866.
- Lennernäs, H., 2014. Regional intestinal drug permeation: biopharmaceutics and drug development. *European journal of pharmaceutical sciences* [online], 57, 333–41. Available from: <http://www.ncbi.nlm.nih.gov/pubmed/23988845> [Accessed 1 Oct 2014].
- Leuner, C. and Dressman, J., 2000. Improving drug solubility for oral delivery using solid dispersions. *European journal of pharmaceuticals and biopharmaceutics* [online], 50 (1), 47–60. Available from: <http://www.ncbi.nlm.nih.gov/pubmed/10840192>.
- Li, B., Zhu, J., Zheng, C., and Gong, W., 2008. A novel system for three-pulse drug release based on ‘tablets in capsule’ device. *International Journal of Pharmaceutics*, 352 (1–2), 159–164.
- Li, D. X., Oh, Y. K., Lim, S. J., Kim, J. O., Yang, H. J., Sung, J. H., Yong, C. S., and Choi, H. G., 2008. Novel gelatin microcapsule with bioavailability enhancement of ibuprofen using spray-drying technique. *International Journal of Pharmaceutics*, 355 (1–2), 277–284.
- Li, X. K., Lu, H., Cao, G. P., Qian, Y. H., Chen, L. H., Zhang, R. H., Liu, H. L., and Shi, Y. H., 2014. Experimental study of the synergistic plasticizing effect of carbon dioxide and ibuprofen on the glass transition temperature of poly(methyl methacrylate). *Industrial and Engineering Chemistry Research*, 53 (14), 5873–5885.
- Li, Y., Pan, H., Duan, H., Chen, J., Zhu, Z., Fan, J., Li, P., Yang, X., and Pan, W., 2018. Double-layered osmotic pump controlled release tablets of actarit: In vitro and in vivo evaluation. *Asian Journal of Pharmaceutical Sciences* [online], 000, 1–9. Available from: <https://doi.org/10.1016/j.ajps.2018.05.009>.
- Lindenberg, M., Kopp, S., and Dressman, J. B., 2004. Classification of orally

- administered drugs on the World Health Organization Model list of Essential Medicines according to the biopharmaceutics classification system. *European journal of pharmaceutics and biopharmaceutics* [online], 58, 265–78. Available from: <http://www.ncbi.nlm.nih.gov/pubmed/15296954> [Accessed 8 Oct 2014].
- Liou, T.-M., Chan, C.-Y., and Shih, K.-C., 2010. Effects of actuating waveform , ink property , and nozzle size on piezoelectrically driven inkjet droplets. *Microfluidics and Nanofluidics*, 8, 575–586.
- Liu, D., Yu, S., Zhu, Z., Lyu, C., Bai, C., Ge, H., Yang, X., and Pan, W., 2014. Controlled delivery of carvedilol nanosuspension from osmotic pump capsule: In vitro and in vivo evaluation. *International journal of pharmaceutics* [online], 475 (1–2), 496–503. Available from: <http://www.ncbi.nlm.nih.gov/pubmed/25219321> [Accessed 6 Nov 2014].
- Liu, Y., Genzer, J., and Dickey, M. D., 2016. ‘2D or not 2D’: Shape-programming polymer sheets. *Progress in Polymer Science* [online], 52, 79–106. Available from: <http://dx.doi.org/10.1016/j.progpolymsci.2015.09.001>.
- Llabot, J. M., Manzo, R. H., and Allemandi, D. A., 2002. Double-layered mucoadhesive tablets containing nystatin. *AAPS PharmSciTech* [online], 3 (3), E22. Available from: <http://www.pubmedcentral.nih.gov/articlerender.fcgi?artid=2784051&tool=pmc&entrez&rendertype=abstract>.
- Lu, L., Zheng, J., and Mishra, S., 2014. A Layer-To-Layer Model and Feedback Control of Ink-Jet 3-D Printing. *IEEE/ASME Transactions on Mechatronics*, 20 (3), 1056–1068.
- Lu, Y., Tang, N., Lian, R., Qi, J., and Wu, W., 2014. Understanding the relationship between wettability and dissolution of solid dispersion. *International Journal of Pharmaceutics*, 465 (1–2), 25–31.
- Luan, E., Zheng, Z., Li, X., Gu, H., and Liu, S., 2016. Inkjet-assisted layer-by-layer printing of quantum dot/enzyme microarrays for highly sensitive detection of organophosphorous pesticides. *Analytica chimica acta* [online], 916, 77–83. Available from: <http://www.ncbi.nlm.nih.gov/pubmed/27016441>.

- Luebbert, C., Klanke, C., and Sadowski, G., 2018. Investigating phase separation in amorphous solid dispersions via Raman mapping. *International Journal of Pharmaceutics* [online], 535 (1–2), 245–252. Available from: <https://doi.org/10.1016/j.ijpharm.2017.11.014>.
- Madelung, P., Bertelsen, P., Jacobsen, J., Müllertz, A., and Østergaard, J., 2017. Dissolution enhancement of griseofulvin from griseofulvin-sodium dodecyl sulfate discs investigated by UV imaging. *Journal of Drug Delivery Science and Technology* [online], 39, 516–522. Available from: <http://dx.doi.org/10.1016/j.jddst.2017.05.010>.
- Mahajan, A., Frisbie, C. D., and Francis, L. F., 2013. Optimization of aerosol jet printing for high-resolution, high-aspect ratio silver lines. *ACS Applied Materials and Interfaces*, 5 (11), 4856–4864.
- Malewar, N., Avachat, M., Kulkarni, S., and Pokharkar, V., 2015. Design and evaluation of novel barrier layer technologies for controlling venlafaxine hydrochloride release from tablet dosage form. *Pharmaceutical Development and Technology*, 20 (5), 588–597.
- Mandwal, P. S., Patel, P. R., Agarwal, K. M., and Surana, S. J., 2012. Q-absorbance and multicomponent UV - Spectrophotometric methods for simultaneous estimation of rosuvastatin calcium and fenofibrate in pharmaceutical formulation. *Der Pharmacia Lettre*, 4 (4), 1054–1059.
- Marizza, P., Keller, S. S., and Boisen, A., 2013. Inkjet printing as a technique for filling of micro-wells with biocompatible polymers. *Microelectronic Engineering* [online], 111, 391–395. Available from: <http://dx.doi.org/10.1016/j.mee.2013.03.168>.
- Markovsky, E., Baabur-Cohen, H., Eldar-Boock, A., Omer, L., Tiram, G., Ferber, S., Ofek, P., Polyak, D., Scomparin, A., and Satchi-Fainaro, R., 2012. Administration, distribution, metabolism and elimination of polymer therapeutics. *Journal of controlled release* [online], 161, 446–60. Available from: <http://www.ncbi.nlm.nih.gov/pubmed/22286005> [Accessed 8 Nov 2013].
- Mascia, S., Heider, P. L., Zhang, H., Lakerveld, R., Benyahia, B., Barton, P. I.,

- Braatz, R. D., Cooney, C. L., Evans, J. M. B., Jamison, T. F., Jensen, K. F., Myerson, A. S., and Trout, B. L., 2013. End-to-end continuous manufacturing of pharmaceuticals: integrated synthesis, purification, and final dosage formation. *Angewandte Chemie* [online], 52, 12359–63. Available from: <http://www.ncbi.nlm.nih.gov/pubmed/24115355> [Accessed 21 Oct 2014].
- Al Masum, A., Sharmin, F., Islam, S. M. A., and Reza, S., 2015. Enhancement of Solubility and Dissolution Characteristics of Ibuprofen by Solid Dispersion Technique. *Journal of Pharmaceutical Sciences*, 11 (1), 1–6.
- Mau, R., Oldorf, P., Peters, R., and Seitz, H., 2016. Adjusting inkjet printhead parameters to deposit drugs into micro-sized reservoirs. *Current Directions in Biomedical Engineering* [online], 2 (1), 387–390. Available from: <http://www.degruyter.com/view/j/cdbme.2016.2.issue-1/cdbme-2016-0086/cdbme-2016-0086.xml>.
- McNamara, D. P., Childs, S. L., Giordano, J., Iarriccio, A., Cassidy, J., Shet, M. S., Mannion, R., O'Donnell, E., and Park, A., 2006. Use of a glutaric acid cocrystal to improve oral bioavailability of a low solubility API. *Pharmaceutical research* [online], 23 (8), 1888–97. Available from: <http://www.ncbi.nlm.nih.gov/pubmed/16832611> [Accessed 24 Aug 2014].
- Mehrdad, A., Shekaari, H., and Niknam, Z., 2013. Fluid Phase Equilibria Effect of ionic liquid on the intrinsic viscosity of polyvinyl pyrrolidone in aqueous solutions. *Fluid Phase Equilibria* [online], 353, 69–75. Available from: <http://dx.doi.org/10.1016/j.fluid.2013.06.003>.
- Melzig, S., Niedbalka, D., Schilde, C., and Kwade, A., 2018. Spray drying of amorphous ibuprofen nanoparticles for the production of granules with enhanced drug release. *Colloids and Surfaces A: Physicochemical and Engineering Aspects* [online], 536 (June 2017), 133–141. Available from: <https://doi.org/10.1016/j.colsurfa.2017.07.028>.
- Mohamad, A. and Dashevsky, A., 2006. pH-independent pulsatile drug delivery system based on hard gelatin capsules and coated with aqueous dispersion Aquacoat ECD. *European journal of pharmaceutics and biopharmaceutics* :

official journal of Arbeitsgemeinschaft für Pharmazeutische Verfahrenstechnik e.V [online], 64 (2), 173–9. Available from:
<http://www.ncbi.nlm.nih.gov/pubmed/16814532> [Accessed 26 Mar 2014].

Montenegro-Nicolini, M., Miranda, V., and Morales, J. O., 2017. Inkjet Printing of Proteins: an Experimental Approach. *The AAPS Journal* [online], 19 (1), 234–243. Available from: <http://link.springer.com/10.1208/s12248-016-9997-8>.

Morgen, M., Bloom, C., Beyerinck, R., Bello, A., Song, W., Wilkinson, K., Steenwyk, R., and Shamblin, S., 2012. Polymeric nanoparticles for increased oral bioavailability and rapid absorption using celecoxib as a model of a low-solubility, high-permeability drug. *Pharmaceutical research* [online], 29 (2), 427–40. Available from:
<http://www.pubmedcentral.nih.gov/articlerender.fcgi?artid=3264876&tool=pmc-entrez&rendertype=abstract> [Accessed 4 Dec 2014].

Moribe, K., Limwikrant, W., Higashi, K., and Yamamoto, K., 2012. Structural evaluation of probucol nanoparticles in water by atomic force microscopy. *International Journal of Pharmaceutics* [online], 427 (2), 365–371. Available from: <http://dx.doi.org/10.1016/j.ijpharm.2012.02.020>.

Mrsny, R. J., 2012. Oral drug delivery research in Europe. *Journal of controlled release* [online], 161, 247–53. Available from:
<http://www.ncbi.nlm.nih.gov/pubmed/22342473> [Accessed 18 Nov 2013].

Nakagawa, Y., Ohta, S., Nakamura, M., and Ito, T., 2017. 3D inkjet printing of star block copolymer hydrogels cross-linked using various metallic ions. *RSC Advances*, 7 (88), 55571–55576.

Newbury, R. W. and Bates, D. J., 2017. *Dynamics of Flowing Water* [online]. Methods in Stream Ecology. Elsevier Inc. Available from:
<http://dx.doi.org/10.1016/B978-0-12-416558-8.00004-4>.

Ng, Y. C., Yang, Z., McAuley, W. J., and Qi, S., 2013. Stabilisation of amorphous drugs under high humidity using pharmaceutical thin films. *European Journal of Pharmaceutics and Biopharmaceutics* [online], 84 (3), 555–565. Available from: <http://dx.doi.org/10.1016/j.ejpb.2013.01.008>.

- Nutalapati, S. R. K., 2012. US2012/0258173A1: Functionally-coated Multilayer Tablets.
- Østergaard, J., 2018. UV imaging in pharmaceutical analysis. *Journal of Pharmaceutical and Biomedical Analysis* [online], 147, 140–148. Available from: <https://doi.org/10.1016/j.jpba.2017.07.055>.
- Østergaard, J., Lenke, J., Sun, Y., and Ye, F., 2014. UV Imaging for In Vitro Dissolution and Release Studies: Initial Experiences. *Dissolution Technologies* [online], 21 (4), 27–38. Available from: <http://www.scopus.com/inward/record.url?eid=2-s2.0-84916217720&partnerID=tZOtx3y1>.
- Østergaard, J., Wu, J. X., Naelapää, K., Boetker, J. P., Jensen, H., and Rantanen, J., 2014. Simultaneous UV imaging and Raman spectroscopy for the measurement of solvent-mediated phase transformations during dissolution testing. *Journal of Pharmaceutical Sciences*, 103 (4), 1149–1156.
- Pan, Y., Pang, W., Lv, J., Wang, J., Yang, C., and Guo, W., 2017. Solid state characterization of amlodipine–oxalic acid co-crystal and co-amorphous complexes: The effect of different amlodipine polymorphs. *Journal of Pharmaceutical and Biomedical Analysis* [online], 138, 302–315. Available from: <http://dx.doi.org/10.1016/j.jpba.2017.02.005>.
- Panakanti, R. and Narang, A. S., 2015. Impact of excipient interactions on drug bioavailability from solid dosage forms. *Excipient Applications in Formulation Design and Drug Delivery*, 273–310.
- Pandhi, T., Kreit, E., Aga, R., Fujimoto, K., Sharbati, M. T., Khademi, S., Chang, A. N., Xiong, F., Koehne, J., Heckman, E. M., and Estrada, D., 2018. Electrical Transport and Power Dissipation in Aerosol-Jet-Printed Graphene Interconnects. *Scientific Reports*, 8 (1), 1–10.
- Papós, K., Kása, P., Ilič, I., Blatnik-Urek, S., Regdon, G., Srčić, S., Pintye-Hódi, K., and Sovány, T., 2015. Effect of the surface free energy of materials on the lamination tendency of bilayer tablets. *International Journal of Pharmaceutics*, 496 (2), 609–613.

- Pataky, K., Braschler, T., Negro, A., Renaud, P., Lutolf, M. P., and Brugger, J., 2012. Microdrop printing of hydrogel bioinks into 3D tissue-like geometries. *Advanced Materials*, 24 (3), 391–396.
- Pavec, M., Navratil, J., Soukup, R., and Hamacek, A., 2018. A Bowtie Antenna Prepared by Aerosol Jet and Embroidering Technology. *Proceedings of the International Spring Seminar on Electronics Technology*, 2018–May, 1–4.
- Pavurala, N. and Achenie, L. E. K., 2013. A mechanistic approach for modeling oral drug delivery. *Computers & Chemical Engineering* [online], 57, 196–206. Available from: <http://linkinghub.elsevier.com/retrieve/pii/S0098135413001956> [Accessed 28 Oct 2014].
- Pawar, I. A., Joshi, P. J., Kadam, A. D., Pande, N. B., Kamble, P. H., Hinge, S. P., Banerjee, B. S., Mohod, A. V, and Gogate, P. R., 2014. Ultrasonics Sonochemistry Ultrasound-based treatment approaches for intrinsic viscosity reduction of polyvinyl pyrrolidone (PVP). *Ultrasonics - Sonochemistry* [online], 21 (3), 1108–1116. Available from: <http://dx.doi.org/10.1016/j.ultsonch.2013.12.013>.
- Petereit, H.-U., Rudolph, M., Beckert, T., and Dressman, J., 2004. CA2502371A1: Multilayer Dosage Forms, which Contain Active Substances and which Comprise a Neutral Core, and an Inner and Outer Coating Consisting of Methacrylate Copolymers and Methacrylate Monomers.
- Pickard, B. S., 2017. Genomics of Lithium Action and Response. *Neurotherapeutics*, 14 (3), 582–587.
- Plachetka, J. R., Gilbert, D. L., and Kothapalli, V. M., 2002. CA2509023A1: Multilayer Dosage Forms Containing NSAIDS and Triptans.
- Plumb, K., 2005. Continuous Processing in the Pharmaceutical Industry. *Chemical Engineering Research and Design* [online], 83 (A6), 730–738. Available from: <http://linkinghub.elsevier.com/retrieve/pii/S0263876205727556> [Accessed 27 Oct 2014].
- Podczec, F., 2011. Theoretical and experimental investigations into the delamination tendencies of bilayer tablets. *International Journal of*

Pharmaceutics [online], 408 (1–2), 102–112. Available from:
<http://dx.doi.org/10.1016/j.ijpharm.2011.02.007>.

Podczec, F. and Al-Muti, E., 2010. The tensile strength of bilayered tablets made from different grades of microcrystalline cellulose. *European Journal of Pharmaceutical Sciences* [online], 41 (3–4), 483–488. Available from:
<http://dx.doi.org/10.1016/j.ejps.2010.08.002>.

Podczec, F., Drake, K. R., Newton, J. M., and Haririan, I., 2006. The strength of bilayered tablets. *European Journal of Pharmaceutical Sciences*, 29 (5), 361–366.

Prabhu, S., Ortega, M., and Ma, C., 2005. Novel lipid-based formulations enhancing the in vitro dissolution and permeability characteristics of a poorly water-soluble model drug, piroxicam. *International journal of pharmaceutics* [online], 301, 209–16. Available from: <http://www.ncbi.nlm.nih.gov/pubmed/16046087> [Accessed 6 Nov 2014].

Prachi, S., Prajapati, S. K., K, S. U., Shipra, S., and Ali, A., 2012. A Review on the Self Micro Emulsifying Drug Delivery System: An Approach to Enhance the Oral Bioavailability of Poorly Water Soluble Drugs. *International Research Journal of Pharmacy*, 3 (9), 1–6.

Prasanth, V. V, Modi, M. P., Mathew, S. T., and Services, A. P., 2012. Pulsatile: A Tool for Circadian Rhythm - A Review. *Journal of Drug Delivery & Therapeutics*, 2 (1), 58–65.

Puranik, P. K., Ashok, K. S., Dilip, G. D., and Prabha, M., 2011.

BIOPHARMACEUTICAL CLASSIFICATION SYSTEM AND BIOWAVER : AN OVERVIEW. *International Research Journal of Pharmacy*, 2 (5), 66–71.

Qi, X., Jiang, Y., Li, X., Zhang, Z., and Wu, Z., 2015. Zero-order release three-layered tablet with an acemetacin solid dispersion core and a hydroxypropyl methylcellulose capped matrix. *Journal of Applied Polymer Science*, 132 (24), 1–7.

Quinten, T., Andrews, G. P., Beer, T., Suerens, L., Bouquet, W., Jones, D. S., Hornsby, P., Remon, J. P., and Vervaet, C., 2012. Preparation and Evaluation of

Sustained-Release Matrix Tablets Based on Metoprolol and an Acrylic Carrier Using Injection Moulding. *AAPS PharmSciTech*, 13 (4), 1197–1211.

- Quinten, T., Beer, T. De, Vervaet, C., and Remon, J. P., 2009. Evaluation of injection moulding as a pharmaceutical technology to produce matrix tablets. *European Journal of Pharmaceutics and Biopharmaceutics*, 71, 145–154.
- Quinten, T., Gonnissen, Y., Adriaens, E., Beer, T. De, Cnudde, V., Masschaele, B., Van Hoorebeke, L., Siepmann, J., Remon, J. P., and Vervaet, C., 2009. Development of injection moulded matrix tablets based on mixtures of ethylcellulose and low-substituted hydroxypropylcellulose. *European Journal of Pharmaceutical Sciences*, 37 (3–4), 207–216.
- Raijada, D., Genina, N., Fors, D., Wisaeus, E., Peltonen, J., Rantanen, J., and Sandler, N., 2013. A Step Toward Development of Printable Dosage Forms for Poorly Soluble Drugs. *Journal of Pharmaceutical Sciences*, 102, 3694–3704.
- Ranade V.V. and Hollinger M.A., 2004, Drug Delivery Systems, MyiLibrary. 2nd ed., pp63-114, Boca Ranton, Florida: CRC Press
- Rasenack, N. and Müller, B. W., 2005. Poorly Water-soluble Drugs for Oral Delivery – A Challenge for Pharmaceutical Development. *Pharmazeutische Industrie*, 67 (3), 323–326.
- Raut Desai, S. and Rohera, B. D., 2014. Formulation, in vitro evaluation and study of variables on tri-layered gastro-retentive delivery system of diltiazem HCl. *Drug Development and Industrial Pharmacy*, 40 (3), 380–389.
- Rautio, J., Kumpulainen, H., Heimbach, T., Oliyai, R., Oh, D., Järvinen, T., and Savolainen, J., 2008. Prodrugs: design and clinical applications. *Nature reviews. Drug discovery* [online], 7, 255–70. Available from: <http://www.ncbi.nlm.nih.gov/pubmed/18219308> [Accessed 3 Oct 2014].
- Roberts, A. D. and Zhang, H., 2013. Poorly water-soluble drug nanoparticles via solvent evaporation in water-soluble porous polymers. *International journal of pharmaceutics* [online], 447, 241–50. Available from: <http://www.ncbi.nlm.nih.gov/pubmed/23499755> [Accessed 15 Nov 2013].

- Ross, S., Scoutaris, N., Lamprou, D., Mallinson, D., and Douroumis, D., 2015. Inkjet printing of insulin microneedles for transdermal delivery. *Drug Delivery and Translational Research*, 5 (4), 451–461.
- Rossmann, M., Braeuer, A., and Schluecker, E., 2014. Supercritical antisolvent micronization of PVP and ibuprofen sodium towards tailored solid dispersions. *Journal of Supercritical Fluids* [online], 89, 16–27. Available from: <http://dx.doi.org/10.1016/j.supflu.2014.02.010>.
- Rowe, C. ., Katstra, W. ., Palazzolo, R. ., Giritlioglu, B., Teung, P., and Cima, M. ., 2000. Multimechanism oral dosage forms fabricated by three dimensional printingTM. *Journal of Controlled Release* [online], 66 (1), 11–17. Available from: <http://linkinghub.elsevier.com/retrieve/pii/S0168365999002242>.
- Roy, P. and Shahiwala, A., 2009. Multiparticulate formulation approach to pulsatile drug delivery: Current perspectives. *Journal of Controlled Release* [online], 134 (2), 74–80. Available from: <http://dx.doi.org/10.1016/j.jconrel.2008.11.011>.
- Russe, I. S., Brock, D., Knop, K., Kleinebudde, P., and Zeitler, J. A., 2012. Validation of terahertz coating thickness measurements using X-ray microtomography. *Molecular Pharmaceutics*, 9 (12), 3551–3559.
- Saerens, L., Dierickx, L., Lenain, B., Vervaet, C., Remon, J. P., and Beer, T. De, 2011. Raman spectroscopy for the in-line polymer-drug quantification and solid state characterization during a pharmaceutical hot-melt extrusion process. *European Journal of Pharmaceutics and Biopharmaceutics* [online], 77 (1), 158–163. Available from: <http://dx.doi.org/10.1016/j.ejpb.2010.09.015>.
- Sahoo, D. K., Sahu, P. K., and Patro, C. S., 2014. New validated isocratic RP-HPLC method for assay of fenofibrate. *International Journal of Pharmacy and Pharmaceutical Sciences*, 6 (SUPPL. 2), 169–172.
- Sailaja, U., Thayyil, M. S., Kumar, N. S. K., and Govindaraj, G., 2016. Molecular dynamics of amorphous pharmaceutical fenofibrate studied by broadband dielectric spectroscopy. *Journal of Pharmaceutical Analysis* [online], 6 (3), 165–170. Available from: <http://dx.doi.org/10.1016/j.jpha.2014.09.003>.
- Salary, R. (Ross), Lombardi, J. P., Rao, P. K., and Poliks, M. D., 2017. Online

Monitoring of Functional Electrical Properties in Aerosol Jet Printing Additive Manufacturing Process Using Shape-From-Shading Image Analysis. *Journal of Manufacturing Science and Engineering* [online], 139 (10), 101010. Available from:

<http://manufacturingscience.asmedigitalcollection.asme.org/article.aspx?doi=10.1115/1.4036660>.

Salary, R. (Ross), Lombardi, J. P., Samie Tootooni, M., Donovan, R., Rao, P. K., Borgesen, P., and Poliks, M. D., 2016. Computational Fluid Dynamics Modeling and Online Monitoring of Aerosol Jet Printing Process. *Journal of Manufacturing Science and Engineering* [online], 139 (2), 021015. Available from:
<http://manufacturingscience.asmedigitalcollection.asme.org/article.aspx?doi=10.1115/1.4034591>.

Sander, A., 2014. Droplet Size Distribution Obtained by Atomization with Two-Fluid Nozzles in a Spray Dryer, (12), 2073–2084.

Sant, V. P., Smith, D., and Leroux, J.-C., 2004. Novel pH-sensitive supramolecular assemblies for oral delivery of poorly water soluble drugs: preparation and characterization. *Journal of controlled release* [online], 97, 301–12. Available from: <http://www.ncbi.nlm.nih.gov/pubmed/15196757> [Accessed 10 Nov 2013].

Satheesh Madhav, N. V. and Kala, S., 2011. Review on microparticulate drug delivery system. *International Journal of PharmTech Research*, 3 (3), 1242–1254.

Savjani, K. T., Gajjar, A. K., and Savjani, J. K., 2012. Drug solubility: importance and enhancement techniques. *ISRN pharmaceutics* [online], 2012 (100 mL), 195727. Available from:
<http://www.pubmedcentral.nih.gov/articlerender.fcgi?artid=3399483&tool=pmc-entrez&rendertype=abstract> [Accessed 11 Nov 2013].

Schaber, S. D., Gerogiorgis, D. I., Ramachandran, R., Evans, J. M. B., Barton, P. I., and Trout, B. L., 2011. Economic Analysis of Integrated Continuous and Batch

- Pharmaceutical Manufacturing: A Case Study. *Industrial & Engineering Chemistry Research* [online], 50, 10083–10092. Available from:
<http://pubs.acs.org/doi/abs/10.1021/ie2006752>.
- Scoutaris, N., 2010. Home based formulation of personalised medicines by means of inkjet printing technique, (September).
- Scoutaris, N., Alexander, M. R., Gellert, P. R., and Roberts, C. J., 2011. Inkjet printing as a novel medicine formulation technique. *Journal of Controlled Release* [online], 156, 179–185. Available from:
<http://dx.doi.org/10.1016/j.jconrel.2011.07.033>.
- Scoutaris, N., Chai, F., Maurel, B., Sobocinski, J., Zhao, M., Moffat, J. G., Craig, D. Q., Martel, B., Blanchemain, N., and Douroumis, D., 2016. Development and Biological Evaluation of Inkjet Printed Drug Coatings on Intravascular Stent. *Molecular Pharmaceutics*, 13 (1), 125–133.
- Scoutaris, N., Hook, A. L., Gellert, P. R., Roberts, C. J., Alexander, M. R., and Scurr, D. J., 2012. ToF-SIMS analysis of chemical heterogenities in inkjet micro-array printed drug/polymer formulations. *Journal of Materials Science: Materials in Medicine*, 23 (2), 385–391.
- Scoutaris, N., Ross, S., and Douroumis, D., 2016. Current Trends on Medical and Pharmaceutical Applications of Inkjet Printing Technology. *Pharmaceutical Research* [online], 33 (8), 1799–1816. Available from:
<http://dx.doi.org/10.1007/s11095-016-1931-3>.
- Seifert, T., Baum, M., Roscher, F., Wiemer, M., and Gessner, T., 2015. Aerosol Jet Printing of Nano Particle Based Electrical Chip Interconnects. *Materials Today: Proceedings* [online], 2 (8), 4262–4271. Available from:
<http://dx.doi.org/10.1016/j.matpr.2015.09.012>.
- Seifert, T., Sowade, E., Roscher, F., Wiemer, M., Gessner, T., and Baumann, R. R., 2015. Additive Manufacturing Technologies Compared: Morphology of Deposits of Silver Ink Using Inkjet and Aerosol Jet Printing. *Industrial & Engineering Chemistry Research*, 54, 769–779.
- Sevda, R. R., Ravetkar, A. S., and Shirote, P. J., 2011. UV spectrophotometric

- estimation of rosuvastatin calcium and fenofibrate in bulk drug and dosage form using simultaneous equation method. *International Journal of ChemTech Research*, 3 (2), 629–635.
- Shah, S., Maddineni, S., Lu, J., and Repka, M. a, 2013. Melt extrusion with poorly soluble drugs. *International journal of pharmaceutics* [online], 453, 233–52. Available from: <http://www.ncbi.nlm.nih.gov/pubmed/23178213> [Accessed 21 Oct 2014].
- Shankar, R., Groven, L., Amert, A., Whites, K. W., and Kellar, J. J., 2011. Non-aqueous synthesis of silver nanoparticles using tin acetate as a reducing agent for the conductive ink formulation in printed electronics. *Journal of Materials Chemistry* [online], 21 (29), 10871. Available from: <http://xlink.rsc.org/?DOI=c0jm04521g>.
- Shen, S.-C., NG, W. K., Chai, L., Dong, Y.-C., and Tan, R. B. H., 2010. Stabilized Amorphous State of Ibuprofen by Co-Spray Drying With Mesoporous SBA-15 to Enhance Dissolution Properties. *Journal of Pharmaceutical Sciences*, 99 (4), 1997–2007.
- Shen, S. C., Ng, W. K., Chia, L., Hu, J., and Tan, R. B. H., 2011. Physical state and dissolution of ibuprofen formulated by co-spray drying with mesoporous silica: Effect of pore and particle size. *International Journal of Pharmaceutics* [online], 410 (1–2), 188–195. Available from: <http://dx.doi.org/10.1016/j.ijpharm.2011.03.018>.
- Shen, Y. C., 2011. Terahertz pulsed spectroscopy and imaging for pharmaceutical applications: A review. *International Journal of Pharmaceutics* [online], 417 (1–2), 48–60. Available from: <http://dx.doi.org/10.1016/j.ijpharm.2011.01.012>.
- Singh, M., Haverinen, H. M., Dhagat, P., and Jabbour, G. E., 2010. Inkjet printing-process and its applications. *Advanced Materials*, 22 (6), 673–685.
- Sinka, I. C., Burch, S. F., Tweed, J. H., and Cunningham, J. C., 2004. Measurement of density variations in tablets using X-ray computed tomography. *International Journal of Pharmaceutics*, 271 (1–2), 215–224.
- Skořepová, E., Bím, D., Hušák, M., Klimeš, J., Chatziadi, A., Ridvan, L.,

- Boleslavská, T., Beránek, J., Šebek, P., and Rulišek, L., 2017. Increase in solubility of poorly-ionizable pharmaceuticals by salt formation: A case of agomelatine sulfonates. *Crystal Growth and Design*, 17 (10), 5283–5294.
- Solanki, N. G., Tahsin, M., Shah, A. V., and Serajuddin, A. T. M., 2018. Formulation of 3D Printed Tablet for Rapid Drug Release by Fused Deposition Modeling: Screening Polymers for Drug Release, Drug-Polymer Miscibility and Printability. *Journal of Pharmaceutical Sciences* [online], 107 (1), 390–401. Available from: <https://doi.org/10.1016/j.xphs.2017.10.021>.
- Soleimani-Gorgani, A., 2016. *Inkjet Printing* [online]. Printing on Polymers. Elsevier Inc. Available from: <http://linkinghub.elsevier.com/retrieve/pii/B9780323374682000142>.
- Song, W. H., Yeom, D. W., Lee, D. H., Lee, K. M., Yoo, H. J., Chae, B. R., Song, S. H., and Choi, Y. W., 2014. In situ intestinal permeability and in vivo oral bioavailability of celecoxib in supersaturating self-emulsifying drug delivery system. *Archives of pharmacal research* [online], 37, 626–35. Available from: <http://www.ncbi.nlm.nih.gov/pubmed/23852645> [Accessed 4 Dec 2014].
- Soppimath, K. S., Aminabhavi, T. M., Kulkarni, a R., and Rudzinski, W. E., 2001. Biodegradable polymeric nanoparticles as drug delivery devices. *Journal of controlled release : official journal of the Controlled Release Society*, 70 (1–2), 1–20.
- Steiner, G., 2008. Fenofibrate for cardiovascular disease prevention in metabolic syndrome and type 2 diabetes mellitus. *The American journal of cardiology* [online], 102 (12A), 28L–33L. Available from: <http://dx.doi.org/10.1016/j.amjcard.2008.09.072>.
- Stella, V. J. and Nti-Addae, K. W., 2007. Prodrug strategies to overcome poor water solubility. *Advanced drug delivery reviews* [online], 59, 677–94. Available from: <http://www.ncbi.nlm.nih.gov/pubmed/17628203> [Accessed 13 Nov 2014].
- Stevenson, C. L., Santini, J. T., and Langer, R., 2012. Reservoir-based drug delivery systems utilizing microtechnology. *Advanced drug delivery reviews* [online],

64, 1590–602. Available from:

<http://www.pubmedcentral.nih.gov/articlerender.fcgi?artid=3430809&tool=pmc-entrez&rendertype=abstract> [Accessed 11 Nov 2013].

Sukeshini A., M., Meisenkothen, F., Gardner, P., and Reitz, T. L., 2013. Aerosol Jet® Printing of functionally graded SOFC anode interlayer and microstructural investigation by low voltage scanning electron microscopy. *Journal of Power Sources* [online], 224, 295–303. Available from: <http://dx.doi.org/10.1016/j.jpowsour.2012.09.094>.

Sun, Y., Chen, X., Zhou, X., Zhu, J., and Yu, Y., 2015. Droplet-in-oil array for picoliter-scale analysis based on sequential inkjet printing. *Lab Chip* [online], 15 (11), 2429–2436. Available from: <http://xlink.rsc.org/?DOI=C5LC00356C>.

Sun, Y. and Østergaard, J., 2017. Application of UV Imaging in Formulation Development. *Pharmaceutical Research*, 34 (5), 929–940.

Swei, J. and Talbot, J. B., 2002. Viscosity Correlation for Aqueous Polyvinylpyrrolidone (PVP) Solutions, 0–1.

Tait, J. G., Witkowska, E., Hirade, M., Ke, T. H., Malinowski, P. E., Steudel, S., Adachi, C., and Heremans, P., 2015. Uniform Aerosol Jet printed polymer lines with 30 µm width for 140 ppi resolution RGB organic light emitting diodes. *Organic Electronics: physics, materials, applications* [online], 22, 40–43. Available from: <http://dx.doi.org/10.1016/j.orgel.2015.03.034>.

Tajane, S. R., Kholwal, B. B., Suryawanshi, S. S., and Tarkase, K. N., 2012. CURRENT TRENDS IN PULSATILE DRUG DELIVERY SYSTEMS. *International Journal of Pharmaceutical Sciences and Research*, 3 (02), 358–366.

Takale, A. A., Gadhawe, M. V, and Gaikwad, D. D., 2012. Microparticles in Drug Delivery System: A Review. *International Journal of Institutional Pharmacy and Life Sciences*, 2 (2), 349–359.

Talbot, E. L., Yow, H. N., Yang, L., Berson, A., Biggs, S. R., and Bain, C. D., 2015. Printing small dots from large drops. *ACS Applied Materials and Interfaces*, 7 (6), 3782–3790.

- Tangri, P. and Khurana, S., 2011. Pulsatile Drug Delivery Systems: Methods and Advances. *International Journal of Drug Formulation and Research*, 2 (3), 100–102.
- Testa, B., 2004. Prodrug research: futile or fertile? *Biochemical pharmacology* [online], 68, 2097–106. Available from: <http://www.ncbi.nlm.nih.gov/pubmed/15498500> [Accessed 2 Dec 2014].
- Thomas, L. H., Wales, C., Zhao, L., and Wilson, C. C., 2011. Paracetamol Form II: An Elusive Polymorph through Facile Multicomponent Crystallisation Routes. *Crystal Growth & Design*, 11, 1450–1452.
- Thybo, P., Pedersen, B. L., Hovgaard, L., Holm, R., and Mullertz, A., 2008. Characterization and physical stability of spray dried solid dispersions of probucol and PVP-K30. *Pharmaceutical development and technology*, 13 (5), 375–386.
- Tipduangta, P. and Pharm, B., 2016. Crystallisation of Amorphous Fenofibrate and Potential of the Polymer Blend Electrospun Matrices to Stabilise in its Amorphous Form, (November).
- Tipduangta, P., Takiuddin, K., Belton, P., and Qi, S., 2015. A New Low Melting-Point Polymorph of Fenofibrate Prepared via Talc Induced Heterogeneous Nucleation.
- Tiwari, G., Srivastawa, B., Pandey, S., Tiwari, R., Rai, A., Pandey, P., and Bhati, L., 2011. In vitro -in vivo correlation and biopharmaceutical classification system. *Chronicles of Young Scientists* [online], 2 (3), 126. Available from: <http://www.cysonline.org/text.asp?2011/2/3/126/90888> [Accessed 8 Jan 2015].
- Torchilin, V., 2011. Tumor delivery of macromolecular drugs based on the EPR effect. *Advanced drug delivery reviews* [online], 63 (3), 131–5. Available from: <http://www.ncbi.nlm.nih.gov/pubmed/20304019> [Accessed 21 Jan 2014].
- Torchilin, V. P., 2004. Targeted polymeric micelles for delivery of poorly soluble drugs. *Cellular and molecular life sciences* [online], 61, 2549–59. Available from: <http://www.ncbi.nlm.nih.gov/pubmed/15526161> [Accessed 27 Nov 2013].

- Tran, T. H., Ramasamy, T., Truong, D. H., Choi, H.-G., Yong, C. S., and Kim, J. O., 2014. Preparation and Characterization of Fenofibrate-Loaded Nanostructured Lipid Carriers for Oral Bioavailability Enhancement. *AAPS PharmSciTech* [online], 15 (6), 1509–1515. Available from: <http://link.springer.com/10.1208/s12249-014-0175-y>
- Uddin, M. J., Scoutaris, N., Klepetsanis, P., Chowdhry, B., Prausnitz, M. R., and Douroumis, D., 2015. Inkjet printing of transdermal microneedles for the delivery of anticancer agents. *International Journal of Pharmaceutics* [online], 1–10. Available from: <http://linkinghub.elsevier.com/retrieve/pii/S0378517315000629>.
- Ursan, I. D., Chiu, L., and Pierce, A., 2013. Three-dimensional drug printing: a structured review. *Journal of the American Pharmacists Association* [online], 53 (2), 136–44. Available from: <http://www.ncbi.nlm.nih.gov/pubmed/23571620>.
- Vakili, H., Kolakovic, R., Genina, N., Marmion, M., Salo, H., Ihalainen, P., Peltonen, J., and Sandler, N., 2015. Hyperspectral imaging in quality control of inkjet printed personalised dosage forms. *International Journal of Pharmaceutics* [online], 483 (1–2), 244–249. Available from: <http://linkinghub.elsevier.com/retrieve/pii/S0378517314009314>.
- Vanarase, A. U., Osorio, J. G., and Muzzio, F. J., 2013. Effects of powder flow properties and shear environment on the performance of continuous mixing of pharmaceutical powders. *Powder Technology* [online], 246, 63–72. Available from: <http://dx.doi.org/10.1016/j.powtec.2013.05.002>.
- Varghese, S. and Ghoroi, C., 2017. Improving the wetting and dissolution of ibuprofen using solventless co-milling. *International Journal of Pharmaceutics* [online], 533 (1), 145–155. Available from: <http://dx.doi.org/10.1016/j.ijpharm.2017.09.062>.
- Varshosaz, J. and Ghassami, E., 2015. Enhancement of Dissolution Rate of Fenofibrate By Spray Drying Technique : Comparison of Eudragit E-100 ,

Solutol ® Hs15 and Hydroxypropyl Cellulose As Carriers, 63.

- Vasconcelos, T., Sarmiento, B., and Costa, P., 2007. Solid dispersions as strategy to improve oral bioavailability of poor water soluble drugs. *Drug discovery today* [online], 12 (23–24), 1068–75. Available from: <http://www.ncbi.nlm.nih.gov/pubmed/18061887> [Accessed 11 Nov 2013].
- Vercammen, Y. and Luppen, J. Van, 2013. ToF-S-SIMS molecular 3D analysis of micro-objects as an alternative to ion beam erosion at large depth : application to single inkjet dots, 2053–2064.
- Verstraete, G., Samaro, A., Grymonpré, W., Vanhoorne, V., Van Snick, B., Boone, M. N., Hellemans, T., Van Hoorebeke, L., Remon, J. P., and Vervaet, C., 2018. 3D printing of high drug loaded dosage forms using thermoplastic polyurethanes. *International Journal of Pharmaceutics* [online], 536 (1), 318–325. Available from: <https://doi.org/10.1016/j.ijpharm.2017.12.002>.
- Vialpando, M., Backhuijs, F., Martens, J. a, and Van den Mooter, G., 2012. Risk assessment of premature drug release during wet granulation of ordered mesoporous silica loaded with poorly soluble compounds itraconazole, fenofibrate, naproxen, and ibuprofen. *European journal of pharmaceutics and biopharmaceutics : official journal of Arbeitsgemeinschaft für Pharmazeutische Verfahrenstechnik e.V* [online], 81 (1), 190–8. Available from: <http://www.ncbi.nlm.nih.gov/pubmed/22306694>.
- Vikaas, B. and Arun, N., 2012. The Biopharmaceutical Classification System (BCS): Present Status and Future Prospectives. *International Research Journal of Pharmacy*, 3 (9), 7–11.
- Vogt, M., Kunath, K., and Dressman, J. B., 2008. Dissolution enhancement of fenofibrate by micronization, cogrinding and spray-drying: Comparison with commercial preparations. *European Journal of Pharmaceutics and Biopharmaceutics*, 68 (2), 283–288.
- Vojinović, T., Medarević, D., Vranić, E., Potpara, Z., Krstić, M., Djuriš, J., and Ibrić, S., 2018. Development of ternary solid dispersions with hydrophilic polymer and surface adsorbent for improving dissolution rate of carbamazepine. *Saudi*

Pharmaceutical Journal, 26 (5), 725–732.

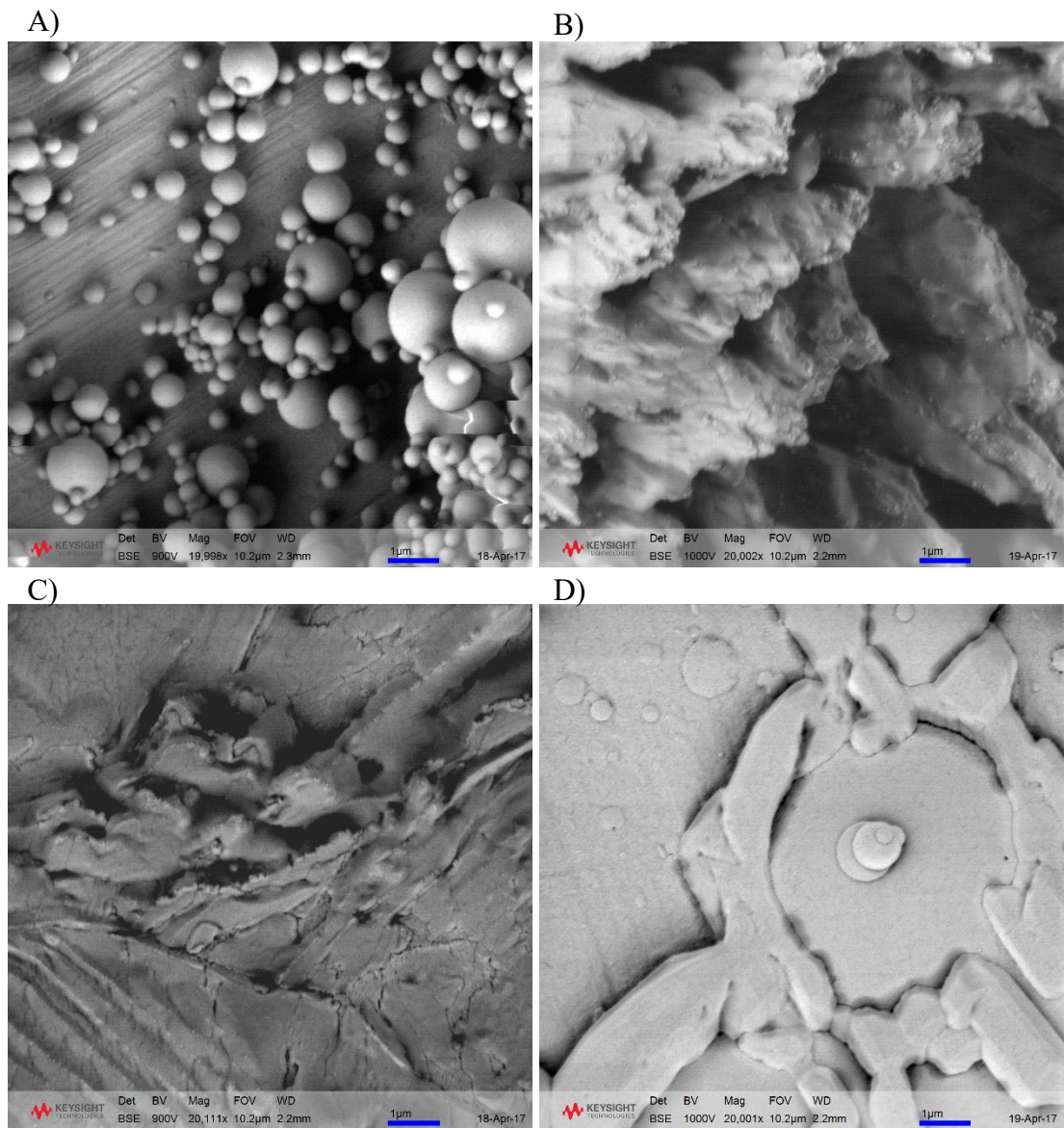
- Vuddanda, P. R., Alomari, M., Dodoo, C. C., Trenfield, S. J., Velaga, S., Basit, A. W., and Gaisford, S., 2018. Personalisation of warfarin therapy using thermal ink-jet printing. *European Journal of Pharmaceutical Sciences*, 117 (September 2017), 80–87.
- Wang, K., Chang, Y. H., Zhang, C., and Wang, B., 2016. Conductive-on-demand: Tailorable polyimide/carbon nanotube nanocomposite thin film by dual-material aerosol jet printing. *Carbon* [online], 98, 397–403. Available from: <http://dx.doi.org/10.1016/j.carbon.2015.11.032>.
- Ward, A., Walton, K., Box, K., Østergaard, J., Gillie, L. J., Conway, B. R., and Asare-Addo, K., 2017. Variable-focus microscopy and UV surface dissolution imaging as complementary techniques in intrinsic dissolution rate determination. *International Journal of Pharmaceutics*, 530 (1–2), 139–144.
- Wei, J., Wang, J., Su, S., Wang, S., Qiu, J., Zhang, Z., Christopher, G., Ning, F., and Cong, W., 2015. 3D printing of an extremely tough hydrogel. *RSC Adv.* [online], 5 (99), 81324–81329. Available from: <http://xlink.rsc.org/?DOI=C5RA16362E>.
- Werner, C., Godlinski, D., Zöllmer, V., and Busse, M., 2013. Morphological influences on the electrical sintering process of Aerosol Jet and Ink Jet printed silver microstructures. *Journal of Materials Science: Materials in Electronics*, 24 (11), 4367–4377.
- Wheeler, J. S. R., Longpré, A., Sells, D., McManus, D., Lancaster, S., Reynolds, S. W., and Yeates, S. G., 2016. Effect of polymer branching on degradation during inkjet printing. *Polymer Degradation and Stability* [online], 128, 1–7. Available from: <http://linkinghub.elsevier.com/retrieve/pii/S0141391016300350>.
- Wheeler, J. S. R., Reynolds, S. W., Lancaster, S., Romanguera, V. S., and Yeates, S. G., 2014. Polymer degradation during continuous ink-jet printing. *Polymer Degradation and Stability* [online], 105 (1), 116–121. Available from: <http://dx.doi.org/10.1016/j.polymdegradstab.2014.04.007>.
- Wickström, H., Nyman, J. O., Indola, M., Sundelin, H., Kronberg, L., Preis, M.,

- Rantanen, J., and Sandler, N., 2017. Colorimetry as Quality Control Tool for Individual Inkjet-Printed Pediatric Formulations. *AAPS PharmSciTech*, 18 (2), 293–302.
- Wickström, H., Palo, M., Rijckaert, K., Kolakovic, R., Nyman, J. O., Määttänen, A., Ihalainen, P., Peltonen, J., Genina, N., de Beer, T., Löbmann, K., Rades, T., and Sandler, N., 2015. Improvement of dissolution rate of indomethacin by inkjet printing. *European Journal of Pharmaceutical Sciences* [online], 75, 91–100. Available from: <http://linkinghub.elsevier.com/retrieve/pii/S0928098715001098>.
- Wiranidchamong, C., Ruangpayungsak, N., Suwattanasuk, P., Shuwisitkul, D., and Tanvichien, S., 2015. Plasticizing effect of ibuprofen induced an alteration of drug released from Kollidon SR matrices produced by direct compression. *Drug Development and Industrial Pharmacy*, 41 (6), 1037–1046.
- Xie, H.-G. and Frueh, F. W., 2005. Pharmacogenomics steps toward personalized medicine. *Personalized Medicine*, 2 (4), 325–337.
- Xie, S., Li, Z., and Yu, Z., 2015. Microneedles for transdermal delivery of insulin. *Journal of Drug Delivery Science and Technology*, 28, 11–17.
- Yadav, V. B. and Yadav, a. V., 2009. Enhancement of solubility and dissolution rate of Fenofibrate by melt granulation technique. *International Journal of PharmTech Research*, 1 (2), 256–263.
- Yang, C., Zhou, E., Miyanishi, S., Hashimoto, K., and Tajima, K., 2011. Preparation of active layers in polymer solar cells by aerosol jet printing. *ACS Applied Materials and Interfaces*, 3 (10), 4053–4058.
- Yang, W.-W. and Pierstorff, E., 2012. Reservoir-based polymer drug delivery systems. *Journal of laboratory automation* [online], 17 (1), 50–8. Available from: <http://www.ncbi.nlm.nih.gov/pubmed/22357608> [Accessed 11 Dec 2013].
- Yawei, Z., Ru, G., Chunyan, L., and Jing, Z., 2013. Design the CCD Tablet Thickness Measurement System Based on Laser Triangulation Method, 748, 521–524.

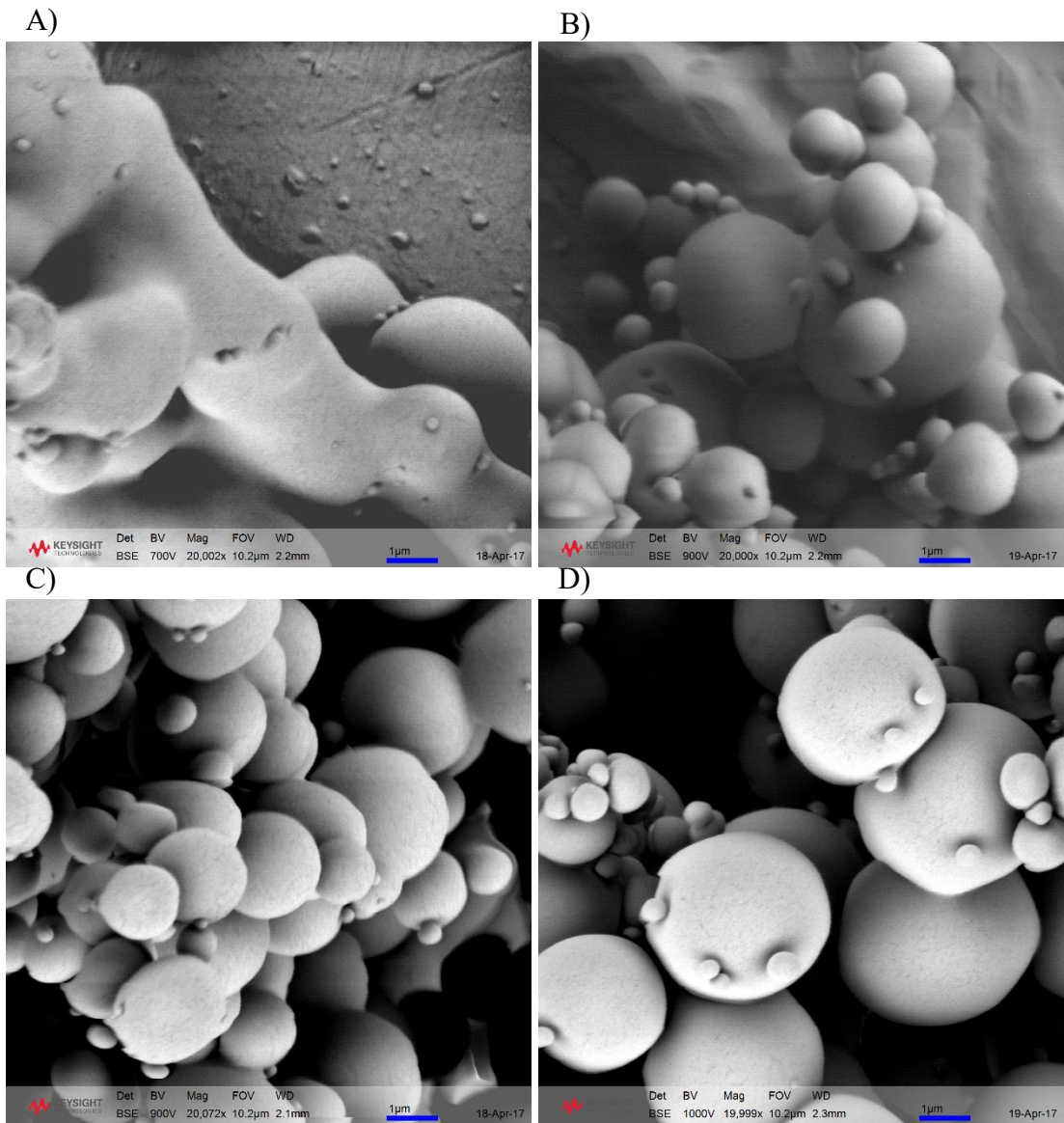
- Yeoman, A., Sayre, C., and Santorella, E., 2016. US2016/0302410A1: Multicomponent and Multilayer Compacted Tablets.
- Yousaf, A. M., Kim, D. W., Yong, C. S., Kim, J. O., and Choi, H.-G., 2015. Enhanced oral bioavailability of fenofibrate using polymeric nanoparticulated systems : physicochemical characterization and in vivo investigation. *International Journal of Nanomedicine*, 10, 1819–1830.
- Yun, Y. H., Kim, J. D., Lee, B. K., Cho, Y. W., and Lee, H. Y., 2009a. Polymer Inkjet Printing : Construction of Three-Dimensional Structures at Micro-Scale by Repeated Lamination. *Macromolecular Research*, 17 (3), 197–202.
- Yun, Y. H., Kim, J. D., Lee, B. K., Cho, Y. W., and Lee, H. Y., 2009b. Polymer inkjet printing: Construction of three-dimensional structures at micro-scale by repeated lamination. *Macromolecular Research*, 17 (3), 197–202.
- Yun, Y. H., Kim, J. D., Lee, B. K., Yoo, B., Lee, J. H., and Cho, Y. W., 2009. Construction of micro-patterned polymer structures by piezoelectric inkjet printing. *Polymer - Plastics Technology and Engineering*, 48 (12), 1318–1323.
- Zema, L., Loreti, G., Melocchi, A., Maroni, A., and Gazzaniga, A., 2012. Injection Molding and its application to drug delivery. *Journal of Controlled Release* [online], 159, 324–331. Available from: <http://dx.doi.org/10.1016/j.jconrel.2012.01.001>.
- Zhang, M., Li, H., Lang, B., O'Donnell, K., Zhang, H., Wang, Z., Dong, Y., Wu, C., and Williams, R. O., 2012. Formulation and delivery of improved amorphous fenofibrate solid dispersions prepared by thin film freezing. *European Journal of Pharmaceutics and Biopharmaceutics* [online], 82 (3), 534–544. Available from: <http://dx.doi.org/10.1016/j.ejpb.2012.06.016>.
- Zhang, Y. J., Gallis, B., Taya, M., Wang, S., Ho, R. J. Y., and Sasaki, T., 2013. pH-responsive artemisinin derivatives and lipid nanoparticle formulations inhibit growth of breast cancer cells in vitro and induce down-regulation of HER family members. *PloS one* [online], 8 (3), e59086. Available from: <http://www.pubmedcentral.nih.gov/articlerender.fcgi?artid=3597601&tool=pmc-entrez&rendertype=abstract> [Accessed 14 Jan 2015].

Appendices

Appendix 1: SEM



A1.1: SEM of PVP K30 (A), fenofibrate (B), 2:1 (C) and 1:1 (D) fenofibrate:PVP K30 taken at x20K magnification.



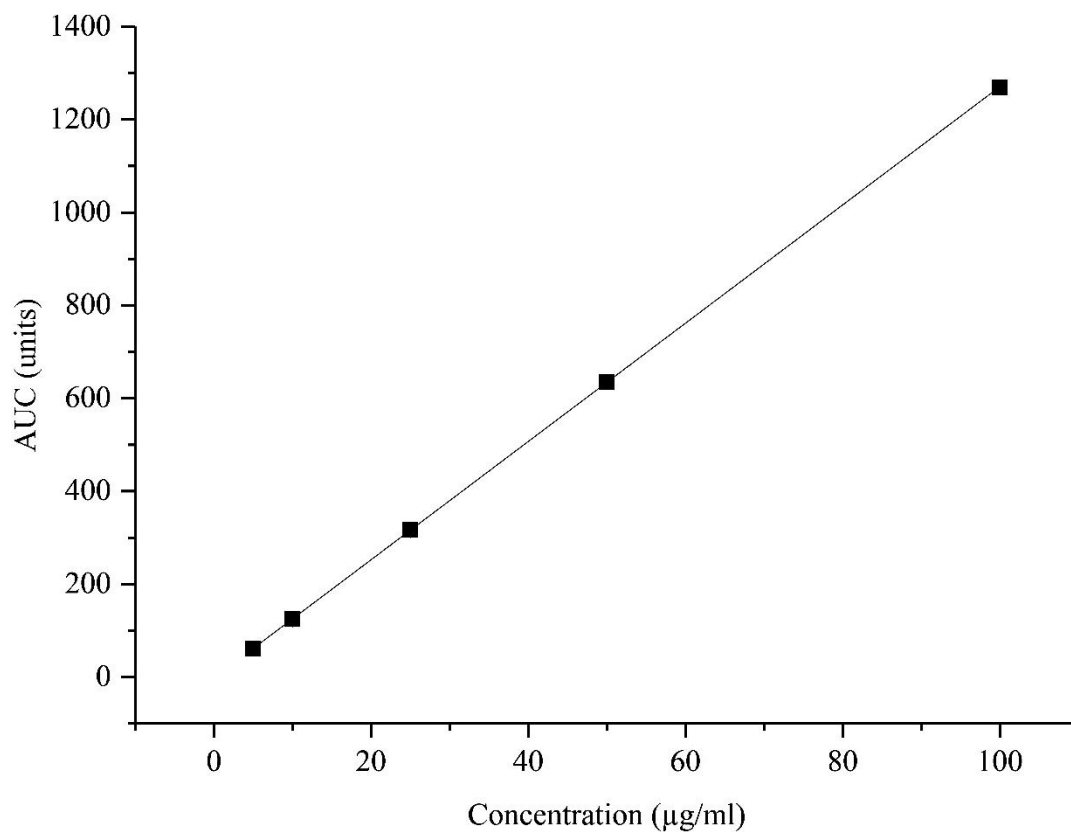
A1.2: SEM of 2:3 (A), 1:2 (B), 1:3 (C) and 1:4 (D) fenofibrate:PVP K30 taken at x20K magnification.

Appendix 2: Printer Capabilities

A2.1: Examples of percentage success and failure of printing using the aerosol jet, based on the number of samples discarded

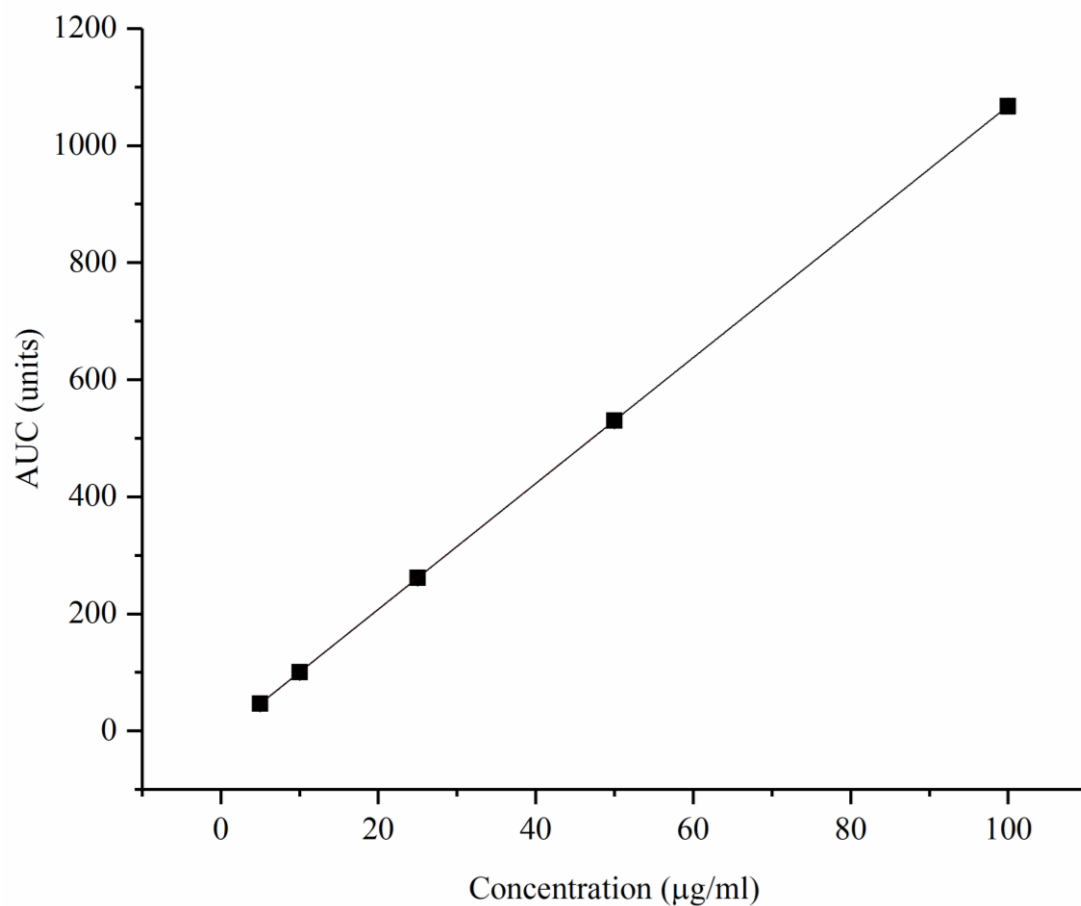
Deposition (mm diameter)	Ink	Nozzle Size (μm)	Speed (mm/s)	Layer(s) (n)	Success (%)	Failure (%)
5	1:1 FNF:PVP	100	3	1	0	100
5	1:1 FNF:PVP	150	3	1	66.67	33.33
5	1:1 FNF:PVP	200	3	1	100	0
5	1:1 FNF:PVP	250	3	1	66.67	33.33
5	1:1 FNF:PVP	300	3	1	100	0
2	1:1 FNF:PVP	250	3	1	100	0
7	1:1 FNF:PVP	250	3	1	60	40
10	1:1 FNF:PVP	250	3	1	88.89	11.11
5	1:1 FNF:PVP	250	3	2	72.73	27.27
5	1:1 FNF:PVP	250	3	3	100	0
5	1:1 FNF:PVP	250	3	4	91.67	8.33
5	1:1 FNF:PVP	250	3	5	50	50

5	1:1 FNF:PVP	250	1	1	37.5	62.5
5	1:1 FNF:PVP	250	2	1	9.09	90.91
5	1:1 FNF:PVP	250	4	1	25	75
5	1:1 FNF:PVP	250	5	1	50	50
5	1:1 FNF:PVP	250	6	1	25	75
5	1:1 FNF:PVP	250	9	1	100	0

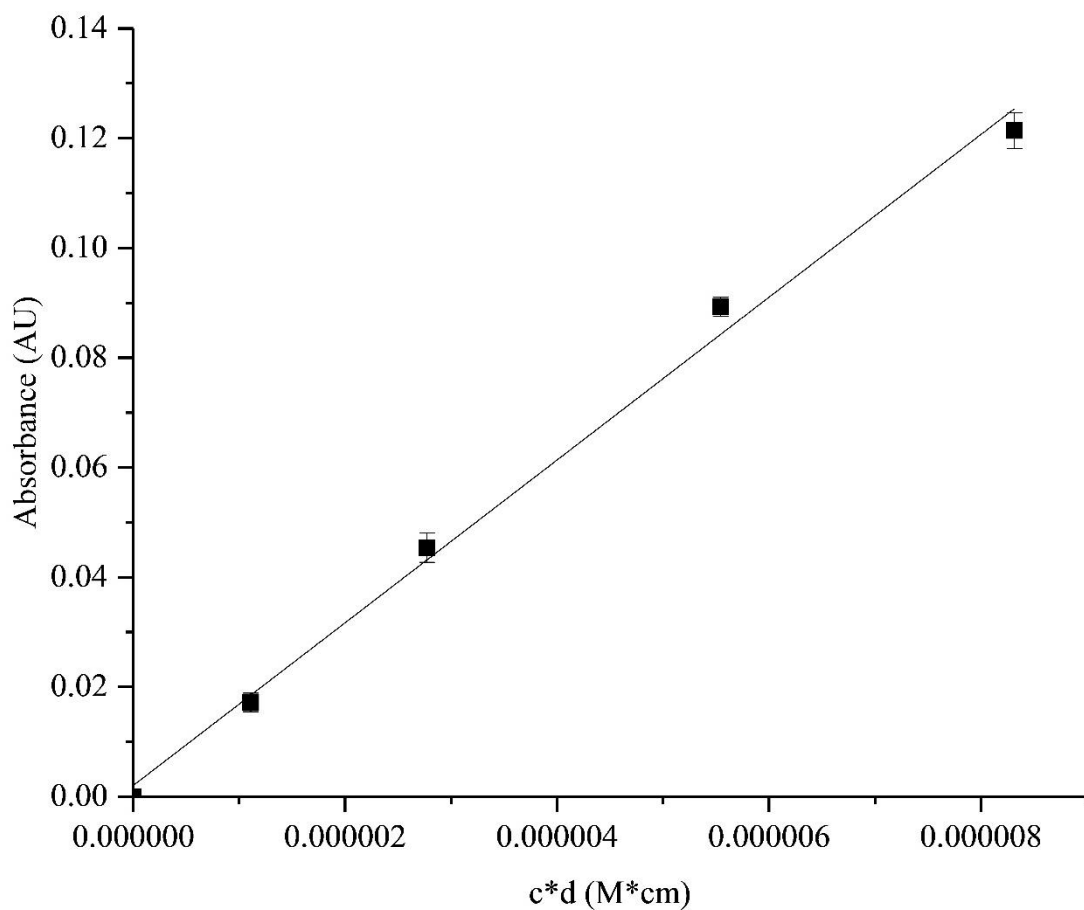


A2.2: Average calibration curve for UHPLC of fenofibrate over a range of 5-100µg/ml using the 80:20 acetonitrile:acidified water method at 280 nm, where $r^2=1$ and $n=9 \pm$ standard error with 95% confidence intervals of 1213.88 units and 1247.58 units, 606.69 units and 624.66 units, 296.80 units and 317.61 units, 115.41 units and 127.43 units, and 53.13 units and 66.10 units for 100, 50, 25, 10 and 5 µg/ml respectively.

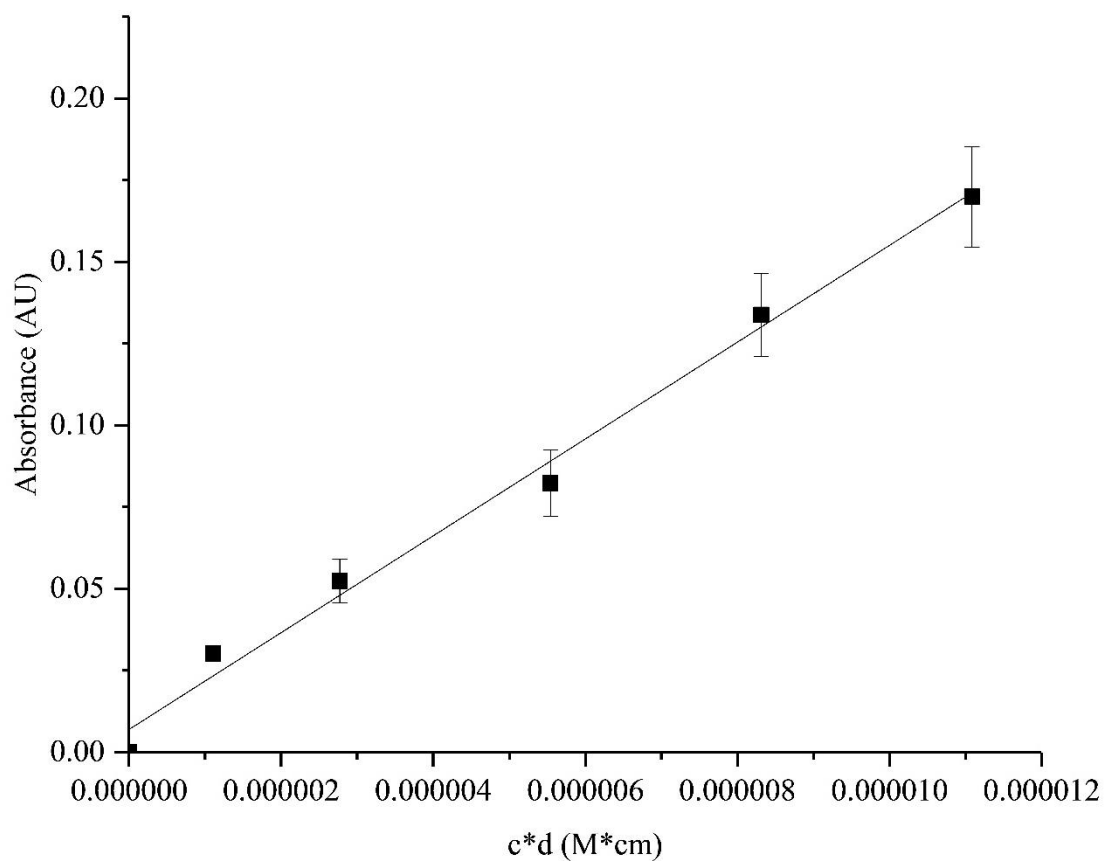
Appendix 3: Calibration curves for SDI



A3.1: Average calibration curve for UHPLC of ibuprofen over a range of 5-100µg/ml using the 60:40 acetonitrile:acidified water method at 214 nm where $r^2=1$ and $n=4 \pm$ standard error with 95% confidence intervals of 1025.87 units and 1109.23 units, 504.39 units and 555.84 units, 242.54 units and 280.25 units, 84.48 units and 115.84 units, and 31.53 units and 61.31 units for 100, 50, 25, 10 and 5 µg/ml.

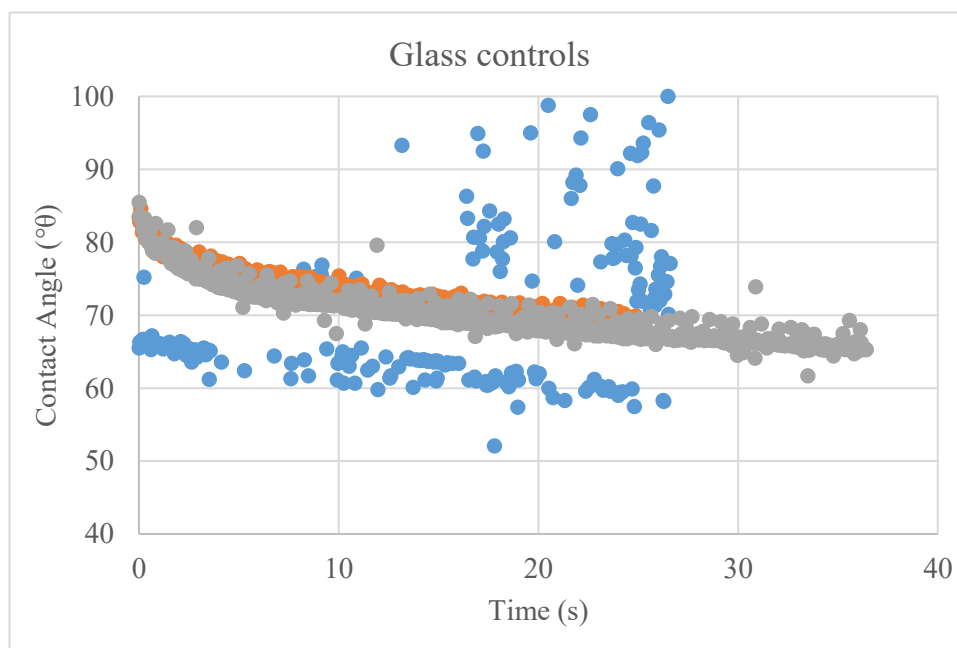
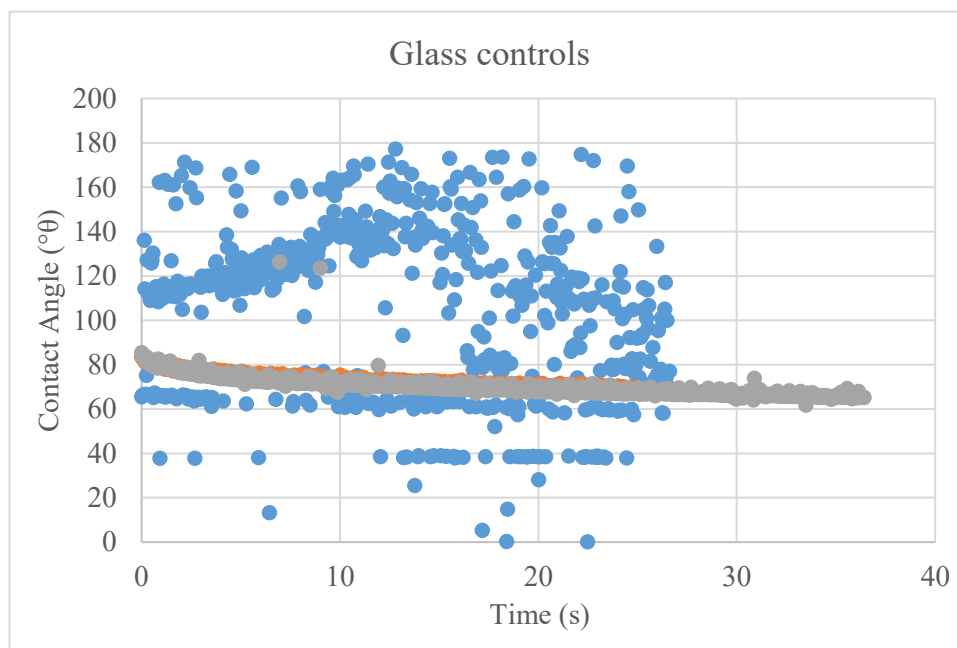


A3.2: Calibration curve generated using the Sirius Analytical SDI for fenofibrate over a range of 1-10 μ g/ml in a 90:10 SIF:methanol solution, where $y=14831x+0.002$, $r^2=0.9948$ and $P=0$. $n=3\pm$ standard error with 95% confidence intervals of 0.00994 units and 0.0244 units, 0.03389 units and 0.05686 units, 0.08182 units and 0.09682 units, and 0.10742 units and 0.13537 units for 1, 2.5, 5, 7.5 and 10 μ g/ml respectively.

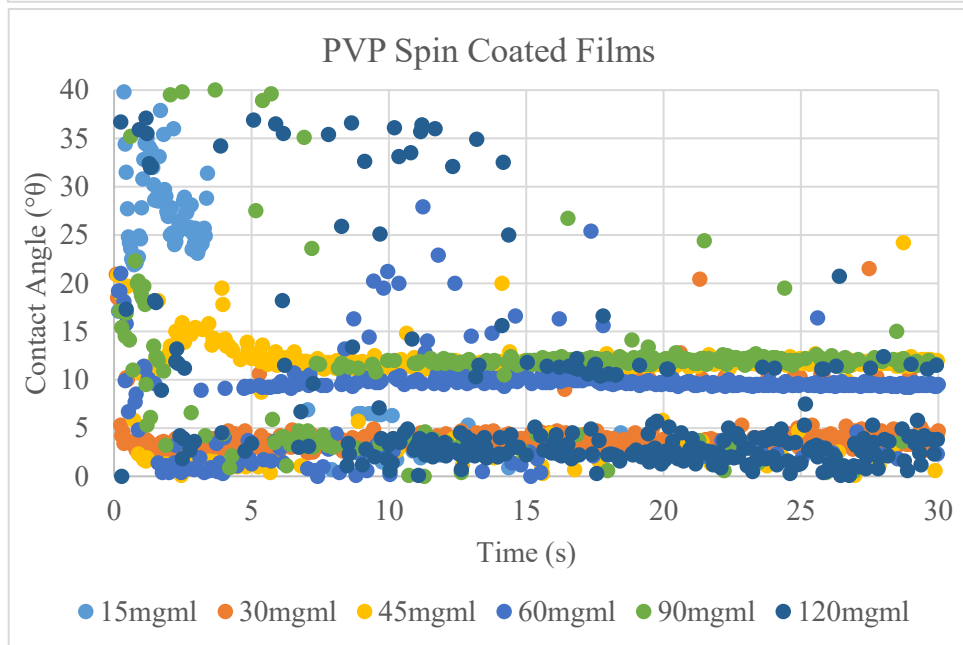
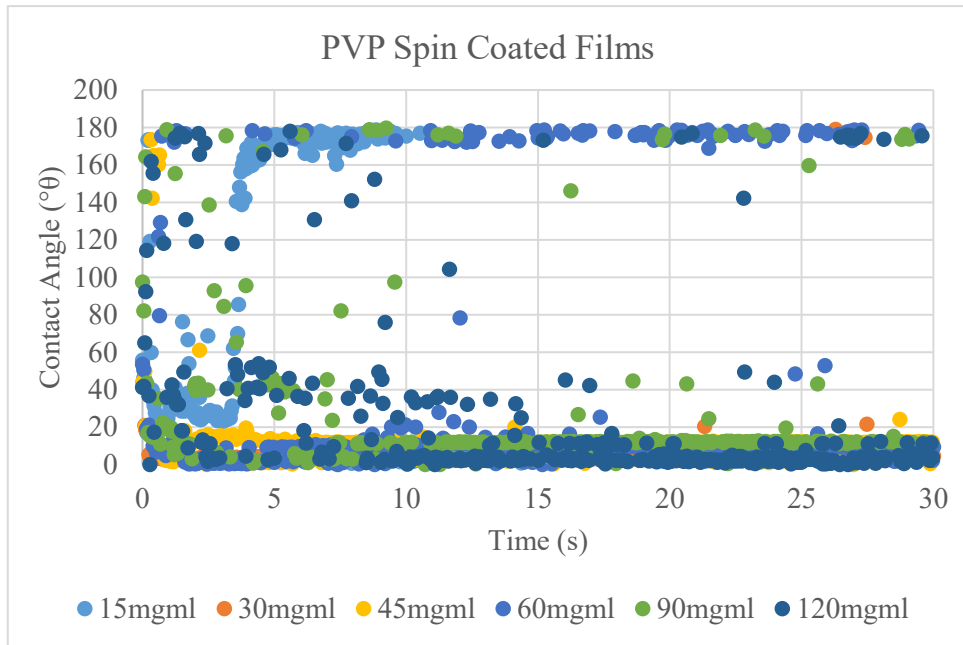


A3.3: Calibration curve generated using the Sirius Analytical SDI for ibuprofen over a range of 1-10 μ g/ml in SIF (using a 1ml methanol stock), where $y=14806x+0.007$, $r^2=0.9915$ and $P=0$. $n=3\pm$ standard error with 95% confidence intervals of 0.02229 units and 0.03813 units, 0.02359 units and 0.08115 units, 0.03883 units and 0.12576 units, 0.07909 units and 0.18849 units, and 0.10381 units and 0.23604 units for 1, 2.5, 5, 7.5 and 10 μ g/ml respectively.

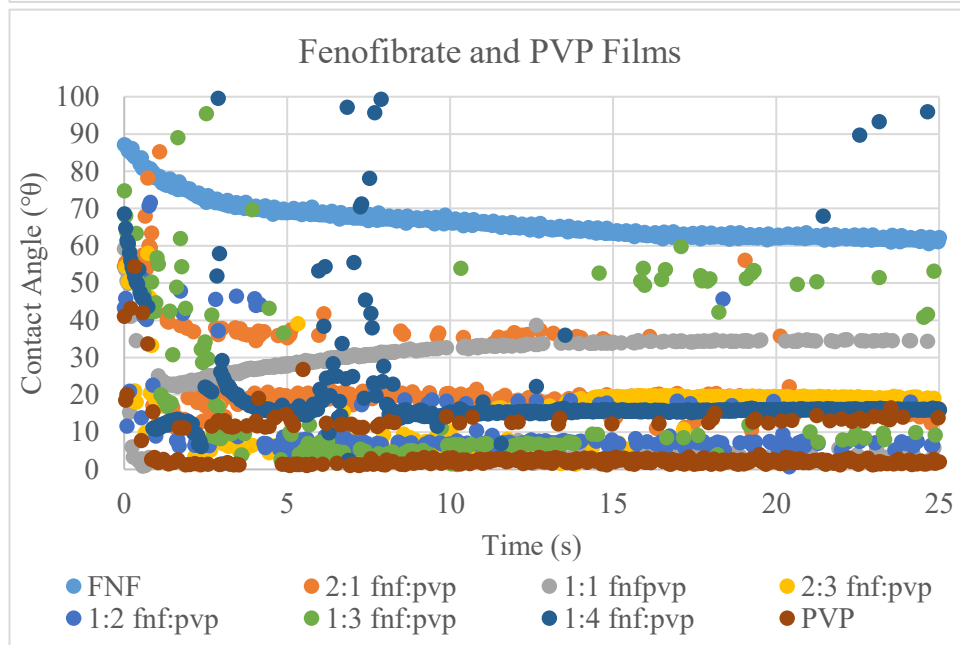
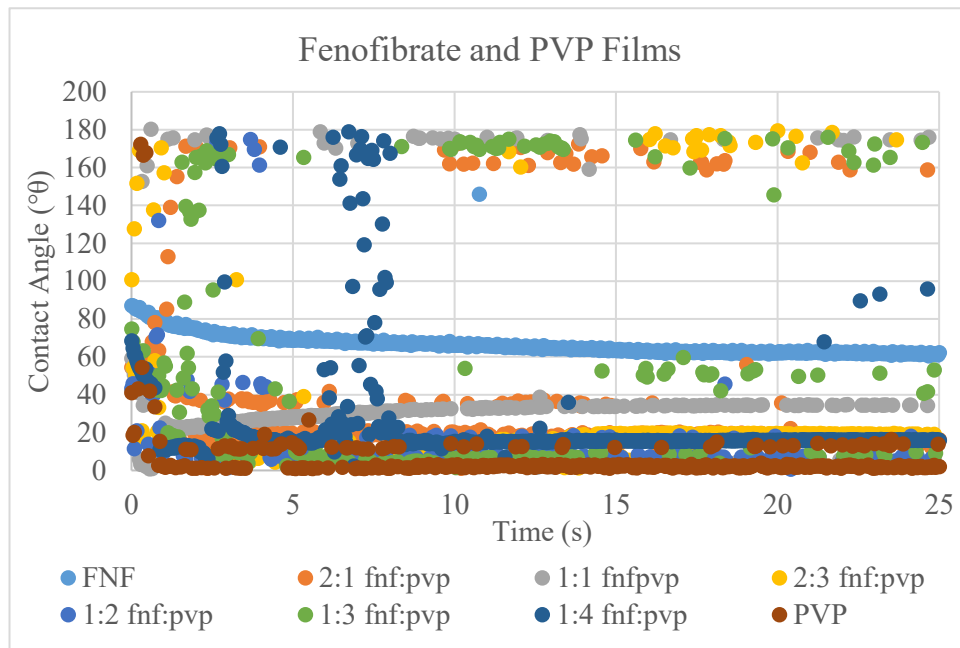
Appendix 4: Contact Angle



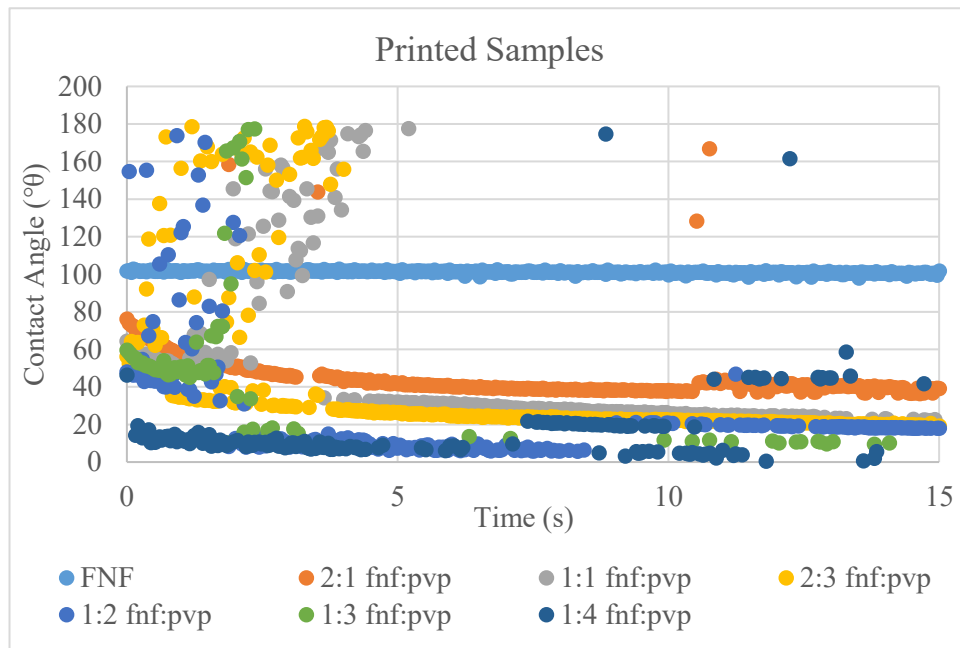
A4.1: Contact angle of glass coverslips over a 30 second period.



A4.2: Contact angle of PVP spin coated samples over a 30 second period.

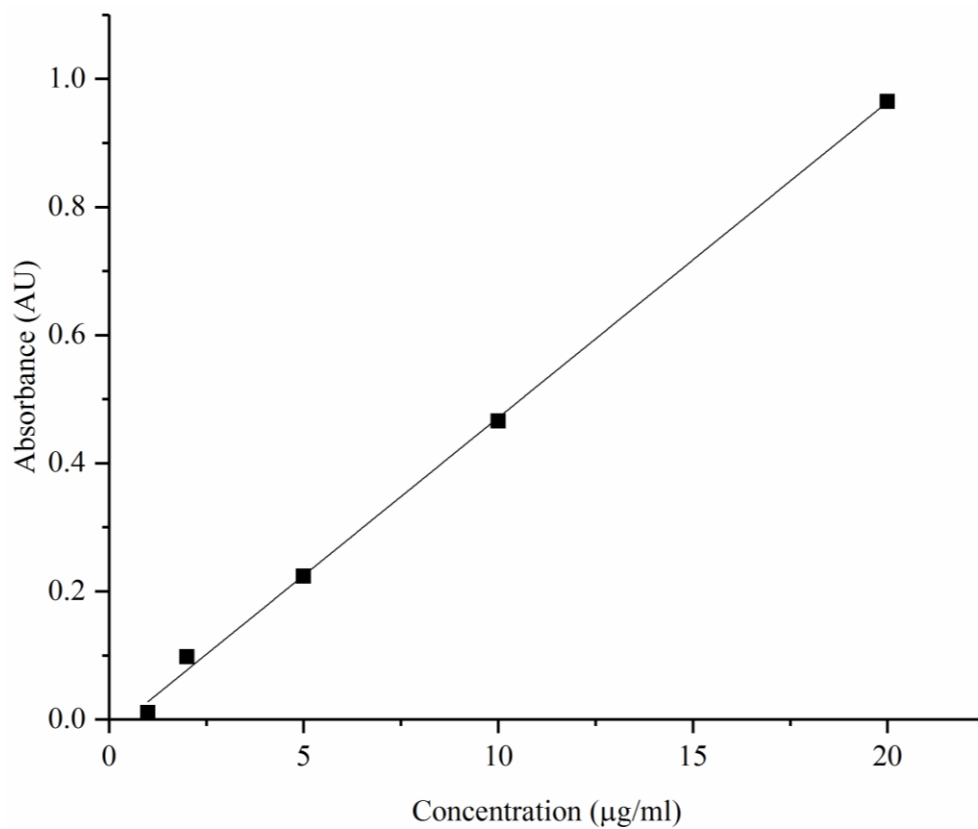


A4.3: Contact angle of fenofibrate and PVP spin coated samples over a 30 second period.



A4.4: Contact angle of fenofibrate and PVP printed samples over a 30 second period.

Appendix 5: Calibration for USP IV



A5: Calibration curve for ibuprofen in SIF using the USP IV flow cell system coupled with the UV spectrometer at 222 nm, where $y=0.0493x-0.0215$ and $r^2 = 0.9987$.